1990

Dynamics Of Lightweight Roofs

Magdy Elsayed Kassem

DYNAMICS OF LIGHTWEIGHT ROOFS

by

Magdy Elsayed Ali Mahmoud Kassem

Faculty of Engineering Science
Department of Civil Engineering

Submitted in partial fulfilment
of the requirements for the degree of
Doctor of Philosophy

Faculty of Graduate Studies
The University of Western Ontario
London, Ontario
June, 1990

ISBN 0-315-59079-3

ABSTRACT

The use of lightweight roofs for long span structures has become popular. Architects find these structures attractive because they allow for a wide scope of innovative design, and can be cost effective and aesthetically pleasing. Although extensive research has already been devoted to many aspects of lightweight structures, this thesis examines the effects of wall openings on self-supported roofs backed by cavities, the nature of the response of air-supported roofs to turbulent wind, and theoretical methods for response prediction.

The first part of the study comprises a free vibration analysis of self-supported, lightweight roofs backed by cavities with openings. A simplified theoretical approach is formulated to evaluate the modal parameters of the roof-air system considering air leakage through the openings, the pneumatic stiffness, and the structural and acoustical damping of the system. The accuracy of the approximate formulae is assessed by comparison with a complex eigenvalue analysis. An exact solution is derived to evaluate the modal parameters for a circular membrane roof backed by a cavity with openings. Closed form solutions are presented for the damped response of circular membrane roofs backed by cavities with openings.

Free vibration laboratory experiments were conducted on two different structural models to verify the theoretical approach. The first model had a membrane roof, and the second had a flexible plate roof. The effects of wall

openings and volume scaling on the roof-air system were examined and the experimental results were then compared with the theoretical ones.

The second part of the study is an examination of the behaviour of air-supported structures. The free vibration of cylindrical and spherical air-supported structures is investigated analytically for different internal pressures and enclosure volumes and the results are compared with those obtained from a finite element solution.

Wind tunnel tests were conducted on an aeroelastic model of a hemispherical, air-supported structure to investigate the wind-induced response and the internal pressure fluctuations. Parameters considered in the aeroelastic experiments included different gradient wind speeds, exposures, enclosure volumes and internal pressures.

A semi-analytical approach is established for predicting the wind-induced response of air-supported structures. This approach depends on external pressure measurements and static deflections. A rigid hemispherical model was tested in a boundary layer wind tunnel to measure the external pressures for different exposure conditions. For different internal pressures, the static deflections were calculated theoretically using the finite element method. The predicted response results of the semi-analytical approach agree well with the experimental results.

To my son Hossam

To my unborn child

To my wife Magda

To my parents

To my whole family

Acknowledgements

I would like to express my thanks to Prof. M. Novak for all his help in the creation of this thesis. His interest, enthusiasm, assistance and encouragement during the past four years inspired me to work hard. The fact that he spent so much of his valuable time making sure that my work was on the right track helped me immeasurably. His efforts have earned my respect and my gratitude.

Special thanks are to Prof. B. J. Vickery for his great advice and help during the wind tunnel experiments. Thanks are also due to Professors A. G. Davenport and D. J. Harman for their help and encouragement in every facet of this thesis.

I also would like to thank Messrs. H. Edney, M. Slattery, H. Cook and Bob Kager of the Mechanical Shop for their help in constructing the four models used in this study. Thanks are also to the staff of The Boundary Layer Wind Tunnel for their assistance and advice during the course of the wind tunnel experiments.

But mostly, I would like to thank my wife Magda and my son Hossam Kassem for their kindness, patience and help. Also, from the bottom of my heart, I would like to thank my parents and my whole family, back home; without their encouragement, support and patience I would never have made it this far.

The author would like to further acknowledge the financial support received for the present work from the National Research Council of Canada.

TABLE OF CONTENTS

Page

Page

Page

Page

LIST OF PHOTOGRAPHIC PLATES

LIST OF TABLES

LIST OF FIGURES

LIST OF APPENDICES

NOMENCLATURE

The following symbols are used

A = roof area;

A_w = area of wall, (A_{wall});

A_1, A_2 = areas of the equivalent piston and openings, respectively;

A_o = area of wall openings;

a = radius of roof;

a_1 ,a_2 = radii of the effective area of the roof and one opening, respectively;

B = constant;

b_1, b_2 = arguments in the membrane equation;

C = constant;

C_F, C_L = local inverse slopes of fan and leakage pressures versus flow characteristics, respectively;

C_p = mean pressure coefficient;

C_p' = RMS pressure coefficient;

$\hat{C_p}$ = peak pressure coefficient;

$C_p^{\vee}$ = minimum pressure coefficient;

c = damping constant;

c_{a1}, c_{a2} = acoustical damping constants for the roof and openings, respectively;

c_s, c_t = structural damping constants of the roof;

c_s, c_t = total damping constants of the roof, $c_t=c_s+c_{a1}$;

c_o = speed of sound in air;

D = rigidity in the shell governing equation;

D = in-plane projection of a circular cross-section;

d = diameter of the model;

dP = excess pressure inside the enclosure;

dV = volume change inside the enclosure;

E = Young's modulus of elasticity;

F = dynamic axial force;

f = frequency in cycle per second (Hz);

f_m, f_p = model and prototype frequencies, respectively;

f_1, f_2 = fundamental frequencies associated with the symmetrical modes with no nodal lines;

f_{ij} = frequency of the ij mode where i = number of nodal lines and j = order of the mode;

H = roof height;

h = roof thickness;

I_B = influence surface of displacement at point B;

Im (μ_j) = imaginary part of μ_j;

J_k = Bessel function of the first kind and k order;

K_{ij} = force at i due to unit displacement at j;

K_p = pneumatic stiffness of the roof;

K_s = generalized structural stiffness of the roof;

k^2, k_1^2 = frequency arguments in the membrane characteristic equation;

L = characteristic length of the structure;

L_j = maximum potential energy of mode j;

L_m, L_p = characteristic lengths of the model and prototype, respectively;

L = actual thickness of the wall opening;

L' = the effective length of the air mass at openings;

M_j = generalized mass of mode j;

m , m_A = membrane mass and added mass per unit area, respectively;

m_m, m_p = mass per unit area of the model and prototype, respectively;

m_S, m_V = structural and virtual masses of the roof per unit area, respectively;

m_1, m_2 = generalized mass of the roof and effective air mass at openings, respectively;

m_2' = effective air mass at openings per unit area;

m = integer;

n = normal vector to the roof surface;

N = number of wall openings;

$p(r,\theta,t)$ = dynamic uniform, harmonic excitation in polar coordinates r and θ at time t;

$\bar{P}$ = mean pressure component;

p' = fluctuating component of pressure;

p = load amplitude;

$\bar{p}$ = load amplitude;

P, P_o = pressure and equilibrium pressure of the enclosure, respectively;

P_{max}, P_{min} = maximum and minimum wind pressures, respectively;

Q = strength of a source of acoustic radiation;

q = dynamic mean wind pressure;

q(t) = generalized coordinate;

q_o = internal pressure in air-supported structures;

R = radius;

R_e = Reynolds number;

RMS = root mean square;

R_{pij} = cross-correlation function of pressures on panel i and j;

Re (μ_j) = real part of μ_j;

r = radius;

$R_1(x)$ = frequency dependent function in the acoustical damping coefficient;

$S_F(f)$ = force spectrum;

$S_p(f)$ = pressure spectrum;

$S_w(f)$ = response spectrum;

s = area of the surface;

T = sampling period;

t = time;

T_A = kinetic energy of the air surrounding the structure;

T_M = kinetic energy of the structure;

T_o = tension force per unit length of the membrane roof;

t_m, t_p = time in model and prototype, respectively;

U = gradient wind speed;

$\bar{U}$ = mean wind speed (gradient);

U_H = mean wind speed at the top of the model;

U_{max} = maximum wind speed;

$\forall$ = volume of the enclosure;

V_o = equilibrium volume of the enclosure;

V_m, V_p = velocity in model and prototype, respectively;

$V_1(r,\theta,t)$ = dynamic displacement of the roof;

$\forall_{chamber}$ = volume of chamber;

$\forall_{model}$ = volume of model;

$\bar{v}_1$ = average displacement of the roof;

$v_2(t)$ = motion of the air mass through openings;

$\ddot{v}_1$, $\dot{v}_1$ = acceleration and velocity of the piston, respectively;

$\ddot{v}_2$, $\dot{v}_2$ = acceleration and velocity of the air mass at openings, respectively;

v_{1j}, v_{2j} = modal amplitudes of the equivalent piston and the air mass at openings in mode j, respectively;

W_A = work done by the roof;

W_j = work done by damping force $P(\delta)$ in mode j;

w = membrane displacement;

$\bar{w}$ = mean component of response;

w' = fluctuating component of response;

x = $2\omega a/c_o$;

$z(t)$ = generalized coordinate;

α = ratio of opening areas to the effective area of the roof;

α' = ratio of opening areas to the roof plane area;

α_1, α_2 = dimensionless parameters;

β = dimensionless ratio;

β_i, i=1,4 = arguments in the equations;

γ = air specific heat ratio;

Δ = determinant;

$\delta(t)$, $\dot{\delta}(t)$ = effective displacement and velocity, respectively;

ϵ = dimensionless ratio = ω_H/ω_p;

ϵ_1 = energy of pulsation of the acoustical surface;

ϵ_2 = argument in the membrane equation, m_2'/m;

ζ_{ac} = acoustical damping;

ζ_j = damping ratio of mode j;

ζ_p = pneumatic damping;

ζ_s = generalized structural damping ratio;

ζ_1, ζ_2 = damping ratios of the fundamental symmetrical modes with no nodal lines;

ζ_{ij} = damping ratio of the ij mode where i = number of nodal lines and j = order of mode;

η = dimensionless ratio;

θ = an angle;

λ, λ_1 = frequency functions in the characteristic equation of cylindrical air-supported structures;

λ_L = length scale;

λ_R = rigidity scale;

λ_{To} = tension per unit length scale;

λ_V = velocity scale;

$\lambda_{\forall}$ = volume scale;

λ_f = frequency scale;

λ_m = mass per unit area scale;

λ_t = time scale;

$\lambda_{\zeta s}$ = structural damping scale;

λ_ρ = density scale;

μ_j = complex eigenvalue of mode j;

ρ_m, ρ_p = model and prototype densities, respectively;

ρ_s = density of the structure;

ρ_o = air density;

ρ = radius of curvature;

σ_U = RMS value of wind speed;

σ_w = RMS value of response w;

τ = time constant;

ϕ = an angle;

$\phi(\theta)$ = shape function in the angle θ;

$\{\phi\}$ = complex mode vector;

$\chi_1(x)$ = function in the added mass equation;

$\psi(r)$ = shape function in polar coordinate r;

$\psi(r,\theta)$ = shape function in polar coordinates r and θ;

ω_H = Helmholtz frequency;

ω_j = undamped frequency of mode j;

ω_j' = damped frequency of mode j;

ω_n = natural frequency of vibration;

ω_p = pneumatic frequency of the roof;

ω_o = fundamental frequency of the roof in vacuum;

ε = dynamic amplification factor;

∞ = infinity; and

∇^2 = Laplacian operator in the membrane equation.

CHAPTER 1

INTRODUCTION, OUTLINE, AND PREVIEW

1.1 INTRODUCTION

During recent decades, the use of lightweight roofs has become increasingly popular. Lightweight roofs, such as cable roofs and air-supported structures, can cover long spans and are economical. With the current trend towards longer roof spans for sporting facilities and special industrial buildings, lightweight roofs are likely to remain the most economical alternative. Some well-known examples of lightweight structures include the German Pavilion at EXPO'67 and the Olympic Stadium in Montreal, the Olympic Swimming Complex in Tokyo, the Munich Pavilion at the 1972 Olympics, and the Calgary Olympic Coliseum (the Saddledome). Examples of lightweight structures are shown in Plates (1.1) to (1.3), and in Figure (1.1).

The design of lightweight roofs involves many difficult problems; among them are the potentially destructive vibration or flutter of the roof, and the effect of gusting turbulent wind. Therefore, wind tunnel tests on scaled models are recommended to investigate these effects and to test stiffening systems that might mitigate the potentially destructive oscillations, should they occur.

The topic of lightweight structures is very broad; therefore, the present study is limited to a narrow area and is focused on the roof-air interaction for two different types of roofs: self-supported, large span roofs backed by cavities with

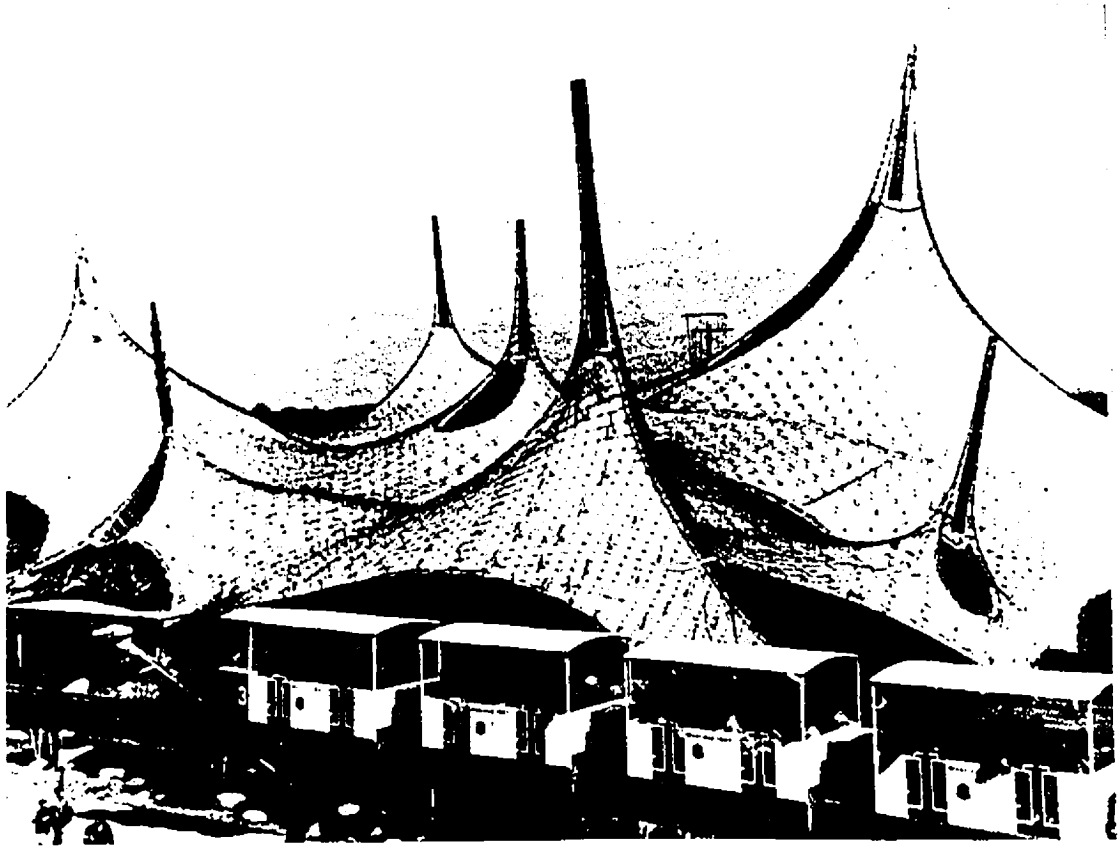

Plate (1.1): West Germany's pavilion at EXPO'67 in Montreal (Dent, 1971)

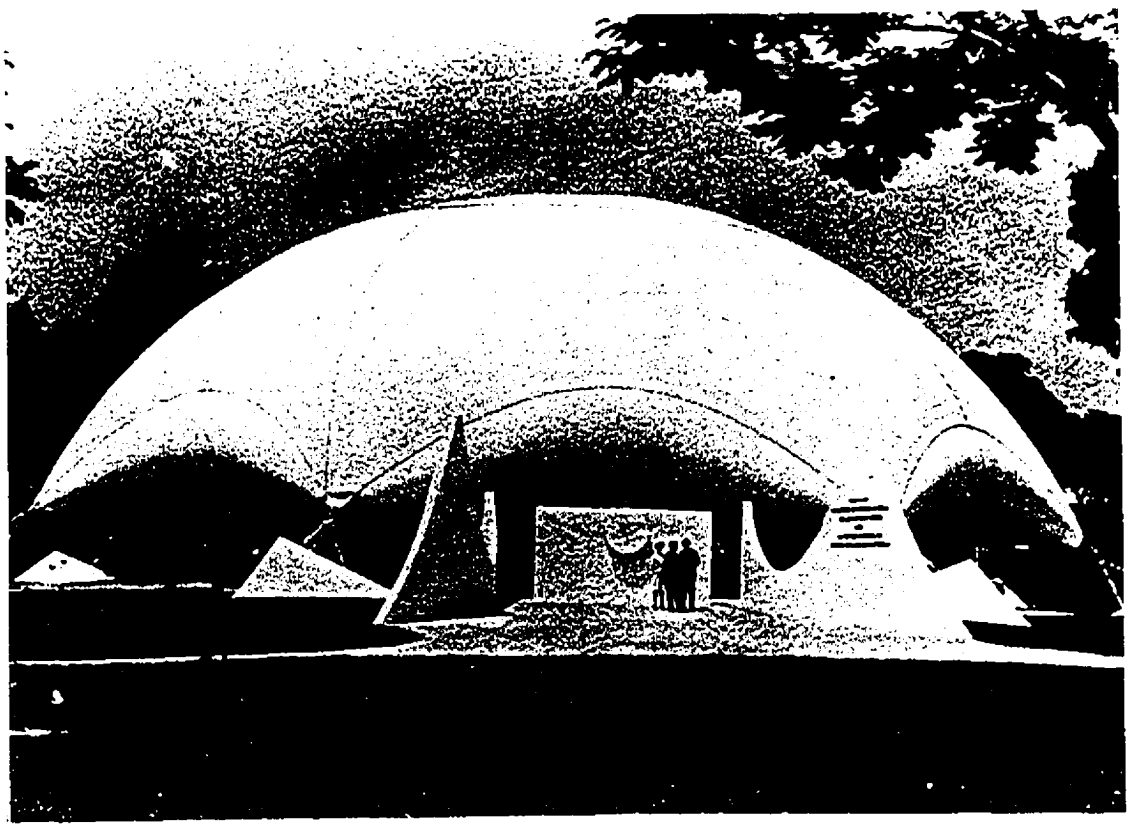

Plate (1.2): Air inflated exhibition pavilion of the U.S. Atomic Energy Commission (Dent, 1971)

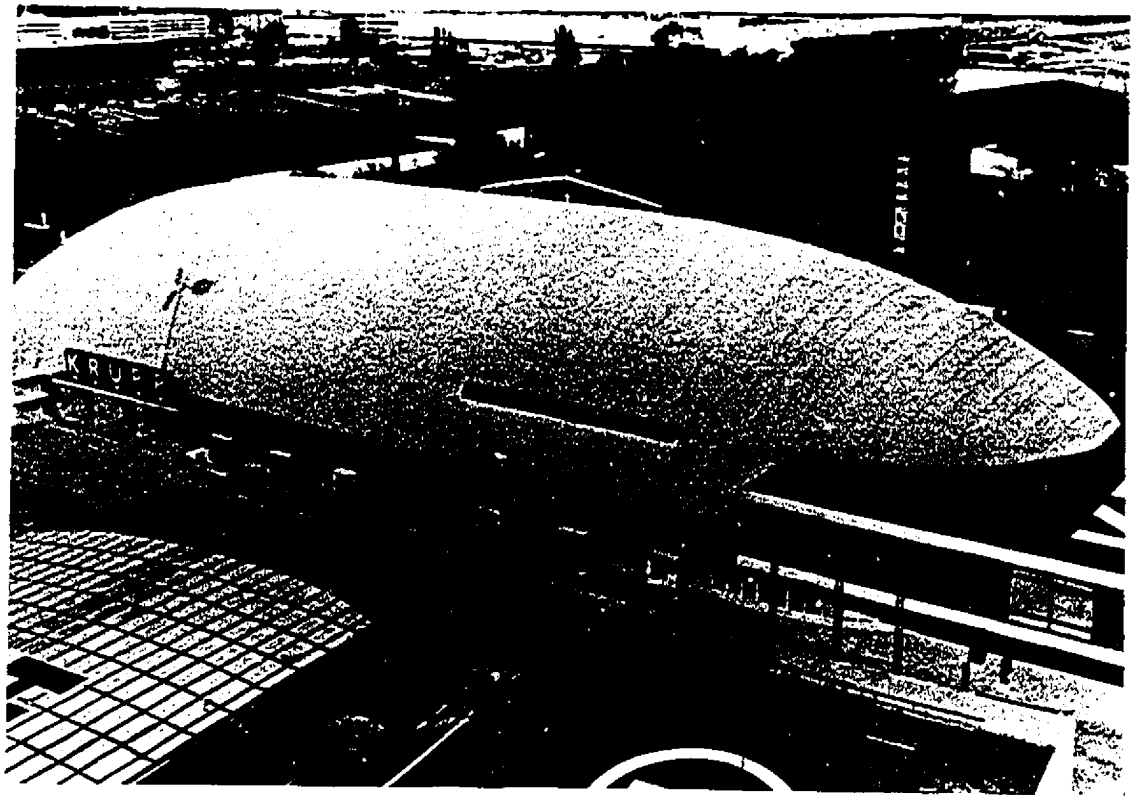

Plate (1.3): Krupp's air-supported exhibition pavilion at Hanover (Dent, 1971)

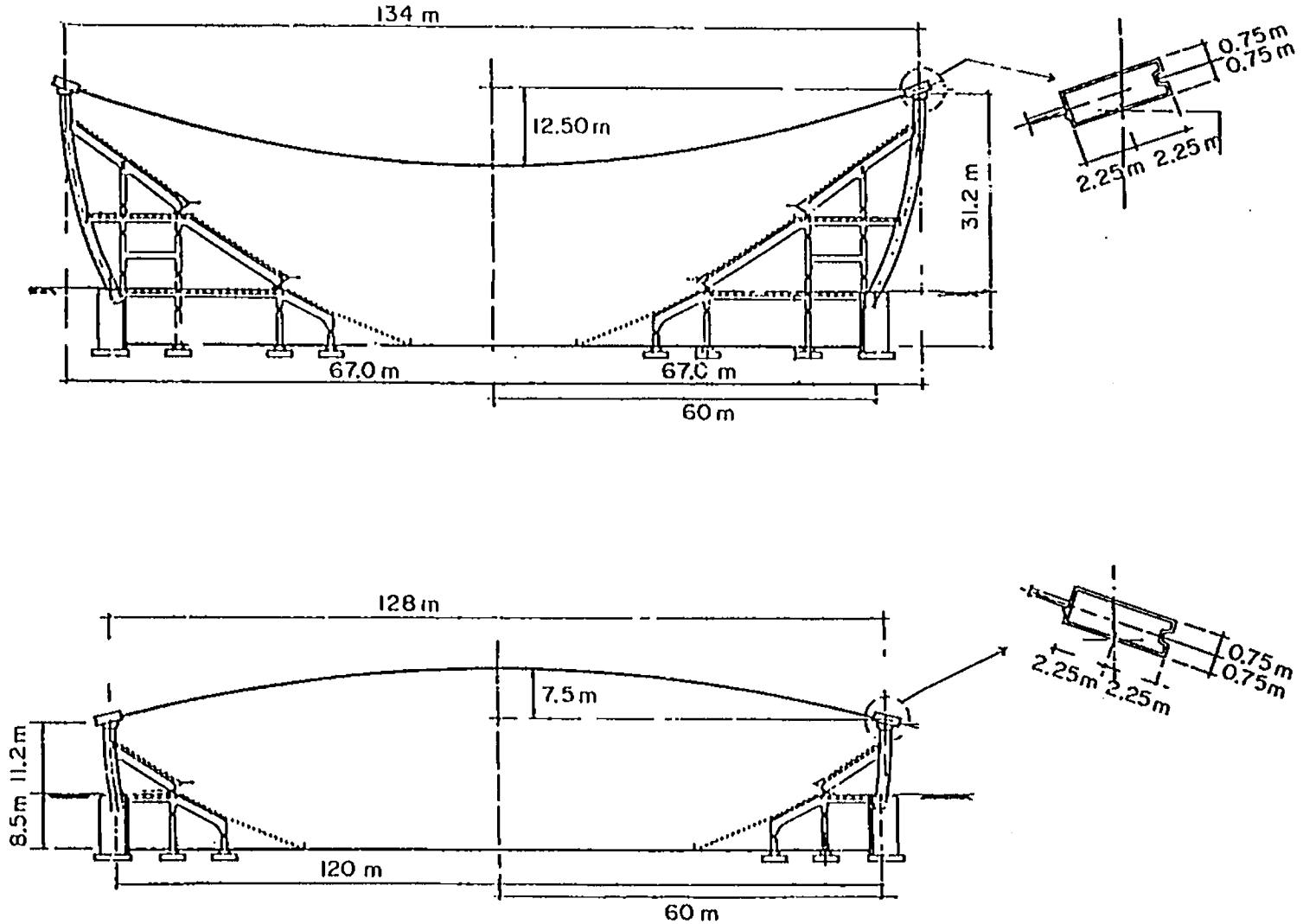

Fig.(1.1): Elevation views of the Calgary Olympic Coliseum (Bobrowski, 1981)

openings; and air-supported structures.

1.2 OUTLINE:

1.2.1 Self-Supported, Large Span Roofs Backed by Cavities With Openings

This part of the thesis comprises a theoretical and experimental examination of the effects of air leakage through openings, and the acoustical damping on the free vibration characteristics of self-supported, lightweight roofs. The objectives of the study are to understand the behaviour of these roofs for the condition of still air, and to examine the effects of wall openings on the roof natural frequencies and modal damping ratios. The outline of this investigation is summarized below:

- To review the previous work done on the topic of lightweight roofs;
- To investigate the roof-air interaction and the effect of air leakage through wall openings for the condition of still air;
- To develop a simplified theoretical approach to evaluate the modal parameters of the roof-air system considering the structural and acoustical damping from the roof and the openings;
- To formulate closed form solutions for the damped response of circular membrane roofs backed by cavities with openings;
- To assess the accuracy of the approximate formulae for the roof modal parameters;

- To review the similarity requirements and techniques for free vibration and wind tunnel testing;
- To verify the theoretical approach by conducting free vibration laboratory experiments on two structural models: one with a membrane roof and the second with a flexible plate roof; and
- To examine the effects of volume scaling on the free vibration characteristics of the roof for the condition of still air.

1.2.2 Air-Supported Structures

The second part of the thesis comprises a theoretical study and wind tunnel tests on aeroelastic and rigid models of a hemispherical air-supported structure. The objectives are to understand the nature of the response of the structure to turbulent wind, and to establish a theoretical method for response prediction. The outline of this part is as follows:

- To review the previous research done on the topic of air-supported structures;
- To formulate analytical solutions for the modal parameters of both cylindrical and spherical forms, and to compare the solutions with those obtained using a finite element method;
- To examine the effects of different internal pressures and enclosure volumes on the free vibration characteristics of hemispherical air-supported structures;

- To investigate the wind-induced response of an aeroelastic hemispherical air-supported model;
- To investigate the internal pressure fluctuations of the aeroelastic model for different wind speeds, exposures, enclosure volumes, and internal pressures;
- To conduct pressure tests on a rigid model to measure the external wind pressures acting on the hemispherical structure;
- To establish a semi-analytical procedure for predicting the wind-induced response of air-supported structures; and
- To prove the applicability of the semi-analytical approach by comparing the predicted wind-induced response results for the hemispherical air-supported model with the experimental data obtained in the aeroelastic tests.

1.3 PREVIEW

Chapter 2 is a brief review of previous research and basic considerations for lightweight roofs.

In Chapter 3, the free vibration of self-supported, large span roofs backed by cavities with openings is theoretically investigated for the condition of still air. Formulae are derived for the evaluation of the modal properties and the response to harmonic loading of circular membrane roofs backed by cavities with openings.

Chapter 4 describes an experimental free vibration investigation on two structural models conducted to verify the theoretical approach formulated in Chapter 3.

Chapter 5 is a brief review of previous research and basic considerations for air-supported structures.

In Chapter 6, the free vibration of cylindrical and spherical air-supported structures is theoretically studied. The analytical results are compared with those obtained using a finite element method.

In Chapter 7, the results of an experimental investigation into the wind-induced response and internal pressure fluctuations are presented for an aeroelastic hemispherical air-supported model.

Chapter 8 describes a semi-analytical approach for predicting the wind-induced responses of air-supported structures based on pressure measurements on rigid models. The predicted results are compared with the aeroelastic test results for the hemispherical air-supported model.

Finally, conclusions and recommendations for further research are given in Chapter 9.

CHAPTER 2

REVIEW OF BASIC CONSIDERATIONS FOR LIGHTWEIGHT ROOFS

2.1 REVIEW OF PREVIOUS WORK

Extensive research into the general mechanics of lightweight roofs such as cable roofs has been conducted [e.g. (Zetlin, 1968), and (Krishna, 1978)]. However, few studies have considered the aerodynamics of such roofs, which is of primary concern here. Some examples of studies that have considered aerodynamic effects are summarized below.

Howell (1973) conducted some experiments to investigate the wind response of a large suspension roof with a positive Gaussian curvature for both open country and urban exposures. The effect of air leakage on the dynamic behaviour of the roof was not considered in the analysis.

El-Ashkar (1974) investigated the initial nonlinear deflection of a flat suspension roof under static loads. The dynamic behaviour of suspension roofs under aerodynamic and acoustical pressures was examined. The effect of the enclosure under the roof was studied both theoretically and experimentally considering wall openings. Visualization tests were conducted to predict the flow characteristics near the model.

Tryggvason and Isyumov (1977) examined the requirement for scaling the elastic properties of tensioned surfaces. For pneumatic structures, modifications were developed for scaling the internal pressure that allow rational velocity scales

to be used. Tryggvason (1977) also emphasized the importance of scaling the pneumatic stiffness and suggested the exaggeration of the internal volume by a factor of $1/\lambda_v^2$, where λ_v is the velocity scale. This scaling was confirmed by the studies due to Holmes (1979) and El-Ashkar (1983).

Holmes (1979) investigated the mean and fluctuating wind-induced pressures inside buildings using experimental and computer simulation techniques. The mean and RMS internal pressure coefficients were both found to be monotonically increasing functions of the ratio of the windward to the leeward opening areas. The case of a single windward opening was treated as a damped Helmholtz resonator. Inertia effects were found to produce a resonant amplification in the response of the internal pressure to turbulent external pressures, and to a step change in the external pressure. It was concluded that these effects are unlikely to be of much practical significance except in the case of a sudden large opening, such as that due to a window failure, occurring in a somewhat rigid building.

Stathopoulos, Surry and Davenport (1979) examined the wind-induced internal pressures using models of low-rise rigid buildings of different geometries and internal volumes. Three models for buildings with variable side-wall and end-wall openings and three background porosities (opening area ratios of 0.0, 0.5 and 3.0% of the total surface area) were used. The results showed that the internal pressures were dynamic but their magnitudes were generally lower than those of

the local external pressures. For windward openings, the internal pressure coefficients were generally positive except for cases with high background porosity combined with small openings, where they became zero or slightly negative. The results also showed that the lower the background porosity, the smaller the size of the wall opening necessary to make the internal pressure insensitive to further increase of the wall openings.

Irwin and Wardlaw (1979) investigated the effect of wind on the forces imparted to the Montreal Olympic Stadium by the deployed retractable fabric roof that is attached to the fixed part of the roof covering the stands. They found the effects of the added mass and the acoustical damping to be important. The measured deflections of the model roof due to wind were significant. No signs of aerodynamic instability were observed on the model. They concluded that the acoustical damping is an important factor in the vibration of membrane roofs.

Davenport and Surry (1983) showed that the interior pressures in buildings are amenable to more detailed analysis and that useful information on them can be easily derived from wind tunnel data on external pressures. The uncertainties in the internal pressure can be expressed in statistical terms which are related to the area of the opening and the interior volume. Davenport and Surry (1983) referred to the importance of calculating the internal pressure in cases where a building is in close proximity to a neighbour lying in its wake. The problem of air-infiltration being controlled by the internal pressure regime was also discussed.

El-Ashkar and Novak (1983) studied the behaviour of large circular cable roofs with wall openings in turbulent wind. They found from free vibration experiments that the first symmetrical mode is strongly dependent on the number of wall openings. The kettledrum frequency was not identified in these experiments. This could be attributed to the high damping associated with the kettledrum frequency. El-Ashkar (1983) suggested that the behaviour of a cable roof backed by a cavity with openings in still air could be similar to that of a Helmholtz resonator. No signs of instability were observed at the wind velocities considered.

Pneumatic effects in air-supported structures were investigated analytically by Kind (1984), who considered an automatically ventilated model. Kind (1984) indicated that the pneumatic damping (internal pressure increase directly proportional to the rate of volume decrease) could become high for large air-supported structures. A formula for the pneumatic damping of the volume-displacing modes of motion, ζ_p, considering only pressure and inertia forces, was given as

$$\zeta_p = 1/(2\ \omega_n\ \tau) \tag{2.1}$$

In the above equation ω_n is the circular frequency of vibration and τ is a time constant that is a function of the internal pressure, the number of air changes per hour, the enclosure volume, and the instantaneous fan and leakage volume flow rates. Kind (1984) concluded that the pneumatic stiffness is expected to be the dominant pneumatic effect in most small air-supported structures, unless the

air change rates are unusually high or the internal overpressure is unusually low.

Vickery (1986) studied the problem of internal pressures generated by wind action for conventional structures. The objective was to examine the validity of a "gust factor" approach for the evaluation of the peak internal pressures for both nominally sealed but leaky buildings and buildings with discrete openings. The dynamic internal pressure component was determined primarily by the time constant of the building and the gust factor was determined by the turbulence intensity. The uncertainties regarding the distribution of leakage paths and the effects of openings caused by premature failures of doors and windows were addressed.

Liu and Rhee (1986) examined the nature of wind-induced Helmholtz oscillations of air pressure in building cavities by testing an impermeable rigid building model. The model had a single room and a single windward opening of four different sizes. The Helmholtz resonance was present in all the different types of flow studied. The spectral peaks showed that the internal pressure generated by different flows fluctuated at the Helmholtz frequency.

Draisey (1987) investigated the influence of wall openings on the dynamic behaviour of large span roofs under wind excitation. Both theoretical and experimental studies showed that the main factors affecting the response were the area of wall openings and the terrain roughness. The experimental observations supported the general trend of the theoretical ones. The venting of the walls

resulted in increases of the dynamic response by an order of magnitude. The difference between the predicted and observed dynamic motions was about ± 25%. This difference was attributed to the inappropriate discharge coefficients used for the vents.

Recently, Vickery and Georgiou (1989) studied the problem of wall venting on the dynamic response of roofs to wind excitation using an exact and a simplified approach. The simplified approach included only the first volume changing mode and N wall openings. The mass of the air passing through the vents was ignored. Both the exact and simplified solutions were generally in good agreement, with a maximum difference of about ± 20%. For a large venting area the system approaches a single degree of freedom system with a stiffness stemming from the roof alone. At very small venting areas the system approaches a single degree of freedom system with a stiffness stemming from both the elastic stiffness of the roof and the pneumatic stiffness. In the theoretical evaluation of the wind-induced response, the coefficient of damping, c_j, due to the pressure loss through openings was evaluated by linearizing the flow equation at the opening about the mean values. This linearization yields

$$c_j = \rho_o \bar{U}_R A_j \{ c_L |\overline{\Delta C_{pj}}| \}^{\frac{1}{2}} \qquad (2.2)$$

where ρ_o is the air density; $\bar{U}_R$ is the reference wind speed; A_j is the area of the j^{th} opening; c_L is the loss coefficient; and ΔC_{pj} is the difference between the mean external and internal pressure coefficients, $\bar{C}_{pj} - \bar{C}_{po}$, across the j^{th} opening. This is adequate if $|\overline{\Delta C_{pj}}|$ is large compared to $\widetilde{\Delta C_{pj}}$ (the RMS coefficient of the

fluctuations in the pressure difference), but is inadequate as $\overline{|\Delta C_{Pj}|}$ approaches zero. Linearization here was suggested to be approached in a fashion similar to that used in the linearization of Morison's Equation (Vickery, 1989). For the case of $\overline{|\Delta C_{Pj}|} = 0$, linearization by least squares was used.

In summary, previous work dealing with self-supported structures was to investigate the effects of wall openings on the wind-induced response and the internal pressure fluctuations, and to study the flow characteristics near the openings. The effects of wall openings on the free vibration characteristics of cable roofs were experimentally investigated by El-Ashkar (1983), but questions remained unanswered about the transition from the kettledrum frequency to the helmholtz frequency, and about the effect of wall openings on modal damping.

To answer these questions, a free vibration analysis of self-supported, lightweight roofs backed by cavities with openings is conducted in the first part of this study. A simplified theoretical approach is formulated to evaluate the modal parameters of the roof-air system considering air leakage through the openings, pneumatic stiffness, and structural and acoustical damping of the system. The accuracy of the approximate formulae is assessed by comparison with a complex eigenvalue analysis. An exact solution is derived to evaluate the modal parameters for a circular membrane roof backed by a cavity with openings. Closed form solutions are presented for the damped response of circular membrane roofs backed by cavities with openings.

In addition, free vibration laboratory experiments were conducted on two different structural models to verify the theoretical approach. The first model had a membrane roof, and the second had a flexible plate roof. The effects of wall openings and volume scaling on the roof-air system were examined.

2.2 THE ADDED MASS

Vibration of a structure in a fluid such as air is generally coupled to motions of the surrounding air. This means that the natural frequencies of a structure in a fluid must be found from the coupled structure-fluid analysis. When the roof vibrates, it undergoes alternate accelerations and decelerations as does the surrounding air. The total effective mass is therefore not just that of the roof, but also an additional amount (the added mass) due to the surrounding air (Irwin and Wardlaw, 1979). The added mass may also be referred to as additional, induced, hydrodynamic or aerodynamic mass. The virtual or apparent mass includes both the actual mass of the structure and the added mass of air (Campbell, 1982).

The added mass depends on the shape of the roof, the nature of the motion and the density of the fluid (Campbell, 1982). In most civil engineering structures, the added mass is small in comparison to the structure mass, and so can be ignored when computing the natural frequencies of the structure or examining the structural response. For lightweight roofs, this is not so as the added mass of the surrounding air is of the same order of magnitude as the roof mass, if not greater (Irwin and Wardlaw, 1979).

The added mass for a sphere of a surface area A, whose surface pulsates with a radial velocity, uniform over the surface, can be obtained by working out the kinetic energy imparted to the air, while ignoring the compressibility of air (Milne-Thompson, 1968). This added mass of the outside air per unit surface area is

$$m_A = 0.282\ \rho_o\ A^{\frac{1}{2}} \tag{2.3a}$$

where ρ_o is the air density. Thus, if the surface is a membrane of mass per unit area m_S, the virtual mass, m_v, per unit area is

$$m_v = m_S + m_A \tag{2.3b}$$

In the example used by Irwin and Wardlaw (1979), for a fabric membrane roof covering a stadium of an area A = 18000 m^2 and m_S = 2.2 kg/m^2, the added mass m_A = 46.6 kg/m^2, which is an order of magnitude greater than the membrane mass.

Irwin and Wardlaw (1979) presented a simple formula for calculating the added mass of air for a membrane with respect to the membrane mass. For a stadium with a membrane roof that is almost flat, it was suggested that the problem be solved by determining the kinetic energy T_A of the surrounding air, assuming the membrane vibrations are small and the equilibrium position of the membrane is flat. The kinetic energy of the air, T_A, (which is equal to the work done by the roof to generate the motion, W_A) can be written as (Lamb, 1932)

$$T_A = W_A = -\tfrac{1}{2}\ \rho_o \iint_S \phi\ \frac{\partial \phi}{\partial n}\ ds \tag{2.4}$$

where s is the surface area of the membrane, ϕ is the velocity potential and $\partial\phi/\partial n$ is the gradient of ϕ normal to the membrane surface. The kinetic energy, T_m, of a membrane of uniform mass m_s is

$$T_m = \tfrac{1}{2} m_s \int_s (\frac{dw}{dt})^2 \, ds \tag{2.5}$$

where w and dw/dt are the membrane displacement and velocity, respectively. Expressions for ϕ and $\partial\phi/\partial n$ were evaluated (based on an assumed mode shape of the membrane). This ratio of the kinetic energies was used as a measure of the ratio of the added mass of the air on both sides of the membrane to the membrane generalized mass (Irwin and Wardlaw, 1979). This ratio can be written as

$$\frac{T_A}{T_m} = \frac{5\pi}{32} \frac{\rho_o A^{\frac{1}{2}}}{m_s} \tag{2.6a}$$

Substituting with A, m_s and ρ_o as before gives

$$\frac{T_A}{T_m} = 37 \tag{2.6b}$$

Thus, the added mass effect can be large. Values of the added mass for different types of cross-sections, bodies and plates with different boundary conditions are given by Blevins (1979).

Campbell (1982) carried out computations for calculating the added mass of air for thin flat plates of rectangular and circular forms using distributions of discrete sources and sinks, for a motion perpendicular to their planes or for a rotation about a principal axis in an ideal fluid. The same method was used to obtain the added mass of air for thin diaphragms with different normal velocity distributions.

Kinsler and Frey (1962) gave a formula for the added mass of air for a piston as

$$m_A = \rho_o A (c_o/\omega) \chi_1(2\omega a/c_o) \quad (2.7)$$

where A is the piston area; ω is the circular frequency; c_o is the speed of sound in the air; a is the piston radius and

$$\chi_1(x) = \frac{4}{\pi} \left(\frac{x}{3} - \frac{x^3}{3^2.5} + \frac{x^5}{3^2.5^2.7} - \dots \right) \quad (2.8)$$

where $x = 2\omega a/c_o$. The function $\chi_1(x)$ is shown in Figure (2.1) for different values of x. For small values of x ($x << 1$) this function can be approximated by the first term of Equation (2.8). On the other hand when x is large, this function converges such that $\chi_1(x) \approx 4/(\pi x)$. Thus, for low frequencies of vibration ($x << 1$), the added mass as given by Kinsler and Frey (1962) becomes

$$m_A = 8 \rho_o a^3/3 \quad (2.9)$$

The added mass in Equation (2.9) is equivalent to that of an imaginary cylinder of the medium having the same radius as the piston and a length $\Delta L = 8a/(3\pi)$. Equation (2.9) is the same as given by Campbell (1982).

The result of the added mass loading is generally to decrease the resonant frequency from the usual value given by $\omega_o^2 = K/m_s$ to $\omega_o^2 = K/(m_s+m_A)$. Since the added mass is usually significant for lightweight roofs, the decrease in the resonant frequency resulting from the presence of the air medium may be marked. For high frequencies of vibration, the added mass is given by Kinsler and Frey (1962) as

$$m_A = 2 \rho_o c_o^2 a/\omega^2 \quad (2.10)$$

Thus, the effect of the added mass is much less at high frequencies than it is at low frequencies (Kinsler and Frey, 1962). To show this, computed values of the mass loading for a piston of 0.1 m radius vibrating in water are plotted as a function of the frequency in Figure (2.2) given by Kinsler and Frey (1962).

2.3 THE ACOUSTICAL DAMPING

Kinsler and Frey (1962) suggested a formula for calculating the damping constants due to sound wave radiation for a piston assuming the sound waves radiate from the piston in the same manner as they do for a simple source mounted on an infinite baffle. This formula is

$$c_a = \rho_o c_o A R_1(2 \frac{\omega}{c_o} a) \tag{2.11}$$

in which

$$R_1(x) = \frac{x^2}{2.4} - \frac{x^4}{2.4^2.6} + \frac{x^6}{2.4^2.6^2.8} - .... \tag{2.12}$$

where $x = 2\omega a/c_o$, and a, A are the radius and the effective area of the piston, respectively. The function $R_1(x)$ is also shown in Figure (2.1) for different values of x.

Irwin and Wardlaw (1979) also estimated the magnitude of the acoustical damping of an almost flat sealed membrane roof, assuming it behaves approximately as a source of acoustic radiation, of strength Q, on an infinite horizontal plane. The natural frequencies are usually low enough that the wave length of the radiated sound is much larger than the roof dimensions (Irwin and Wardlaw, 1979). The energy emitted per cycle of pulsation of the source, ϵ_1, is

$$\epsilon_1 = \rho_o \frac{\pi f Q^2}{c_o} \tag{2.13}$$

where f is the frequency in Hz (Rayleigh, 1945). The strength of the source is related to the roof motion by

$$Q = \iint_S \dot{w}\, ds \tag{2.14}$$

where $\dot{w}$ is the normal velocity of the roof surface and the integral is over the outside surface of the roof. The roof velocity of vibration could be expressed as

$$\dot{w}(x,y,t) = \psi(x,y)\, \dot{q}(t) \tag{2.15}$$

where x and y are the horizontal coordinates of a point on the roof; q is the generalized deflection, $\dot{q}$ is the first derivative of q with respect to time, and ψ is the mode shape. Substituting Equation (2.15) into Equation (2.14) gives

$$\epsilon_1 = \frac{\rho_o f}{c_o} \dot{q}^2 \overline{\psi}^2 A^2 \tag{2.16}$$

where

$$\overline{\psi} = (1/A) \iint_S \psi\, ds \tag{2.17}$$

and A is the roof area as before (Irwin and Wardlaw, 1979). The energy emitted per cycle of pulsation, ϵ_1, must be equal to the work done by the roof per cycle of oscillation

$$W = 2\, \pi\, m_v\, \zeta_{ac} \iint_S \dot{w}^2\, ds \tag{2.18}$$

where ζ_{ac} is the acoustical damping ratio. Substituting Equation (2.15) into Equation (2.18) yields the following non-dimensional expression for the acoustical damping ratio ζ_{ac} as

$$\zeta_{ac} = \frac{1}{2} \frac{\rho_o f A}{c_o m_v} \left(\overline{\psi}^2 / \overline{\psi^2} \right) \tag{2.19}$$

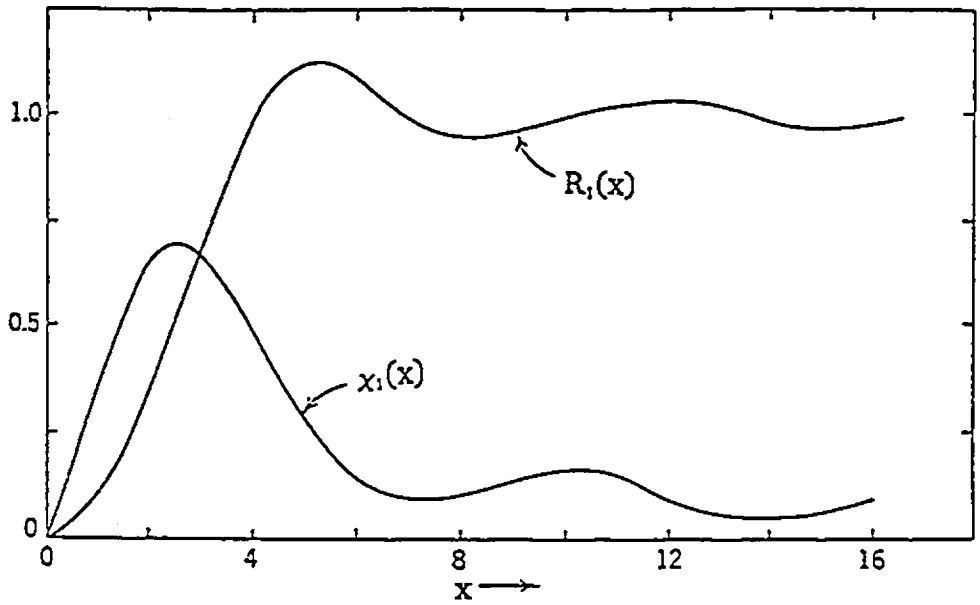

Fig. (2.1): Functions $R_1(x)$ and $\chi_1(x)$ Piston impedance functions (Kinsler and Frey, 1962)

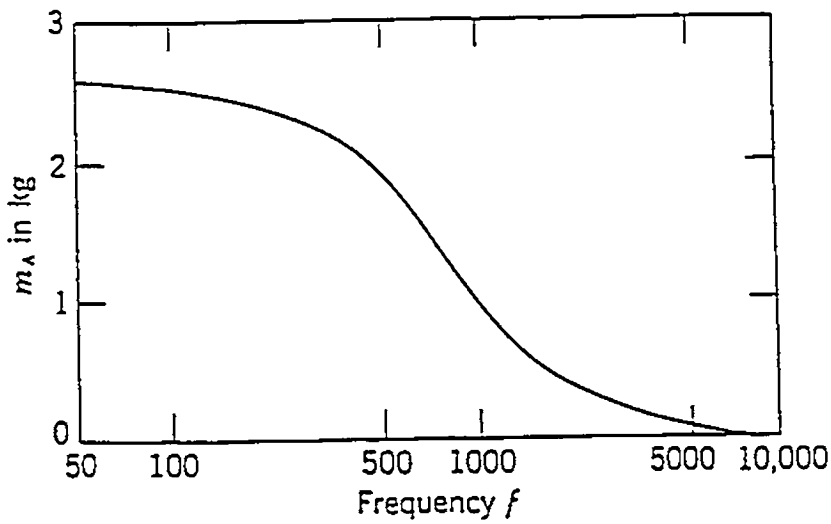

Fig. (2.2): Added mass of a vibrating piston radiating into water (Kinsler and Frey, 1962)

where

$$\bar{\psi}^2 = (1/A) \iint_S \psi^2 \, ds \qquad (2.20)$$

Thus, for the volume displacing modes of vibration (the antisymmetrical modes in this thesis) $\bar{\psi} = 0$, the acoustical damping is zero. The value of ζ_{ae} is generally between 0.02 to 0.8 depending on the parameters of Equation (2.19), and in most fabric structures reaches a high value (Irwin and Wardlaw, 1979).

Irwin and Wardlaw (1979) also investigated the scaling of the acoustical damping. They showed that to model the acoustical damping effect correctly, the non-dimensional parameter $\rho_o fA/(c_o m_v)$ must be the same on the model as at full scale. In this parameter, ρ_o is the air density, c_o is the speed of sound in air, U is the mean wind speed, f is the frequency in Hz, A is the roof area and m_v is the virtual mass per unit area at the full scale. It follows that the Mach number, U/c_o, should be the same at both scales. In many wind tunnels, Mach number scaling cannot be achieved, but the use of wind velocities lower than those required by Mach number scaling can be regarded as conservative (Irwin and Wardlaw, 1979). This is shown from the following:

$$\zeta_{ae} = \frac{\rho_o fA}{2c_o m_v} = \frac{1}{2} \left(\frac{\rho L}{m_v}\right) \left(\frac{fL}{U}\right) \left(\frac{A}{L^2}\right) \left(\frac{U}{c_o}\right) \qquad (2.21)$$

in which L is the characteristic length of the roof. In the above equation each quantity enclosed in brackets is a non-dimensional parameter. If U/c_o is less than that at full scale but the other non-dimensional parameters are the same as at full scale, then the model value of ζ_{ae} becomes smaller which is conservative (Irwin

and Wardlaw, 1979). For a roof with leakage around its edge (as for a roof of a stadium with openings) under wind excitation, the acoustical damping may be reduced due to the losses in the flow around the edge, but the aerodynamic damping may be increased.

CHAPTER 3

THEORETICAL ANALYSIS OF FREE VIBRATION OF SELF-SUPPORTED, LIGHTWEIGHT ROOFS BACKED BY CAVITIES WITH OPENINGS

3.1 INTRODUCTION

Self-supported, lightweight roofs over large unobstructed areas such as sports arenas must have sufficient integrity to provide adequate safety. Such structures must also have openings (usually located in the circumferential walls) to allow for ventilation and for the movement of the incoming and departing crowd. The presence of such openings has a marked influence on the dynamic characteristics of the roof. The air enclosed in the cavity under the roof and its leakage through the wall openings affect the internal pressure and accordingly influence the dynamic behaviour of the roof. The roof behaviour is also affected by the sound waves radiating from the vibrating roof that generate acoustical damping. These effects are particularly important for lightweight roofs such as cable roofs.

While many studies have been devoted to the dynamics of lightweight roofs, only a few investigators have considered the roof-air interaction and the air leakage. El-Ashkar (1983), and El-Ashkar and Novak (1983) studied a hyperbolic paraboloid roof and a flat circular membrane in still air and under wind excitation. Draisey (1987) investigated a circular plate roof exposed to wind and this study was expanded by Vickery and Georgiou (1989).

The key difference between this study and that of Vickery and Georgiou (1989) is that they were interested in the response of naturally ventilated roofs due to wind, with the air flowing into the building from one side and leaking out of the other side. Friction damping at openings was the main source of damping, and the acoustical damping due to sound radiation from both the roof and the openings was not considered.

This study is focused on the behaviour of lightweight roofs backed by cavities with openings for the conditions of still air. The effects of wall openings, internal pressure changes due to the roof vibration, and structural as well as acoustical damping from both the roof and openings are accounted for. Free vibration experiments were conducted on two different structural models to examine these effects, and to investigate the effect of volume scaling on the modal parameters of the roof-air system. The first model had a membrane roof, and the second had a flexible plate roof. The opening areas were increased by increasing the number of openings, keeping the area of each opening constant. This was done to maintain a constant effective length of the volume of air at each opening area ratio. The internal volume of each model was exaggerated by a factor of $1/\lambda_V^2$ where λ_V is the velocity scale, as required by the pneumatic stiffness scaling

This chapter is focused on the theoretical analysis, while the free vibration experiments and the comparisons between the theoretical and experimental results are discussed in Chapter 4.

In this chapter, the roof-air interaction and the effect of air leakage through the openings in the building walls are theoretically investigated for the condition of still air. Structural damping is accounted for and acoustical damping is considered for the roof as well as the openings. Approximate formulae are derived for the evaluation of the modal parameters of the roof-air system using a two-mass theoretical model for a roof backed by a cavity. The accuracy of the derived modal damping formula is assessed by comparisons with a complex eigenvalue analysis and an exact solution of a circular membrane roof backed by a cavity with openings.

The theoretical approaches are used in a parametric study of two roofs with prototype properties. The first has approximately the basic parameters of the Calgary Olympic Coliseum and the second roof is similar but has lighter mass per unit area. The analysis presented can be extended to include moving air which introduces pressure coefficients at the openings. Closed form solutions are also derived for the damped response of circular membrane roofs backed by cavities with or without openings. The accuracy of these formulae is assessed.

3.2 ASSUMPTIONS OF THE SIMPLIFIED ANALYSIS

Large span, lightweight roofs are often of complex shapes, e.g., hyperbolic paraboloids. The vibration modes of such structures are, therefore, usually analyzed using numerical techniques such as the finite element method. The roof response is, in general, nonlinear but its dynamic part can be approximated as a

linear, small amplitude oscillation about the deflection due to static loading.

The acoustical damping and the changes in the internal pressure depend on the amount of air displaced, not on the exact shape of the moving surface. Therefore, for the evaluation of these effects, the vibrating roof may be replaced by an equivalent rigid piston such that the product of its area and displacement is equal to the air volume displaced by the actual roof. Given the complex shapes of lightweight roofs, the solution of the governing equations of motion is difficult and usually does not lead to closed form expressions.

In the analysis of the roof response formulated here, the roof is replaced by an equivalent generalized piston in the individual vibration modes. The roof motion in each individual vibration mode is described by one generalized degree-of-freedom, and the motion of the air masses at the openings is described by another degree-of-freedom. Thus, the roof backed by a cavity with openings is replaced by a two-mass system as shown in Figure (3.1), with the same enclosed volume. The air pressure is evaluated using the equivalent piston and introduced into the governing equations of motion.

The displacement of the roof may be written in polar coordinates r and θ for each mode as

$$v(r,\theta,t) = \psi(r,\theta)\, q(t) \tag{3.1}$$

where q(t) is the generalized coordinate, t is time and $\psi(r,\theta)$ is the j^{th} mode shape relative to the static deflection normalized so that $\psi(0,\theta) = 1$. The generalized

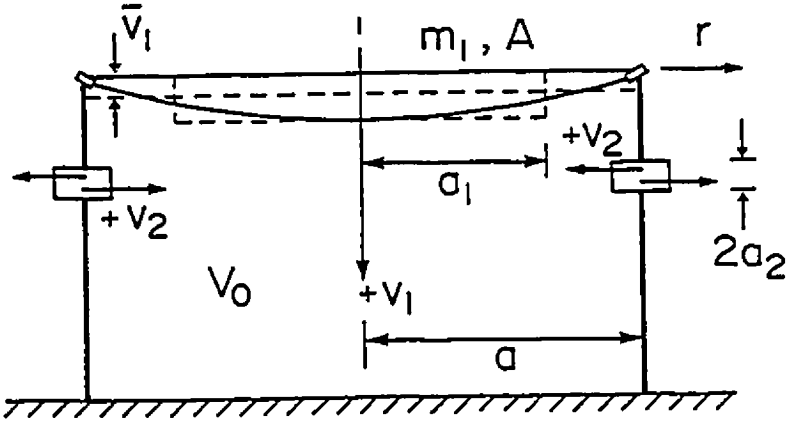

(a)

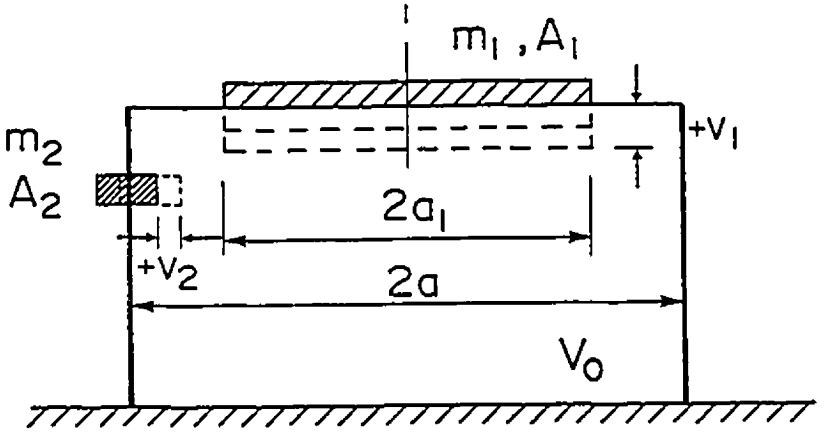

(b)

Fig. (3.1): Schematic of vibrating roof backed by cavity with openings and its theoretical model

mass associated with the mode $\psi(r,\theta)$ is

$$m_j = \int_A m(r,\theta)\cdot\psi^2(r,\theta)\, dA \tag{3.2}$$

where A is the area of the roof, and m is its mass per unit area. This mass comprises the actual mass of the roof and the added air mass that accounts for the inertia forces of the vibrating air. The generalized structural stiffness of the roof is

$$K_s = m_j\, \omega_j^2 \tag{3.3}$$

where ω_j is the j^{th} natural frequency of the roof. The effective area of the roof is defined as

$$A_1 = \int_A \psi(r,\theta)\, dA \tag{3.4}$$

The generalized structural damping ratio of the roof vibration in air is denoted by

$$\zeta_s = \frac{c_s}{2m_j\omega_j} \tag{3.5}$$

where c_s is the structural damping coefficient.

It is further assumed that the forces associated with the air movement and the structural damping have only a small effect on the shape of the roof vibration modes. This is a plausible assumption, because the internal air pressure is uniformly distributed over the roof and the structural damping also can be assumed to be proportional to either the mass or the stiffness matrices. The undamped modes of the roof vibrating in a vacuum can first be established and then substituted in Equations (3.2) to (3.5) to define the parameters of the generalized piston. While this representation is applicable to any mode, the

numerical examples of this part are limited to the fundamental modes, since they are most affected by the air in the cavity and the acoustical effects.

3.3 THE ROOF-AIR INTERACTION SYSTEM

3.3.1 Masses

Using the previously outlined assumptions, the roof backed by a cavity with openings is replaced by a two-mass system as shown in Figure (3.1b). In this model, m_1 is the generalized mass of the roof, and m_2 is the effective air mass at the openings. If the openings are assumed to be of equal areas, their effective air mass can be expressed as

$$m_2 = \rho_o A_2 L' \tag{3.6}$$

where ρ_o is the air density, A_2 is the total area of openings, and L' is the effective length of the air mass at each opening. This effective length can be calculated as (Kinsler and Frey, 1962)

$$L' = L + \delta a_2 \tag{3.7}$$

where L is the true thickness of the wall at the opening, δ is an empirical constant ranging from 0.8 to 1.7, and a_2 is the radius of the typical opening. The constant δ depends on whether the opening has flanged ends or not.

3.3.2 Pressures

When the roof vibrates, the enclosed air volume and the internal pressure change. The alterations of the volume, ~~V~~, are assumed to be adiabatic, i.e., $P V^{\gamma} = P_o V_o^{\gamma}$, where γ is the ratio of specific heat of air at constant pressure to the

specific heat of air at constant volume; P_o and V_o are the equilibrium pressure and volume of the enclosure, respectively (Kinsler and Frey, 1962). Then, the excess pressure inside the enclosure due to the motions $v_1(t)$ of the equivalent piston (the generalized coordinate of the roof at its centre), and $v_2(t)$ of the air masses can be written as

$$dp = -\frac{\gamma P_o}{V_o} dV = -\frac{\gamma P_o}{V_o} (A_1 v_1 + A_2 v_2) \tag{3.8}$$

where A_1 and A_2 are the areas of the equivalent piston and openings, respectively.

3.3.3 Governing Equations of Free Undamped Vibration

The governing equations of free undamped vibration of the roof-air system can be written as follows:

For the roof

$$m_1 \ddot{v}_1 + (K_s + \frac{\gamma P_o A_1^2}{V_o}) v_1 + \frac{\gamma P_o A_1 A_2}{V_o} v_2 = 0 \tag{3.9a}$$

and for the openings

$$m_2 \ddot{v}_2 + \frac{\gamma P_o A_1 A_2}{V_o} v_1 + \frac{\gamma P_o A_2^2}{V_o} v_2 = 0 \tag{3.9b}$$

Equations (3.9a) and (3.9b) can be written in a matrix form as

$$[m]\{\ddot{v}\} + [k]\{v\} = \{0\} \tag{3.10}$$

in which the dots indicate differentiation with respect to time, t, and the mass matrix is

$$[m] = \begin{bmatrix} m_1 & 0 \\ 0 & m_2 \end{bmatrix} \tag{3.11}$$

The stiffness matrix in Equation (3.10) is

$$[k] = \begin{bmatrix} k_s + \frac{\gamma P_o A_1^2}{V_o} & \frac{\gamma P_o A_1 A_2}{V_o} \\ \frac{\gamma P_o A_1 A_2}{V_o} & \frac{\gamma P_o A_2^2}{V_o} \end{bmatrix} \tag{3.12}$$

3.4 FREE UNDAMPED VIBRATION

The solutions for the undamped displacements $v_1(t)$ and $v_2(t)$ in Equations (3.9a) and (3.9b) can be written as

$$v_1(t) = v_1 \sin \omega_j t \tag{3.13}$$

$$v_2(t) = v_2 \sin \omega_j t \tag{3.14}$$

Substituting Equations (3.13) and (3.14) into Equations (3.9a) and (3.9b) yields

$$(K_{11} - m_1\omega_j^2)v_1 + K_{12}v_2 = 0 \tag{3.15a}$$

$$K_{21}v_1 + (K_{22} - m_2\omega_j^2)v_2 = 0 \tag{3.15b}$$

Solving the eigenvalue problem, two natural frequencies of the roof-air system are obtained as

$$\omega_{1,2}^2 = \frac{1}{2}\left(\frac{K_{11}}{m_1} + \frac{K_{22}}{m_2}\right) \pm \left[\frac{1}{4}\left(\frac{K_{11}}{m_1} - \frac{K_{22}}{m_2}\right)^2 + \frac{K_{12}^2}{m_1 m_2}\right]^{\frac{1}{2}} \tag{3.16}$$

Substituting the two frequencies ω_j; j = 1, and 2; into Equations (3.15a) and (3.15b) one at a time, the two ratios v_1/v_2 of the displacements can be calculated. These ratios represent the associated undamped vibration modes which are

$$a_j = \frac{v_{1j}}{v_{2j}} = \frac{-K_{12}}{K_{11} - m\omega_j^2} = \frac{K_{22} - m_2\omega_j^2}{-K_{21}} \quad \text{and} \quad j = 1, 2 \tag{3.17}$$

To distinguish the vibration amplitudes of the two modes, double subscripts are introduced. The first subscript identifies the amplitudes of the masses m_1 or m_2; the second subscript indicates the frequency and mode with which the amplitudes v_{ij} are associated. The two ratios in Equation (3.17) characterize the vibration modes shown in Figures (3.2a) and (3.2b).

For a parametric study of the roof-air system the following dimensionless ratios are defined: (denoting the pneumatic stiffness $K_p = \gamma P_o A_1^2/V_o$)

1. $\alpha = A_2/A_1$ = the ratio of the opening areas to the effective area of the roof;
2. $\beta = \omega_o/\omega_p$ = the ratio of the natural frequency of the roof in air to the pneumatic frequency, $\omega_p = (K_p/m_1)^{1/2}$. As β increases, the kettledrum frequency of the system increases and vice versa.

Two other dimensionless parameters are used which are ϵ and η. The parameter ϵ represents the ratio of the Helmholtz frequency (assuming that the roof is very rigid) to the pneumatic frequency of the roof, i.e., $\epsilon = \omega_H/\omega_p$. The parameter η represents the ratio of the roof generalized mass to the air masses at openings, i.e., $\eta = m_1/m_2$. These parameters depend on the opening area ratio, α, and the pneumatic frequency, ω_p.

Dividing Equations (3.9a) and (3.9b) by m_1 and m_2 respectively, using the parameters mentioned above, and substituting into Equation (3.16) yields the following undamped frequency equation

$$\omega_{1,2}/\omega_p = \{\tfrac{1}{2}[\beta^2+1+\eta^2] \pm [\tfrac{1}{2}(\beta^2+1-\eta^2)^2+\epsilon\alpha^2]^{1/2}\}^{1/2} \qquad (3.18)$$

Equation (3.18), which is another version of Equation (3.16), relates the natural frequencies of the roof-air system to the four dimensionless parameters α, β, ϵ and η in a closed form solution. The most important of these parameters is the first parameter, α, as described in Section 3.6. Equations (3.16) and (3.18) satisfy the three limiting cases of the problem. The first is the "kettledrum frequency", when there are no wall openings, i.e., $\alpha = 0$. The second is when the opening areas increase beyond any limit; i.e., $A_2 \to \infty$ and $V_o \to \infty$, which yields the natural frequency of the roof vibrating in still air, ω_o. The last limiting case is obtained when the roof is very rigid and $\alpha \to 0$ giving the well-known frequency of a Helmholtz resonator, ω_H.

3.5 FREE DAMPED VIBRATION

In still air, the primary sources of roof damping are the structural damping, c_s, the acoustical damping arising from the wall openings, c_{a2}, and the external acoustical damping associated with the radiation of energy from the roof surface in the form of sound waves, c_{a1}. Kinsler and Frey (1962) indicated that in still air friction damping at openings is small compared to the acoustical damping. Therefore, friction damping at openings is not considered in this analysis. For cases where there is flow through the openings due to wind, friction damping becomes more important. Another source of damping is the pneumatic damping in automatically ventilated, air-supported structures as reported by Kind (1982). This damping is not applicable here as the structures considered are self-supported, naturally ventilated structures.

3.5.1 Damping

For the two mass system adopted, the structural damping coefficient of the roof, c_s, is

$$c_s = 2\zeta_s m_j \omega_j \tag{3.19}$$

in which the structural damping ratio, ζ_s, is usually estimated.

The damping constants c_{a1} and c_{a2} due to sound wave radiation can be calculated for the masses m_1 and m_2, respectively, using Equation (2.11) given by Kinsler and Frey (1962). The main assumption is that sound waves radiate from the roof and the openings in the same manner that they do for a simple source mounted on an infinite baffle. With this assumption, the acoustical damping constants ,c_{a1} and c_{a2}, are calculated as:

$$c_{a1} = \rho_o c_o A_1 R_1(2 \frac{\omega}{c_o} a_1) \tag{3.20}$$

$$c_{a2} = \rho_o c_o A_2 R_1(2 \frac{\omega}{c_o} a_2) \tag{3.21}$$

in which c_o is the speed of sound in air; $R_1(x)$ is as given in Equation (2.12) and Figure (2.1), where $x = 2\omega a_i/c_o$, $i = 1, 2$; and a_1 and a_2 are the radii of the effective areas of the roof and the openings, respectively. For a non-circular wall opening with area, A_2, the effective radius can be taken as $a_2 = (A_2/\pi)^{1/2}$.

3.5.2 Governing Equation of Free Damped Vibration

With these damping coefficients considered, the governing equations of the roof-air system free damped vibration can be written as follows:

For the roof

$$m_1\ddot{v}_1 + (c_s + c_{a1})\dot{v}_1 + (K_s + \frac{\gamma P_o A_1^2}{V_o})v_1 + \frac{\gamma P_o A_1 A_2}{V_o} v_2 = 0 \qquad (3.22a)$$

and for the openings

$$m_2\ddot{v}_2 + c_{a2}\dot{v}_2 + \frac{\gamma P_o A_1 A_2}{V_o}\dot{v}_1 + \frac{\gamma P_o A_2^2}{V_o} v_2 = 0 \qquad (3.22b)$$

in a matrix form

$$[m]\{\ddot{v}\} + [c]\{\dot{v}\} + [k]\{v\} = \{0\} \qquad (3.23)$$

in which the damping matrix is

$$[c] = \begin{bmatrix} c_s + c_{a1} & 0 \\ 0 & c_{a2} \end{bmatrix} \qquad (3.24)$$

The free damped vibration is analyzed in two ways; accurately - as a complex eigenvalue problem, and approximately - using energy considerations.

3.5.3 Complex Eigenvalue Analysis

In this approach, the modal damping of the roof-air system is established from the complex eigenvalues obtained by the solution of the homogeneous governing equation of damped vibration, Equation (3.23). Adding the identity $[m]\{\dot{v}\} = [m]\{\dot{v}\}$ to Equation (3.23), the governing equation is obtained in the reduced form, i.e.,

$$[B]\{\dot{Z}\} + [K]\{Z\} = \{0\} \qquad (3.25)$$

in which

$$[R] = \begin{bmatrix} [0] & [m] \\ [m] & [c] \end{bmatrix} \tag{3.26}$$

$$[K] = \begin{bmatrix} -[m] & [0] \\ [0] & [k] \end{bmatrix} \tag{3.27}$$

$$\{Z\} = \begin{Bmatrix} \{\dot{v}\} \\ \{v\} \end{Bmatrix} \quad \text{and} \quad \{0\} = \begin{Bmatrix} \{0\} \\ \{0\} \end{Bmatrix} \tag{3.28}$$

The solution to Equation (3.25) can be written as

$$\{z(t)\} = e^{\mu t} \{\phi\} \tag{3.29}$$

where μ = the complex eigenvalue and $\{\phi\}$ = the complex mode vector, which is also called the non-classical mode shape (Novak and El-Hifnawy, 1983). Substituting Equation (3.29) into Equation (3.25), an eigenvalue problem is obtained whose solution yields two pairs of complex conjugate eigenvalues, μ_j, and two pairs of complex conjugate eigenvectors. From the complex eigenvalues, the approximate undamped frequency follows as

$$\omega_j = |\mu_j| \tag{3.30}$$

and the damped frequency as

$$\omega_j' = \text{Im}\,(\mu_j) \tag{3.31}$$

The modal damping ratio is

$$\varsigma_j = -\,\text{Re}\,(\mu_j)/\,|\mu_j| \quad \text{and} \quad j = 1, 2 \tag{3.32}$$

In this study, the EISPACK subroutine RGG was used to calculate the complex eigenvalues from Equations (3.25) to (3.28). It is efficient and has accuracy checks for ill-conditioned matrices. Other subroutines were also used for comparisons such as the MATHLIB subroutine EIGZF.

3.5.4 Modal Damping from Energy Considerations

The modal damping ratios of a roof backed by a cavity with openings can also be evaluated approximately using energy considerations. The basic assumption is that the damped vibration modes can be represented by the undamped modes. This is an acceptable assumption, at least for damping ratios much smaller than the critical damping. The advantage of this approach is that a very simple formula for the modal damping ratios from all damping sources is obtained.

The work done during a period of steady-state vibration, $T = 2\pi/\omega_j$ by the damping forces $P(\dot{\delta})$ is, in general,

$$W = \int_0^T P(\dot{\delta})\, d\delta(t) \tag{3.33}$$

in which δ is the effective displacement. For the roof-air system, shown in Figure (3.1), vibrating harmonically with the natural frequency ω_j and modal amplitudes v_{1j} and v_{2j} given by Equation (3.17), the displacements δ_{ij} are defined as

$$\begin{aligned} \delta_{1j} &= \delta_{1j} \sin \omega_j t \\ \delta_{2j} &= \delta_{2j} \sin \omega_j t \end{aligned} \tag{3.34}$$

where $\delta_{1j} = v_{1j}$ and $\delta_{2j} = v_{2j}$. The damping force is

$$P(\delta) = [(c_s + c_{a1})v_{1j} + c_{a2}v_{2j}]\, \omega_j \cos \omega_j t \tag{3.35}$$

in which the acoustical damping coefficients, c_{aj}, $j = 1, 2$ are related to the motions of the roof and the mass in the openings, respectively, and c_s is the structural damping constant of the roof. With this damping, Equation (3.33) yields the work done as

$$W_j = \pi\omega_j [(c_s+c_{a1})v_{1j}^2 + c_{a2}v_{2j}^2] \tag{3.36}$$

In free vibration, the maximum potential energy of the system is the same as the maximum kinetic energy, i.e.,

$$L_j = \tfrac{1}{2} (m_1v_{1j}^2 + m_2v_{2j}^2)\, \omega_j^2 \tag{3.37}$$

in which the generalized mass of the mode j is

$$M_j = m_1v_{1j}^2 + m_2v_{2j}^2 \tag{3.38}$$

The damping ratio of the j^{th} mode is

$$\varsigma_j = \frac{W_j}{4\pi L_j} \tag{3.39}$$

For structural damping stemming only from the roof, the damping constant is, by Equation (3.19), $c_s = 2m_j\varsigma_j\omega_j$ and M_j is reduced to $m_j\, v_{1j}^2$. Then, the total damping ratio of the j^{th} mode of the roof-air system becomes

$$\varsigma_j = \frac{1}{2\omega_j M_j} [(c_s+c_{a1})v_{1j}^2 + c_{a2}v_{2j}^2] \tag{3.40}$$

in which ς_s is the structural damping ratio estimated for the roof in air; the acoustical damping constants c_{a1} and c_{a2} are given by equation (3.20); and v_{ij} is the undamped modal amplitude chosen to arbitrary scale in the ratio specified by Equation (3.17), i.e., for example, $v_{2j} = 1$ and $v_{1j} = a_j$.

The advantage of the energy approach is that it uses the undamped modes of vibration which can be obtained for instance by the subroutine NROOT or by other means; also, frequency dependent damping such as the acoustical damping can be readily accommodated. The energy approach is, however, approximate. Its accuracy can be assessed by a comparison with the complex eigenvalue analysis

previously formulated, which yields modal damping derived directly from the damped vibration mode shapes.

3.6 APPLICATIONS AND DISCUSSION OF THE THEORETICAL RESULTS

3.6.1 Free Undamped Vibration Results

To illustrate the effects of wall openings, an example using the basic parameters of the hyperbolic paraboloid cable roof of the Calgary Olympic Coliseum (Bobrowski, 1987) is used. To this end, the fundamental vibration mode of the roof, measured with regard to its static deflection, is represented by the vibration mode of a circular membrane having the same area, mass per unit area, and tension per unit of length as the prototype. Such a simple representation was found to be feasible by El-Ashkar (1983).

In Figures (3.3a) and (3.3b), the ratios ω_j / ω_p are plotted for both modes versus the dimensionless opening area ratio $\alpha = A_2/A_1$ and denoted as undamped. The corresponding vibration modes by Equation (3.17) are shown in Figures (3.2a) and (3.2b). The fundamental undamped frequency, ω_1, monotonically decreases as the opening area decreases and vanishes with $A_2 \to 0$. This corresponds to the Helmholtz oscillator behaviour as is also indicated by the first vibration mode, Figures (3.2a) and (3.2b), for which the two masses move in phase and the roof movement, v_1, vanishes with $A_2 \to 0$. In the second mode, the two masses move in antiphase and the undamped frequency, ω_2, approaches the kettledrum frequency as $A_2 \to 0$.

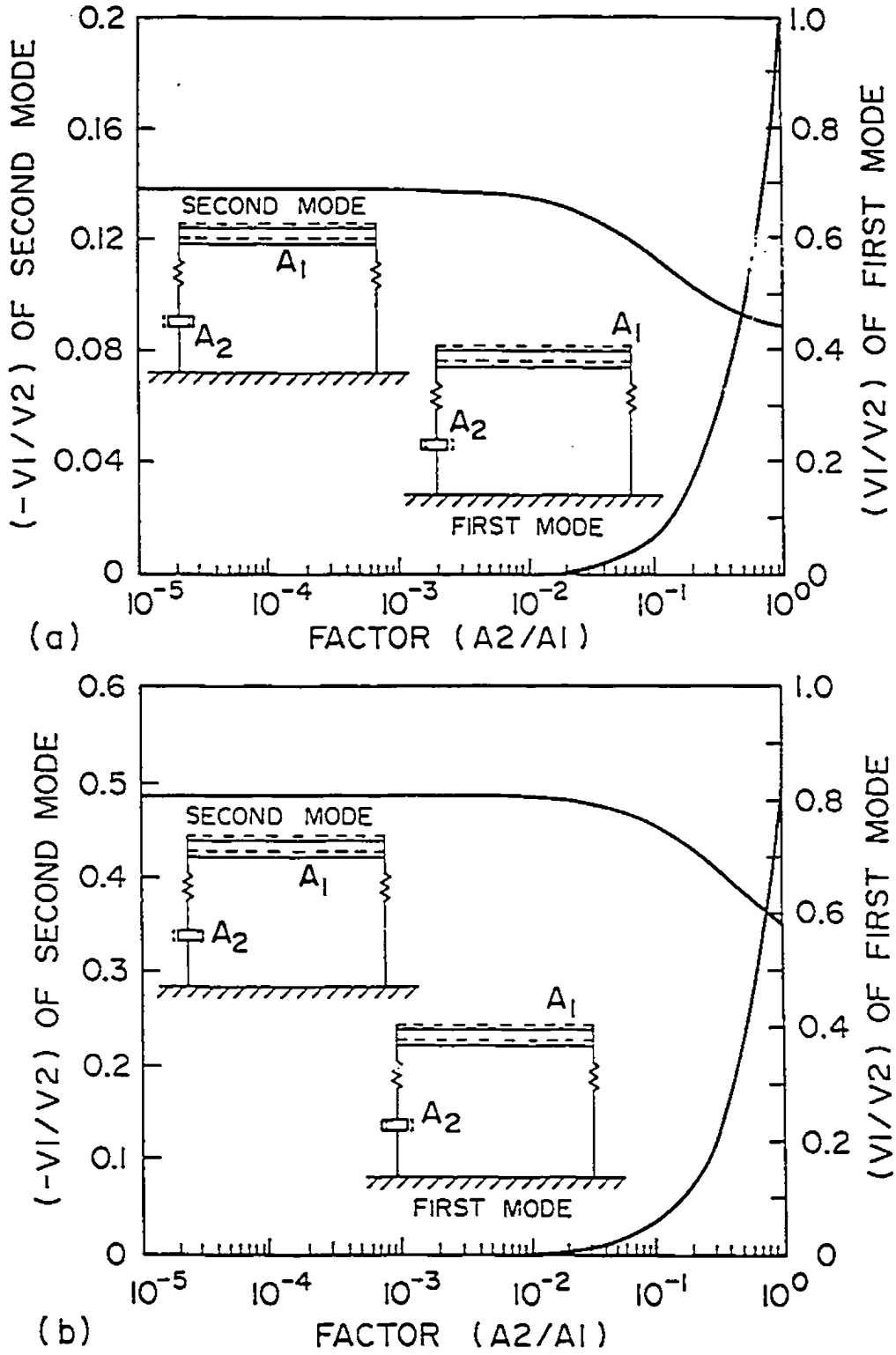

Fig. (3.2): Leakage effect on roof undamped vibration modes: (a) the simplified Calgary Olympic Coliseum roof and (b) the lighter roof

For comparison, the roof is reanalysed with all its parameters the same as before except the weight per unit plan area, which is taken as one third that of the first example. Such a lighter roof may be applicable in regions of little or no snowfall. The corresponding mode shapes and natural frequencies are shown for the lighter roof in Figures (3.2b) and (3.3b), respectively. The trend of the undamped frequencies is similar for both roofs.

3.6.2 Free Damped Vibration Results

3.6.2.1 Complex Eigenvalue Approach Results

Considering the structural damping ratio equal to 1%, the acoustical damping due to the roof vibration, and the air leakage through the wall openings; the damped frequencies of the Calgary Olympic Coliseum (simplified as a flat membrane) and those of the lighter roof were calculated using Equation (3.31) and are plotted in Figures (3.3a) and (3.3b). For the heavier roof, Figure (3.3a), the first frequency is negligibly affected by damping while the second frequency starts deviating from the undamped frequency quite rapidly once the opening area ratio A_2/A_1 exceeds about 0.2 and ultimately drops to zero. For the lighter roof, Figure (3.3b), similar behaviour occurs in the first mode; the behaviour of the second mode becomes clear when the damping is examined.

The marked deviation of the damped frequencies from the undamped ones is associated with the dramatic increases in modal damping that results from the wall openings. This is illustrated in Figures (3.4a) and (3.4b) in which the

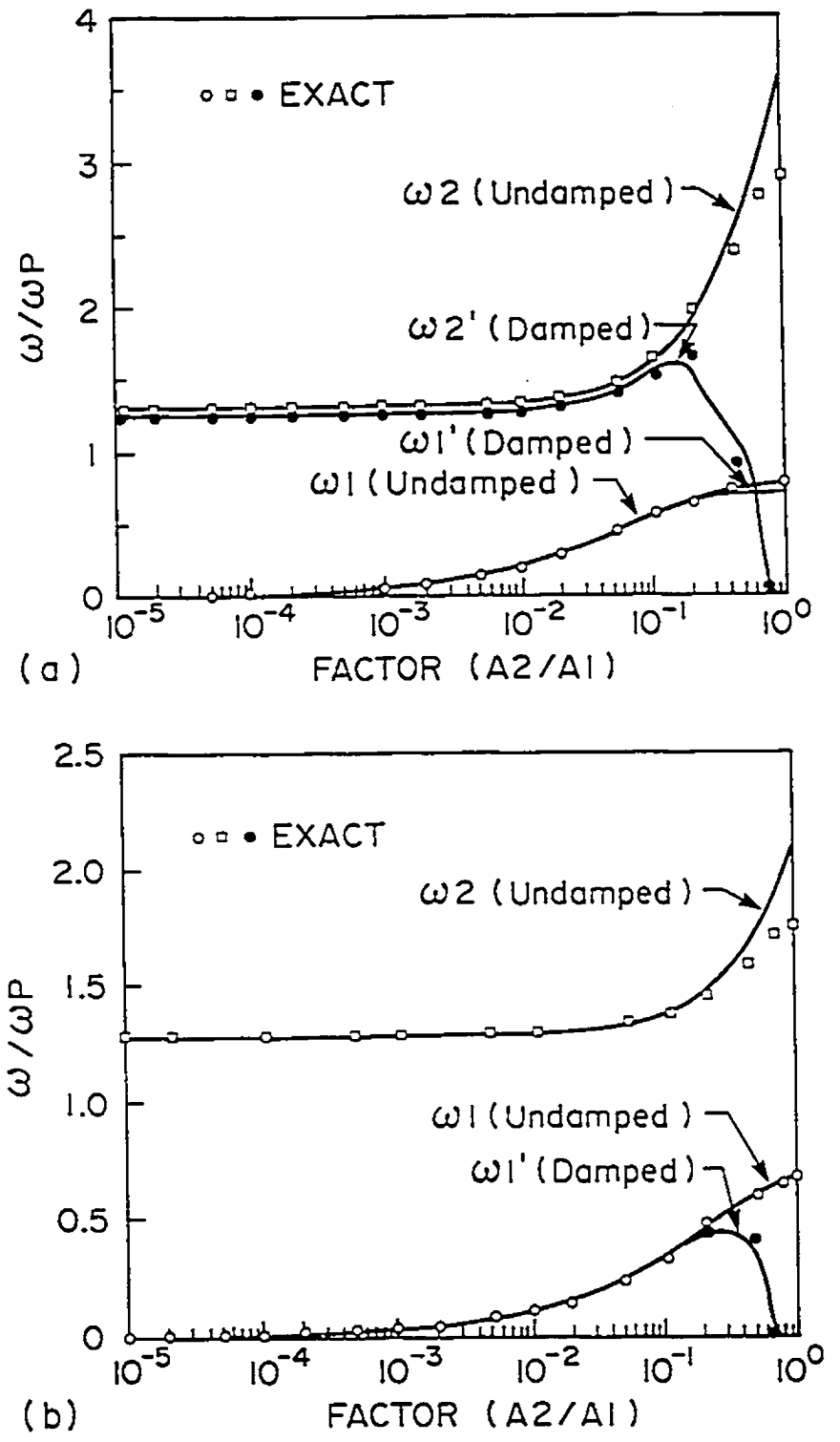

Fig. (3.3): Leakage effect on roof fundamental frequencies: (a) the simplified Calgary Olympic Coliseum roof and (b) the lighter roof

damping ratios, calculated by Equation (3.32), are plotted for the simplified Calgary roof and for the lighter roof versus different opening ratios, $\alpha = A_2/A_1$. For both modes, the damping rapidly increases with the increase of the opening area ratio and may even lead to overdamped conditions for which the natural frequency vanishes. For the heavier roof, Figure (3.4a), this is observed for the second (kettledrum) mode and large opening ratios for which the damping ratio of the first (Helmholtz) mode is less than critical, but quite high.

For the lighter roof, Figure (3.4b), the damping ratio of first mode rapidly increases with the opening area and reaches critical values of $\varsigma_1 = 1$ or more for very large opening ratios. The damping of the second mode is more than critical throughout, which corresponds to the absence of damped natural frequencies ω_j' in Figure (3.4b). Therefore, the kettledrum frequency of the lighter roof vanishes because this vibration mode is overdamped. This explains why in El-Ashkar's free vibration experiments (1983), the kettledrum frequency could not be found. This was the case even for $A_2 \to 0$, when high damping stems from the roof acoustical damping.

In the study of El-Ashkar and Novak (1983), the transition from the Helmholtz frequency to the kettledrum frequency was not established. The opinion was that when the opening area becomes very small, causing the Helmholtz frequency to approach zero, an abrupt jump to the kettledrum frequency should occur as shown in dashed lines in Figure (3.5) given by El-Ashkar (1983).

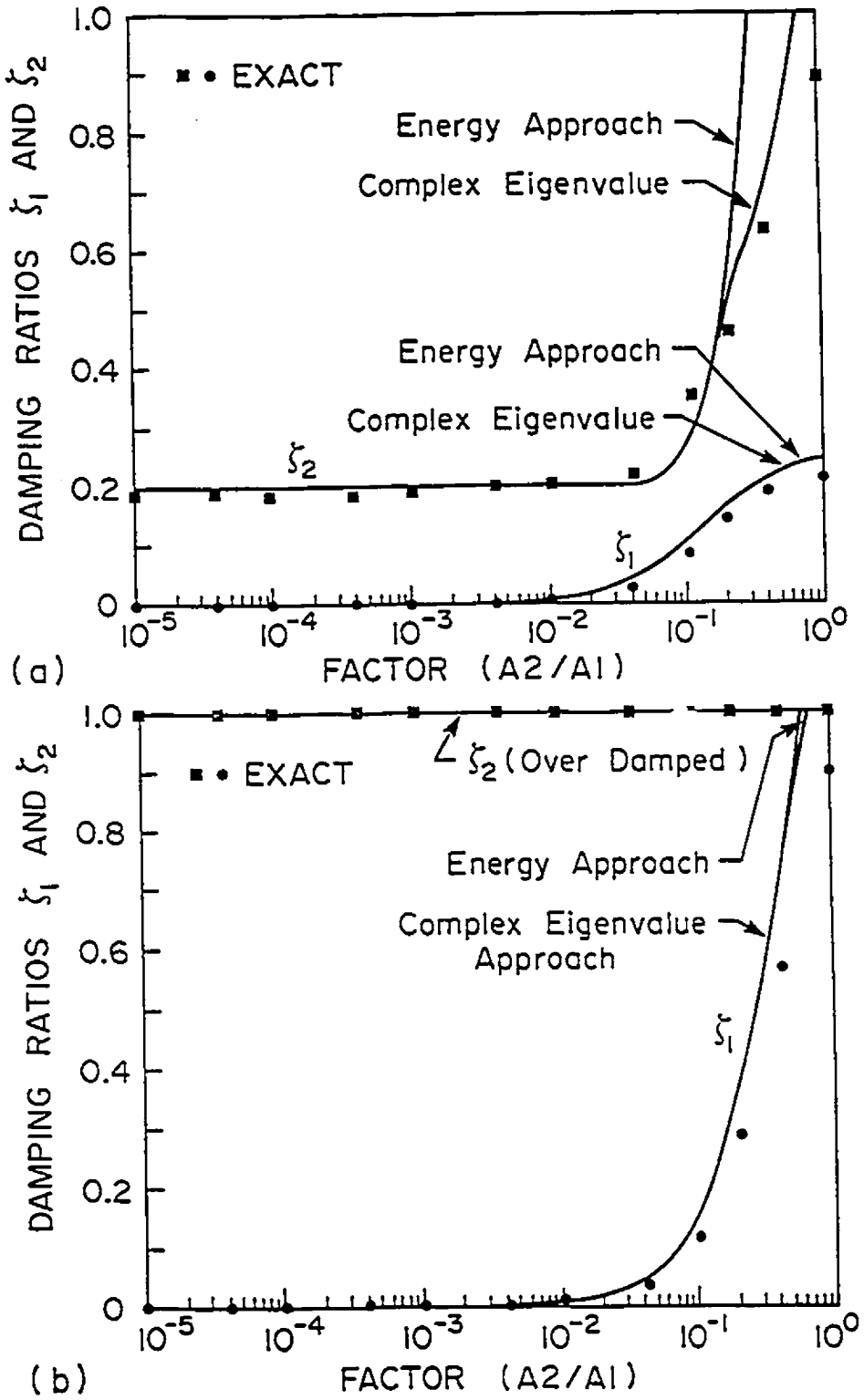

Fig. (3.4): Leakage effect on roof total damping: (a) the simplified Calgary Olympic Coliseum roof and (b) the lighter roof

However, Figures (3.3b) and (3.4b) suggest that the Helmholtz and the kettledrum frequencies follow two separate theoretical branches in the frequency versus opening area plot. In Figure (3.5), the dimensionless parameter β_1 is equivalent to the opening area ratio α in the present study.

In Table (3.1) the theoretical results are compared with the experimental data of El-Ashkar (1983), for a roof with several opening ratios. The natural frequencies are shown as the ratio ω_1'/ω_p in which ω_1' is the damped frequency of the first symmetrical mode and $\omega_p=(K_p/m_1)^{\frac{1}{2}}$ is the pneumatic frequency. The agreement is excellent for the natural frequencies and poor for the damping ratios. It may be noted that because of the very light membrane used by El-Ashkar, the damping ratios were not established accurately. Data for the second symmetrical mode of the lighter roof are not shown because this mode is overdamped.

3.6.2.2 Comparison between Complex Eigenvalue and Energy Approaches

The damping ratios calculated for the roofs in the two examples by Equation (3.40) with $\zeta_s = 0.01$ are plotted against the opening area ratio A_2/A_1 in Figures (3.4a) and (3.4b). The damping ratios calculated rigorously from the complex eigenvalues by Equation (3.32) are also shown. The damping ratios established from energy considerations are in excellent agreement with the more accurate values for all realistic opening ratios, i.e., $A_2/A_1 < 0.30$ (30%) and in some cases even for larger opening ratios. For the first mode of the heavier roof and for both modes of the lighter roof, almost perfect agreement is obtained for

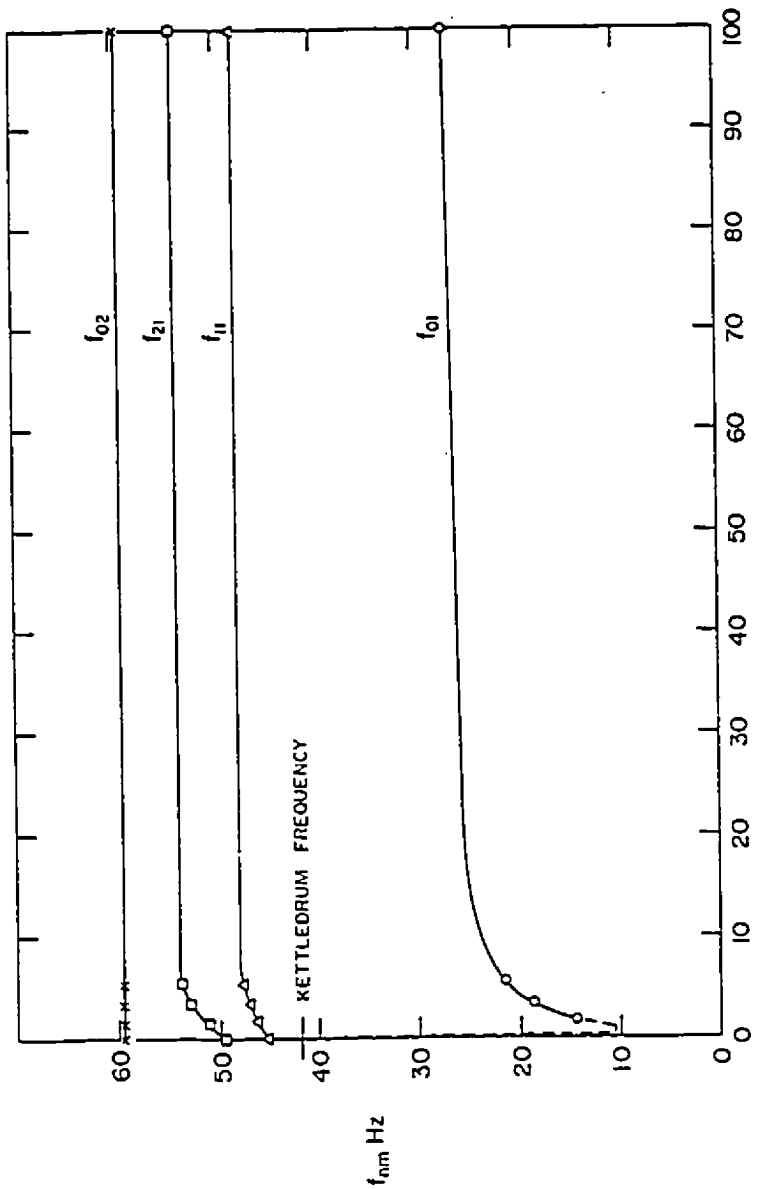

Fig. (3.5) : Effect of openings on fundamental frequencies in El-Ashkar's experiments (1983)

TABLE (3.1): COMPARISON OF THEORETICAL RESULTS WITH EXPERIMENTS DESCRIBED IN EL-ASHKAR AND NOVAK (1983)

(FIRST SYMMETRICAL MODE)

Opening Area Ratio (%)	Frequency Ratio ω_1'/ω_p		Damping ratio ζ_1 (%)		
			Theory		Experiment
	Theory	Experiment	Complex Eigenvalue	Energy Approach	
3.17	0.200	0.220	2.90	2.90	2.22
6.30	0.277	0.265	5.00	5.00	2.62
9.44	0.331	0.320	10.01	10.00	2.76

the entire range of the A_2/A_1 ratio. In the overdamped cases, no vibratory motion exists.

3.7 CHARACTERISTIC EQUATION OF A CIRCULAR MEMBRANE BACKED BY A CAVITY WITH OPENINGS

To assess further the accuracy of the approximate two-mass model of the roof-air system, an exact solution is formulated for the free damped vibration of a circular membrane roof, backed by a cavity with openings. The effects of the air leakage through wall openings, the internal pressure changes due to the roof vibration, and the structural as well as acoustical damping radiating from both the roof and the openings are considered.

3.7.1 Free Damped Vibration

In this analysis, $v_1 = v_1(r,\theta,t)$ is the membrane dynamic displacement, $v_2 = v_2(t)$ is the motion of the air mass through the openings, m is the mass per unit of plan area, and T_o is the tension force per unit length. The volume change due to the membrane motion can be expressed by the average displacement of the membrane, i.e.,

$$\bar{v}_1(t) = \frac{1}{\pi a^2} \int_A v_1(r,\theta,t)\, dA \tag{3.41}$$

where a and A are the radius and plan area of the membrane. The pressure increment in the enclosure caused by the two motions v_1 and v_2 can be written as

$$dp = -\frac{\gamma P_o}{V_o} (A \bar{v}_1 + A_2 v_2) = -\frac{\gamma P_o}{V_o} A_2 \left(\frac{\bar{v}_1}{\alpha} + v_2\right) \tag{3.42}$$

in which the opening area ratio is $\alpha' = A_o/A$. With this pressure increment, the governing equation of a circular membrane (Kinsler and Frey, 1962) backed by a cavity becomes

$$\frac{\partial^2 v_1}{\partial t^2} - \frac{T_s}{m}\left(\frac{\partial^2 v_1}{\partial r^2} + \frac{1}{r}\frac{\partial v_1}{\partial r} + \frac{1}{r}\frac{\partial^2 v_1}{\partial \theta^2}\right) + \frac{\gamma P_o A_o}{V_o}\left(\frac{\bar{v}_1}{\alpha'} + v_2\right) + \frac{(c_s + c_{ac})}{m}\frac{\partial v_1}{\partial t} = 0 \qquad (3.43a)$$

and for the motion of the air mass at openings

$$\frac{\partial v_2}{\partial t} + \frac{\gamma P_o A_o}{m_o V_o}\left(\frac{\bar{v}_1}{\alpha'} + v_2\right) + \frac{c_{ac}}{m_o}\frac{\partial v_2}{\partial t} = 0 \qquad (3.43b)$$

in which m_o, P_o, V_o, A_o, c_s, c_{ac} and c_o are as given before in section 3.5. In these equations, $\bar{v}_1$ is an integral function of the mode of vibration. The solution to [illegible] can be written as

$$\begin{Bmatrix} v_1(r,\theta,t) \\ v_2(t) \end{Bmatrix} = \begin{Bmatrix} v_{1o}(r,\theta) \\ v_{2o} \end{Bmatrix} e^{j\omega t} \qquad (3.44)$$

in which ω is the common frequency and v_{1o} and v_{2o} are complex amplitudes. For the [illegible] modes of vibration, the term $\bar{v}_1$ [illegible] variables. Substituting [illegible] into [illegible] and [illegible] results

[illegible] (3.45a)

[illegible] (3.45b)

Using the [illegible] and the orthogonality as well as [illegible] integrating over [illegible] the [illegible] can be [illegible] in the form

[illegible] (3.46)

in which C is a complex constant whose dimension is that of v_1 (i.e., length) and f(r) is a dimensionless function which satisfies the boundary condition f(a) = 0. Then, the value of $\bar{v}_1$ becomes a constant equal to β_2 C which can be obtained from Equation (3.41). Thus, Equation (3.43b) can be rewritten as

$$v_2 = -\frac{b_2 \bar{v}_1}{\alpha'[b_2+\mu^2+(c_{a2}/m_2)\mu]} \tag{3.47a}$$

or

$$\frac{v_2}{C} = -\frac{b_2 \beta_2}{\alpha'[b_2+\mu^2+(c_{a2}/m_2)\mu]} \tag{3.47b}$$

where $b_2 = \gamma P_o A_2^2/(m_2 V_o)$ and v_2/C is the ratio describing how the motion of the air masses at the openings relates to the roof motion at the centre of the membrane. Substituting Equation (3.47) into Equation (3.45a) and allowing v_2 to act in phase and in antiphase with the roof motion yields

$$\frac{d^2v_1}{dr^2} + \frac{1}{r}\frac{dv_1}{dr} + k^2 v_1 - \frac{b_1 m}{T_o \alpha'}\beta_2 C \pm \frac{m\, b_1\, b_2\, C\, \beta_2}{\alpha' T_o[b_2+\mu^2+(c_{a2}/m_2)\mu]} = 0 \tag{3.48}$$

where

$$k^2 = -(m\omega^2 + c_{a1})/T_o \quad , \quad c = c_{a1} + c_{a2} \quad \text{and} \quad b_1 = \gamma P_o A_1/(mV_o) \tag{3.49}$$

Equation (3.48) can be written in the form

$$\frac{d^2v_1}{dr^2} + \frac{1}{r}\frac{dv_1}{dr} + k^2 v_1 = -\frac{b_1 m}{T_o \alpha'}\beta_2 C \pm \frac{m\, b_1\, b_2\, C\, \beta_2}{\alpha' T_o[b_2+\mu^2+(c_{a2}/m_2)\mu]} \tag{3.50}$$

The right hand side of Equation (3.50) is a function of $\bar{v}_1$ and is equal to a constant C_m. The complete solution of Equation (3.50) is the sum of two terms, one being the general solution of the homogeneous equation with the right hand [illegible] and the other being the particular solution [illegible]

[illegible] (3.51)

where J_o is Bessel function of the first kind and zero order. Applying the boundary conditions gives

$$v_1(a) = 0 = J_o(ka) + \frac{C_2}{k^2} \tag{3.52a}$$

or

$$C_2 = -k^2 C J_o(ka) \tag{3.52b}$$

Substituting Equation (3.52b) into Equation (3.51) yields

$$v_1(r) = C [J_o(kr) - J_o(ka)] \tag{3.53}$$

With the mode shape as in Equation (3.53), after applying the boundary conditions and rearranging the resulting expression, the characteristic equation for the free damped vibration of a membrane backed by a cavity with openings can be written as

$$J_o(ka) = -\alpha_1 [1 \pm \frac{1}{\{1 + (k_1 a)^2/(\alpha_1 \alpha')\}}] \frac{J_2(ka)}{(ka)^2} \tag{3.54}$$

in which J_i; i = 0, and 2; are Bessel functions of the first kind and order zero and two respectively, and

$$k_1^2 = (m_2' \mu^2 + c_{a2}\mu/A_2)/T_o \quad \text{and} \quad m_2' = m_2/A_2 \tag{3.55a}$$

$$\alpha_1 = \gamma_7 P_o a^2/T_o V_o \quad \text{and} \quad \alpha' = A_2/A \tag{3.55b}$$

In the above equation A is the total area of the roof; m_2 is the air mass at openings per unit area; and α_1 is a dimensionless parameter which expresses the relative importance of the restoring forces stemming from the enclosed air in the cavity and the tension forces applied to the membrane.

Equation (3.54) can be solved numerically by trial and error to obtain the complex eigenvalues μ_j for a specific opening area α'; then the damped frequencies and modal damping of the roof-air system can be calculated from Equations (3.31) and (3.32) in Section 3.5. This process is repeated for several opening area ratios. The results of this procedure are shown as dots, circles and squares in Figures (3.3) and (3.4).

3.7.2 Free Undamped Vibration

The free undamped frequencies of vibration can also be obtained with the same procedure as in the free damped case, by neglecting the damping terms c_{11}, c_{12} and c_{22} in Equations (3.43a) and (3.43b). Denoting $\epsilon_2 = m_2'/m$ and $k^2 = \omega^2 m/T_o$, the characteristic (frequency) equation of the membrane for the free undamped case becomes

$$J_o(ka) = -\alpha_1 \left[1 \pm \frac{1}{\{1 - \epsilon_2(ka)^2/(\alpha_1\alpha')\}}\right] \frac{J_2(ka)}{(ka)^2} \qquad (3.56)$$

3.7.3 Limiting Cases of the Characteristic Equation

Equation (3.54) contains all the three limiting cases of the problem, which are listed below:

1. For the opening area $A_2 \to 0$, $m_2 \to 0$, and Equation (3.54) reduces to the well-known equation of the kettledrum, i.e.,

$$J_o(ka) = -\alpha_1 \frac{J_2(ka)}{(ka)^2} \qquad (3.57)$$

2. For the opening area and the enclosure volume increasing beyond any limit, $A_2 \to \infty$, $V_2 \to \infty$, and Equation (3.54) reduces to

$$J_o(ka) = 0 \tag{3.58}$$

which is the well known frequency equation for a membrane vibrating in air, whose roots are ka = 2.405, 5.52, 8.654, 11.792, ...

3. For a very rigid membrane, $T_o \to \infty$, $\alpha_1 \to 0$, $k \to 0$, $v_1 = 0$, and the system becomes a Helmholtz oscillator whose frequency is given by

$$\omega_H^2 = \frac{\gamma P_o A_2^2}{V_o} \tag{3.59}$$

Equation (3.59) yields the frequency of a Helmholtz oscillator with openings, internal pressure, and volume similar to those of the structure. This frequency is substantially higher than the fundamental frequency of the flexible roof backed by a cavity with openings.

3.7.4 Comparison between Exact and Simplified Analysis

Using Equations (3.54) and (3.56) both the damped and undamped frequencies were calculated for the simplified Calgary Olympic Coliseum roof and the lighter roof. The resulting modal parameters are plotted in Figures (3.3a) and (3.3b) and shown as dots, circles and squares. The results of the approximate two-mass theory are generally in very good agreement with those of Equations (3.16) and (3.31). However, the simplified theoretical approach gives somewhat higher values of undamped frequencies of the second mode for opening area ratios $A_v/A_r \geq 0.5$. This difference is not of practical importance because such openings are unrealistically large and, in this range, the roof second frequency, f_2, tends to vanish because of overdamping. It may be mentioned that the estimated leakage

through doors and windows for the Calgary Olympic Coliseum corresponds to an opening area ratio of about 5% to 8%.

The damping ratios of the roof-air system, calculated from the complex eigenvalues μ_j, Equations (3.31) and (3.32), for both roofs, are plotted in Figures (3.4a) and (3.4b) and denoted as exact. The agreement with the values from the two-mass model is very good except for higher values of A_2/A_1 for which the "exact" damping ratios are lower than those calculated using the simplified approach. Some of the differences observed, though not of great practical importance, are probably due to the approximate nature of the much simpler two-mass model, the use of which is well-justified by the often complex shapes of lightweight roofs and the associated computational effort.

3.8 HARMONIC RESPONSE OF A CIRCULAR MEMBRANE BACKED BY A CAVITY WITH OPENINGS

A closed form solution is derived for the damped response of a circular membrane backed by a cavity with openings. The effects of the wall openings, the internal pressure changes due to the roof vibration, and the structural as well as the acoustical damping for both the roof and the openings are accounted for in the analysis. The derived solution and the assessment of its accuracy are described below.

In the analysis formulated below, the uniform harmonic loading is $P(r,\theta,t) = \bar{P} \exp(i\omega t)$ where $\bar{P}$ is the load amplitude, $i^2 = -1$, and ω is the circular

frequency of the loading. Using the same symbols as in Section 3.7, the governing equation of motion of a circular membrane (Kinsler and Frey, 1962) backed by a cavity with openings under harmonic pressure can be written as

$$\frac{\partial^2 v_1}{\partial t^2} - \frac{T_o}{m}\left(\frac{\partial^2 v_1}{\partial r^2} + \frac{1}{r}\frac{\partial v_1}{\partial r} + \frac{1}{r}\frac{\partial^2 v_1}{\partial \theta^2}\right) + \frac{\gamma P_o A_2}{V_o}\left(\frac{\bar{v}_1}{\alpha} + v_2\right)$$

$$+ \frac{(c_s + c_{a1})}{m}\frac{\partial v_1}{\partial t} = \frac{\bar{P}}{m} e^{i\omega t} \qquad (3.60a)$$

The governing equation of motion of the air mass at the openings is

$$\frac{\partial^2 v_2}{\partial t^2} + \frac{\gamma P_o A_2^2}{m_2 V_o}\left(\frac{\bar{v}_1}{\alpha} + v_2\right) + \frac{c_{a2}}{m_2}\frac{\partial v_2}{\partial t} = 0 \qquad (3.60b)$$

In equations (3.60a) and (3.60b), $\bar{v}_1$ is an integral function of the mode of vibration. The solution of Equation (3.60) can be written as

$$\begin{Bmatrix} v_1(r,\theta,t) \\ v_2(t) \end{Bmatrix} = \begin{Bmatrix} v_1(r,\theta) \\ v_2 \end{Bmatrix} e^{i\omega t} \qquad (3.61)$$

For the symmetrical modes of vibration, the term $\partial^2 v_1 / \partial \theta^2$ vanishes. Substituting Equation (3.61) into Equations (3.60a) and (3.60b) yields

$$-\omega^2 v_1 - \frac{T_o}{m}\left(\frac{d^2 v_1}{\partial r^2} + \frac{1}{r}\frac{dv_1}{dr}\right) + \frac{\gamma P_o A_2}{V_o}\left(\frac{\bar{v}_1}{\alpha} + v_2\right)$$

$$+ i\frac{(c_s + c_{a1})}{m}\omega v_1 = \frac{\bar{P}}{m} \qquad (3.62a)$$

$$-\omega^2 v_2 + \frac{\gamma P_o A_2^2}{m_2 V_o}\left(\frac{\bar{v}_1}{\alpha} + v_2\right) + i\frac{(c_s + c_{a1})}{m_2}\omega v_2 = 0 \qquad (3.62b)$$

From Equation (3.62b), the displacement of the air masses at openings, v_2 can be written as

$$v_2 = -\frac{b_2 \bar{v}_1}{\alpha\,[b_2 - \omega^2 + i\omega(c_{a2}/m_2)]} \qquad (3.63)$$

where $b_2 = \gamma P_o A_2^2/(m_2 V_o)$. Equation (3.62a) can be arranged in the form

$$\frac{d^2v_1}{dr^2} + \frac{1}{r}\frac{dv_1}{dr} + k^2v_1 = -\frac{\bar{P}}{T_o} + \frac{b_1 m}{T_o}\left(\frac{\bar{v}_1}{\dot{\alpha}} + v_2\right) \tag{3.64a}$$

or

$$\frac{d^2v_1}{dr^2} + \frac{1}{r}\frac{dv_1}{dr} + k^2v_1 = -\frac{\bar{P}\beta_3}{T_o} \tag{3.64b}$$

where

$$\beta_3 = 1 - (b_1 m/\bar{P})\left(\frac{\bar{v}_1}{\dot{\alpha}} + v_2\right) \tag{3.65a}$$

and

$$k^2 = (m\omega^2 - ic_t\omega)/T_o \tag{3.65b}$$

The right hand side of Equation (3.64) is a constant. Thus, the complete solution of Equation (3.64) can be written as

$$v_1(r) = C\,J_o(kr) - \frac{\bar{P}\beta_3}{k^2T_o} \tag{3.66}$$

Applying the boundary condition, $v_1(a) = 0$, gives the value of the constant C as

$$C = \frac{\bar{P}\beta_3}{k^2T_o}\,\frac{1}{J_o(ka)} \tag{3.67}$$

Substituting Equation (3.67) into Equation (3.66) yields the amplitude of the membrane displacement, i.e.,

$$v_1(r) = \frac{\bar{P}\beta_3}{k^2T_o}\left[\frac{J_o(kr) - J_o(ka)}{J_o(ka)}\right] \tag{3.68}$$

The average displacement of the membrane can be written as

$$\bar{v}_1 = \frac{\bar{P}\beta_3}{k^2T_o}\left[\frac{J_2(ka)}{J_o(ka)}\right] \tag{3.69}$$

Substituting Equation (3.63) into Equation (3.65) gives

$$\beta_3 = 1 - (\alpha_1 T_o/\bar{P}a^2)\,\beta_4\,\bar{v}_1 \tag{3.70}$$

where

$$\beta_4 = [1 - \frac{1}{\{1 - (k_1a)^2/(\alpha_1\alpha')\}}] \frac{J_2(ka)}{(ka)^2} \tag{3.71}$$

and

$$k_1^2 = (m_2'\omega^2 - ic_{a2}\omega/A_2)/T_o \tag{3.72}$$

Thus, the displacement of the membrane becomes

$$v_1(r,t) = \frac{\bar{P}\beta_3}{k^2T_o} [\frac{J_o(kr)}{J_o(ka)} - 1] e^{i\omega t} \tag{3.73}$$

It can be seen that the amplitude of vibration is frequency dependent and that it is directly proportional to the amplitude of the harmonic loading $\bar{P}$, and inversely proportional to the tension T_o. When the frequency ω of the harmonic loading corresponds to any of the free oscillation frequencies of the membrane, the amplitude reaches a finite maximum value, depending on the damping of the membrane. For undamped cases, the value of k^2 is real and equal to $m\omega^2/T_o$, instead of $(m\omega^2 - ic_t\omega)/T_o$.

Limiting Cases

Equation (3.73) contains the two limiting cases of the problem, which are listed below:

1. For the opening area $A_2 \to 0$, $m_2 \to 0$, $\beta_4 \to 1$, $\beta_3 \to \beta_5$, and Equation (3.73) reduces to Equation (3.74) for the response equation of a membrane backed by a closed cavity under harmonic uniform pressure, which is

$$w(r,t) = \frac{\bar{P}\beta_5}{k^2T_o} [\frac{J_o(kr)}{J_o(ka)} - 1] e^{i\omega t} \tag{3.74}$$

where

$$\beta_5 = 1 - (\gamma P_o \pi a^2/\bar{P}V_o)\ \bar{w} \tag{3.75}$$

2. For the opening area increasing beyond any limit $A_2 \to \infty$, $V_o \to \infty$, $\beta_4 \to 0$, $\beta_3 \to 1$, and Equation (3.73) reduces to that of a membrane vibrating in air under uniform harmonic loading, which is

$$w(r,t) = \frac{\bar{P}}{k^2 T_o}\left[\frac{J_o(kr)}{J_o(ka)} - 1\right] e^{i\omega t} \tag{3.76}$$

Equation (3.73) can be used to calculate the damping ratios at the natural frequencies of vibration, ω_o. After calculating the resonant amplitude under harmonic uniform pressure, the dynamic amplification at the roof centre is

$$\varepsilon = \frac{v_1(r=0,\omega=\omega_m)}{v_1(r=0,\omega=0)} \tag{3.77}$$

where

$$\omega_m = \omega_o\ (1 - 2\ \zeta^2)^{1/2} \tag{3.78}$$

The dynamic amplification factor also can be written as

$$\varepsilon = \frac{1}{[2\zeta(1-\zeta^2)]^{1/2}} \approx \frac{1}{2\ \zeta} \tag{3.79}$$

Thus, from Equation (3.76), the modal damping ratio is

$$\zeta = 0.707\ [\ 1 - \{\ 1 - (1/\varepsilon^2)\ \}^{1/2}\ ]^{1/2} \approx 1/(2\varepsilon) \tag{3.80}$$

For a specific value of α', Equations (3.77) to (3.80) can be solved initially by assuming $\omega_m = \omega_o$, which can be calculated from either Equation (3.16) or Equation (3.56). New values of ω_m, ε, and ζ are recalculated and the process is

repeated until convergence is reached. This procedure is followed for different opening area ratios.

The damping ratios calculated in this way are also in very good agreement with the values of the two mass model, Figures (3.4a) and (3.4b), except for higher values of A_2/A_1 for which the "exact" damping ratios are lower than those calculated using the simplified approach.

CHAPTER 4

EXPERIMENTS WITH FREE VIBRATION OF SELF-SUPPORTED, LIGHTWEIGHT ROOFS BACKED BY CAVITIES WITH OPENINGS

4.1 INTRODUCTION

The design and construction of self-supported, large span, lightweight roofs require an examination of their dynamic behaviour to secure a safe and serviceable design. For most cases, an experimental study becomes necessary because either the problem is too complex for theoretical treatment or the analysis is too expensive. In addition, most theories are based on approximations and simplifying assumptions. The experiments in this chapter are conducted to provide a method of verifying the theory outlined in Chapter 3 and to further explore the behaviour of these roofs.

Two structural models were used in this study. The first was a large span, self-supported membrane roof and the second was a flexible large span, lightweight plate roof. The main objective of the experimental free vibration investigation is to study the effect of wall openings and volume scaling on the dynamic behaviour of self-supported, lightweight roofs backed by cavities with openings.

In this study, the similarity requirements, instrumentation and testing procedure are described. Also, experimental observations and the comparison of the experimental results with the theoretical results are given.

4.2 SIMILARITY REQUIREMENTS

The basis of the experimental work on models is that all forces can be scaled in the same proportion to those of the corresponding full-scale forces. The dimensional analysis of all variables yields a proportionality constant which is a function of a dimensionless group of parameters. Once a unique relationship has been established between the proportionality constant and its dimensionless group, the value of the constant can be found for different dimensionless numbers. In many cases, the scaling requirements for one dimensionless parameter make it difficult to scale another one correctly. A continuation to this discussion is given in the wind tunnel study of Chapter 7. Detailed data on aeroelastic modelling and techniques to simulate free vibration of structures and the effects of wind on them are given by Tryggvason and Isyumov (1977).

The length, mass, and time scaling parameters are defined as follows:

$$\text{Length scale} = \frac{L_m}{L_p} = \lambda_L \tag{4.1}$$

$$\text{Density scale} = \frac{\rho_m}{\rho_p} = \lambda_\rho \tag{4.2}$$

$$\text{Velocity scale} = \frac{U_m}{U_p} = \lambda_V \tag{4.3}$$

In the equations above, the subscript m refers to the model and the subscript p refers to the prototype. The dimensions of the model are determined by the length scale, λ_L, which is constrained by the scaling of the boundary layer thickness and the integral length scale of the wind turbulence. The length scale may also be dictated by other constraints.

The frequency scale, λ_f, is

$$\lambda_f = \frac{f_m}{f_p} = \frac{\lambda_V}{\lambda_L} \tag{4.4}$$

The reciprocal of the frequency scale is the time scale, λ_t, which is given by

$$\lambda_t = \frac{T_m}{T_p} = \frac{\lambda_L}{\lambda_V} \tag{4.5}$$

For a roof system that is attached to a rigid structure, the following physical quantities may have significance in determining its behaviour: ρ, μ, g, c_o, U, ρ_s, L_s, E_s, and ς_s in which c_o is the speed of sound in air; ρ, μ, and U are the density, dynamic viscosity, and velocity of the air, respectively; g is the acceleration of gravity; ρ_s, L_s, and E_s are the density, typical dimension, and the modulus of elasticity of the structure, respectively; and finally ς_s is the damping ratio of the structure.

Using the Buckingham π theorem, a minimum of five non-dimensional parameters are required, Whitbread (1965), which are:

1. Reynolds number $R_e = \frac{\rho UL}{\mu}$ (4.6)
2. Cauchy Number $= \frac{E_s}{\rho U^2}$ (4.7)
3. Density ratio $= \frac{\rho_s}{\rho}$ (4.8)
4. Froude Number $= \frac{U^2}{gL}$ (4.9)
5. Damping ratio $= \varsigma_s$ (4.10)

Another dimensionless parameter is the Mach number which is important for scaling the pneumatic damping (Irwin and Wardlaw, 1979). In the free vibration experiments in this chapter, Reynolds and Froude numbers are not

relevant. The discussions of Reynolds and Froude numbers is continued in Section 7.2.

Similarity of the inertial, elastic and damping forces for lightweight structures requires the equality of the following non-dimensional quantities (Tryggvason and Isyumov, 1977):

Similarity of inertial effects - ρ_s/ρ

Similarity of elastic effects - $E_s/\rho U^2$

Similarity of structural damping - ζ_s

4.2.1 The Mass Density Scaling

The mass density scaling parameter of the structure, which represents the inertial similarity, requires that

$$[\frac{\rho_s}{\rho}]_m = [\frac{\rho_s}{\rho}]_p \qquad (4.13)$$

Hence,

$$[\frac{m}{\rho L}]_m = [\frac{m}{\rho L}]_p \qquad (4.14)$$

where m is the mass per unit area. Thus, the mass per unit area scaling, λ_m, is

$$\lambda_m = m_m/m_p = \lambda_L \qquad (4.15)$$

4.2.2 The Elasticity Scaling

For pure membrane action, the elastic similarity implies the similarity of tensile force per unit length. Allowing the non-dimensional parameter, $E_s/\rho U^2$ to be rewritten as $E_s h/\rho U^2 L$, where h is the thickness of membrane and L is the building characteristic dimension, then

$$\left[\frac{E_s h}{\rho U^2 L}\right]_m = \left[\frac{E_s h}{\rho U^2 L}\right]_p \tag{4.16}$$

and with $\rho_m = \rho_p = \rho_{air}$, then

$$\frac{[E_s h]_m}{[E_s h]_p} = \lambda_L \lambda_v^2 \tag{4.17}$$

In Equation (4.17) λ_V is the velocity scale, therefore, the scaling of the tension per unit length scaling is

$$\lambda_{To} = \lambda_L \lambda_v^2 \tag{4.18}$$

Similarly, for a flexible plate roof the rigidity scaling, λ_R, requires that

$$\left[\frac{E_s h^3}{\rho U^2 L^3}\right]_m = \left[\frac{E_s h^3}{\rho U^2 L^3}\right]_p \tag{4.19}$$

Thus,

$$\lambda_R = \lambda_L^3 \lambda_v^2 \tag{4.20}$$

4.2.3 Dynamic Stiffness Scaling

The stiffness of lightweight roofs backed by cavities depends on the tension force in the case of membrane roofs or the roof rigidity in case of plate roofs, and the internal pressure resulting from the volumetric changes of the enclosed volume underneath the roof. Correct scaling of the internal pressure changes due to the roof motion is important for maintaining the dynamic similarity of the roof.

Tryggvason et al. (1977) showed that the similarity of fluctuating internal pressures can be maintained for low wind tunnel speeds by distorting the internal volume according to the following relation:

$$\lambda_{\forall} = \forall_m / \forall_p = \lambda_L^3 \lambda_v^2 \tag{4.21}$$

in which λ_v is the internal volume scaling. This volume scaling implies exaggerating the model volume by $1/\lambda_v^2$ beyond that required by the length scale. In practice it is not difficult to provide an additional volume (beneath the turntable floor) to provide the distorted internal volume.

4.2.4 Damping Similarity

The structural damping ratio, ς_s, of the model is usually assumed to be similar to that of the prototype, i.e., the structural damping scaling parameter, λ_{ς_s}, equals one.

In most cases where the pneumatic forces of the internal volume play a role (for volume changing motions of a sealed roof) the acoustical damping is also important. Irwin and Wardlaw (1979) investigated the scaling of the acoustical damping. It was shown that to model the acoustical damping effect correctly, the Mach number, U/c_o, should be the same at both model and full scales. However, it was shown that relaxing Mach number scaling can be regarded as conservative.

Kind (1982 and 1984) analytically investigated the pneumatic effects in air-supported structures. The analysis was limited to the volume displacing modes of vibration. It was concluded that both the pneumatic stiffness (internal pressure increase directly proportional to volume decrease) and the pneumatic damping (internal pressure increase directly proportional to the rate of volume decrease) are important for most air-supported structures. For such structures, it was suggested that a non-dimensional pneumatic damping scaling parameter, λ_{ς_p}, should be

maintained as

$$\lambda_{\zeta_p} = \frac{L^2}{\rho U(C_L+C_F)} \tag{4.23}$$

where C_F and C_L are the local inverse slopes of the fan and leakage pressure versus flow characteristics, respectively. The fan effect is not considered in this study; therefore the scaling by Equation (4.23) is not implemented. It should be mentioned that the pneumatic damping is of much less importance in naturally ventilated, self-supported structures.

4.2.5 Summary of Aeroelastic Scaling Requirements

The aeroelastic modelling requirements for the free vibration experiments in this chapter can be summarized as follows:

1. All dimensions of the structure are scaled according to λ_L.
2. The internal volume is scaled according to $\lambda_{\forall} = \lambda_L^3/\lambda_V^2$.
3. The mass per unit area of the roof is scaled according to $\lambda_m = \lambda_L$.
4. The elasticity similarity for the membrane roof is scaled according to $\lambda_{T_0} = \lambda_V^2\lambda_L$, and the rigidity of the plate roof is scaled according to $\lambda_R = \lambda_V^2\lambda_L^3$.
5. The similarity of the structural damping is based on $\lambda_{\zeta_s} = 1$.

4.3 CONSTRUCTION OF THE MODELS

4.3.1 The Prototypes

4.3.1.1 Prototype 1

The first structure type considered is a stadium with a horizontal circular membrane roof of 126.75 m in diameter and 42 m in height. The membrane of the roof is considered to be 20 cm thick lightweight concrete panels supported by a prestressed cable mesh anchored in a ring beam resting on a rigid circular wall. The membrane action is obtained by grouting the lightweight concrete panels to the pretensioned cables to form a monolithic membrane.

The total mass per unit area of prototype 1 is about 292.5 kg/m^2 which includes the masses of the lightweight concrete, the cable net and the plastic waterproof cover. The structure enclosed volume is 5.40 x 10^5 m^3 and the fundamental frequency of the roof is taken as 0.20 Hz.

4.3.1.2 Prototype 2

The second structure type considered is that of a similar stadium but with a lightweight, flexible plate roof. This structure may be suitable for an area subject to little or no snowfall. This type of structure might comprise a truss system or any other supporting system that behaves in a flexural way resting on the outside ring wall. Such a system may not be very practical but it is suitable for the experiment. The roof total mass per unit area of prototype 2 is assumed to be 58.5 kg/m^2 and the structure enclosed volume is the same as that of

prototype 1.

4.3.2 Models

The main considerations in designing the two models used in this experimental study were easy construction, easy adjustment of the membrane tension in model 1, and easy replacement of the roofs. The length scale was determined after an extensive study of the material properties of various membranes and plates.

4.3.2.1 Roof of model 1

At first, a 0.254 mm thick tetrafluroethylene membrane (teflon) was chosen. However, this material was not used because of its nonlinear properties. Finally, a 0.50 mm thick neoprene membrane was used. With this material, a geometric scaling of λ_L = 1:390 was determined which allowed through elasticity scaling a velocity scale of 1: 3, and the model was constructed to satisfy the various similarity requirements mentioned earlier. The membrane roof was attached to the wall by a clamping ring and the membrane tension was adjusted using a movable aluminum clamping ring as shown in Figure (4.1).

A summary of the various scaling parameters of model 1 is presented in Table (4.1). The numerical values for the membrane model and the corresponding prototype scaling are also given in Table (4.2). A plan and a vertical cross-section of this model showing the model set-up are given in Figures (4.1) and (4.2). Also, a photograph of the model is given in Plate (4.1).

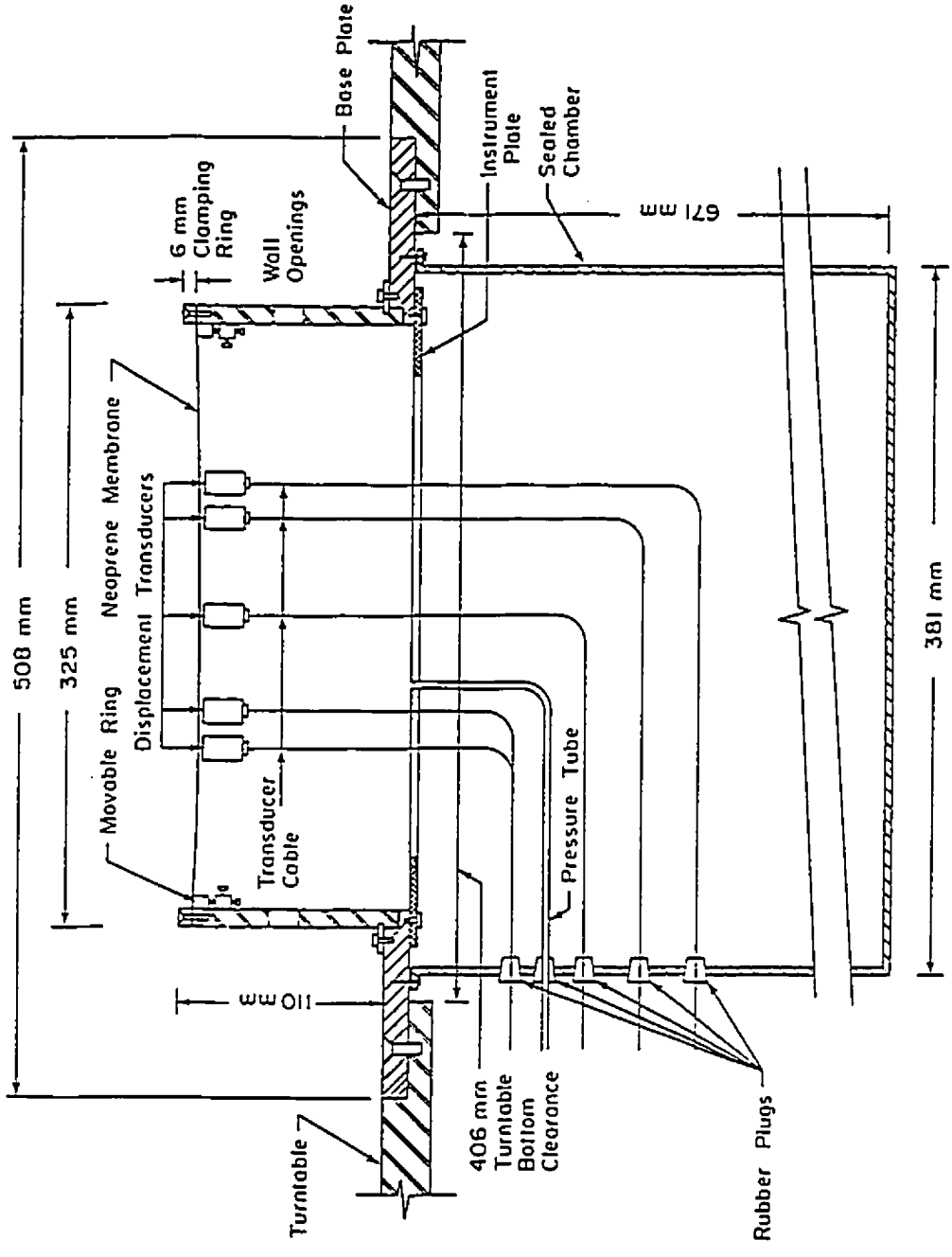

Fig. (4.1): Vertical cross-section of the membrane roof model

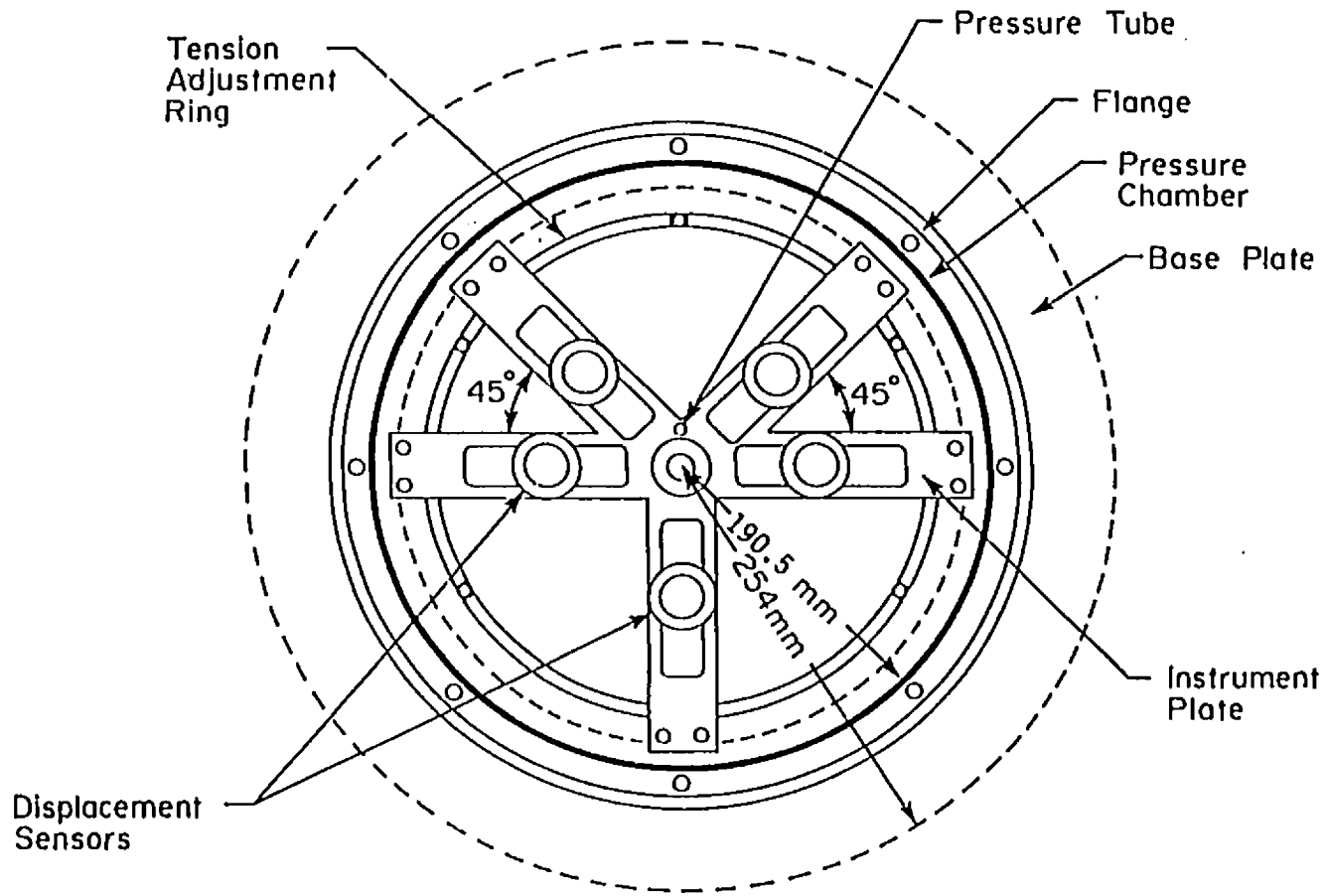

Fig. (4.2): Cross-sectional plan of the membrane roof model

TABLE (4.1): SUMMARY OF AEROELASTIC SCALING PARAMETERS OF THE MEMBRANE STRUCTURE (MODEL 1)

No.	Parameter	Scaling	Numerical value
1	length	$\lambda_L=L_m/L_p$	2.564×10^{-3} (1 : 390)
2	Internal volume	$\lambda_w=\lambda_L^3/\lambda_V^2$	1.517×10^{-7}
3	Mass/unit area	$\lambda_m=\lambda_L$	2.564×10^{-3} (1 : 390)
4	Weight/unit area	$\lambda_w=\lambda_L$	2.564×10^{-3} (1 : 390)
5	Time	$\lambda_t=\lambda_L/\lambda_V$	7.69×10^{-3} (1 : 130)
6	Frequency	$\lambda_f=\lambda_V/\lambda_L$	130 (130 : 1)
7	Velocity	$\lambda_V=V_m/V_p$	0.333 (1 : 3)
8	Force	$\lambda_F=\lambda_L^2\lambda_V^2$	7.305×10^{-7}
9	Pressure	$\lambda_p=\lambda_V^2$	0.111 (1 : 9)
10	Tension/unit area	$\lambda_{To}=\lambda_L\lambda_V^2$	2.849×10^{-4}

TABLE (4.2): AEROELASTIC SCALING OF THE MEMBRANE STRUCTURE

(MODEL 1)

No.	Parameter	Prototype		Model	
		Quantity	Dimension	Quantity	Dimension
1	Roof diameter	126.75	m	32.5	cm
2	Height	42.9	m	11.0	cm
3	Mass/unit area	292.5	kg/m^2	0.75	kg/m^2
4	Weight/unit area	2869.4	N/m^2	7.36	N/m^2
5	Modulus of elasticity	46.53	MN/m^2	5.17	MN/m^2
6	Enclosed volume	5.41×10^5	m^3	8.21×10^4	cm^3
7	Fundamental frequency	0.2	Hz	26.0	Hz

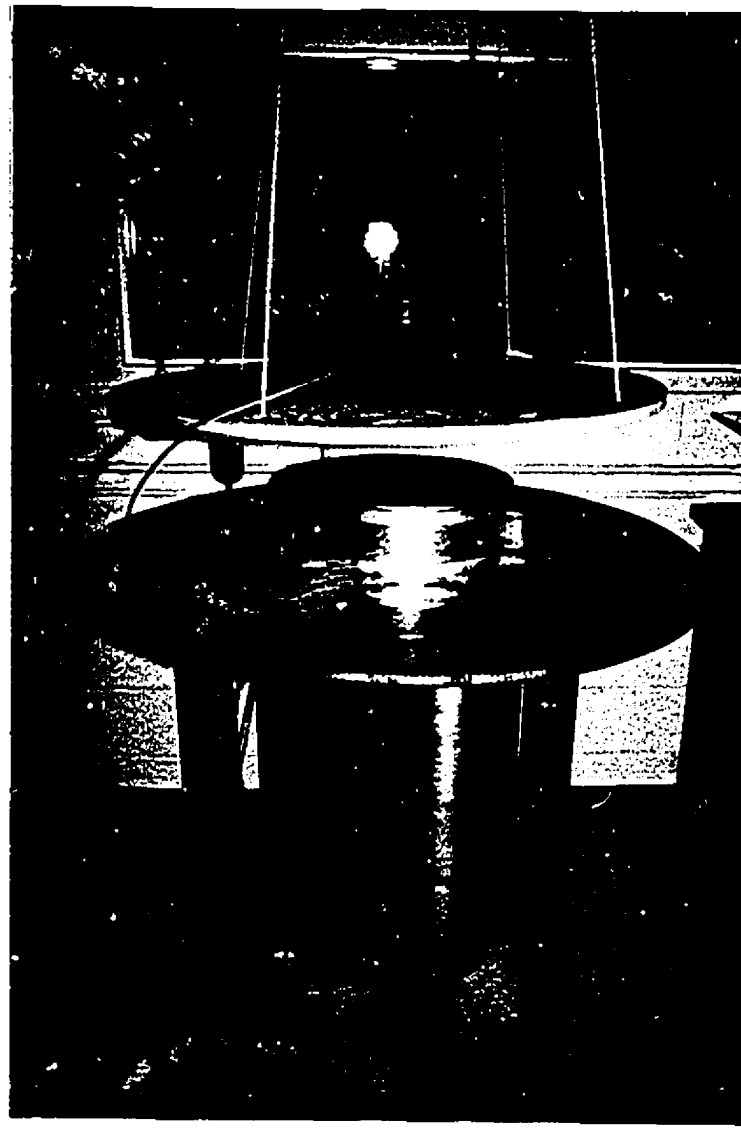

Plate (4.1): The membrane roof model

4.3.2.2 Roof of model 2

In the second model of this study, the roof was modelled as a clamped circular lightweight plate. Several considerations governed the design of this model. The most important were the linear behaviour of the roof material without the possibility of creep, and the resonant frequencies of the roof (not to exceed those which are the maximum measurable frequencies by the available instruments). The roof material selected was 3.0 mm Rohacell 51 foam sheet. This selection was based on its availability and on its deflection/thickness ratio (which was less than 0.10), as linear bending deflections were desired. The roof was fixed to the walls by a strong adhesive material (RTV glue). The fundamental frequency of the model with the base open was 45.0 Hz.

A summary of the various scaling parameters of the model is presented in Table (4.3). The numerical values for the model and the corresponding prototype scaling are given in Table (4.4). A vertical cross-section of the model is given in Figure (4.3). Also, a photograph of the model is given in Plate (4.2).

4.3.3 Other Parts of The Models

The walls of the two models were rigid and made from an aluminum material 10 mm thick. To simulate wall openings (windows and doors in the prototype), four groups of three symmetrical circular holes of 30 mm in diameter each, were drilled in the circular wall at mid-height, spaced 90° apart, as shown in Figure (4.4). The ratio of the opening areas to the wall area, α', could be

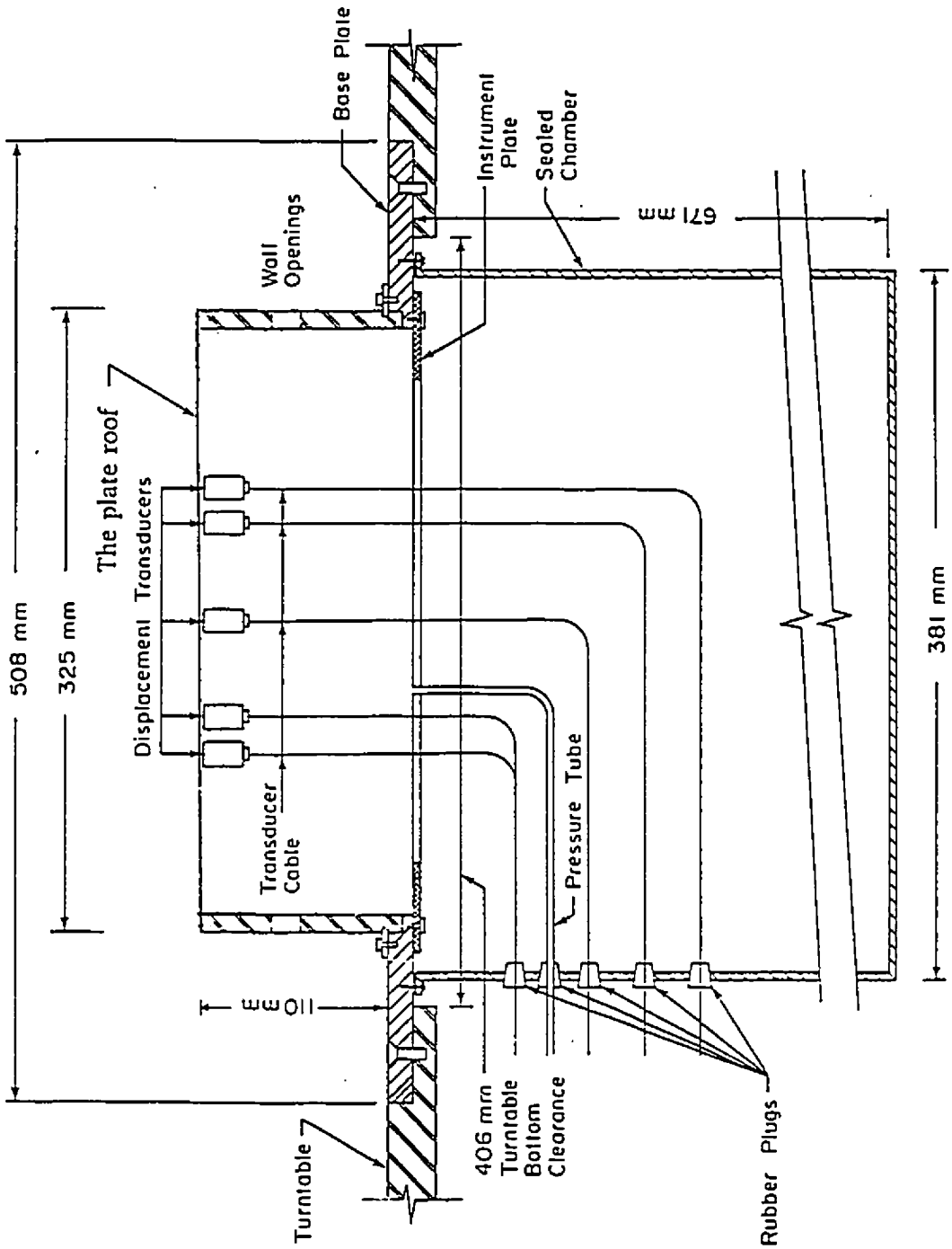

Fig. (4.3): Vertical cross-section of the plate roof model

TABLE (4.3): SUMMARY OF AEROELASTIC SCALING PARAMETERS OF THE PLATE ROOF STRUCTURE (MODEL 2)

No.	Parameter	Scaling	Numerical value
1	length	$\lambda_L = L_m/L_p$	2.564×10^{-3} (1 : 390)
2	Internal volume	$\lambda_v = \lambda_L^3/\lambda_V^2$	6.74×10^{-8}
3	Mass/unit area	$\lambda_m = \lambda_L$	2.564×10^{-3} (1 : 390)
4	Weight/unit area	$\lambda_w = \lambda_L$	2.564×10^{-3} (1 : 390)
5	Time	$\lambda_t = \lambda_L / \lambda_V$	5.13×10^{-3} (1 : 195)
6	Frequency	$\lambda_f = \lambda_V/\lambda_L$	195 (195 : 1)
7	Velocity	$\lambda_V = V_m/V_p$	0.5 (1 : 2)
8	Force	$\lambda_F = \lambda_L^2\lambda_V^2$	1.644×10^{-6}
9	Pressure	$\lambda_p = \lambda_V^2$	0.25 (1 : 4)

TABLE (4.4): AEROELASTIC SCALING OF THE PLATE ROOF STRUCTURE

(MODEL 2)

No.	Parameter	Prototype		Model	
		Quantity	Dimension	Quantity	Dimension
1	Roof diameter	126.75	m	32.5	cm
2	Height	42	m	11.0	cm
3	Mass/unit area	58.5	kg/m^2	0.15	kg/m^2
4	Weight/unit area	574.0	N/m^2	1.47	N/m^2
5	Modulus of elasticity	6.30×10^8	N/m^2	7.0×10^7	N/m^2
6	Enclosed volume	5.41×10^5	m^3	3.65×10^4	cm^3
7	Fundamental frequency	0.23	Hz	45.0	Hz

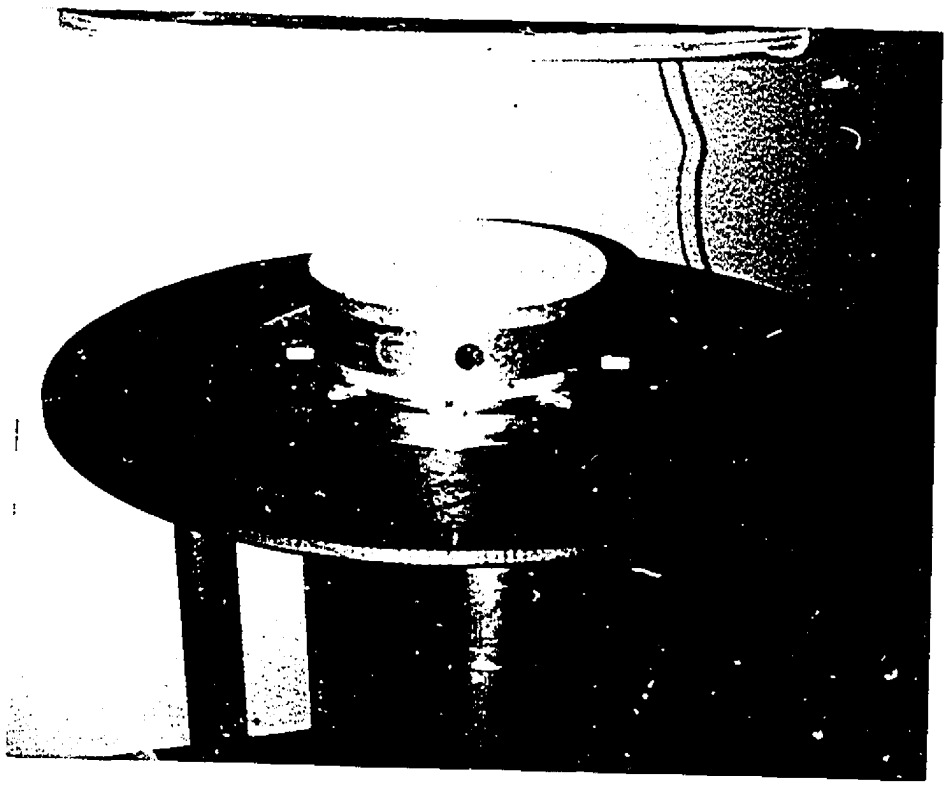

Plate (4.2): The plate roof model

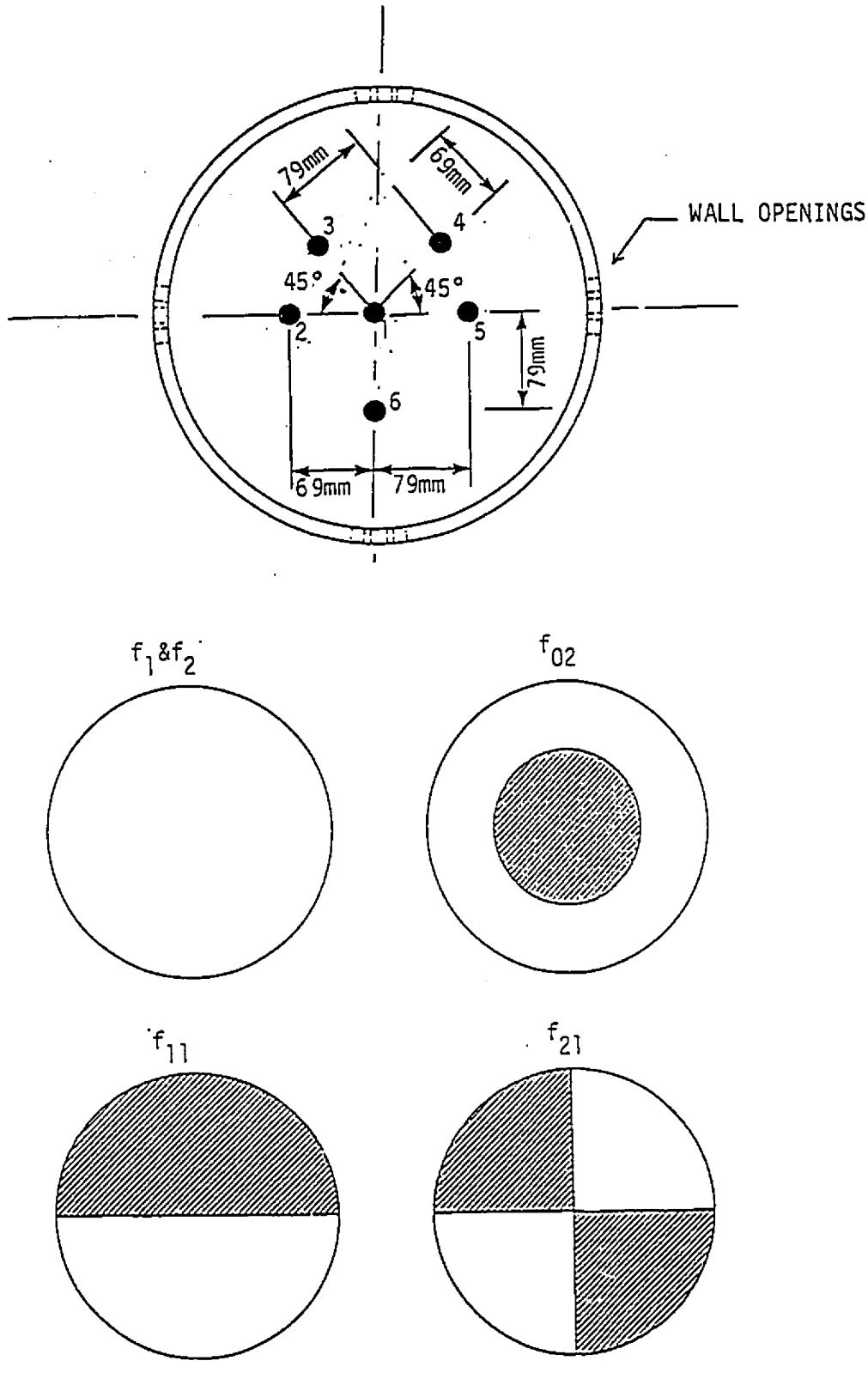

Fig. (4.4): Kaman displacement sensors arrangement and mode shapes

varied from 0.0 % to 7.8 % by using a rigid aluminum circular band embracing the walls. The circular band could cover one, two or three openings of each group to give values of 5.2 %, 2.6 % or 0.0 %, respectively. For α' = 7.8 % the band was removed from the models. These opening area ratios were chosen on the basis that, for the Calgary Olympic Coliseum, the estimated leakage rate corresponds to an opening area ratio of about 5% to 8%.

A chamber was mounted below the models to satisfy the corresponding internal volume scaling as shown in Figures (4.1) and (4.3). The chamber was sealed to prevent any air leakage from the models by inserting a rubber strip between the model base and the chamber flange.

4.4 INSTRUMENTATION AND CALIBRATION

The instrumentation used in this study comprised six vertical displacement sensors and one pressure transducer. The displacement sensors measure the change in the reactance of the air gap between the vibrating surface and the probe. These sensors allowed simultaneous deflection measurements at six different locations. The displacement sensors were Kaman non-contact reactance sensors and were located below the roof surface as shown in Figures (4.1) and (4.3). Probe positioning holes were provided in the instrument plate to orient the transducers normal to the roof surface. The sensors were calibrated prior to each experiment.

The locations of the sensors are given in Figures (4.2), (4.3) and (4.4) for both model 1 and 2. This arrangement facilitates the separation of the symmetrical modes of vibrations from the antisymmetrical ones. The displacements at all probes were monitored to confirm the mode identification and for comparison purposes.

Electrical leads for various sensors were passed through the side of the chamber and carefully sealed. Small aluminum foil targets (0.015 mm thick and of 9 mm diameter) were glued to the inner surface of the roof at the Kaman probes. Baffles were placed into the pressure chamber to avoid any acoustic resonance. A further consideration was the complete sealing of the models on the mounting board as any small leakage may negate the results. An internal pressure tap was connected to the instrument plate inside the model and, with the openings closed, the model was pressurized and the resulting pressure was monitored to detect any leakage.

4.5 TEST PROCEDURE

After calibrating the sensors, the membrane model was tuned by excitation with a loudspeaker, having the base board and the opening band removed as shown in Plate (4.1). This was done to simulate the membrane vibration without an enclosed cavity. The tension in the membrane was uniformly adjusted in all directions until a resonance occurred with the loudspeaker exciting the membrane at 26.0 Hz which is equivalent to 0.2 Hz in the prototype scale.

The test procedure was the same for both models. After setting up the experiment for each model as shown in Figure (4.5), the wall opening area was set to different ratios and for each ratio the models were excited in still air using the loudspeaker. Two types of excitations were used: random and harmonic. The random excitation generated using white noise with a frequency range of 0 to 100 Hz for the first model and 0 to 400 Hz for the second model. These frequency ranges facilitated the determination of the natural frequencies of vibration. Harmonic excitation was then applied stepwise and was used to identify the mode shapes associated with the natural frequencies.

The establishment of the natural frequencies from the power spectra of response to the white noise excitation utilized a Hewlett-Packard Structural Dynamic Analyzer 5423A. The damping ratios and the auto-correlation of the response at each probe location were also obtained using the analyzer. The HP analyzer evaluates the damping by fitting an analytical function to the measured peak of response, from which damping is obtained when convergence between the measured and analytical peaks is reached. The damping ratios obtained represent the total damping of the model. This process was repeated for different opening areas. Examples of the established response spectra at the center of model 1 are shown in Figure (4.6) for different opening ratios. The spectral peaks are very narrow, facilitating a sufficiently accurate determination of the natural frequencies of the system.

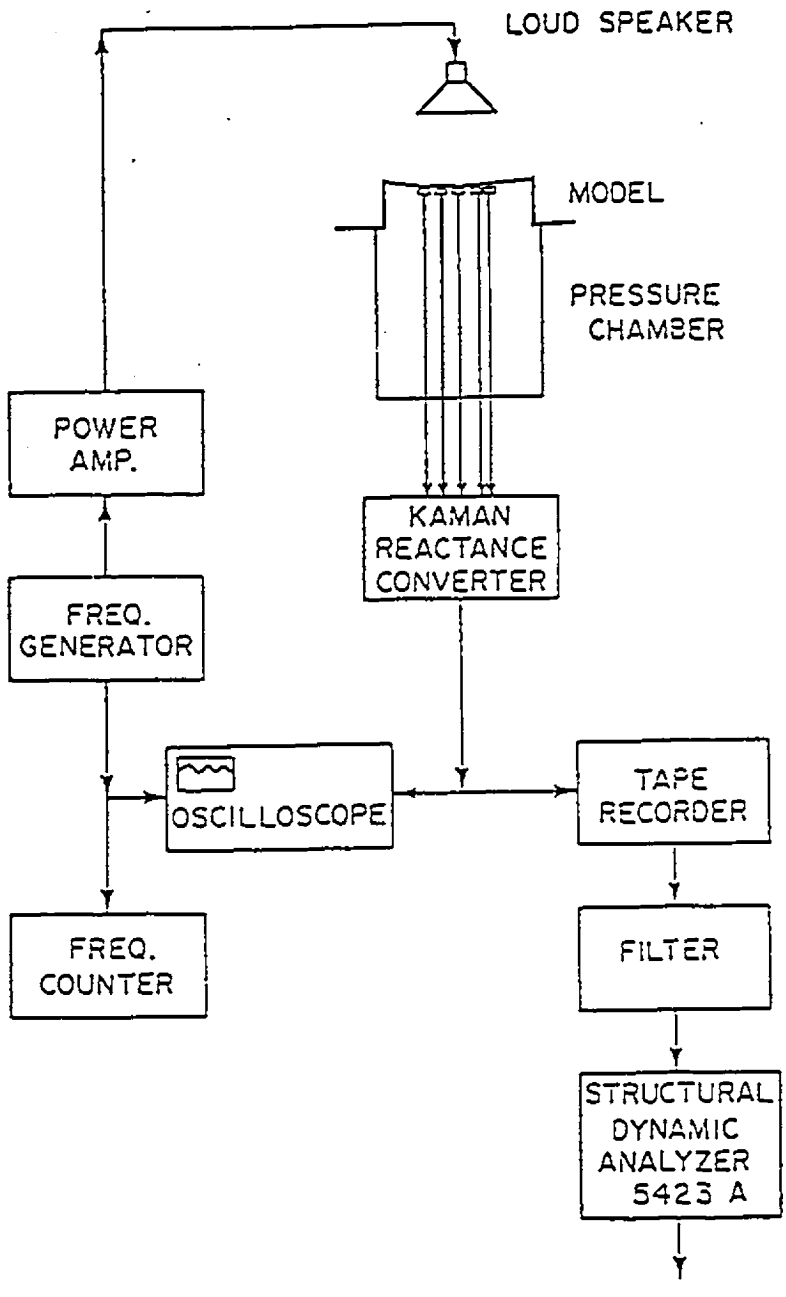

Fig. (4.5): Free vibration experimental set-up

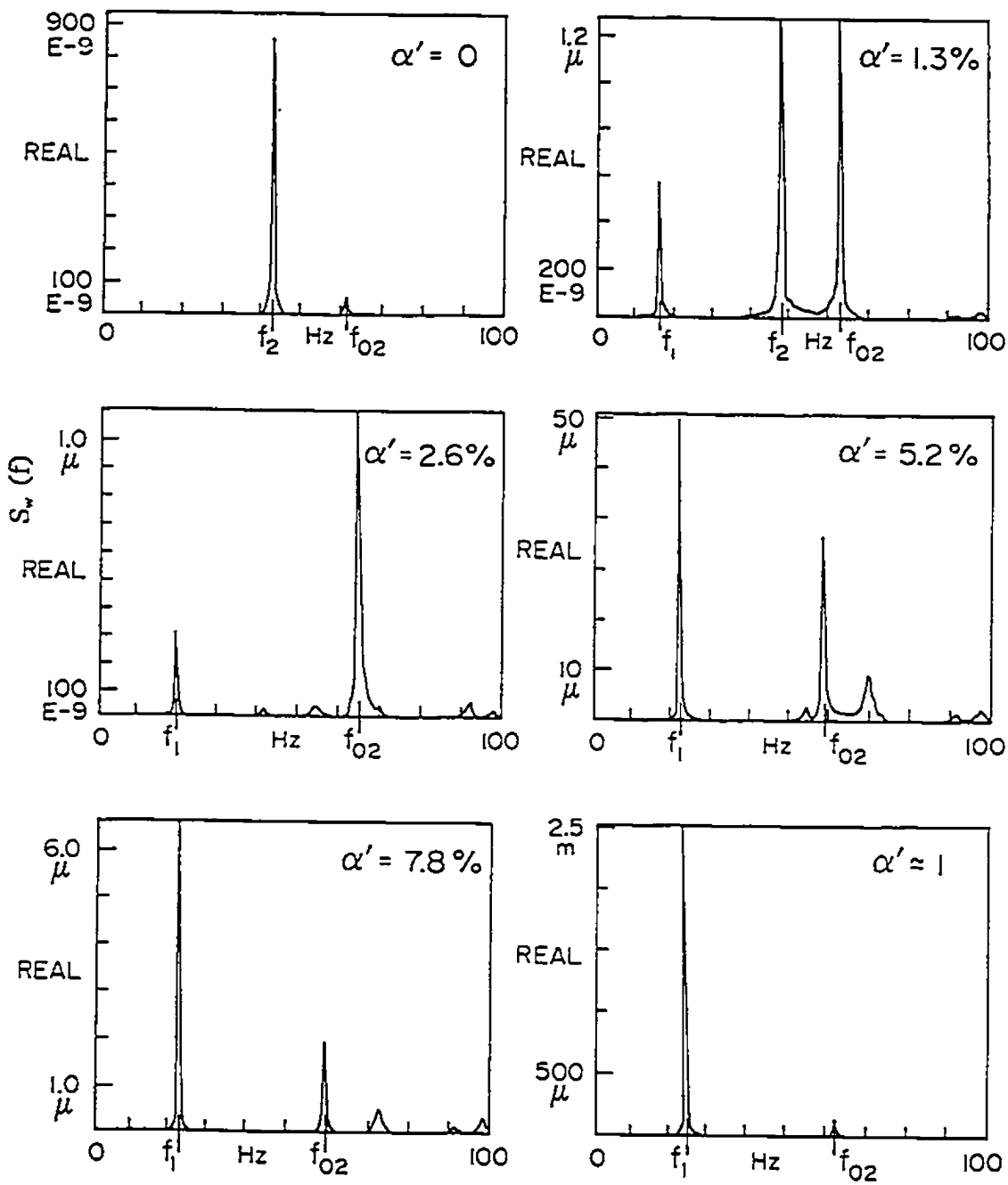

Fig. (4.6): Power spectra of response of the membrane roof to a white noise excitation

When applying harmonic excitation, the positioning of the sensors indicated in Figure (4.4) made it possible to identify the mode shapes, and to distinguish between the frequencies of both the symmetrical and antisymmetrical modes. To confirm the mode shape identification visually, a thin layer of fine white sand was uniformly spread on the surface of the membrane roof. For the plate roof, a thin layer of sawdust was used instead. The roof was then subjected to a harmonic excitation at each natural frequency, previously established for each wall opening ratio. The displacements at all six transducers were monitored while the sand or sawdust travelled toward the points of minimum displacement delineating the nodal lines and circles. Examples of the vibration modes indicated by the nodal lines and circles visualized in this way are displayed in Plates (4.3) to (4.6).

4.6 TEST RESULTS AND THEIR COMPARISON WITH THE THEORY

The experimental and theoretical free vibration results are discussed in this section. The frequency and damping results are plotted against the wall opening ratio $\alpha' = A_o/A_W$, where A_o is the total area of the openings and A_W is the area of the wall. In Figures (4.7) and (4.8), the results for no wall openings are plotted at $\alpha' = 10^{-3}$, and for the models with open bases and without the opening band the results are plotted at $\alpha' = 10^{0}$.

Plate (4.3): The fundamental modes f_1 and f_2 of the membrane model

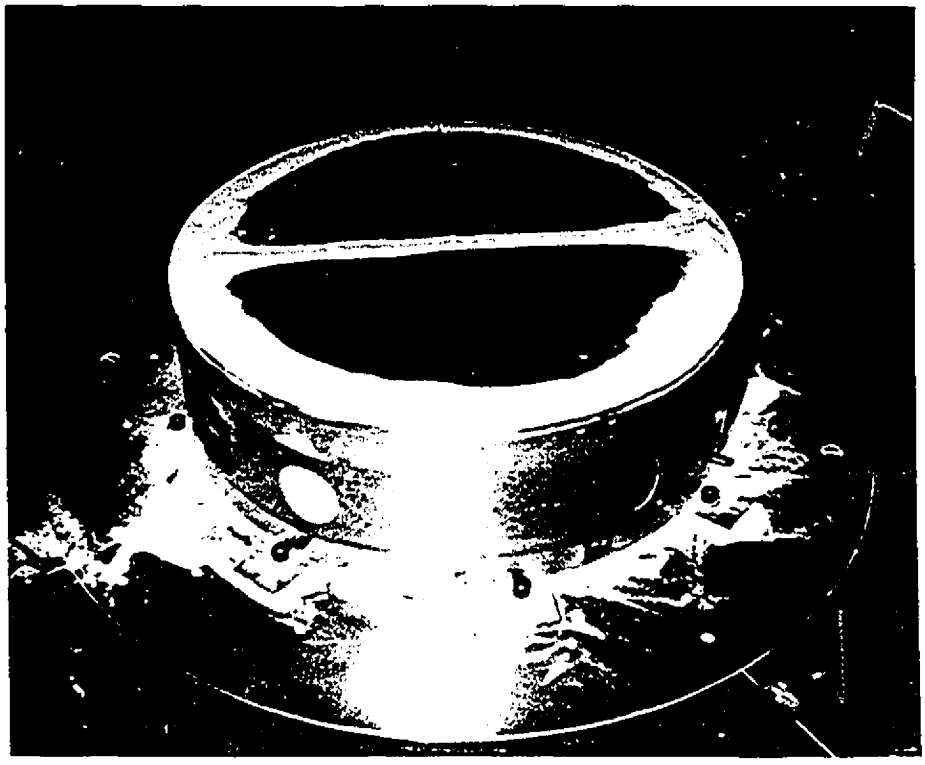

Plate (4.4): The first antisymmetrical mode f_{11} of the membrane model

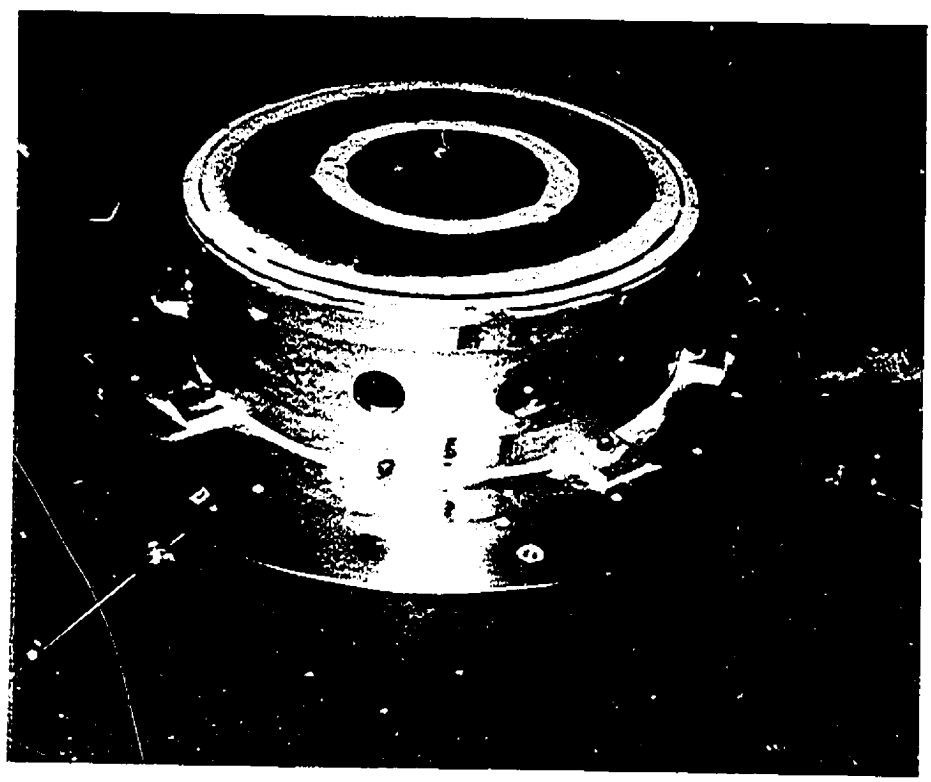

Plate (4.5): The second symmetrical mode f_{02} of the membrane model

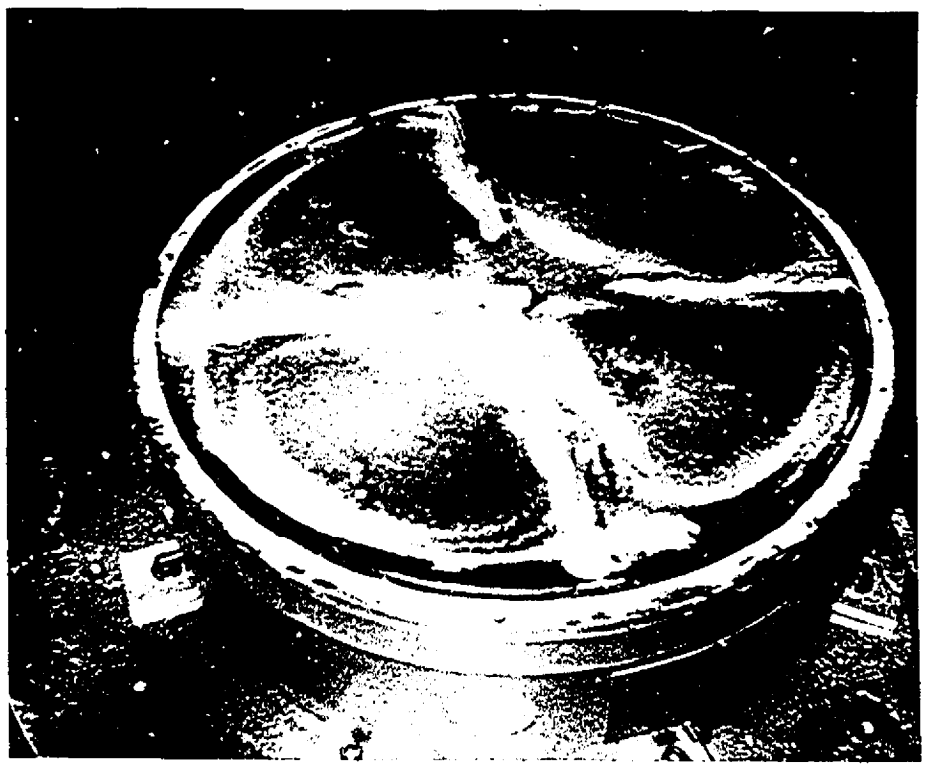

Plate (4.6): The second antisymmetrical mode f_{21} of the membrane model

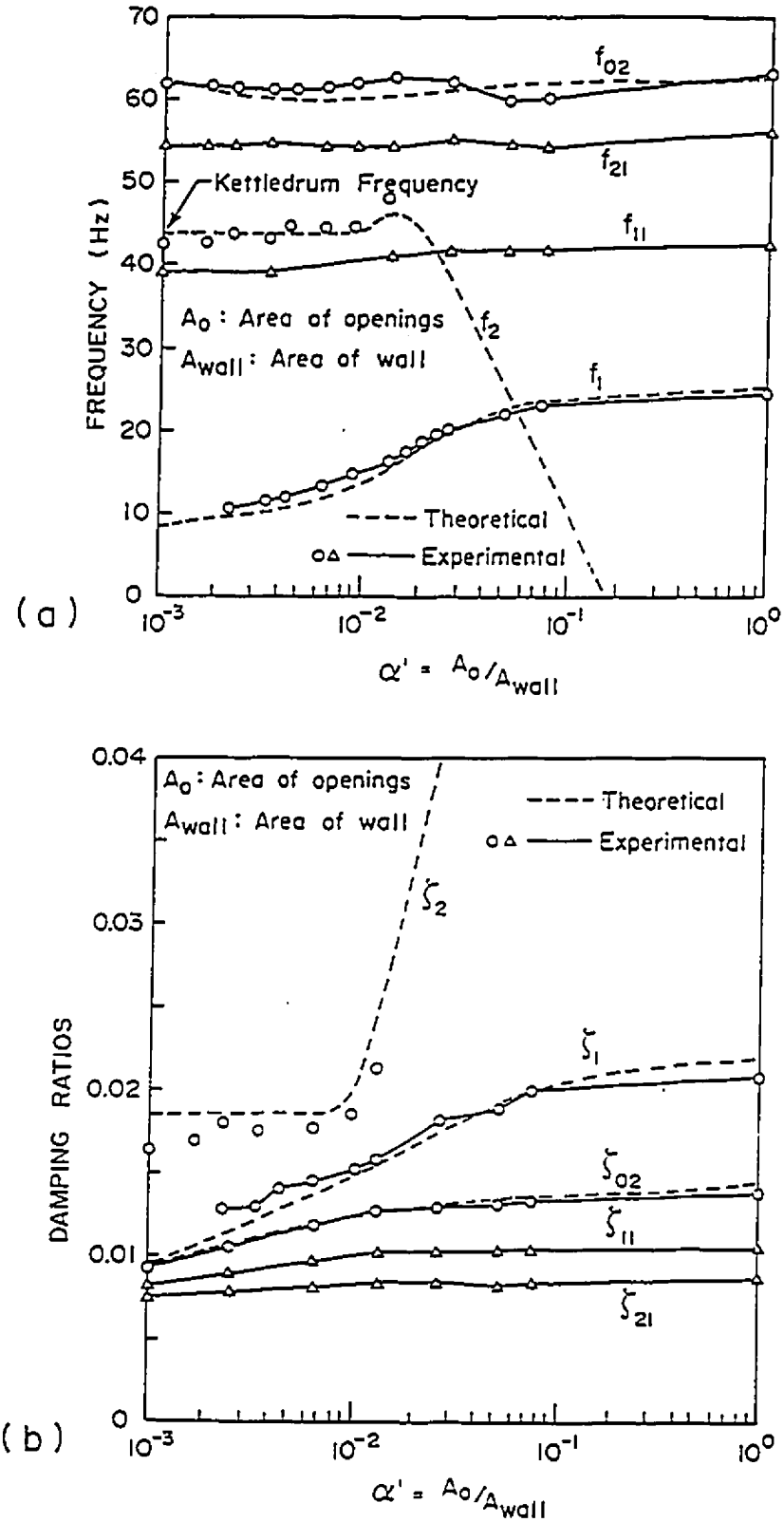

Fig. (4.7): Effect of wall openings on (a) frequencies and (b) damping ratios of the membrane roof.

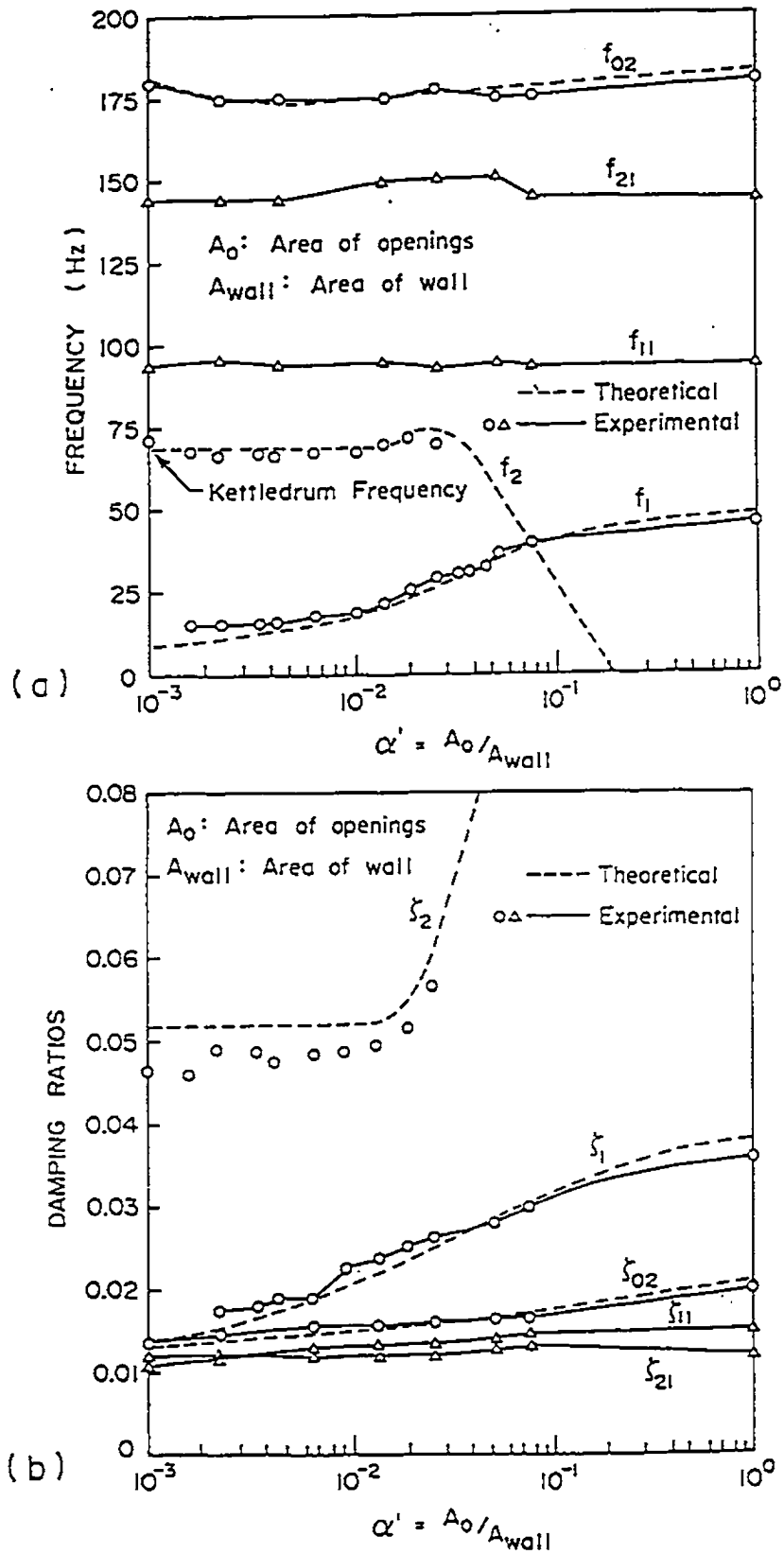

Fig. (4.8): Effect of wall openings on (a) frequencies and (b) damping ratios of the plate roof.

4.6.1 Frequencies of Free Vibration

The natural frequencies of the roof-air system were identified from the power spectra of the roof response, such as those shown in Figure (4.6). For the two models, Figures (4.7a) and (4.8a) show the variations in the natural frequencies with the wall opening ratio α'.

The opening area ratio, α', significantly affects the fundamental frequencies f_1 and f_2 associated with the symmetrical modes having no nodal lines. These frequencies were calculated using the generalized two mass system described in Chapter 3. In these two modes, the roof and the air mass at the openings vibrate in phase or in anti-phase,respectively. For the plate roof, the generalized mass, and stiffness were calculated using the formulas for natural frequencies and mode shapes given by Blevins (1979).

The first frequency, f_1, can be interpreted as one of a Helmholtz oscillator with a flexible wall. For comparison, the theoretical damped frequencies as well as modal damping were calculated from the complex eigenvalues of the generalized two-mass system. Both the structural and acoustical damping for the roofs and the openings were considered. Theoretical natural frequencies of the two models system f_1 and f_2 are plotted (in dashed lines) as shown in Figures (4.7a) and (4.8a).

The frequency f_1 diminishes with the decreasing the opening area ratio, α', and its experimental values agree well with theoretical predictions for most openings. Two extreme cases occur. For the opening area approaching zero, the frequency, f_1, vanishes which is consistent with the standard Helmholtz oscillator. For the wall opening area increasing, the natural frequency approaches that of the roof without the enclosure.

The second frequency of interest, f_2, is also associated with a symmetrical roof vibration mode without nodal lines, but the air mass at the openings moves in and out in anti-phase with the motion of the roof. Therefore, the air pressure on the roof is increased and the frequency, f_2, is higher than f_1 for low values of α'. The variation in the damped frequency, f_2, with the opening area factor, α', is also shown in Figures (4.7a) and (4.8a). For α' approaching zero, i.e. with the openings vanishing, and at very small α', the frequency, f_2, is controlled by the pneumatic stiffness of the enclosure and approaches the "kettledrum" frequency. Increasing the opening area produces a "leaking kettledrum" and has little effect at first, but at a certain α' (0.015 for the first model and about 0.03 for the second model) the damped frequency, f_2, starts rapidly dropping. This drop is caused by the loss of the pneumatic stiffness and is accelerated by a rapid increase in damping. Those frequencies, f_2, that could be reliably identified agree well with the theoretical values.

Other frequency notation used are f_{ij} in which i is the number of nodal lines and j is the order of the mode. For symmetrical mode shapes, i equals zero. The higher mode frequencies, denoted f_{ij} in Figures (4.7a) and (4.8a), are largely insensitive to the magnitude of the wall openings for both symmetrical modes and antisymmetrical modes. For these modes, the air in the enclosure is displaced from one part of the cavity to another instead of undergoing volume changes that, in turn, causes internal pressure changes.

4.6.2 Modal Damping of the Roof-Air System

For various wall opening ratios, α', the total damping ratios were experimentally obtained from the peaks of the auto-spectrum of the roof response to a white noise excitation by the HP analyzer. The analyzer establishes the modal damping by fitting eleven theoretical points to each experimental spectral peak for a chosen bandwidth until the theoretical and experimental spectral peaks are matched. The damping ratios obtained for the two models are plotted in Figures (4.7b) and (4.8b), along with the theoretically predicted values. The damping ratio of the lowest mode shape with the frequency, f_1, is denoted ζ_1. This diminishes with decreasing α' and for most α' its experimental values agree very well with the theoretical ones. For the theoretical evaluation, the structural damping ratio was assumed to be 0.8 % for the membrane and 1.2% for the plate roof.

The second basic modal damping ratio, ζ_2, corresponds to the mode shape with the frequency, f_2, and for small α', the experimental values are in good agreement with the theoretical values. Excellent agreement is also obtained for the damping ζ_{02} pertinent to the symmetrical mode with one nodal circle and a frequency f_{02}. It should be noted that the upper limit of the α' scale corresponds to the completely open base of the model. The modal damping of the higher modes ζ_{02}, ζ_{11}, and ζ_{21} varies with α' only slightly indicating a small growth with the opening area.

Altogether, the experimentally established damping ratios are in good agreement with the theoretical values. The differences observed are insignificant from a practical point of view and at least part of the differences can be attributed to the inaccuracy of the estimated value and character of the structural damping. In other words, these differences may be due to the assumption adopted in the theoretical model that the structural damping is viscous in character. This might not be the case as much of the roof damping comes from the friction at the supports and from the roof hysteresis damping which is frequency independent.

4.6.3 Effect of Enclosure Volume

The last series of experiments was devoted to the study of the effects that the enclosure volume may have on the natural frequencies and damping ratios of the roof-air system. The volume scale expressed by Equation (4.21) suggests that such effects might be present. In this investigation, special attention was paid to

the symmetrical modes of vibration f_1, f_2, and f_{o2}, which are volume changing modes. Both models were used. To study these effects, the volume of the chamber under the model was changed in a few increments by inserting cylinders of rigid styrofoam and the frequencies and damping ratios were established as before.

For model 1, the results are plotted in Figures (4.9a) and (4.9b) for several opening area ratios. The volume factor used to characterize the enclosure is the ratio of the volume of the chamber under the model base to the volume of the cavity above the base. In Figure (4.9a), this ratio is shown as the factor $(\forall_{chamber}/\forall_{model})$. The fundamental frequency can be seen to vary markedly with the chamber volume only with the wall openings absent ($\alpha' = 0$), in which case the frequency decreases with increasing the chamber volume. This is to be expected because with $\alpha' = 0$, the roof behaves as a kettledrum, whose fundamental frequency, f_2, depends on the pneumatic stiffness of the enclosure and thus on its volume.

For $\alpha' > 0$, the fundamental frequencies are lower than those for $\alpha' = 0$, but increase with increasing opening area, and slowly diminish with increasing chamber volume. This is consistent with the behaviour of the Helmholtz oscillator. The effect of the model volume on the frequency f_1 is not significant for values of α' greater than zero because the effect of air compressibility in stiffening the structure diminishes as the openings are introduced.

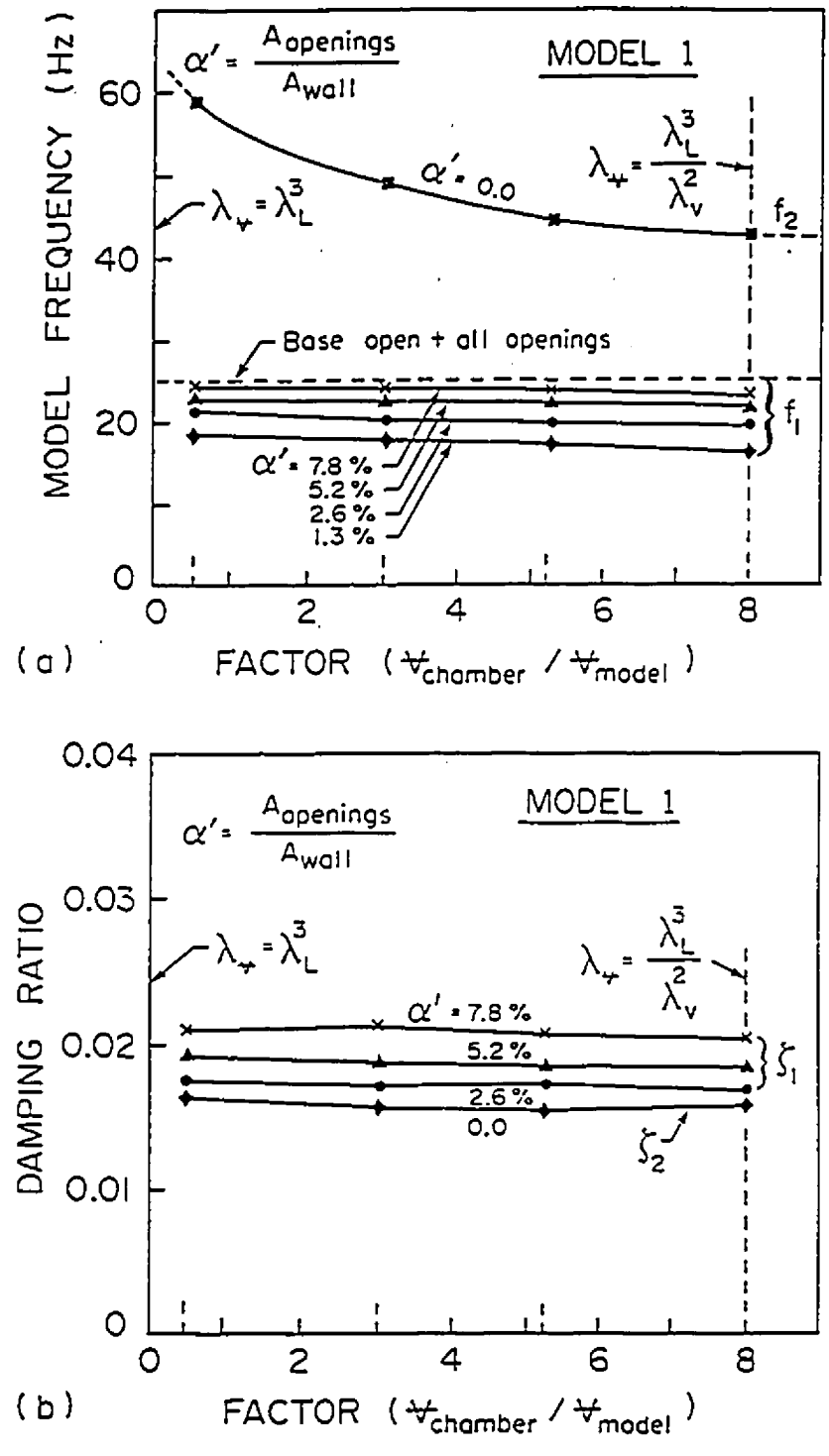

Fig. (4.9): Effect of cavity volume on (a) fundamental frequencies and (b) damping ratios of fundamental modes of the membrane roof

The vertical dashed lines denoted by λ_v in Figures (4.9a) and (4.9b) correspond to the actual volume scale of the model, with the auxiliary chamber present. It can be seen that if the internal volume was scaled according to $\lambda_v = \lambda_L^3$, the kettledrum frequency f_2 for $\alpha' = 0$ would be considerably overestimated and the Helmholtz frequencies ($\alpha' > 0$) would be somewhat overestimated.

Figure (4.9b) shows the effect of the enclosure on the damping ratios of the fundamental modes of model 1. The damping ratios increase with α', but show only a marginal increase with decreasing chamber volume and thus only a very small effect of the volume scaling. A similar trend was observed with the second symmetrical mode f_{o2} which has one nodal circle, but it was not as pronounced as for the symmetrical modes f_1 and f_2. This is because the volume changes involved with the mode f_{o2} are small compared to those of modes f_1 and f_2. In general, all the effects of the enclosure volume diminish with increasing wall openings because the internal pressure contribution diminishes.

CHAPTER 5

REVIEW OF BASIC CONSIDERATIONS FOR AIR-SUPPORTED STRUCTURES

5.1 INTRODUCTION

Air-supported structures have been in use since 1945. These structures are now a common sight in most cities, where they cover exposition halls, tennis courts, and greenhouses. Also, they can serve as inflatable forms in dome construction. The advantages of such structures are speed of erection, low cost, large span capabilities, and stability in seismic regions. The main drawbacks are their vulnerability to snow load, instability in high winds, and accidental deflation due to power or mechanical failure. The almost indefinite span capacity of these structures is a potential advantage and is a challenge to engineers. Examples of air-supported structures are shown in Plates (5.1) and (5.2).

In this chapter, the basic considerations in air-supported structures are briefly covered. These considerations include definitions, stages of construction, loading, and applications of air-supported structures. The previous work on air-supported structures is also reviewed.

5.1.1 Definitions of Pneumatic and Air structures

PNEUMATIC STRUCTURES

A pneumatic structure is a structure fabricated from a strong, flexible, airtight material that is supported by maintaining a pressure differential across the surface of the material (Bird, 1972). Pneumatic structures are classified as air-

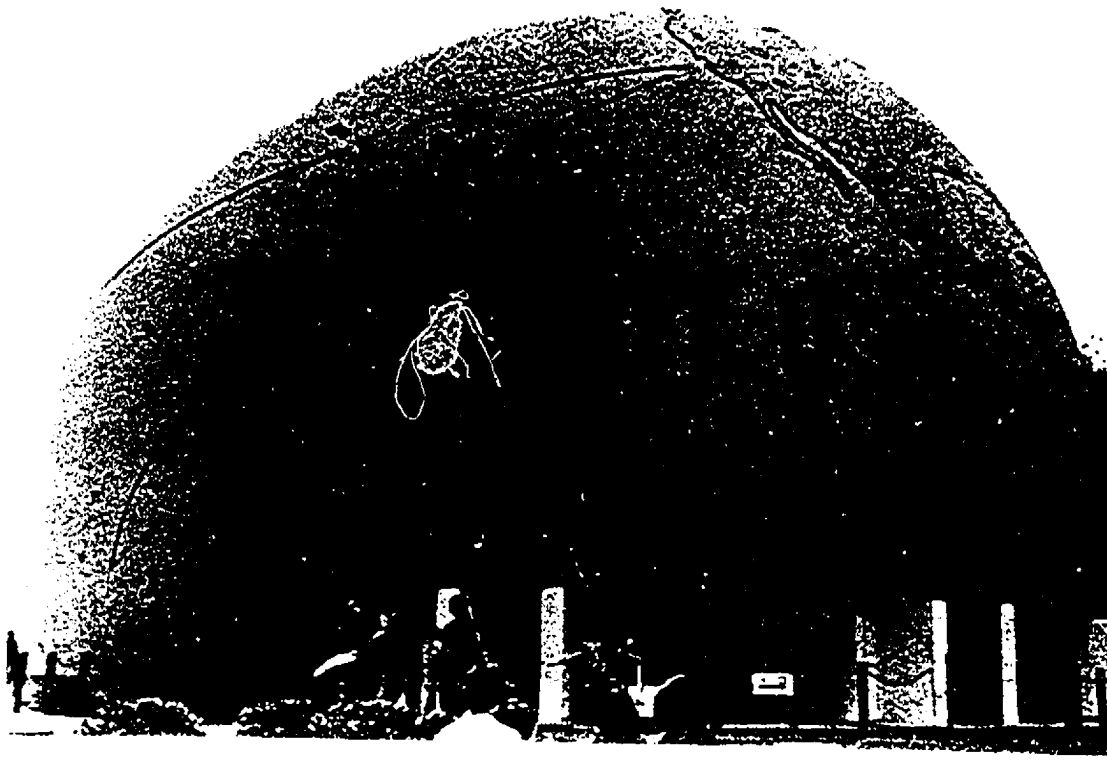

Plate (5.1): Birdair's air-supported structure for U.S. Travel Association Pavilion (Dent, 1971)

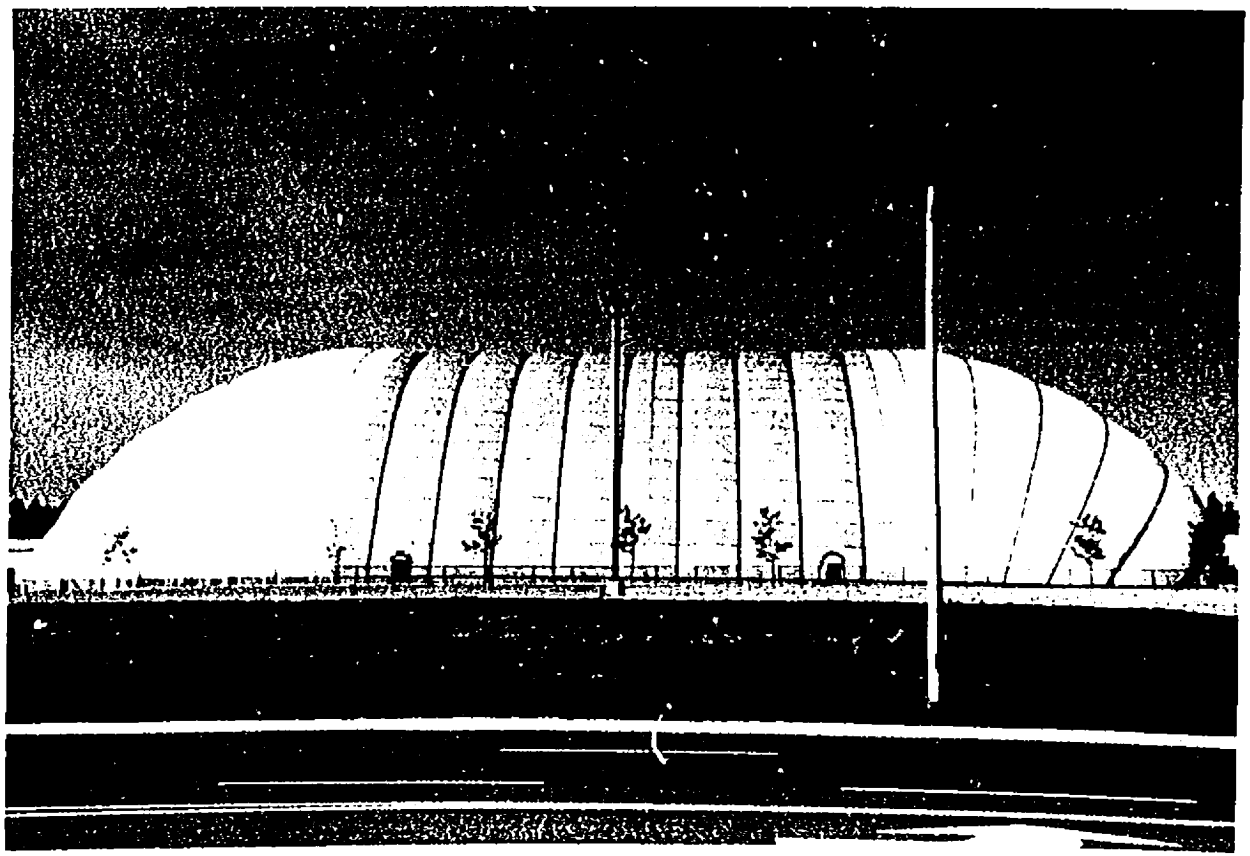

Plate (5.2): Sportsworld air-supported structure, Waterloo, Ontario .

supported structures (sometimes known as air structures), air-inflated structures, and hybrid structures.

Air Structures

An air structure is a form of pneumatic structure used to enclose useful space, i.e., a pneumatic structure that serves as a building or enclosure. Air structures can be classified as follows (Bird, 1972):

1. Air-Supported Structures

An air-supported structure is an air structure in which the entire enclosed space is maintained at a small pressure differential over the ambient atmospheric pressure to support and pretension the membrane that serves as the enclosure. Air-supported membranes can be categorized as:

A. Single Membranes

A single membrane air structure is one in which the structural envelope is a single fabric or any other material that has essentially uniform structural behaviour.

B. Reinforced Membranes

A reinforced membrane air structure is one in which the primary stresses in the structural envelope are reduced by providing cable reinforcements which carry a major share of the imposed loading. This reinforcement may serve to reshape or stabilize the envelope.

C. Multiple Membranes

Among the most innovative advances in air structures is the addition of one or several secondary membranes to the inner side of the primary load bearing membrane. These secondary membranes are usually suspended from various points or lines on the structural membrane creating one or several somewhat stagnant air spaces which can significantly reduce heat losses and gains. Typical multiple membrane systems are displayed in Figure (5.1) given by the Architectural Fabric Structures Institute (AFSI, 1977).

2. Air-inflated structures

Air-inflated structures are those in which inflated structural elements act as columns, beams, or arches to support the enclosing membranes.

3. Hybrid air structures

Air structures that combine air-inflated and structural elements with each other, or with other major structural supports are defined as hybrid air structures.

In air-supported structures, the internal pressure supports the structure just like a column or a beam in a conventional building. All air-supported structures include automatic inflation systems with continuous operation to maintain the internal pressure in the structure. These systems must include primary and secondary blowers to assure back-up inflation capacity, with each blower designed for full capacity (Leonard, 1972).

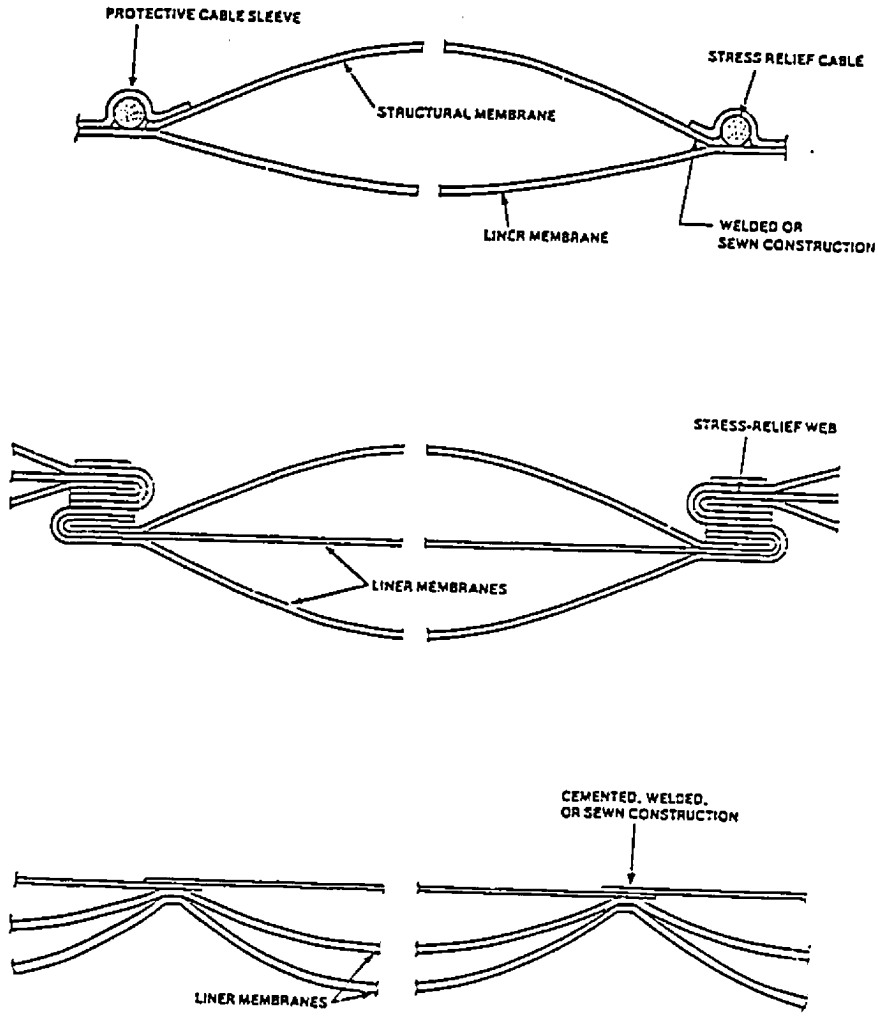

Fig. (5.1): Multiple membrane systems (AFSI, 1977)

5.1.2 Advantages and Disadvantages of Air-Supported Structures

Some advantages of air-supported structure are listed below (Leonard, 1972):

1. They are light in weight and collapsible implying easy transportation and erection of components;
2. The environmental loads are efficiently carried by direct tensile stresses without bending;
3. The leakage of gases through punctures provides an early warning of collapse and repairs can be easily made by patching; and
4. The primary load carrying mechanism is a part of the habitable environment itself, i.e., a pressurized mixture of gases.

The disadvantages of air-supported structures include (Leonard, 1972):

1. Susceptibility to large displacements and wrinkling under concentrated loads;
2. Strength requirements of the material used; and
3. The tendency to respond greatly to dynamic forces.

5.1.3 Applications of Air-Supported Structures as Inflatable Forms

With advances in material technology and the capability to predict nonlinear membrane behaviour, lightweight concrete is now being sprayed over the exterior or the interior of inflated rubber membrane structures (Leonard, 1972). This technique has several advantages:

1. The formwork in its conventional sense is eliminated and less labour is involved in the erection process;
2. If the concrete is sprayed on the interior, the plastic shell serves as a weather protection during construction;
3. The plastic inflatable formwork is light and collapsible; and
4. It can be used to shape the complex formwork necessary for a "freeform" shell.

5.2 STAGES OF CONSTRUCTION

The physical behaviour of an air-supported shell during the application of loads can be divided into three primary phases. The first phase is the **unfolding phase**. This occurs when the shell is inflated from its compact form into its initial unstrained state. The behaviour of the shell in this phase is primarily a problem in mathematical topology (Leonard, 1972).

The second phase in the inflation is the **pressurization phase**. This is the phase in which the shell is deformed from the unstrained state into the final shape. Since the displacements during this inflation process are large, this is a nonlinear problem. Additional nonlinearities in the behaviour may occur because of the nature of the material or the magnitude of the strains (Leonard, 1972).

The final phase is the **in-service phase** in which the shell is fully inflated by the internal pressure and in use. The shell might be subjected to external loads such as wind, ring loads, snow loads, or overpressures. This can be considered as

the superposition of a small displacement problem on the previous nonlinear problem. Large superposed displacement problems can be modeled as a sequence of incremental displacements. Since these small additional displacements interact with the stress resultants of the preceding pressurization phase, the equations specifying the behaviour of the shell during the in-service phase are not completely linear. In all phases of the inflatable shell behaviour, the structure is solely subjected to membrane stresses (Leonard, 1972).

The analytical implications of the behaviour of an air-supported shell are given by Leonard (1972) as follows:

A. Bending rigidity can be neglected;

B. Only tensile principal stresses are admissible;

C. Care must be exercised in the design of the supports to ensure purely membrane states without local instabilities;

D. Irrespective of constitutive relations, solution techniques for nonlinear differential equations (direct, iterative, or incremental) must be used to treat the pressurization phase;

E. Two options are available for the choice of the reference surface; the unrestrained or the pressurized middle surface; and

F. Static or dynamic loads can be handled in a piece-wise fashion in that the prior pressurization can be assumed to have stiffened the shell considerably.

5.3 LOADING

In air-supported structures, the **dead load** of the membrane is usually very small or even negligible compared to other loads. **Snow loads** vary considerably from region to region. Air-supported structures subjected to abnormally heavy snowfalls should be monitored until the danger period is over. The AFSI (1977) recommends that air-supported structures be designed to withstand a triangular distribution of snow (based on the maximum rate of snowfall). This design snow load has the maximum load at the apex, or a horizontal point, decreasing to zero at the 30° slope point as shown in Figure (5.2). The AFSI (1977) also recommends snow loads to be considered as follows:

Method A

Snow loads may be borne by virtue of the inflation pressure only by the static equilibrium required for a given snow load.

Method B

Snowfall may be melted upon contact with the air-supported structure by virtue of the heat loss from the interior. This implies that the interior is heated to a temperature that will provide the heat flow necessary to melt the accumulated snow.

Method C

Snow accumulations in excess of the structure bearing capacity defined by a given inflation pressure may be removed manually, thus ensuring that the

structure will not be overloaded.

Wind loading is primarily a function of wind velocity and the shape of the building, and varies relative to the height above the ground and the dimensions of the structure. Most building codes specify wind loads and pressure intensities at different parts of the building. The wind load distribution on a cylindrical air-supported structure is given by the AFSI (1977) as shown Figure (5.3).

Air-supported structures are known to be the structural type most resistant to seismic forces and usually remain totally unaffected by earthquake loads due to their ability to withstand large deflections and deformations without structural failure (AFSI, 1977).

The membrane of an air-supported structure should be designed to withstand the maximum stress resulting from all possible combinations of loads. This maximum stress must be less than the allowable stress of the membrane, with a considerable factor of safety, as may be required by local codes (AFSI, 1977).

5.4 SPECIAL CONSIDERATIONS

5.4.1 Deflection Characteristics

Because air-supported structures are very flexible, deflections are considerably larger than those in rigid structures. The AFSI (1977) suggests limiting deflection coefficients (not to be exceeded in the design) for both cylindrical and spherical air-supported structures as shown in Figure (5.4). These

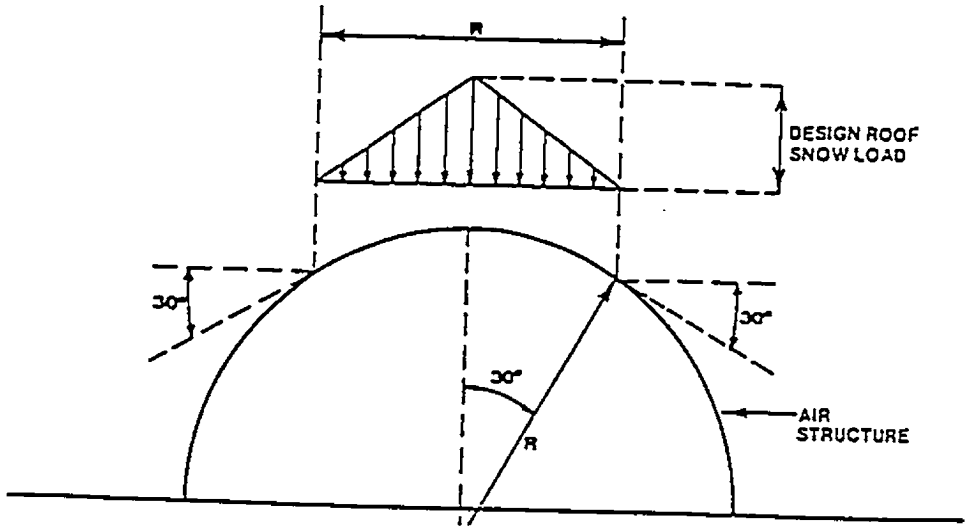

Fig. (5.2): Standard snow load on air-supported structures (AFSI, 1977)

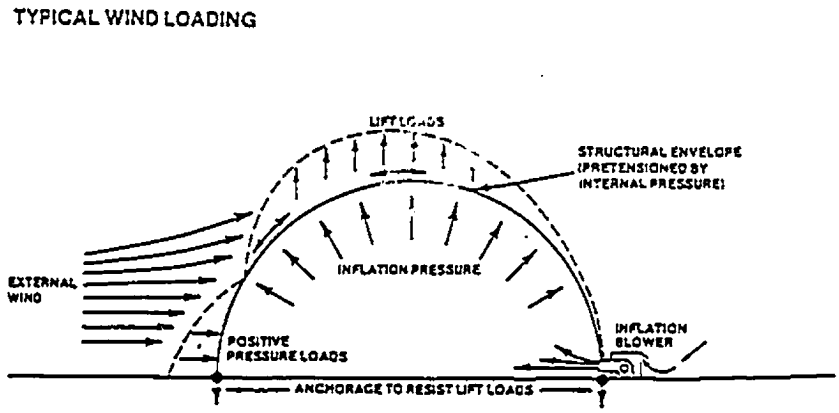

Fig. (5.3): Wind load distribution on a cylindrical roof (AFSI, 1977)

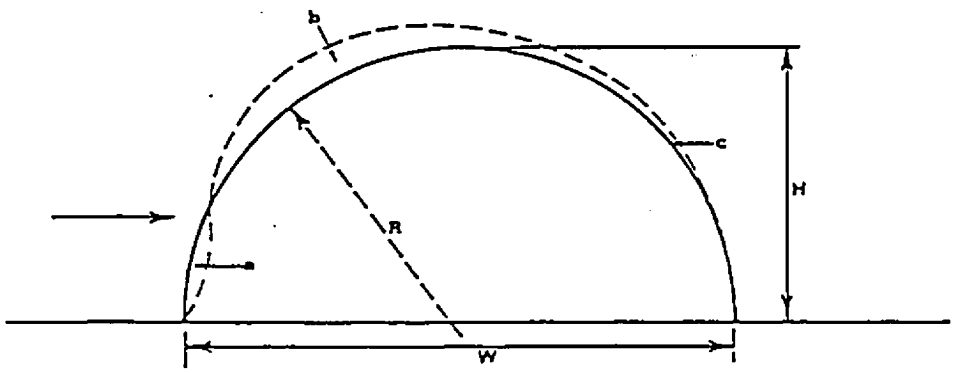

Where R = cross-sectional radius
DEFLECTION AT a, b, or c = (R) (C)
C = coefficient from table below

H/W	CYLINDRICAL			SPHERICAL		
	a	b	c	a	b	c
.3	.051	.017	.025	.043	.014	.024
.4	.074	.028	.041	.068	.022	.033
.5	.100	.040	.060	.090	.032	.050

Based on inflation pressure at .5q for H/W≤.5 and 1.0q for H/W> .5 and for 80 MPH wind velocity. (1 MPH = 0.447m/sec)

Fig. (5.4): Deflection characteristics of air-supported structures (AFSI, 1977)

deflection coefficients were derived from a combination of wind tunnel tests, empirical data, and service experience.

5.4.2 Anchorage Systems

Unlike conventional structures, the foundations for air-supported structures are designed primarily to withstand uplift forces developed by the inflation pressure and the aerodynamic wind loads. Vertical walls above grade or ring beams used to support an air structure must be designed to carry both vertical and horizontal uplift components. The anchorage system securely attaches the membrane to the ring beam or the ground and provides sealing around the perimeter of its base (AFSI, 1977).

5.4.3 Access Doors

Air-supported structures require access openings depending on the application, local codes, and the level of occupancy. **Revolving doors** are usually used to maintain the internal pressure and to allow pedestrian access to air structures. Another type of access doors is the **air lock** which has two sets of doors with an area between them large enough to fit any equipment (AFSI, 1977). Entry occurs by passing through the external door with the pressure in the air lock area equal to the exterior atmospheric pressure. Then, the external door is closed and the air lock pressure is then raised to that of the interior and the internal doors are opened.

5.4.4 Operation and Maintenance

Operation and maintenance are essential to assure the best possible service life for an air-supported structure installation. All parts of the air-supported structure must always be maintained in good serviceable condition. Besides, the entire air structure system is usually inspected at quarterly intervals to insure that the installation is maintained in good operating condition (AFSI, 1977).

Air-supported structures have been shown to be inherently fire resistant. However, it is desirable to control the selection of fabric to avoid the use of flammable materials. Concrete sprayed fabrics or coated fabrics can meet the most stringent flame resistance requirements that may be required by local codes [Leonard (1972) and AFSI (1977)].

5.5 REVIEW OF PREVIOUS WORK

There is an extensive literature dealing with the general mechanics of shells and air-supported structures (Kraus, 1967; Vol'mir, 1972; and Firt, 1983). Many investigators studied the behaviour of these roof under static loads; however, only a limited number of studies were devoted to the aerodynamics of such roofs. This section contains a brief review of the previous studies dealing with air-supported structures.

Uemura (1971) analyzed the membrane tension and deformations of a long cylindrical, inflated single-wall tent under strong wind blowing on its broadside. The analysis was based on finite deformation, membrane theory.

Reitmeier and Punnett (1972) presented various features of the design of large, air-supported spherical domes using cables as the major load-carrying members. The optimization of the profile for minimum aerodynamic loading, which was based upon a finite element method, indicated that a rise to span ratio of 0.20 is most favourable.

For spherical membranes Fournier and Greenberg (1972) presented a graphical superposition of the membrane stress resultants resulting from the dead load, the snow load, and the internal pressure. Haug (1972) investigated the static behaviour of pneumatic structures as elastic structures which undergo large displacements using a finite element method.

The forced vibration of an infinitely long, cylindrical air-supported structure under harmonic loading was analyzed by Firt (1983). The final deflections and elongations of the membrane due to static loads were considered, and the deformed cross-section of the structure was replaced with a system of circular arcs and straight sectors.

Malcolm and Glockner (1978) examined the equilibrium of a central line static load on a cylindrical inflatable structure. Spinelli (1978) described a method to compute the displacements and the internal forces in a cylindrical air-supported membrane under wind loads. Malcolm and Glockner (1979) investigated the optimum cable form for cylindrical air-supported structures. This work was

extended to cover the collapse by ponding of air-supported spherical caps, assuming that the membrane is inextensible (Malcolm and Glockner, 1981).

Vinogradov et al. (1981) showed that the dynamic characteristics of cable-reinforced, air-supported structures are strongly dependent on the internal pressure and static loading including the equivalent static wind pressure. The results indicated that the changes in the natural frequencies can be considered as proportional to the square root of the internal pressure.

Srivastava et al. (1984) conducted wind tunnel experiments on a series of rigid and flexible spherical models to establish the wind pressure distribution. The results suggested that the distribution of the wind pressure coefficient C_p and the displacements of the flexible model depend on the internal pressure q_o and the dynamic wind pressure q.

Mataki et al. (1985) dealt with the wind pressure affecting low-profile cable-reinforced, air-supported structures and their structural characteristics. The study was based on wind tunnel and forced displacement vibration tests on a large-scale model. Williams (1985) described how numerical methods can be used to produce geometrical forms for different classes of curved structures made of fabric or cable nets.

Maaskant and Rooda (1985) studied (both theoretically and experimentally) the behaviour of cylindrical air-supported membranes subjected to a concentrated line load. The results showed that the structure may bifurcate from the symmetrical shape into a nonsymmetrical shape at loads less than the critical buckling load.

Ikoma and Sugizaki (1986) conducted a series of wind pressure measurements and melting snow loading tests on full-scale, air-supported domes. The reinforcing cable stress and the roof vertical displacement were measured when the simulated snow load was applied to the roof model.

Daw (1987) conducted a wind tunnel study on a semicircular cylindrical model to study the motion-dependent aeroelastic forces. A forced model oscillation technique was used to study the dependence of the aeroelastic forces on the turbulence intensity, the wind speed, the amplitude of oscillation, and on the geometric details of the model. The results indicated that for semi-circular structures in cross winds, the aeroelastic coefficients varied with the reduced frequency. The aeroelastic coefficients were independent of the turbulence intensity and were not sensitive to the scaling effects of the Reynolds number.

Daw and Davenport (1989) found that for semi-cylindrical structures, the aerodynamic stiffness was a negative term and reduced the total static stiffness. The aerodynamic damping was positive and increased the resistance to the dynamic movement of the structure. As the structure became heavier and stiffer,

the relative influence of the aeroelastic forces on the response to turbulent wind was reduced. It was concluded that the resonant frequencies and the amplitudes of the motion might be reduced due to the aeroelastic forces.

5.6 SUMMARY

Previous work dealing with the mechanics of air-supported structures was to analyze their static behaviour under concentrated and snow loads, and to study the free undamped vibrations of cylindrical air-supported structures. Other pervious work dealing with the aerodynamics of these structures was to find the minimum internal pressure required to prevent local buckling, to establish wind pressure distribution, to estimate wind-induced response using equivalent static wind pressures, and to study the aerodynamic forces on the response to turbulent wind.

In this study, closed form solutions are derived for the evaluation of natural frequencies and modal damping of cylindrical and shallow spherical air-supported structures, and the accuracy of these solutions is assessed by comparisons with finite element solutions. The free vibration characteristics of a hemispherical air-supported model are examined for different internal pressures and enclosure volumes.

Wind tunnel tests were conducted on the hemispherical aeroelastic model to investigate the wind-induced response and the internal pressure fluctuations for different wind speeds, exposures, enclosure volumes, and internal pressures.

A semi-analytical approach is established to predict the wind-induced response of air-supported structures, which is based on external pressure measurements and static deflections. A rigid hemispherical model was wind-tunnel-tested to measure the external pressures for different exposure conditions. Static deflections were calculated theoretically using a finite element method for different internal pressures.

CHAPTER 6

FREE VIBRATION OF AIR-SUPPORTED STRUCTURES

6.1 Introduction

The natural frequencies and modal damping ratios are very important in the design of air-supported structures, as under dynamic loading every structure vibrates in some of its natural modes. Knowledge of the natural frequencies and modal damping ratios is necessary to investigate the forced vibration under dynamic loads, particularly wind loads.

6.2 FREE VIBRATION OF CYLINDRICAL AIR-SUPPORTED STRUCTURES

The governing equations of air-supported structures represent a special case of the equations of shells whose study has a long history. The vibration of cylindrical shells (with simplified equations) was first studied by Sophie Germaine before 1821. This problem was also investigated by Lord Rayleigh in 1882 and by Love in 1888 (Soedel, 1981). Subsequent developments to the problem were made by Rayleigh (1945), Reissner (1955), Oniashvili (1957), Vlasov (1960), Kalnins (1967), Sharama (1971), Vol'mir (1972), Lissa (1973), Soedel (1981), and others.

A solution to the free undamped vibration of an infinitely long, cylindrical air-supported structure was given by Firt (1983). However, for air-supported structures, the damping is rather high (compared to conventional structures) due to the light weight of the structures. Total damping stems primarily from the

structural and acoustical damping associated with the energy radiated from the roof surface as sound waves. Another damping source is the pneumatic damping which depends on the volume flow rate from fans into the structure, and the leakage rate from the structure (Kind, 1984).

In this section, both the structural and acoustical damping are included in the governing equations of free vibration of cylindrical air-supported structures extending the solution due to Firt (1983). A characteristic equation is derived for the damped free vibration and used to evaluate the modal parameters of natural vibrations. Comparisons are made between the results of the derived equation, a finite element method, and those of Firt (1983).

6.2.1 Assumptions of the Analysis

In this analysis, natural vibrations of cylindrical air-supported structures are investigated using the following assumptions:

1. The structure is infinitely long, and the influence of the ends is neglected.
2. The dynamic deflections of the membrane are small oscillations about the static deflections.
3. The structural and acoustical damping are viscous in character and act uniformly in the radial direction of the membrane.

6.2.2 Differential Equations of Free Damped Vibration

Figure (6.1) shows an infinitely long cylindrical air-supported structure with radius R and central angle α. Figure (6.2) represents an element of length ds and of unit width, cut from the cylindrical air-supported membrane. The static internal pressure is q_o and the static axial force due to the internal pressure is q_oR. The tangential inertia force is m ds $\partial^2v/\partial t^2$, where $v(\theta,t)$ is the tangential displacement, and m is the mass per unit area. The radial inertia force is m ds $\partial^2w/\partial t^2$, where $w(\theta,t)$ is the radial displacement, and θ is an angle as shown in Figure (6.1). The dynamic axial forces acting on the element are F and $F+(\partial F/\partial\theta)d\theta$.

Introducing the structural and acoustical damping terms to the governing equations of a cylindrical air-supported structure, reduced from the shell equation and given by Firt (1983), yields

for the tangential direction

$$m\frac{\partial^2 v}{\partial t^2}\,ds - \left(F + \frac{\partial F}{\partial\theta}\,d\theta + q_o R\right)\cos d\theta + F + q_o R = 0 \qquad (6.1a)$$

and for the radial direction

$$m\,ds\frac{\partial^2 w}{\partial t^2} + c_t\frac{\partial w}{\partial t}\,ds - \left(F + q_o R\right)\cos\left(\frac{\pi}{2} - d\theta\right) + q_o\,ds = 0 \qquad (6.1b)$$

In the above equations, $c_t = c_s + c_a$ where c_t, c_s, and c_a are the total damping, the structural damping, and the acoustical damping coefficients, respectively. As the dynamic deflections are assumed to be very small, the following can be written

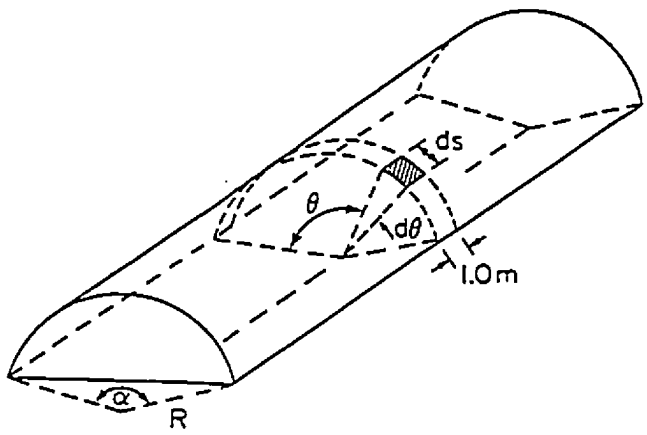

Fig. (6.1) : An infinitely long, cylindrical air-supported structure

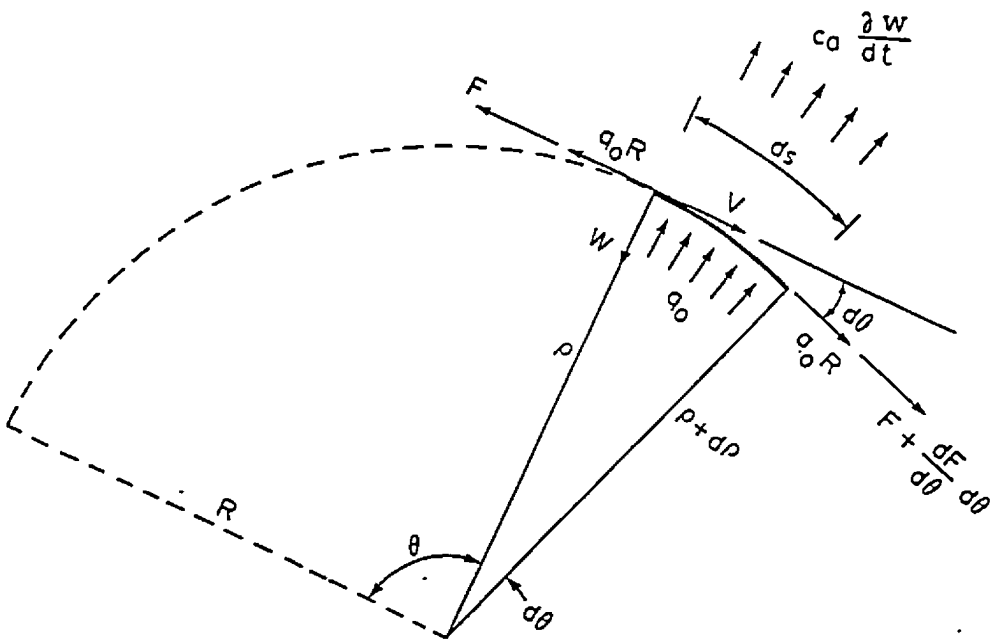

Fig. (6.2) : Forces on an element of a cylindrical air-supported structure

$$\cos d\theta = 1$$

$$\cos\left(\frac{\pi}{2} - d\theta\right) = \sin\theta \; d\theta$$

$$ds = \rho \, d\theta \tag{6.2}$$

where ρ is the instantaneous radius of curvature of the section. Substituting Equations (6.2) into Equations (6.1a) and (6.1b) gives

$$\frac{1}{\rho}\frac{\partial F}{\partial \theta} - m\frac{\partial^2 v}{\partial t^2} = 0 \tag{6.3a}$$

$$\frac{F}{\rho} + q_o\left(\frac{R}{\rho} - 1\right) - m\frac{\partial^2 w}{\partial t^2} - c_t\frac{\partial w}{\partial t} = 0 \tag{6.3b}$$

The following geometric relations hold for a cylindrical membrane with circular cross-section (Soarce, 1967):

$$w = \frac{\partial v}{\partial \theta} \tag{6.4a}$$

$$\frac{R}{\rho} = 1 + \frac{\partial \psi}{\partial \theta} \tag{6.4b}$$

where

$$\psi = \frac{1}{R}\left(\frac{\partial w}{\partial \theta} + \int w \, d\theta\right) \tag{6.5}$$

Substituting Equation (6.5) into Equation (6.6b) gives

$$\frac{1}{\rho} = \frac{1}{R}\left(1 + \frac{1}{R}\frac{\partial^2 w}{\partial \theta^2} + \frac{1}{R}w\right) \tag{6.6}$$

Substituting Equations (6.5) and (6.6) into Equations (6.3a) and (6.3b), and neglecting the higher order product of the quantities F and w and their derivatives yields

$$\frac{1}{R}\frac{\partial^2 F}{\partial \theta^2} - m\frac{\partial^2 w}{\partial t^2} = 0 \tag{6.7a}$$

$$\frac{F}{R} + \frac{q_o}{R}\left(\frac{\partial^2 w}{\partial \theta^2} + w\right) - m\frac{\partial^2 w}{\partial t^2} - c_t\frac{\partial w}{\partial t} = 0 \tag{6.7b}$$

Differentiating Equation (6.7b), and substituting into Equation (6.7a), the following linear partial differential equation of the radial deflection w of the free vibration of the membrane is:

$$\frac{\partial^2 w}{\partial \theta^2} + \frac{\partial^2}{\partial \theta^2}\left(w - \frac{mR}{q_o}\frac{\partial^2 w}{\partial t^2} - \frac{c_t R}{q_o}\frac{\partial w}{\partial t}\right) + \frac{mR}{q_o}\frac{\partial^2 w}{\partial t^2} = 0 \qquad (6.8)$$

The inclusion of damping calls for a complex approach which is quite different from that of Firt (1983). The radial deflection and the dynamic axial force are assumed as

$$w(\theta,t) = w(\theta)\, e^{\mu t} \qquad (6.9)$$

$$F(\theta,t) = F(\theta)\, e^{\mu t} \qquad (6.10)$$

where μ is the complex frequency, $w(\theta)$ is the amplitude of the radial deflection w, and $F(\theta)$ is the amplitude of the dynamic force F. Substituting Equation (6.9) into Equation (6.8) yields

$$\frac{d^4 w}{d\theta^4} + \frac{d^2 w}{d\theta^2}\left(1 - \frac{mR\mu^2}{q_o} - \frac{c_t R\mu}{q_o}\right) + \frac{mR\mu^2}{q_o} w = 0 \qquad (6.11a)$$

or

$$\frac{d^4 w}{d\theta^4} + \frac{d^2 w}{d\theta^2}\left[1 - \lambda\left(1 + \frac{c_t}{\mu m}\right)\right] + \lambda w = 0 \qquad (6.11b)$$

where

$$\lambda = \frac{mR\mu^2}{q_o} \qquad (6.12)$$

Substituting Equations (6.10) and (6.9) into Equation (6.7b) gives the dynamic axial force, F, as

$$F = -q_o\left[\frac{d^2 w}{d\theta^2} + w\left\{1 - \lambda\left(1 + \frac{c_t}{m\mu}\right)\right\}\right] \qquad (6.13)$$

6.2.3 Solution of the Differential Equation

The solution of Equation (6.11b) follows from the standard approach to homogeneous differential equations and can be written as

$$w(\theta) = \sum_{i=1}^{4} A_i \, e^{\beta_i \theta} \tag{6.14}$$

where A_i, i = 1, 2, 3, and 4, are constants. The parameters β_i are the roots of the following characteristic equation:

$$\beta^4 + \lambda_1 \beta^2 + \lambda = 0 \tag{6.15}$$

where

$$\lambda_1 = 1 - \lambda \left(1 + \frac{c_i}{m \mu}\right) \tag{6.16}$$

The parameters λ_1 and β are functions of the internal pressure, the mass per unit area, the radius of the section, and the structural as well as acoustical damping coefficients. Equation (6.15) has two imaginary roots and two real roots, i.e.,

$$\beta_{1,2} = \pm \frac{i}{\sqrt{2}} \left[\lambda_1 + \left(\lambda_1^2 - 4 \lambda \right)^{\frac{1}{2}} \right]^{\frac{1}{2}} \tag{6.17a}$$

and

$$\beta_{3,4} = \pm \frac{1}{\sqrt{2}} \left[-\lambda_1 + \left(\lambda_1^2 - 4 \lambda \right)^{\frac{1}{2}} \right]^{\frac{1}{2}} \tag{6.17b}$$

where $i = \sqrt{-1}$; λ and λ_1 are as given in Equations (6.12) and (6.16), respectively. Thus, the general solution of Equation (6.11) may be written as

$$w(\theta) = A_1 e^{\beta_1 \theta} + A_2 e^{\beta_2 \theta} + A_3 e^{\beta_3 \theta} + A_4 e^{\beta_4 \theta} \tag{6.18}$$

According to Equation (6.5a), the amplitude of the tangential displacement v in the direction of the tangent is given by

$$v(\theta) = \int w \, d\theta = \frac{A_1}{\beta_1} e^{\beta_1 \theta} + \frac{A_2}{\beta_2} e^{\beta_2 \theta} + \frac{A_3}{\beta_3} e^{\beta_3 \theta} + \frac{A_4}{\beta_4} e^{\beta_4 \theta} \tag{6.19}$$

According to Equation (6.18)

$$\frac{dw}{d\theta} = A_1 \beta_1 e^{\beta_1\theta} + A_2 \beta_2 e^{\beta_2\theta} + A_3 \beta_3 e^{\beta_3\theta} + A_4 \beta_4 e^{\beta_4\theta} \qquad (6.20)$$

Then, the amplitude of the angle of rotation of the cross-section ψ of the circular section is

$$R\psi = A_1 \left(\frac{1}{\beta_1} + \beta_1 \right) e^{\beta_1\theta} + A_2 \left(\frac{1}{\beta_2} + \beta_2 \right) e^{\beta_2\theta} + A_3 \left(\frac{1}{\beta_3} + \beta_3 \right) e^{\beta_3\theta} + A_4 \left(\frac{1}{\beta_4} + \beta_4 \right) e^{\beta_4\theta} \qquad (6.21)$$

Differentiating Equation (6.18) with respect to θ gives

$$\frac{d^2w}{d\theta^2} = A_1 \beta_1^2 e^{\beta_1\theta} + A_2 \beta_2^2 e^{\beta_2\theta} + A_3 \beta_3^2 e^{\beta_3\theta} + A_4 \beta_4^2 e^{\beta_4\theta} \qquad (6.22)$$

Substituting Equation (6.22) into Equation (6.13) gives the amplitude of the dynamic force as

$$\frac{F}{q_o} = -A_1 \left(\lambda_1 + \beta_1^2 \right) e^{\beta_1\theta} - A_2 \left(\lambda_1 + \beta_2^2 \right) e^{\beta_2\theta} - A_3 \left(\lambda_1 + \beta_3^2 \right) e^{\beta_3\theta} - A_4 \left(\lambda_1 + \beta_4^2 \right) e^{\beta_4\theta} \qquad (6.23)$$

According to Figure (6.1), the boundary conditions of the cylindrical air-supported structure are

$$w(0) = 0 \,,\; w(\alpha) = 0 \,,\; v(0) = 0 \;\text{ and }\; v(\alpha) = 0 \qquad (6.24)$$

Substituting Equations (6.24) into Equations (6.18) and (6.19) yields the following four homogenous algebraic equations

$$A_1 + A_2 + A_3 + A_4 = 0 \qquad (6.25a)$$

$$A_1 e^{\beta_1\alpha} + A_2 e^{\beta_2\alpha} + A_3 e^{\beta_3\alpha} + A_4 e^{\beta_4\alpha} = 0 \qquad (6.25b)$$

$$\frac{A_1}{\beta_1} + \frac{A_2}{\beta_2} + \frac{A_3}{\beta_3} + \frac{A_4}{\beta_4} = 0 \qquad (6.25c)$$

$$\frac{A_1}{\beta_1} e^{\beta_1\alpha} + \frac{A_2}{\beta_2} e^{\beta_2\alpha} + \frac{A_3}{\beta_3} e^{\beta_3\alpha} + \frac{A_4}{\beta_4} e^{\beta_4\alpha} = 0 \qquad (6.25d)$$

Equations (6.25) are linear with respect to A_i, i = 1, 2, 3, and 4. A condition for the existence of a non-trivial solution is

$$\Delta = \begin{vmatrix} 1 & 1 & 1 & 1 \\ e^{\beta_1\alpha} & e^{\beta_2\alpha} & e^{\beta_3\alpha} & e^{\beta_4\alpha} \\ \frac{1}{\beta_1} & \frac{1}{\beta_2} & \frac{1}{\beta_3} & \frac{1}{\beta_4} \\ \frac{1}{\beta_1} e^{\beta_1\alpha} & \frac{1}{\beta_2} e^{\beta_2\alpha} & \frac{1}{\beta_3} e^{\beta_3\alpha} & \frac{1}{\beta_4} e^{\beta_4\alpha} \end{vmatrix} = 0 \qquad (6.26)$$

Some elements of the determinant in Equation (6.26) are complex, and depend on the structural and acoustical damping coefficients. From Equation (6.26), the characteristic equation for the free damped vibration of an infinitely long cylindrical air-supported structure can be written as:

$$\frac{1}{4\lambda} (\beta_1 - \beta_3)^2 \sinh (\beta_1 \alpha) \sinh (\beta_3 \alpha) = 0 \qquad (6.27)$$

where λ, β_1 and β_3 are given by Equation (6.17). Equations (6.26) or (6.27) can be solved by trial and error, to get the complex frequency λ_j. Equation (6.26) was solved numerically using the LINPACK subroutines CGEDI and CGEFA, and compared with the results of Equation (6.27) to check the results. Substituting the value of λ_j into Equation (6.12), gives pairs of conjugate eigenvalues for each mode j as

$$\mu_j = \mu_{1j} \pm i\, \mu_{2j} \qquad (6.28)$$

From the complex eigenvalue μ_j, the damped frequency is

$$\omega_j' = \text{Im}\, \mu_j = \mu_{2j} \qquad (6.29)$$

and the modal damping ratio is

$$\varsigma_j = \text{Re}\ \mu_j \,/\, |\ \mu_j\ | = \mu_{1j} \,/\, |\ \mu_j\ | \tag{6.30}$$

It must be noted that for free undamped vibration, which is a special case of the damped vibration, $c_r = 0$ and the value of μ_{1j} equals zero. To find the damped mode shape, the value of the characteristic number λ_j is substituted into Equations (6.25) and solved for the ratios A_i/A_1, i = 2, 3, and 4. Also, substituting the characteristic number λ_j given by Equation (6.12) into Equations (6.21) and (6.23) gives the amplitude of the angle of rotation ψ_j and the dynamic axial force F_j for mode j.

It may be mentioned that Firt (1983) studied the criteria for the overall aerodynamic instability of a cylindrical air-supported membrane using an equation formally identical with Equation (6.26). A similar approach was used to define the critical frequency at which the aerodynamic instability occurs. However, the parameters in Firt's solution are quite different from those used in this study and defined by Equation (6.17).

6.3 FREE UNDAMPED VIBRATION OF CYLINDRICAL STRUCTURES

Neglecting the damping terms in Equations (6.1) and (6.2) and following a similar procedure, Firt (1983) derived the equation

$$2\ (\ 1 - \cos a \cosh b\ ) + \frac{b^2 - a^2}{a\ b} \sin a \sinh b = 0 \tag{6.31}$$

where

$$a = \frac{\alpha}{\sqrt{2}} [\ 1 + \lambda + (\ 1 + 6\ \lambda + \lambda^2\ )^{\frac{1}{2}}\ ]^{\frac{1}{2}} \tag{6.32a}$$

$$b = \frac{\alpha}{\sqrt{2}} [-1 - \lambda + (1 + 6\lambda + \lambda^2)^{\frac{1}{2}}]^{\frac{1}{2}} \qquad (6.32b)$$

and

$$\lambda = \frac{mR\omega^2}{q_o} \qquad (6.33)$$

The parameters a and b in Equation (6.31) are different from the parameters β_i, i = 1, 2, 3, and 4 in Equation (6.27), which are damping dependent. The complex eigenvalue μ_{ij} in Equation (6.28) has real and imaginary parts, while the circular frequency ω, in Firt's solution, has only a real part.

6.4 EXAMPLE OF A CYLINDRICAL STRUCTURE

In this example, a cylindrical air-supported structure with a central angle $\alpha = \pi$ is considered. The structure has the following parameters:

Internal pressure	q_o = 50 to 250 Pa
Radius	R = 10.00 m
Mass per unit area	m = 1 kg/m^2

In this study, the internal pressure was varied to investigate its effects on the natural frequencies of the structure.

The finite element program ABAQUS, available on the UWO mainframe, can solve nonlinear problems, such as the problem of pressurizing an air-supported structure in which the displacements are large. The program uses Riks' method rather than the Newton-Raphson iteration solution. Riks' method controls the solutions by using increments of fixed size along the equilibrium path in the load-

displacement space. The accuracy of the solution is controlled by specifying tolerance values. The convergence criterion in the program is that all force residuals must be less than the specified tolerance values and the analysis ends when no increments exceed these specified values.

For comparison purposes, different types of elements were used in analyzing the cylindrical air-supported structure. Among the used elements were a 3-node beam element, B22 as shown in Figure (6.3); a 2-node beam element, B23, as shown in Figure (6.4), and an 8-node membrane element, S8R, as shown in Figure (6.5).

6.4.1 Static Analysis under Standard Snow Load

The AFSI (1977) recommends that air-supported structures be designed to withstand a triangular distribution of snow as shown in Figure (5.2). The maximum load at the apex decreases to zero at the 30° slope point. The maximum design snow load for the roof was taken with a value of 360 N/m at the apex as shown in Figure (6.6). The displaced shape of the cylindrical air-supported structure under snow loads is shown in Figure (6.7). It can be seen that an internal pressure of 150 Pa is sufficient to stabilize the structure under the standard snow load. The maximum displacement was about 1.0 meter at the center, and the displaced shape becomes elliptical as shown in Figure (6.7). The concentrated loads in Figure (6.7) are for a 1.0 m strip of the infinitely long cylindrical air-supported structure.

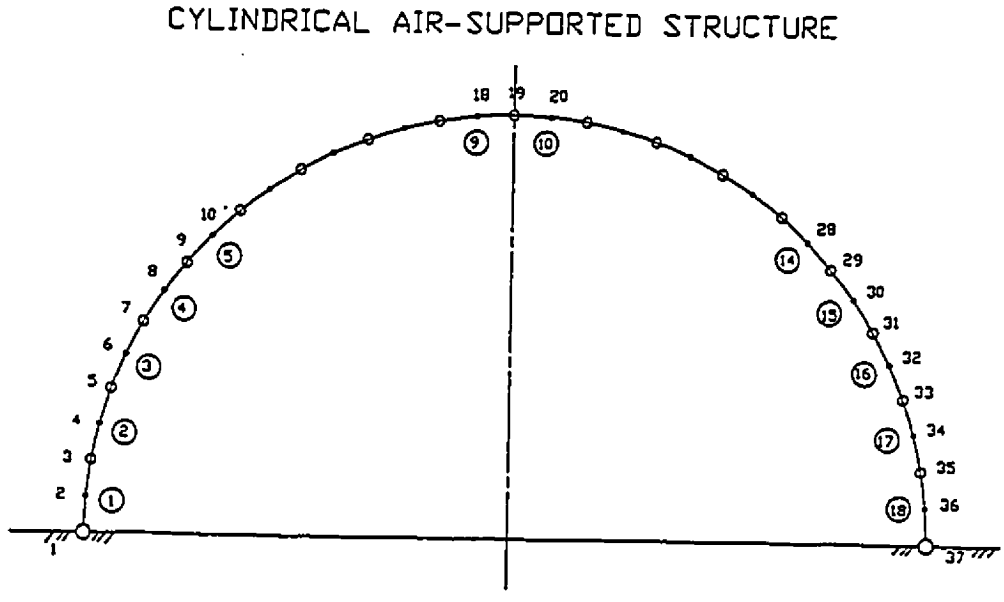

Fig. (6.3): Finite element mesh of the cylindrical air-supported structure (3 node element, B22)

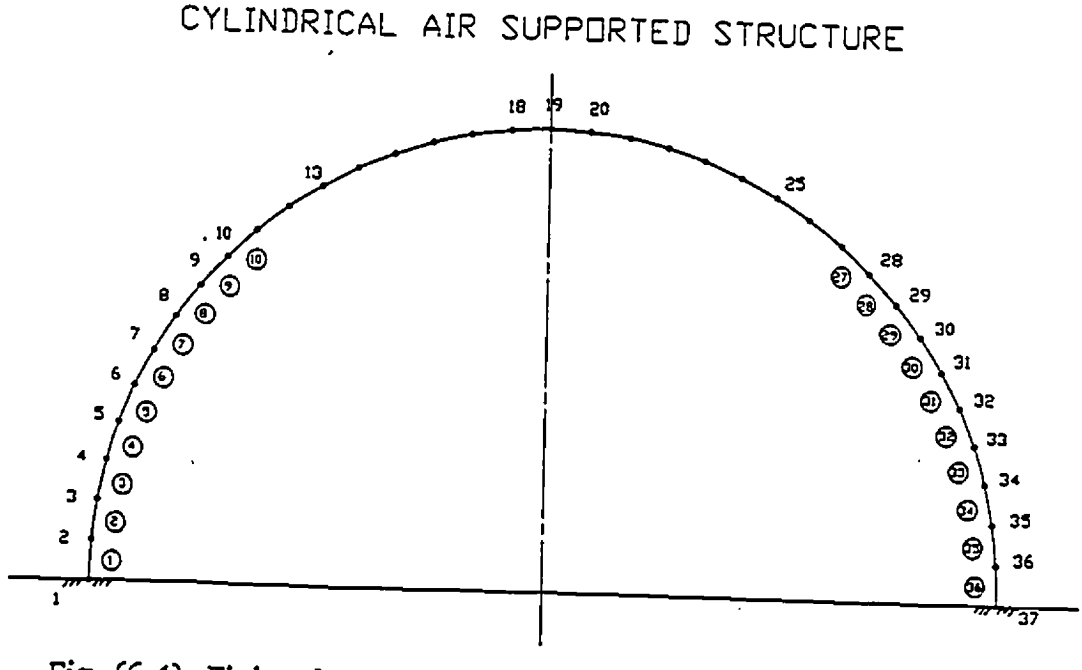

Fig. (6.4): Finite element mesh of the cylindrical air-supported structure (2 node element, B23)

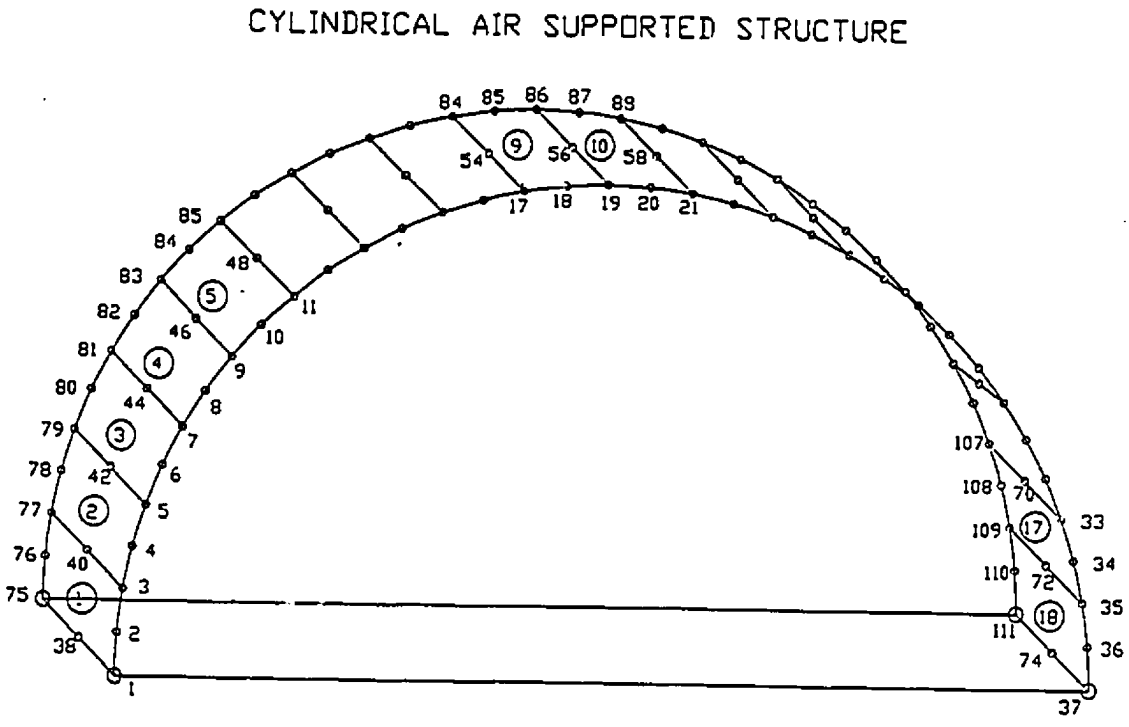

Fig. (6.5): Finite element mesh of the cylindrical air-supported structure (8 node element, S8R)

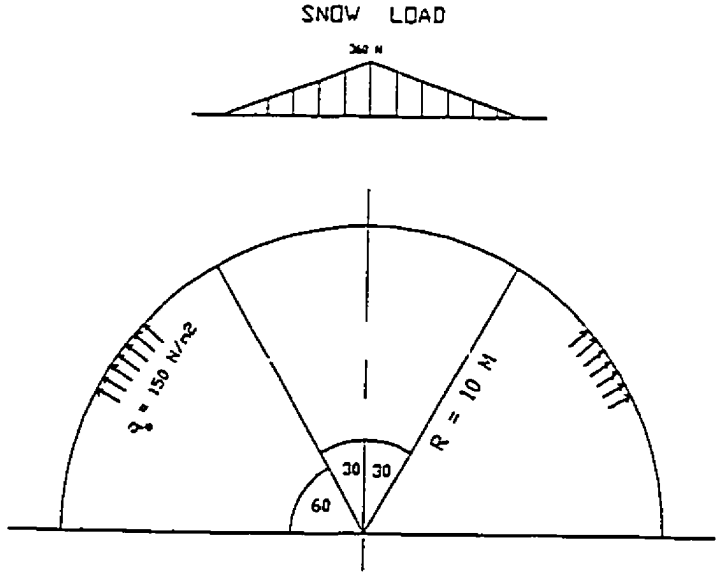

Fig. (6.6): The cylindrical air-supported structure under snow load

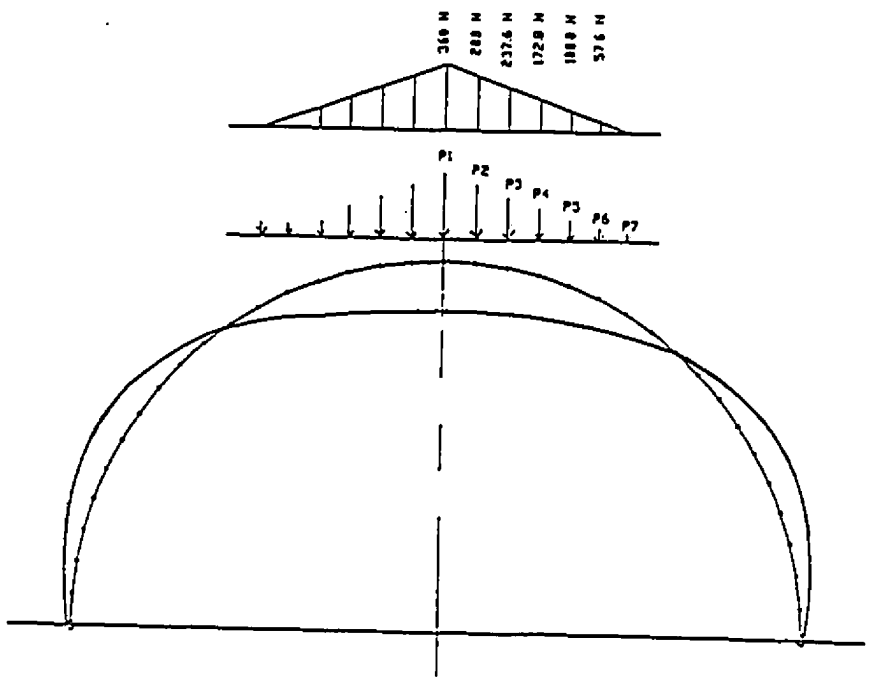

Fig. (6.7): Displaced shape of the cylindrical air-supported structure under snow load

6.4.2 Free Vibration Results

The natural frequency results of the derived characteristic equation, Equation (6.26), and those of the FEM are tabulated in Table (6.1). It can be seen that the maximum difference between the results of the two approaches is about 6%, for the element B22. This shows good agreement of the derived frequency equation with the FEM models. With more elements the difference could be less. However, the CPU computer time for the 8-node membrane element, S8R, was about four times that for other elements.

The effect of varying the internal pressure on the natural frequencies of the cylindrical air-supported structure is shown in Figure (6.8). As the internal pressure increases, the natural frequencies increase. This is expected since the stiffness of the structure depends on the internal pressure (as the pressure increases the stiffness increases). The results of Equation (6.26) and the finite element results are in very good agreement as shown in Table (6.1). The results of Equations (6.26) and (6.27) for c_t equals zero are the same as the undamped frequencies calculated using Firt's equation, Equation (6.31). It must be noted that decreasing the internal pressure q_o might lead to a loss of the membrane stiffness due to partial inflation and subsequently cause substantial decreases in the natural frequencies.

After determining the natural frequencies, the undamped mode shapes were calculated using Equations (6.18) and (6.19). The first symmetrical mode was

TABLE (6.1): ANALYTICAL AND FEM RESULTS FOR NATURAL FREQUENCIES OF THE CYLINDRICAL AIR-SUPPORTED STRUCTURE

	Element Type	ω_1	ω_2	ω_3	ω_4
		(rad/sec)			
FEM	3-Node (B22)	5.15	9.06	14.34	17.10
	2-Node (B23)	4.99	9.13	13.79	16.93
	8-Node (S8R)	4.87	8.90	12.97	16.75
Analytical		5.06	9.46	14.00	18.11

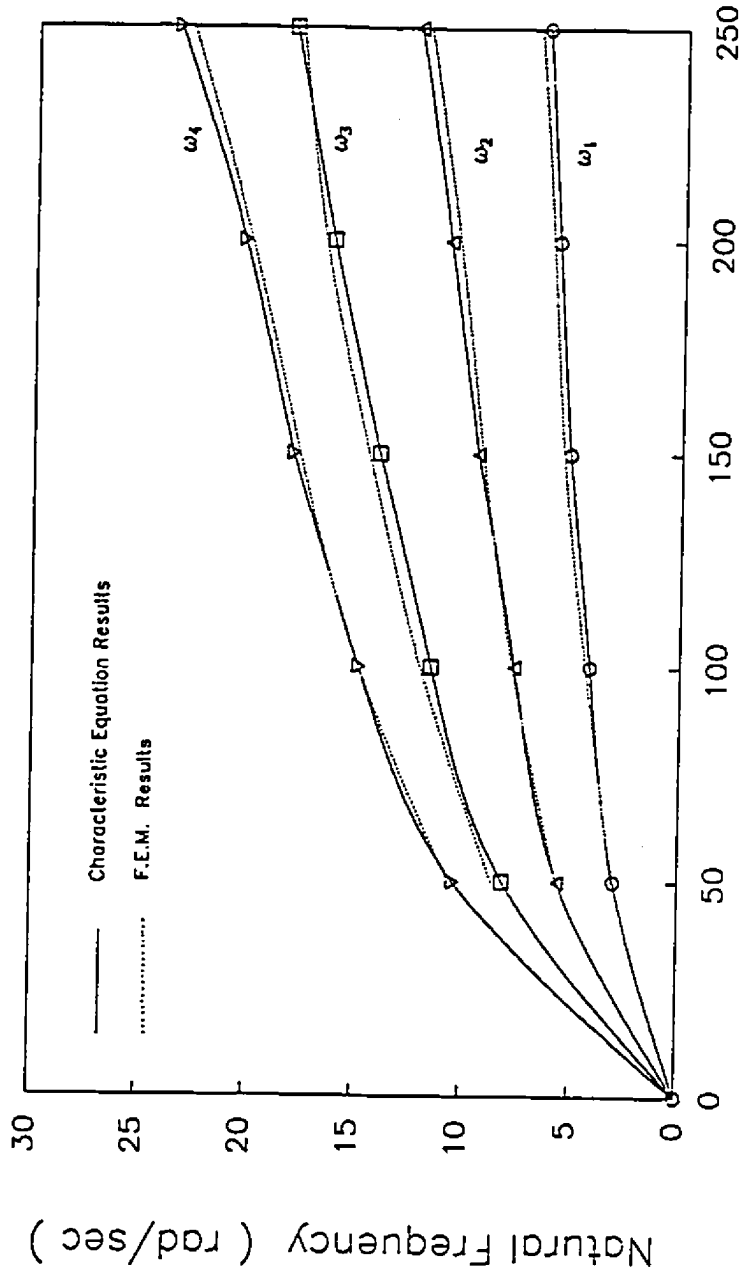

Fig. (6.8): Internal pressure effect on frequencies of the cylindrical air-supported structure

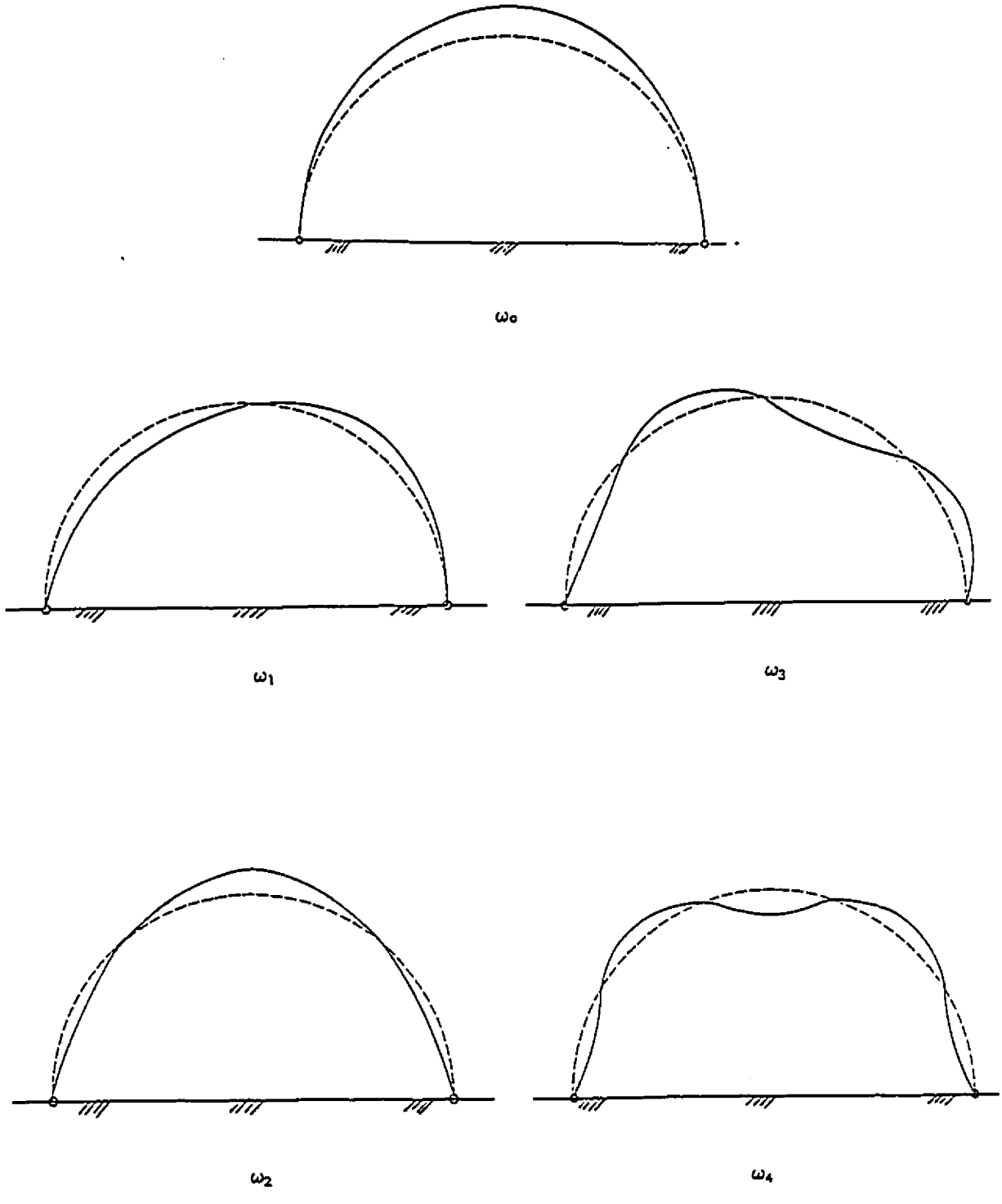

Fig. (6.9): Mode shapes of the cylindrical air-supported structure

obtained by considering the radial displacement alone, and the value of its frequency, ω_o, was 3.74 rad/sec. These mode shapes of vibration are shown in Figure (6.9).

The structural damping ratio was taken equal to 10% since the structure mass is very small. The acoustical damping due to the roof vibration was calculated according to Equation (2.11). With these structural and acoustical damping values, the damped frequencies and the modal damping of the cylindrical air-supported structure were calculated using Equations (6.29) and (6.30). These modal parameters are given in Table (6.2).

In order to examine how long a cylindrical air-supported structure should be to be considered of infinite length, several finite element meshes were analyzed assuming the cylinder is fixed at both ends. A typical mesh of 4-node membrane elements, S4R, is shown in Figure (6.10). The cylindrical air-supported structures were of the same diameter but with variable lengths; the ratio L/D varied from 0.5 to 7, where D is the lateral projection of the structure. It was found that the fundamental frequency decreases as the ratio L/D increases. This reflects the effect of the two ends in stiffening the membrane causing it to behave as a two-way membrane. As the ratio L/D increases, the frequency starts to approach the frequency values calculated from the characteristic equation derived in Subsection 6.2.1. This is because the effect of the two ends of the structure becomes merely local for high values of L/D. From Figure (6.11), it is concluded that cylindrical

TABLE (6.2): MODAL PARAMETERS OF THE CYLINDRICAL AIR-SUPPORTED STRUCTURE ($\alpha = 180°$)

Frequency	ω_1	ω_2	ω_3	ω_4
Undamped Frequencies (rad/sec)	5.06	9.46	14.00	18.11
Damped Frequencies (rad/sec)	5.00	9.28	13.84	17.82
Damping Ratio (%)	10	14.41	10	12.81

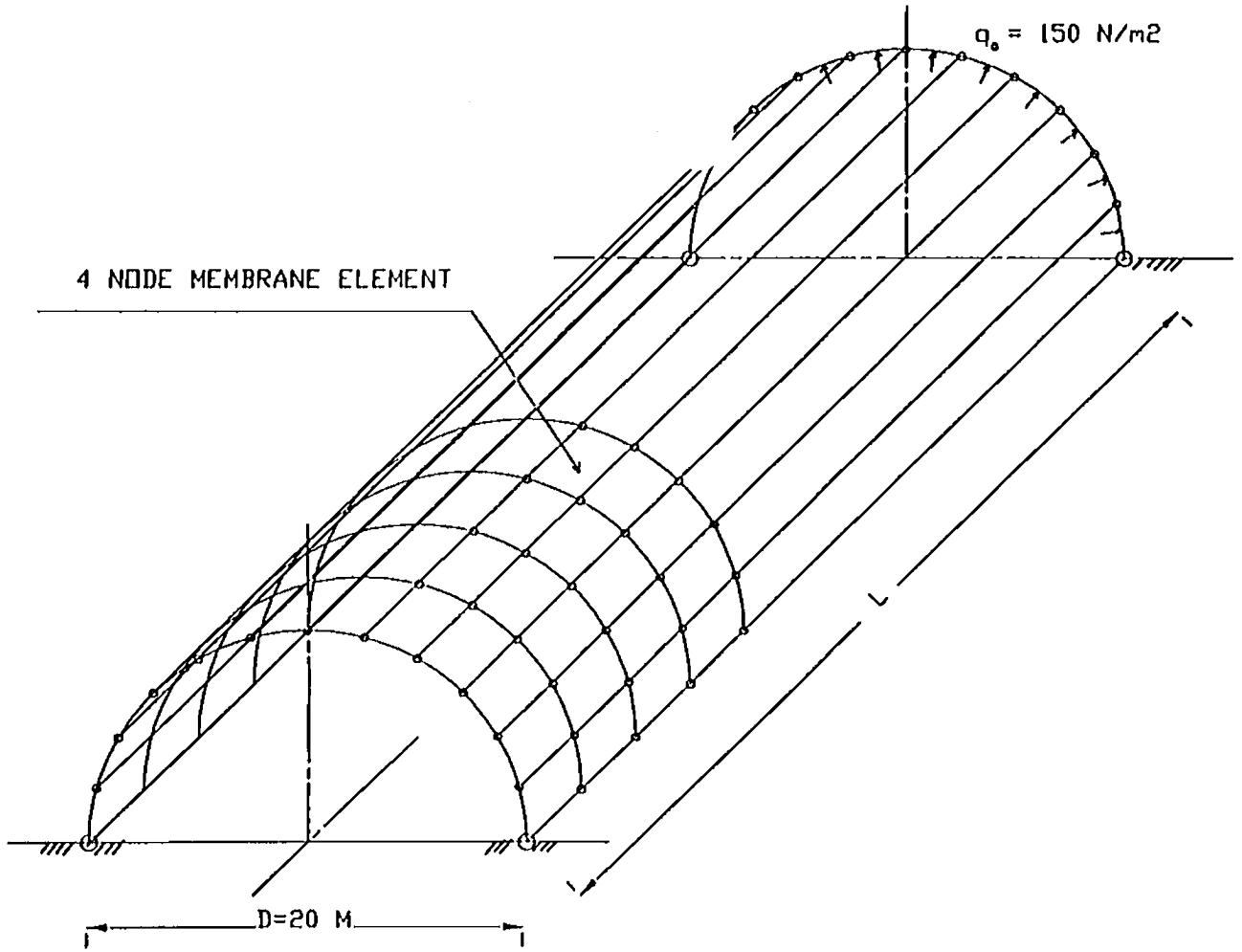

Fig. (6.10): Finite element mesh of the cylindrical air-supported structure with variable L/D (4 node element, S4R)

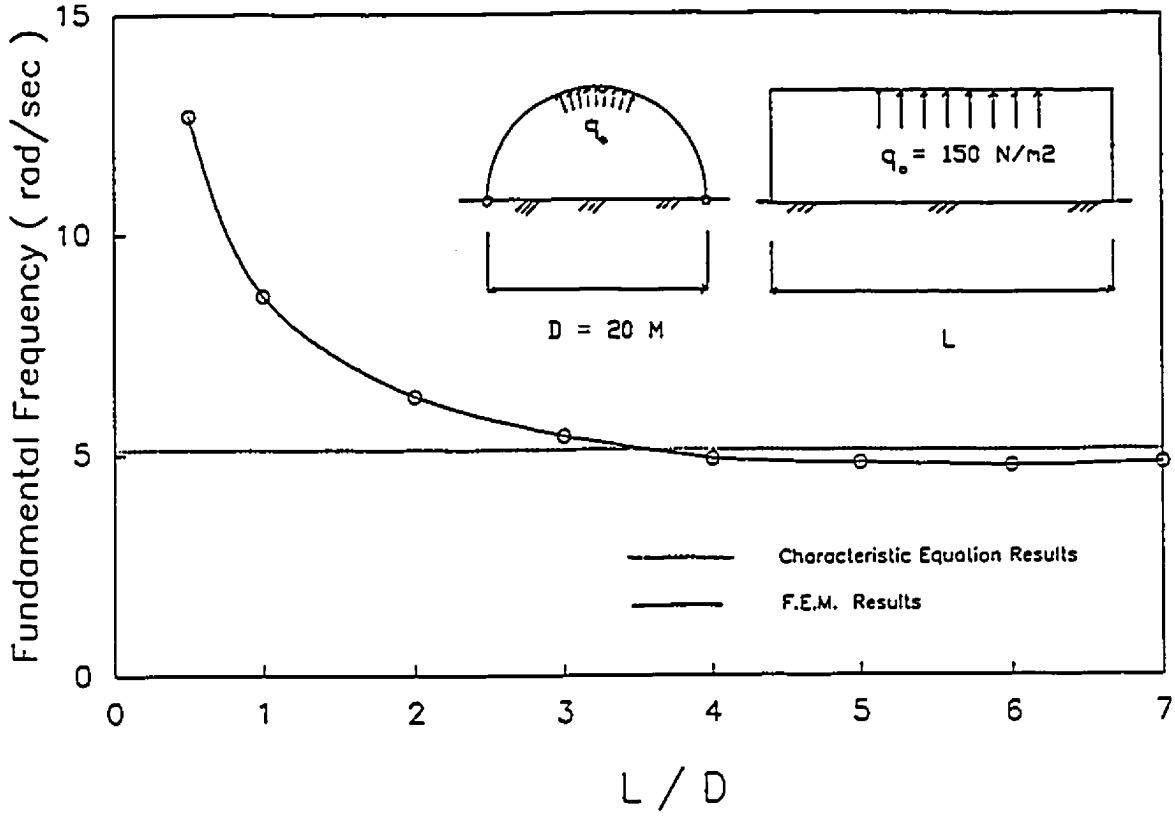

Fig. (6.11): Effect of varying the L/D ratio on the fundamental frequency of the cylindrical air-supported structure

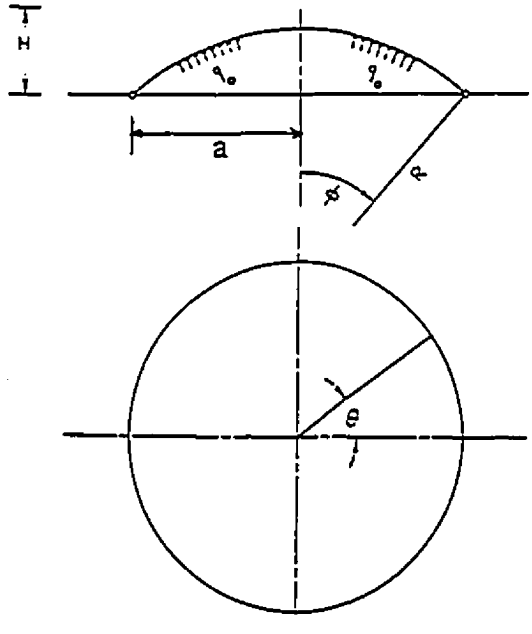

Fig. (6.12): A shallow spherical air-supported structure

air-supported structures of L/D ratios greater than about 4 can be considered as infinitely long.

6.5 FREE VIBRATION OF SHALLOW SPHERICAL AIR-SUPPORTED STRUCTURES

6.5.1 Introduction

Many studies have been devoted to the free undamped vibration of spherical shells. Rayleigh (1945), Reissner (1955), Oniashvili (1957), Vlasov (1960), Nowacki (1963), Kalnins (1967), Vol'mir (1972), Soedel (1973), and Lissa (1973) are among the pioneers in this subject.

In this section, the tension force due to the internal pressure, the enclosure volumetric changes due to the roof vibration, and the structural as well as acoustical damping are introduced into the governing equations of motion of shallow spherical shells. Closed form solutions are derived for the free damped vibration, and used to evaluate the modal parameters of natural vibration. A comparison is made between the results of the derived solutions and on FEM analysis.

The main assumptions of the analysis are as follows:

1. The rise of the structure, H, is less than 1/5 the lateral projection of the structure, 2a, and the membrane is thin, Figure (6.12). Therefore, the deformation during vibration is dominated by the motion perpendicular to the membrane surface, and only the inertia associated with the normal deformation is accounted for in the analysis.

2. The total damping is viscous in character and acts in the radial direction of the membrane.

6.5.2 Governing Equations of Free Damped Vibrations

The governing equations of free undamped vibration of a shallow spherical shell according to Nowacki (1963) are

$$\rho\, h \frac{\partial^2 w}{\partial t^2} + \frac{1}{R} \nabla^2 F + D \nabla^4 w = 0 \tag{6.34}$$

$$\nabla^2 \nabla^2 F - \frac{Eh}{R} \nabla^2 w = 0 \tag{6.35}$$

where

w = transverse motion perpendicular to the membrane surface;

$F = F(r)$ = Airy stress function;

h = thickness of membrane;

ρ = mass density;

R = radius of the spherical shell, Figure (6.12);

E = Young's modulus of Elasticity.

$D = Eh^3/12(1-\nu^2)$; ν is Poisson's ratio; and

$\nabla^2 = \partial^2/\partial r^2 + (1/r)(\partial/\partial r) + \partial^2/\partial\theta^2$;

For a pure membrane action, the shell rigidity is zero, i.e.,

$$D = 0 \tag{6.36}$$

With both the tension, $T_o = \frac{1}{2} q_o R$, due to the internal pressure q_o, and the total damping term ($c_t = c_s + c_a$) added, the equations of free damped vibration of a shallow spherical air-supported structure can be written as

$$\rho h \frac{\partial^2 w}{\partial t^2} + \frac{1}{R} \nabla^2 F - T_o \nabla^2 w + c_t \frac{\partial w}{\partial t} = 0 \tag{6.37}$$

$$\nabla^2 \nabla^2 F - \frac{Eh}{R} \nabla^2 w = 0 \tag{6.38}$$

Substituting Equation (6.38) into Equation (6.37) gives

$$\rho h \frac{\partial^2 w}{\partial t^2} + c_t \frac{\partial w}{\partial t} + \frac{Eh}{R^2} w - T_o \nabla^2 w = 0 \tag{6.39}$$

6.5.3 Solution of the Governing Equations

The radial displacement w of the shallow spherical air-supported structure can be assumed as

$$w(r,t) = w(r)\, e^{\mu t} \tag{6.40}$$

where μ is the complex frequency, and w(r) is the amplitude of radial displacement. For axisymmetrical vibration, the terms with $\partial/\partial\theta$ vanish. Substituting Equation (6.40) into Equation (6.37) yields

$$\nabla^2 w + k^2 w = 0 \tag{6.41}$$

where

$$k^2 = -\frac{1}{T_o} \left(\rho h \mu^2 + c_t \mu + \frac{Eh}{R^2} \right) \tag{6.42}$$

Equation (6.41) is the well-known Bessel differential equation, and the solution can be written as

$$w = A J_o (kr) + B Y_o (kr) \tag{6.43}$$

where A and B are constants, J_o (kr) is a Bessel function of the first kind and zero order, and Y_o (kr) is a Bessel function of the second kind and zero order. Since, Y_o (kr) becomes infinite for r = 0, B must be zero to satisfy the limitation of small displacements, thus,

$$w = A\, J_o\,(kr) \tag{6.44}$$

The boundary condition at the edge of the membrane is w(a) = 0, i.e., $J_o(ka) = 0$, therefore $\lambda_{ij} = ka = 2.405, 5.52, 8.865$, etc., which upon substitution into Equation (6.42) gives

$$\frac{\lambda_{ij}^2}{a^2} = -\frac{1}{T_o}\left(\rho\, h\, \mu^2 + c_t\, \mu + \frac{Eh}{R^2}\right) \tag{6.45}$$

Thus, the complex frequency of vibration, μ_{ij}, can be expressed as

$$\mu_{ij} = \frac{c_t}{2\rho h} \pm i\left[\frac{T_o}{\rho h}\frac{\lambda_{ij}^2}{a^2} + \frac{E}{\rho R^2} - \frac{c_t^2}{4\rho^2 h^2}\right]^{1/2} \tag{6.46}$$

where i and j are the numbers of radial nodal lines and circles, respectively. The complex frequency μ_{ij} can be rewritten as

$$\mu_{ij} = \mu_1 \pm i\, \mu_2 \tag{6.47a}$$

where

$$\mu_1 = \frac{c_t}{2\rho h} \tag{6.47b}$$

and

$$\mu_2 = \left[\frac{T_o}{\rho h}\frac{\lambda_{ij}^2}{a^2} + \frac{E}{\rho R^2} - \frac{c_t^2}{4\rho^2 h^2}\right]^{1/2} \tag{6.47c}$$

Thus, the damped frequency is

$$\omega_{ij}^2 = \left[\omega_{o(ij)}^2 - \frac{c_t^2}{4\rho^2 h^2}\right]^{1/2} \tag{6.48}$$

where

$$\omega_{o(ij)} = \left[\frac{T_o}{\rho h}\frac{\lambda_{ij}^2}{a^2} + \frac{E}{\rho R^2}\right]^{1/2} \tag{6.49}$$

and the modal damping ratio is

$$\zeta_{ij} = \frac{c_r}{2 \rho h \omega_{o(ij)}} \tag{6.50}$$

Substituting Equation (6.44) into Equation (6.38) gives the function, $F(r)$, as

$$F(r) = -\frac{Eh}{k^2 R} A J_o(kr) \tag{6.51}$$

To include the volumetric changes of the cavity due to the roof vibration, and the associated changes in the internal pressure, the change in the volume of the enclosed air is assumed to be $dV = S \bar{w}$, where S is the surface area of the shallow spherical membrane and $\bar{w}$ is the average displacement of the roof. Following the procedure adopted in Subsection 3.3.2, the excess pressure dp inside the structure is

$$dp = -\frac{\gamma q_o}{V_o} dV = -\frac{\gamma q_o}{V_o} S \bar{w} \tag{6.52}$$

where q_o and V_o are the equilibrium pressure and volume of the structure, respectively. Introducing this force to Equation (6.39) and using Equation (6.40) give

$$\nabla^2 w + k^2 w = \frac{\gamma q_o}{T_o V_o} S \bar{w} \tag{6.53}$$

where k^2 is as in Equation (6.42). Equation (6.53) is satisfied by a function of the form

$$w(r) = A [J_o(kr) - J_o(ka)] \tag{6.54}$$

where A is a constant. This solution satisfies the boundary condition that $w(a)=0$.

Substituting Equation (6.54) into Equation (6.53), and taking $S = 2 \pi R H$, gives the following frequency equation

$$J_o (ka) = - \alpha_2 \frac{J_2 (ka)}{(ka)^2} \tag{6.55a}$$

where

$$\alpha_2 = \frac{2 \gamma q_o R_o H}{T_o V_o} \pi a^2 \tag{6.55b}$$

In equation (6.55b) R and H are the radius and rise of the structure, respectively. Equation (6.55a) is numerically solved to get the value of k, then the damped frequencies and modal damping are determined according to Equations (6.42), (6.48) and (6.50).

To include the antisymmetrical modes into the solution of Equation (6.39), the displacement function is assumed to be

$$w = \psi(r) \phi(\theta) e^{\mu t} \tag{6.56}$$

where μ is the complex frequency. Substituting Equation (6.56) into the governing equation of free damped vibration of shallow spherical air-supported structures, Equation (6.39), and rearranging gives

$$\frac{r^2}{\psi} \left(\frac{d^2 \psi}{dr^2} + \frac{1}{r} \frac{d\psi}{dr} \right) + k^2 r^2 = - \frac{1}{\phi} \frac{d^2 \phi}{d\theta^2} \tag{6.57}$$

where k^2 is given by Equation (6.42). Since each side of Equation (6.57) is a function in a different parameter, and because the two sides are equal, each side must be equal to a constant, m^2. The complete solution of Equation (6.57) is

$$w = C J_m (kr) e^{im\theta} e^{\mu t} \quad , \quad m = 0, 1, 2, 3, \ldots \tag{6.58}$$

where C is a constant. The boundary condition $w(a,\theta,t) = 0$ leads to

$$J_m (ka) e^{im\theta} = 0 \tag{6.59}$$

The roots, λ_{ij}, of Equation (6.59) where i and j are the numbers of radial nodal lines and circles, respectively, can be found elsewhere (Blevins, 1979). Substituting the values of λ_{ij} into Equations (6.48) and (6.50) gives the damped frequencies and modal damping, respectively.

Inspection of Equation (6.49) shows that a powerful analogy exists between the natural frequencies of flat circular membranes and shallow spherical membranes. The term $T_o\lambda_{ij}^2/(\rho h a^2)$ in Equation (6.49) represents the natural frequency of a flat circular membrane. Therefore, if a flat circular membrane and a shallow spherical membrane have the same thickness; dimensions on a plane; homogeneous isotropic material; and the same boundary conditions, the mode shapes governing the deformation normal to the surface are identical and the natural frequencies of mode ij are related by

$$\omega_{o(ij)}\Big|_{\substack{\text{shallow}\\ \text{spherical}\\ \text{membrane}}} = \left[\omega_{o(ij)}^2 \Big|_{\substack{\text{flat}\\ \text{circular}\\ \text{membrane}}} + \frac{E}{\rho R^2} \right]^{1/2} \tag{6.60}$$

Equation (6.60) satisfies the limiting case of a flat circular membrane for which $1/R = 0$. This analogy is similar to the analogy made by Soedel (1973)

between the natural frequencies and mode shapes of flat plates and spherically curved panels ($D \neq 0$). It is also possible to relate the natural frequencies and mode shapes of flat rectangular membranes to the natural frequencies of similar shallow cylindrical membranes.

6.6 EXAMPLE OF SHALLOW SPHERICAL STRUCTURES

In this example, a shallow spherical air-supported structure features the following parameters:

Internal pressure	q_o = 50 to 250 Pa
Radius	R = 23.66 m
Mass per unit area	m = 2 kg/m^2
Central angle	$2\phi = 30° \rightarrow 90°$

The internal pressure was varied similar to what was done in the cylindrical air-supported structure discussed earlier. With these data, a comparison between the natural frequencies calculated by the derived frequency equation, Equation (6.49), and the results obtained using the program ABAQUS is made. The finite elements used were 3 node axisymmetrical membrane elements, type SAX2. Both the axisymmetrical and antisymmetrical modes of vibration were calculated using the finite element meshes shown in Figures (6.13) and (6.14). The results of the derived frequency equation, Equation (6.49), and the finite element results are in

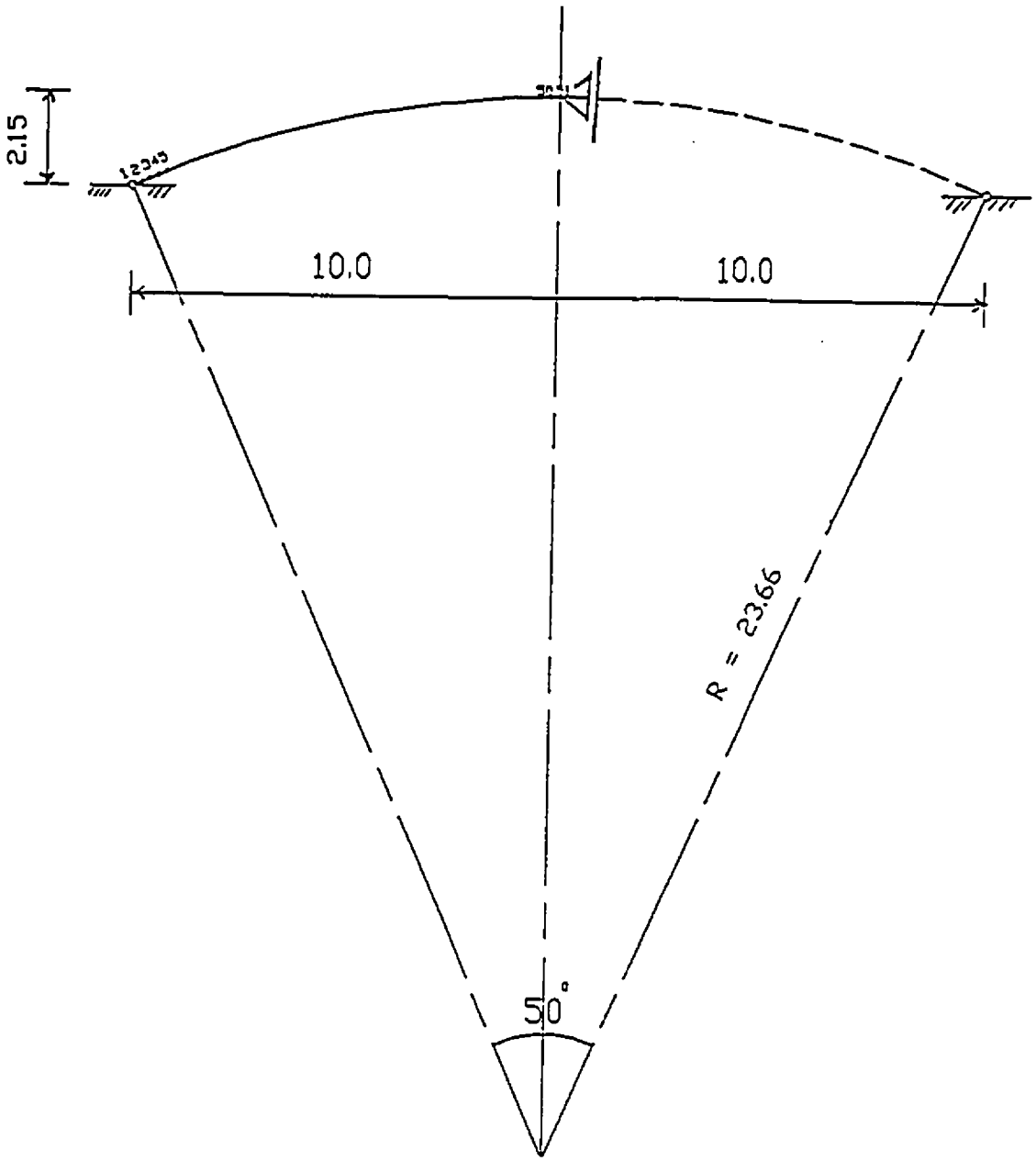

Fig. (6.13): Finite element mesh of the shallow spherical air-supported structure (axisymmetrical modes)

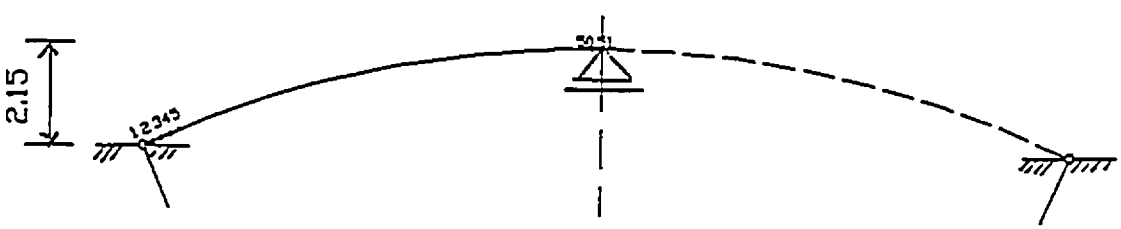

Fig. (6.14): Finite element mesh of the shallow spherical air-supported structure (antisymmetrical modes)

good agreement, as shown in Figures (6.15a) and (6.15b). With more elements, the agreement would be better.

The effect of varying the internal pressure on the natural frequencies is shown in Figures (6.15a) and (6.15b). It can be seen that as the internal pressure increases, the natural frequencies increase as expected. After determining the natural frequencies, the undamped mode shapes were calculated using Equations (6.44), and (6.58). Similar mode shape results were obtained using the finite element program ABAQUS. The axisymmetrical and antisymmetrical mode shapes are shown in Figure (6.16).

The damping ratios of the shallow spherical air-supported structure were calculated using Equation (6.50) and (6.51) derived before, and tabulated in Table (6.3). The structural damping ratio was taken equal to 10% and the acoustical damping due to the roof vibration was calculated according to Equation (2.11). The first axisymmetrical mode shape has the highest damping ratio compared to other modes, because of the high acoustical damping associated with this mode.

To further determine how shallow the spherical air-supported structure should be to use the derived frequency equation, Equation (6.49), different finite element meshes were used with different central angles ranging from 30° to 90°. The results of both Equation (6.49) and those of the FEM analysis are shown in Figures (6.17a) and (6.17b). The agreement between the two approaches is good for ϕ up to 30° (ϕ is half the central angle of the cross-section). For ϕ greater

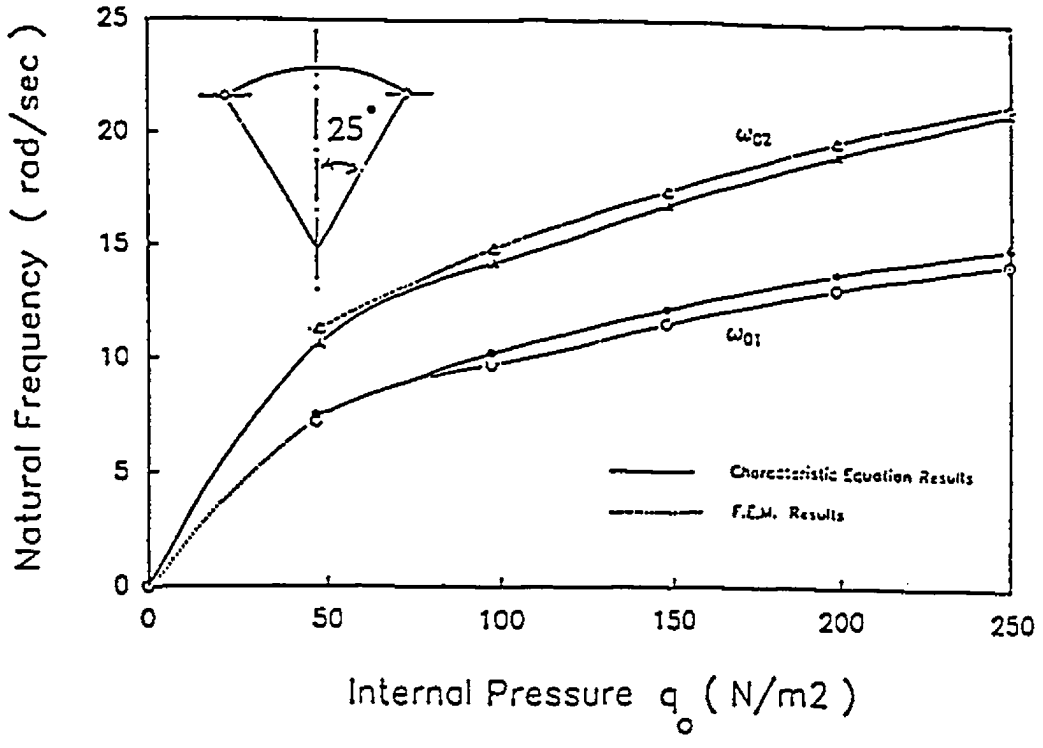

Fig. (6.15a): Internal pressure effect on frequencies of the shallow spherical air-supported structure (axisymmetrical modes)

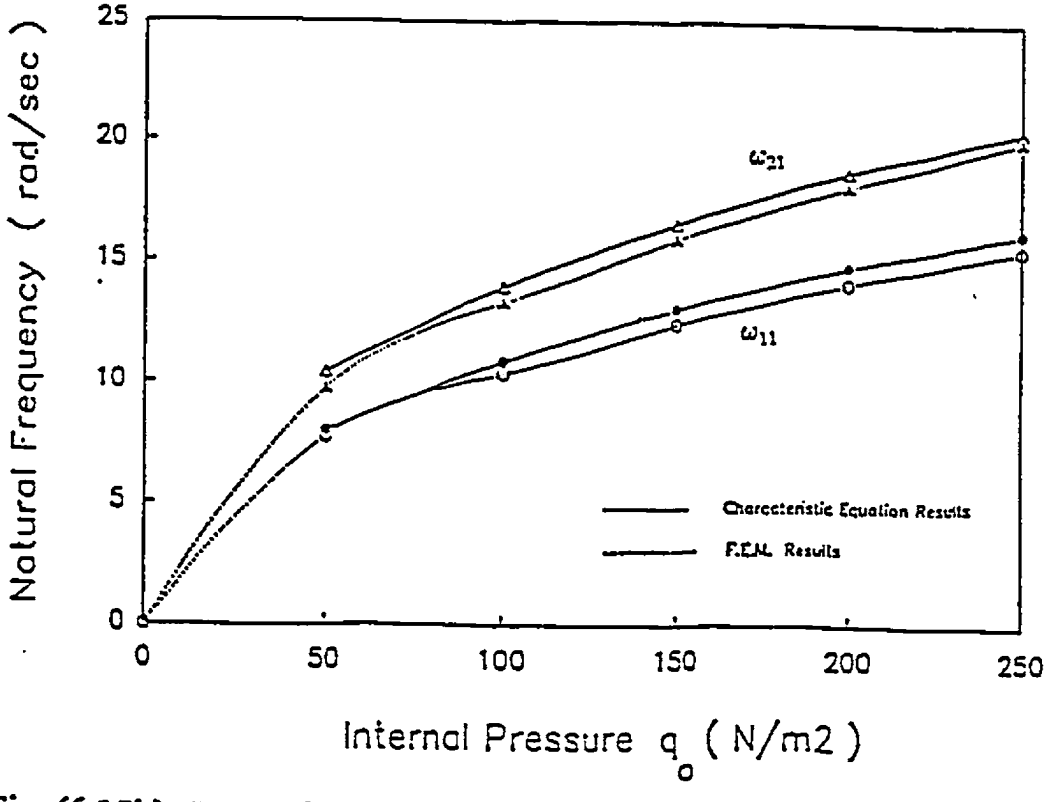

Fig. (6.15b): Internal pressure effect on frequencies of the shallow spherical air-supported structure (antisymmetrical modes)

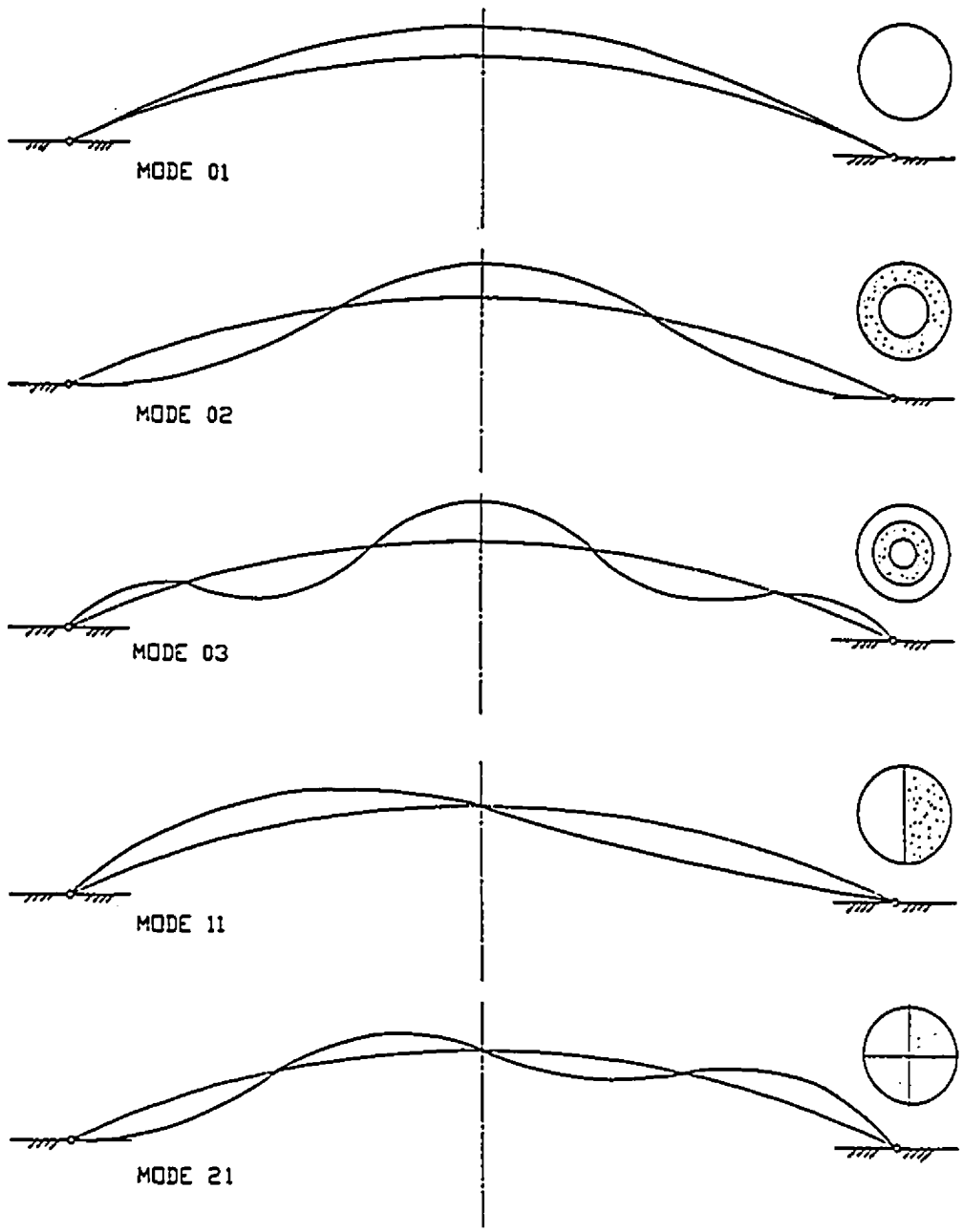

Fig. (6.16): Mode shapes of the shallow spherical air-supported structure

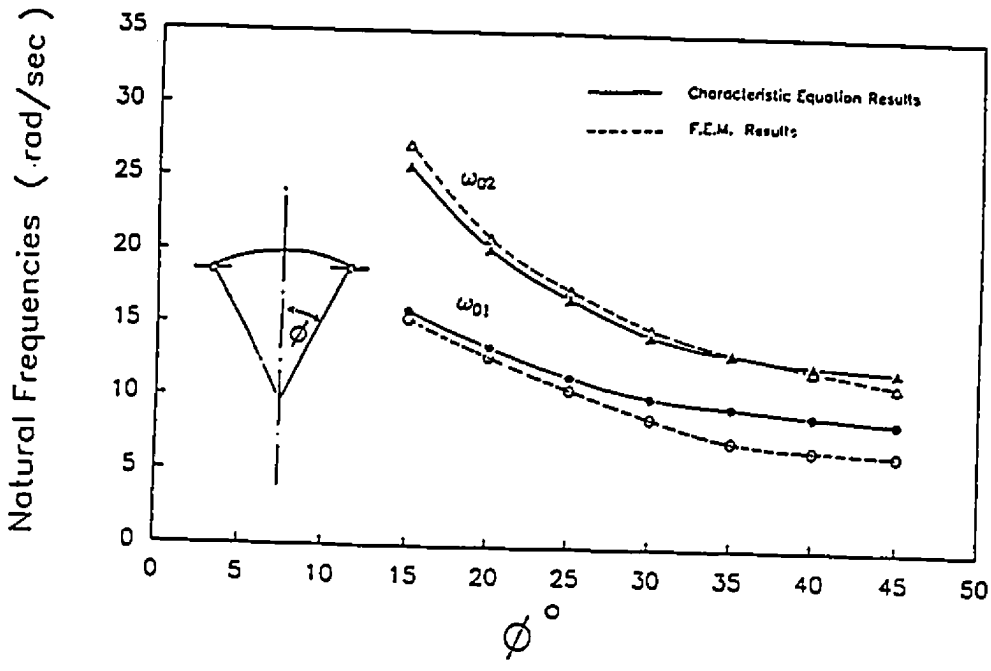

Fig. (6.17a): Comparison of the analytical and FEM results of the shallow spherical air-supported structure (axisymmetrical modes)

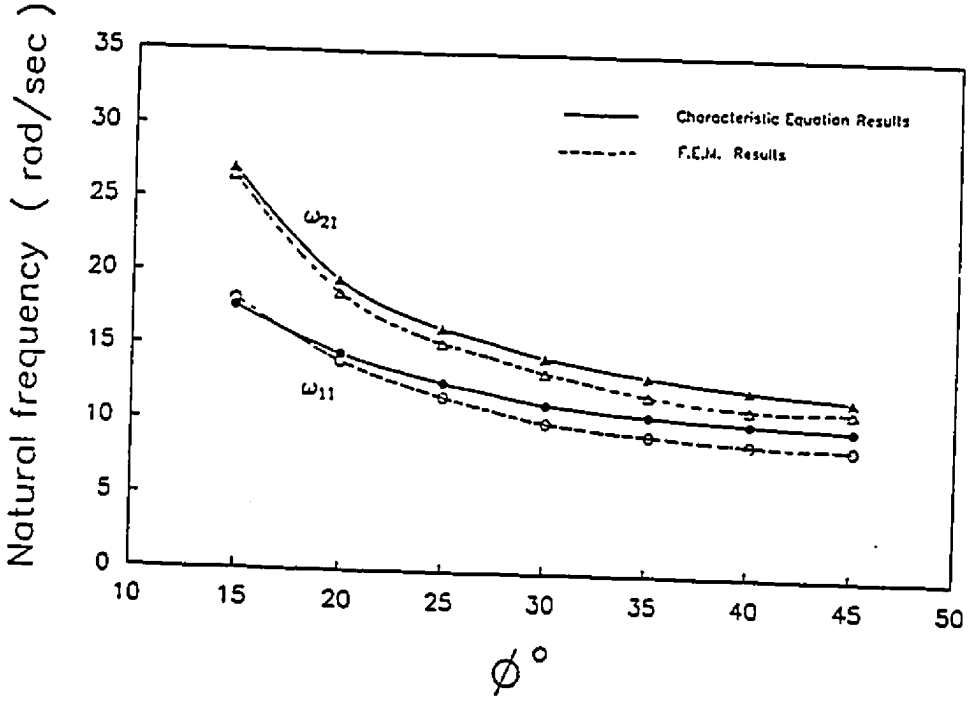

Fig. (6.17b): Comparison of the analytical and FEM results of the shallow spherical air-supported structure (antisymmetrical modes)

TABLE (6.3): MODAL PARAMETERS OF THE SHALLOW SPHERICAL STRUCTURE (ϕ = 25°)

Mode	Axisymmetrical Modes		Antisymmetrical Modes	
	01	02	11	21
Undamped Frequencies (rad/sec)	11.12	17.27	12.50	16.13
Damped Frequencies (rad/sec)	10.66	16.94	12.37	15.97
Damping Ratio (%)	21	13	10	10

than 30°, the derived frequency equation underestimates the natural frequencies, since the tangential deformation becomes significant, and the membrane is no longer shallow. Therefore, it is concluded that the frequency equation derived for shallow spherical air-supported structures is only valid for cross-sections with central angles 2ϕ up to 60°, or with rise to lateral projection ratios less than 1/5.

CHAPTER 7

WIND TUNNEL EXPERIMENTS WITH A HEMISPHERICAL AIR-SUPPORTED STRUCTURE

7.1 INTRODUCTION

Air-supported structures are increasingly being used as permanent building forms; however, since they are very light, there is a potential for strong interaction between the structure and the wind. A survey of failures of air-supported structures indicated that, apart from rain and snow accumulations, the most common causes of failure are inadequate anchorage details, and the instability of the structures at high wind speeds (Malcolm and Glockner, 1978). Therefore, to ensure safe and serviceable design of large span, air-supported structures, an examination of their dynamic behaviour under turbulent wind is necessary.

The general lack of design procedures that consider the dynamic wind effects on air-supported structures or unusual aspects of these roof systems, such as aerodynamic instability, make wind tunnel testing even more desirable. The concern for aerodynamic instabilities calls for aeroelastic testing as opposed to pressure measurements on rigid models, which are used to estimate wind forces on such structures.

In the study described here, an aeroelastic model of a large span, hemispherical, air-supported roof was designed and tested. Construction of the model, its instrumentation, and free vibration as well as wind tunnel testing

procedures are described. The main objectives were to determine the free vibration characteristics of hemispherical air-supported structures, and to find the roof response and the internal pressure fluctuations due to wind loading. Different gradient wind speeds, exposures, enclosed volumes, and internal pressures were employed in the wind tunnel experiments. The internal pressure, as defined in this study, is the differential between the mean pressure within the hemispherical model and the mean ambient outside static pressure.

Comparisons of the experimental free vibration results with the theoretical results are made, along with the aeroelastic test observations. A proposed semi-analytical procedure to predict the wind-induced response of air-supported structures is formulated in Chapter 8. Predicted responses of the hemispherical, air-supported model and their comparisons with the measured ones from the aeroelastic tests are also presented in Chapter 8.

7.2 SIMILARITY REQUIREMENTS

In Section 4.2, it was stated that the scaling requirements for one dimensionless parameter can make it difficult to scale another one correctly. It is rarely possible to simultaneously satisfy the five non-dimensional parameters in Equations (4.6) to (4.10). For example, Reynolds number, R_e, scaling requires

$$[\frac{\rho UL}{\mu}]_m = [\frac{\rho UL}{\mu}]_p \tag{7.1}$$

where L is the structure characteristic dimension; ρ, μ, and U are the density, viscosity, and velocity of air. With both the model and prototype in air under

atmospheric conditions, this equation becomes

$$\lambda_V = 1/\lambda_L \tag{7.2}$$

where λ_L and λ_V are the length and velocity scales, respectively. This condition is very difficult to achieve practically in the wind tunnel; therefore the Reynolds number scaling is often relaxed, and tests for transcritical Reynolds numbers are rare. This simplification leads to model R_e values in conventional boundary layer wind tunnels that are typically two to three orders of magnitude lower than full scale values. For structures with corners, this disparity is generally of little practical importance as the resulting flow-induced forces are not sensitive to R_e variations. This is so because the positions of the flow separation are fixed by the edges.

For curved structures, such as the hemispherical roof, the Reynolds number effect can be significant. However, the wind tunnels available to the author do not allow the very high Reynolds numbers required for proper modelling of a large roof prototype. Therefore, the model was tested at low R_e, i.e. under subcritical flow conditions. This may be justified, at least partly, by the following reasons: the tests are not meant to verify the behaviour of an actual prototype to be erected, rather, they aim at studying the pattern of roof behaviour, and the verification of the proposed semi-analytical method of response prediction. In addition, experiments with circular cylinders indicate that at very high R_e, in the transcritical region in Roshko's terminology, the wake characteristics are closer

to those in the subcritical region than to those in the supercritical region (Roshko, 1961).

The similarity of Froude number, U^2/gL, requires that

$$\left[\frac{U^2}{g\,L}\right]_m = \left[\frac{U^2}{g\,L}\right]_p \tag{7.3}$$

Since the acceleration of gravity, g, is the same for both the model and prototype, this equation reduces to

$$\lambda_V = \sqrt{\lambda_L} \tag{7.4}$$

which is also difficult to achieve in the wind tunnel. Froude number scaling is important where gravitational forces are important. In the current tests, similarity of Froude number was not maintained because the gravitational forces at full scale tend to be small in comparison to the aerodynamic forces in high winds, as a result of the light weight of the air-supported structure. This is an important simplification, since it eliminates the use of the low wind speeds that would be required to match the Froude number in model tests.

In Chapter 2, it was mentioned that to model the acoustical damping effect correctly, the Mach number (U/c_o where c_o is the speed of sound in air) should be the same at both scales. This cannot be achieved in many wind tunnels; however, Irwin and Wardlaw (1979) stated that the use of wind velocities lower than that required by Mach number scaling can be regarded as conservative. For these reasons, the Mach number scaling was not maintained in the current tests. It should be noted that in wind tunnel tests with air-supported models the

acoustical damping may be decreased due to the wind interaction and the aerodynamic damping may be dominant.

Simulation of aerodynamic damping does not need any additional similarity parameters beyond those already considered in this section and in Section 4.2 (Irwin and Wardlaw, 1979).

In summary, the aeroelastic modelling similarity relationships (with the notation used in Chapter 4) for the wind tunnel study of hemispherical air-supported structures are as follows:

1. The turbulent boundary layer flow properties are scaled at a length scale λ_L.
2. The dimensions of the structure are scaled according to λ_L.
3. The internal volume is scaled according to $\lambda_\forall = \lambda_L^3/\lambda_V^2$.
4. The mass per unit area of the roof is scaled according to $\lambda_m = \lambda_L$.
5. The elasticity similarity for the roof is scaled according to $\lambda_{To} = \lambda_V^2\lambda_L$.
6. The internal pressure is scaled according to $\lambda_{qo} = \lambda_V^2$.
7. The similarity of the structural damping is based on $\lambda_{\zeta_s} = 1$.

The determination of the actual scales used is described below.

7.3 MODEL SCALING

The choice of length scales is generally governed by the available roof materials and the scale of the boundary layer wind tunnel. The Boundary Layer Wind Tunnel Laboratory at The University of Western Ontario, London, Ontario,

Canada, can model the atmospheric boundary layer at length scales ranging from 1:300 to 1:500. Within these bounds, the choice of the length scale is determined through the mass scale by the materials available to simulate the structure type considered.

7.3.1 The Prototype

The structure considered is a hemispherical air-supported structure with a projected horizontal circular plan of 120 m in diameter and a mass per unit area of 2.5 kg/m^2. This type of structure may be employed to cover a baseball stadium or an exhibition hall. The membrane of the roof is supported by an internal pressure, and anchored in a ring beam resting on a rigid circular wall, or directly on the ground.

7.3.2 The Model

An extensive study of suitable materials for fabricating the model roof was made. As a result, a 0.05 mm thick polyethelyne material was chosen to simulate the prototype. This material satisfied the mass scaling at a geometrical scale of λ_L = 1:400, which through the elasticity scaling permitted a suitable velocity scale of 1:3.

The stiffness of the air-supported membrane stems primarily from the static membrane tension, and depends on the changes of the internal pressure resulting from the wind-induced volumetric changes of the enclosed volume. Thus, the volume scaling is very important. To satisfy the internal volume scaling, a

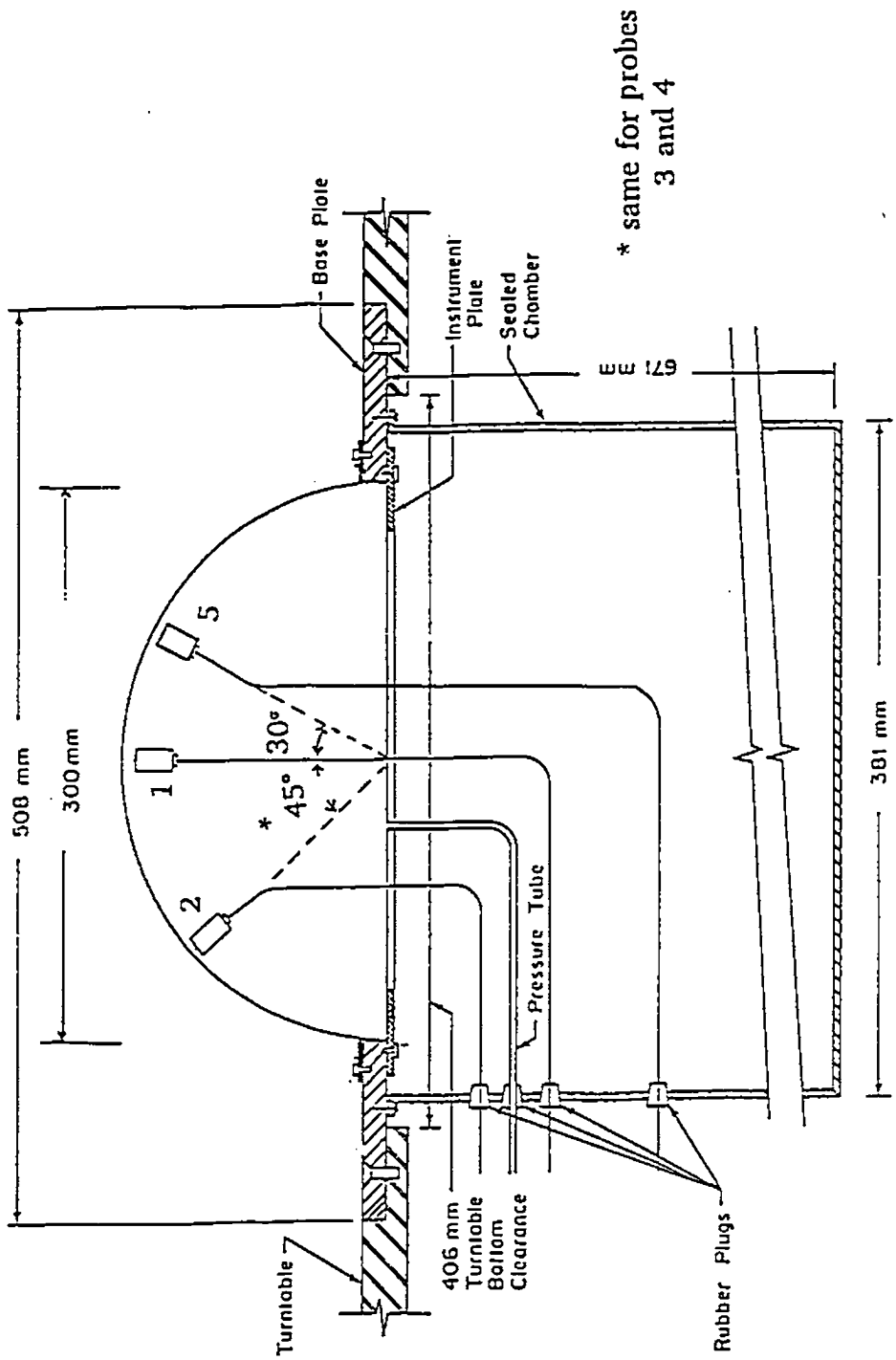

Fig. (7.1): Vertical cross-section of the hemispherical model

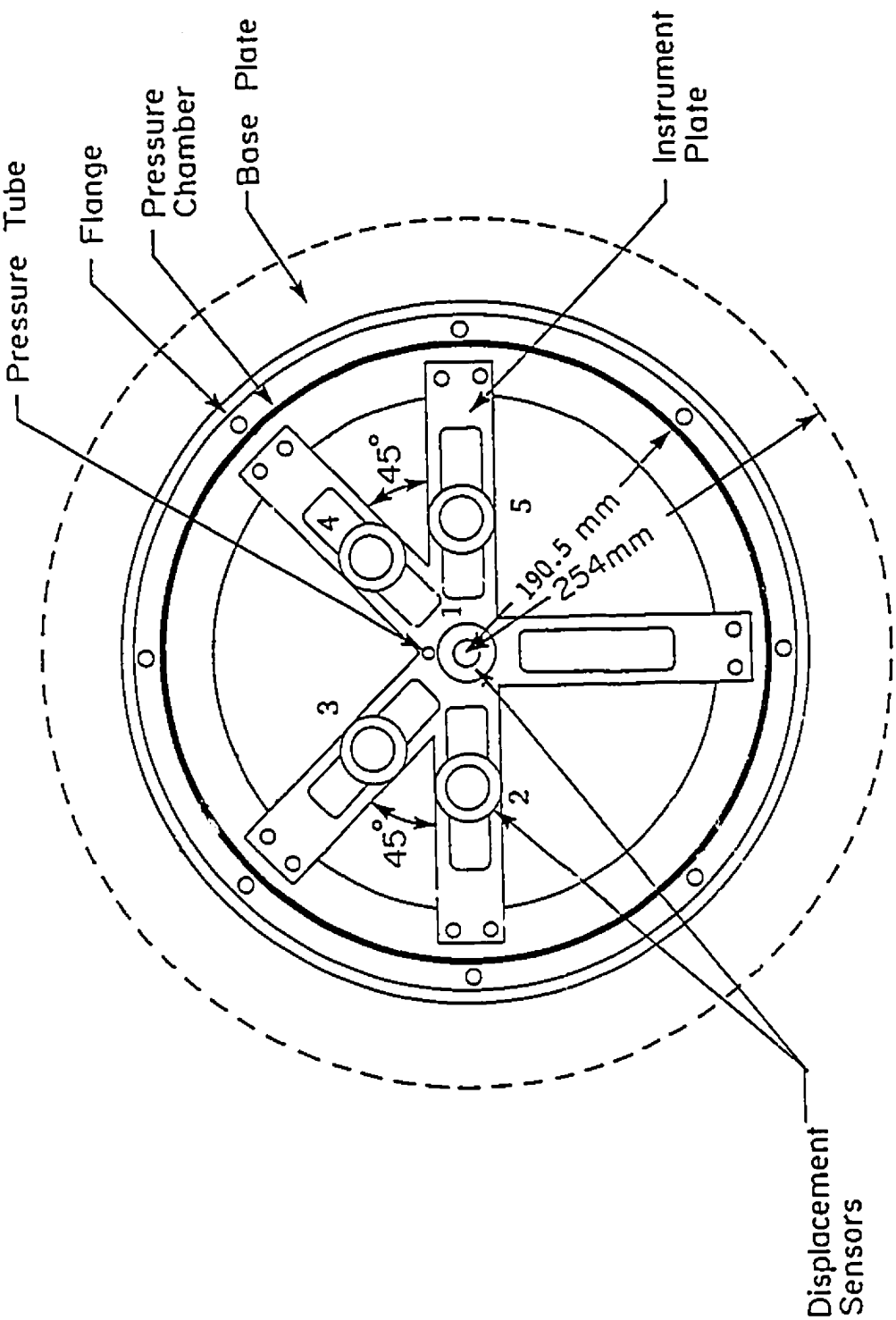

Fig. (7.2): Cross-sectional plan of the hemispherical model

chamber was mounted below the model, as shown in Figures (7.1) and (7.2), to provide the additional volume needed.

A summary of the various scaling parameters of the aeroelastic model is presented in Table (7.1). The numerical values for the model and the prototype scaling are also given in Table (7.2). A plan and a vertical cross-section of the model showing the transducer locations are given in Figures (7.1) and (7.2). Also, a photograph of the model is displayed in Plate (7.1). It must be noted that all results given here are in model scale units, which can be converted to full scale values using the scaling parameters in Table (7.1).

7.4 CONSTRUCTION OF THE MODEL

The membrane model was formed to the required hemispherical shape under pressure and elevated temperature, using a plexiglass mold. Heat was uniformly applied to the circular membrane sheet by a fabricated cylindrical furnace through which heat guns were directed. Simultaneously, a vacuum pump was used to draw the membrane as it expanded to form the required hemispherical shape. This process of baking the hemisphere was a considerable portion of the overall experimental effort. The membrane roof was attached to the base by a clamping ring.

The chamber, below the model, was sealed to prevent any air leakage from the model by inserting a rubber strip between the model base and the chamber flange. Baffles were placed into the chamber to avoid acoustic resonance. To

TABLE (7.1): SUMMARY OF AEROELASTIC SCALING PARAMETERS OF THE HEMISPHERICAL AIR-SUPPORTED ROOF

No.	Parameter	Scaling	Numerical value
1	length	$\lambda_L=L_m/L_p$	2.50×10^{-3} (1 : 400)
2	Internal volume	$\lambda_w=\lambda_L^3/\lambda_V^2$	1.41×10^{-7}
3	Mass/unit area	$\lambda_m=\lambda_L$	2.50×10^{-3} (1 : 400)
4	Weight/unit area	$\lambda_w=\lambda_L$	2.50×10^{-3} (1 : 400)
5	Time	$\lambda_t=\lambda_L/\lambda_V$	7.52×10^{-3} (1 : 133)
6	Frequency	$\lambda_f=\lambda_V/\lambda_L$	133 (133 : 1)
7	Velocity	$\lambda_V=U_m/U_p$	0.33 (1 : 3)
8	Force	$\lambda_F=\lambda_L^2\lambda_V^2$	6.941×10^{-7}
9	Pressure	$\lambda_{qo}=\lambda_V^2$	0.11 (1 : 9)
10	Tension/unit area	$\lambda_T=\lambda_L\lambda_V^2$	2.78×10^{-4}

TABLE (7.2): AEROELASTIC SCALING OF THE HEMISPHERICAL AIR-SUPPORTED ROOF

No.	Parameter	Prototype		Model	
		Quantity	Dimension	Quantity	Dimension
1	Roof diameter	120.00	m	30.0	cm
2	Height	60	m	15.0	cm
3	Mass/unit area	2.50	kg/m^2	6.25×10^{-3}	kg/m^2
4	Weight/unit area	24.53	N/m^2	0.0613	N/m^2
5	Modulus of elasticity	1.35×10^7	N/m^2	1.5×10^6	N/m^2
6	Enclosed volume	4.52×10^5	m^3	0.0636	m^3
7	Fundamental frequency	1.00	Hz	133.0	Hz
8	Gradient wind speed	45	m/sec	15	m/sec

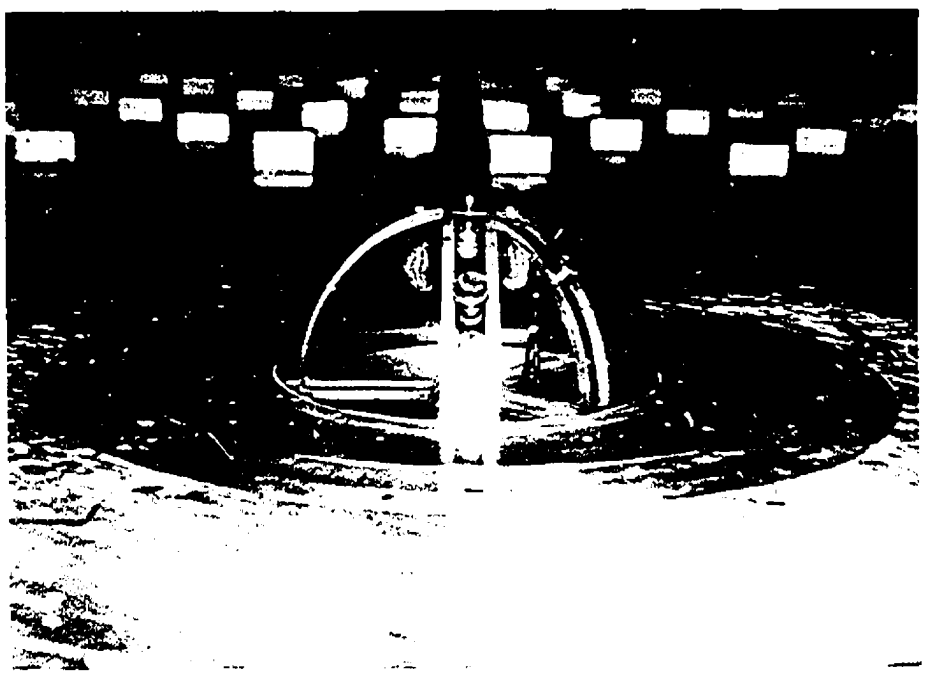

Plate (7.1): The aeroelastic hemispherical air-supported model

facilitate any adjustments inside the model or any change in the positioning of the displacement probes, a sealable circular access door was made in the chamber walls.

7.5 INSTRUMENTATION

The internal volume of the model was pressurized by a high pressure air supply controlled by two needle valves in series. A vacuum pump, controlled by a needle valve, was used to bleed the chamber when needed. A manometer was attached to the chamber to monitor the mean internal pressure and to detect any possible leakage. All pressures were measured with respect to the mean ambient static pressure within the boundary layer wind tunnel. A Setra pressure transducer was connected to the instrument plate inside the model to monitor the internal pressure fluctuations caused by the movement of the roof due to wind pressure.

Five displacement sensors were used in the tests to measure deflections simultaneously at five different locations. The displacement sensors were Kaman non-contact reactance sensors, mounted below the roof surface as shown in Figures (7.1) and (7.2). A transducer positioning frame was fabricated to orient the transducers normal to the membrane surface. This arrangement allowed the identification of both the axisymmetrical and asymmetrical modes of vibrations.

Electrical leads for various sensors were passed through the side of the chamber and carefully sealed. Small aluminum foil targets were glued to the outer surface of the roof at the Kaman probe locations to provide electrical conductivity.

The added mass of the targets was small. The measured membrane displacements were instantaneous values averaged spatially over the area of the probe surface.

7.6 FREE VIBRATION TESTS

An experimental investigation of free vibration was conducted on the hemispherical aeroelastic model to find the natural frequencies, damping ratios and mode shapes of the structure in still air. The objective was to study the effects of internal pressure and volume scaling on the dynamic behaviour of the hemispherical air-supported structure for the condition of still air.

7.6.1 Test Procedure

The aeroelastic model was excited in still air using a loudspeaker. Two types of excitation were used: random and harmonic. The random excitation was generated using white noise with a frequency range of 0 to 400 Hz. Harmonic excitation was then applied stepwise at each natural frequency, and was used to identify the associated mode shapes similar to what was done in Section 4.5. A parametric study was conducted in which three different internal pressures and three different enclosure volumes were considered.

7.6.2 Test Results

7.6.2.1 Frequencies of Free Vibration

Using the HP analyzer, the natural frequencies of the hemispherical air-supported model were identified for all of the internal pressures considered. For comparison, the theoretical damped frequencies were calculated using the finite

element program ABAQUS mentioned previously in Chapter 6. The finite element used in the analysis was a 4 node membrane element, S4R, as shown in Figure (7.3). The first four mode shapes determined theoretically for the hemispherical air-supported structure are shown in Figure (7.3). The experimental and theoretical results of the model frequencies are shown in Figure (7.4), in which the theoretical values are plotted in dashed lines. The frequency notation used here is f_{ij} in which i is the number of nodal lines, and j is the order of the mode; for axisymmetrical mode shapes i equals zero.

The aeroelastic model fundamental frequency was 130 Hz at an internal pressure of about 40 Pa. The frequencies most affected by the internal pressure are the fundamental frequencies f_{01} and f_{02} associated with the first two axisymmetrical modes. The first frequency, f_{01}, can be interpreted as one of a curved, pressurized "kettledrum". It is the most affected by varying the internal pressure, since it is the most volume-changing mode. This frequency decreases with diminishing internal pressure, and its experimental values agree well with the theoretical predictions for most internal pressures. The extreme case occurs when the internal pressure inside the structure approaches zero, which causes the membrane stiffness to decrease, and therefore the frequency f_{01} to approach zero. As the internal pressure increases, the natural frequency of the system increases as the roof becomes stiffer.

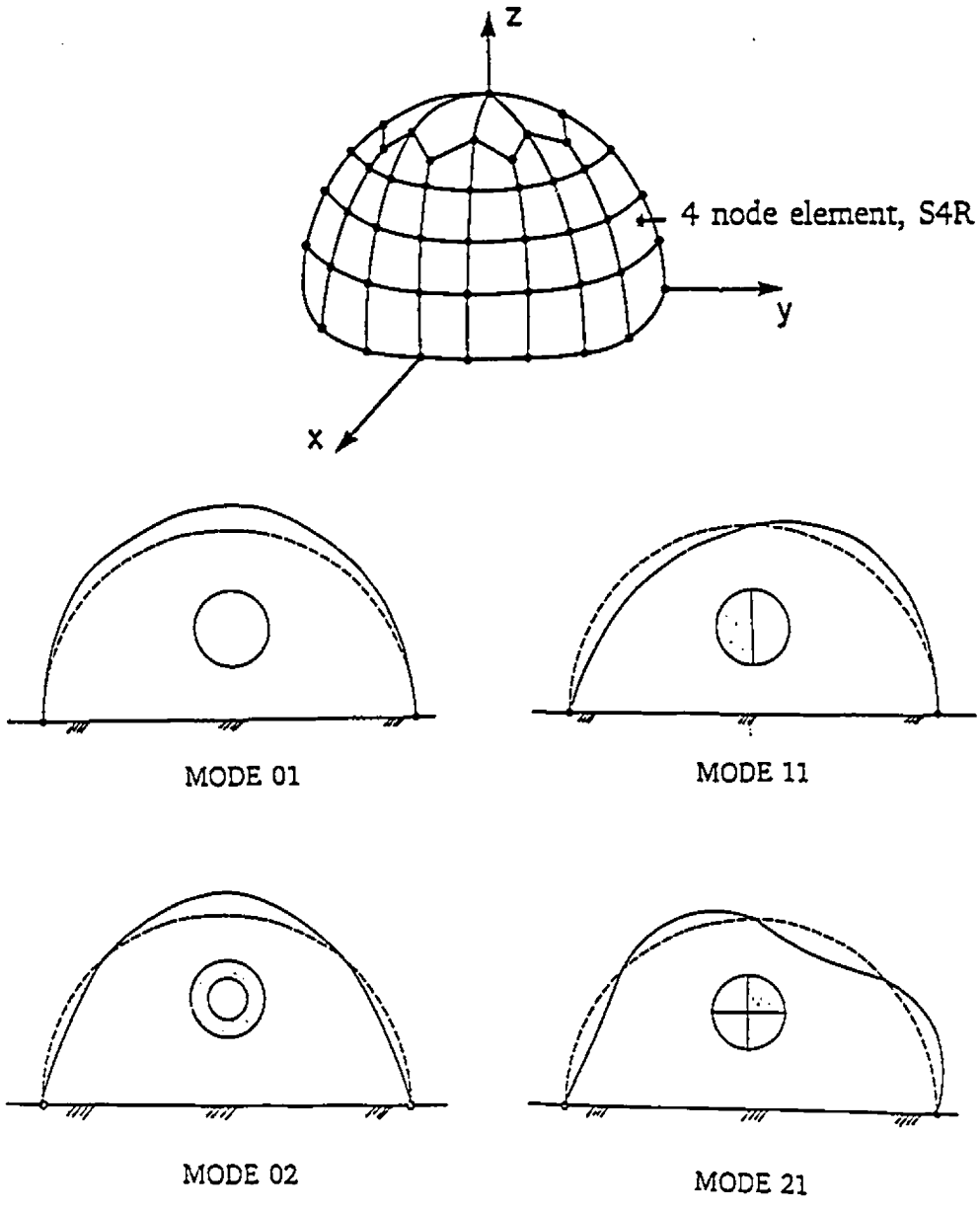

Fig. (7.3): Mode shapes of the hemispherical air-supported structure

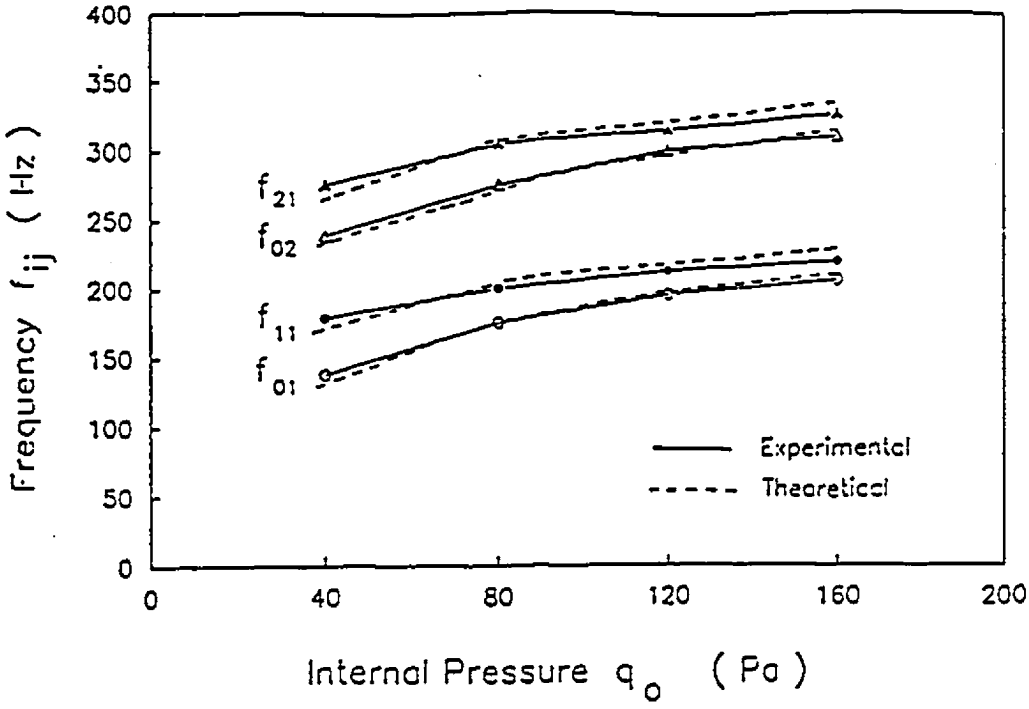

Fig. (7.4) : Effect of internal pressure on frequencies of free vibration

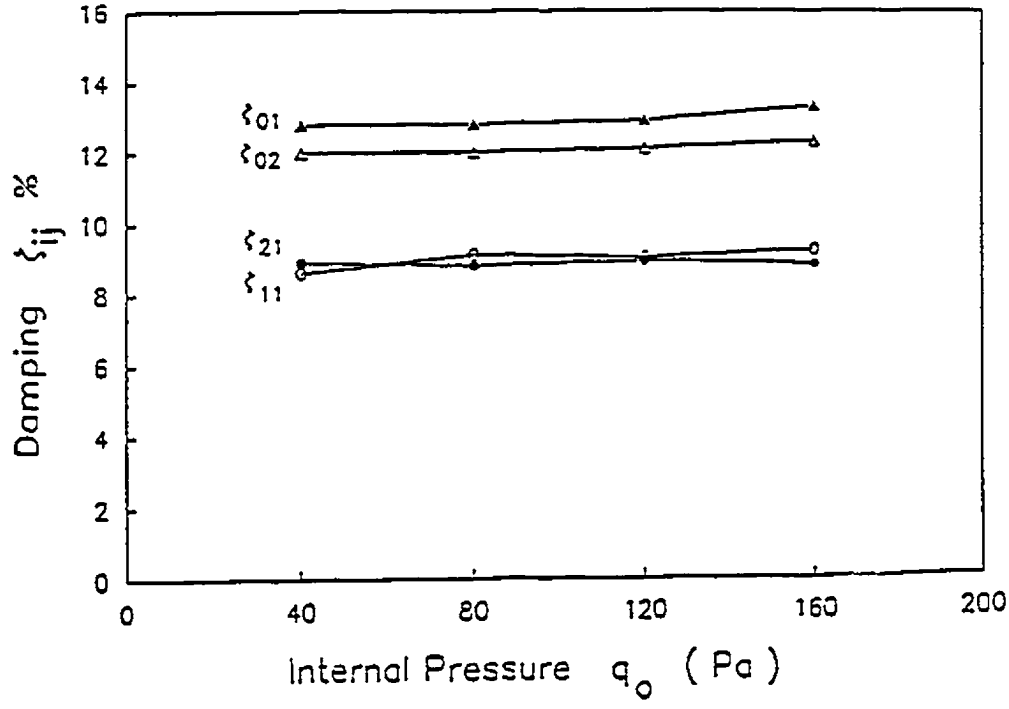

Fig. (7.5) : Effect of internal pressure on damping of free vibration

7.6.2.2 Modal Damping of Free Vibration

For various values of internal pressure, the total damping ratios were experimentally established for the model using the HP analyzer, as mentioned in Section 4.5. The modal damping ratios of the first four modes are plotted in Figure (7.5). The damping ratio of the fundamental mode with frequency, f_{01}, is denoted ζ_{01}. Figure (7.5) shows that the damping is relatively insensitive to the internal pressure for the internal pressure range tested. However, there is a tendency for the damping to be slightly increased by the increase in the internal pressure.

The damping of the axisymmetrical mode f_{01} is higher than that of the second axisymmetrical mode f_{02}, as a result of the first mode being the most volume changing mode. The total damping ratios of the axisymmetrical modes f_{01} and f_{02} are higher than those of the antisymmetrical modes f_{11} and f_{21}. This is so because of the acoustical damping associated with the axisymmetrical modes of vibration.

7.6.2.3 Effect of Enclosure Volume

The volume of the pressure chamber underneath the model was changed in three steps by inserting cylinders of rigid styrofoam. The frequencies and damping ratios were then established as before. The internal pressure was kept constant for the various volumes considered for each test series.

The volume factor used to characterize the enclosure is the ratio of the volume of the chamber under the model base to the volume of the cavity above the base. The measured frequencies and damping ratios are presented in Figure (7.6) and Table (7.3). The fundamental frequency varies with the chamber volume quite markedly and decreases with increasing chamber volume. This is to be expected because the roof behaves as a curved pressurized "kettledrum" whose fundamental frequency, f_{01}, depends on the pneumatic stiffness of the enclosure, and thus on its volume.

Figure (7.6) shows that if the model design was based only on the length scale (i.e., if the volume of the chamber under the model was zero), the fundamental axisymmetrical frequency f_{01} would be considerably overestimated. A similar trend was observed for the second axisymmetrical mode f_{02}, but was not as pronounced as for the first axisymmetrical mode f_{01}, because the volume changes involved are small in comparison.

The damping ratios of the fundamental modes of the model for different enclosure volumes are given in Table (7.3). It can be seen that there is a small increase in the damping ratio, ζ_{01} and ζ_{02}, of the axisymmetrical modes with decreasing chamber volume, and that the enclosure volume has little effect on the antisymmetrical modes, ζ_{11} and ζ_{21}.

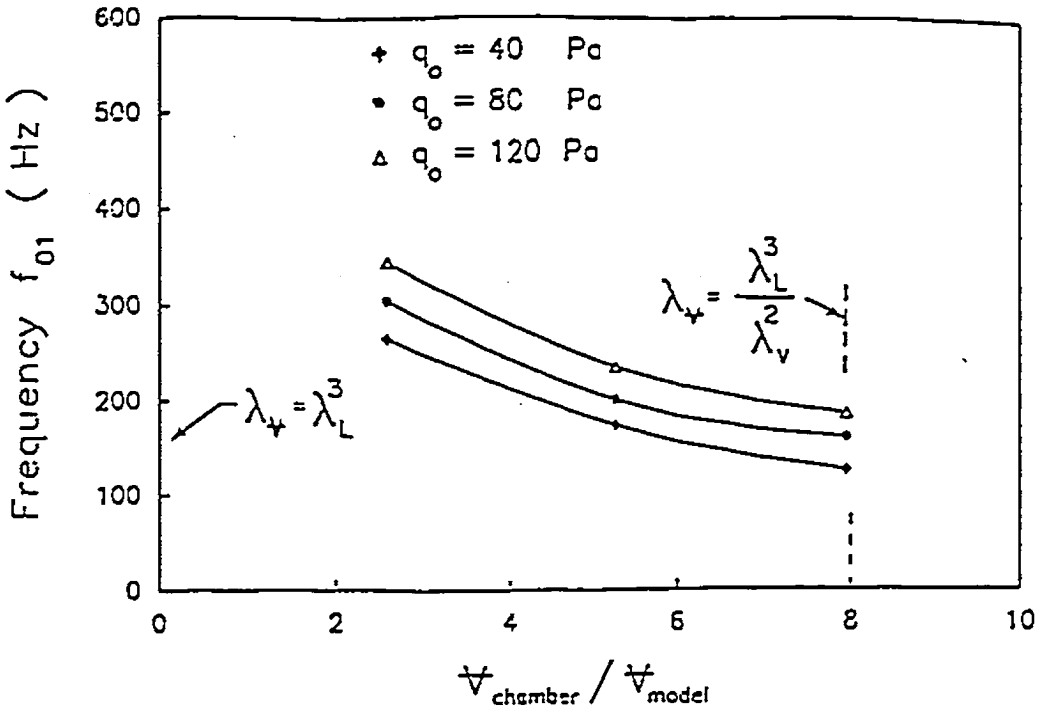

Fig. (7.6) : Effect of cavity volume on fundamental frequency of the hemispherical model

TABLE (7.3): EFFECT OF ENCLOSURE VOLUME ON DAMPING RATIOS

$\forall_{chamber}$ / $\forall_{model}$	Internal pressure (Pa)	Damping Ratios (%)			
		ζ_{01}	ζ_{11}	ζ_{02}	ζ_{21}
8	40	12.9	8.5	12.0	8.9
	80	12.8	9.1	12.0	8.8
	120	12.9	9.0	12.1	8.9
5.33	40	14.0	8.7	12.5	9.0
	80	12.8	9.1	12.0	8.8
	120	12.9	9.0	12.5	8.9
2.66	40	14.5	9.0	12.8	8.8
	80	15.0	9.1	12.5	9.0
	120	14.0	8.8	12.5	8.9

7.7 WIND TUNNEL AEROELASTIC TESTS

7.7.1 Flow Modelling

The experimental work was conducted at the Boundary Layer Wind Tunnel Laboratory (BLWT II) at The University of Western Ontario, London, Ontario, Canada. The experiments were conducted in the high speed tunnel section that has cross-sectional dimensions of 3.4 m high, 2.5 m wide, and is 39 m long. The tunnel is equipped with adjustable-height roughness elements to produce boundary layers appropriate to a wide variety of terrain roughnesses. The tunnel is also equipped with noise dampers to reduce acoustic noise.

Three terrain exposures were simulated in these tests by varying the height of the roughness elements; open country, suburban and urban exposures. The roughness elements have an across flow width of 0.10 m and an along flow depth of 0.05 m, and are distributed with 0.40 m center to center spacing in both directions, upstream and downstream of the test area. The open country, suburban and urban exposures were achieved with the elements in the upstream fetch with heights of 20, 55 and 125 mm, respectively. The wind properties at different heights was measured using a hot wire device mounted on a vertical transversing gear at the model location. The wind tunnel was automatically controlled by an on-line PDP 11/73 computer that also took the measurements.

The properties of the flow measured include the vertical variation of the mean wind speed U(z), and of the standard deviation of the wind velocity

fluctuation, $\sigma_u(z)$ at the test section. Spectra of the wind velocity at the top of the model, the vertical profiles of the mean wind speed, and the longitudinal local turbulence intensity ($\sigma_u(z)/U(z)$) in the test section are shown in Figures (7.7) to (7.12) for different exposures. The local turbulence intensities at the top of the model were about 18.9%, 22.5% and 33.9% for the open country, suburban, and urban exposures, respectively. The heights at the edge of the boundary layer were 1.19, 1.33, and 1.48 m for the open country, suburban, and urban exposures, respectively. The properties of the flow were measured at a gradient wind speed (wind speed at the top of the boundary layer) of about 15 m/sec, $R_e \approx 3.0 \times 10^5$ based on the diameter of the model.

7.7.2 Experimental Procedure

The aeroelastic model was tested in turbulent boundary layer flow conditions simulating natural wind as described above. The model testing was carried out for all combinations of the following four parameters:

1. Exposure: open country, suburban and urban exposures.
2. Internal pressure: 40, 80, and, 120 Pa.
3. Gradient wind speed: 6, 9, 12, and 15 m/sec.
4. Volume of the enclosure: volume ratios of 9:1, 6:1, and 3:1.

The volume of the model was varied in order to investigate the effects of air compressibility on the wind-induced response and the internal pressure fluctuations. The model was also rotated to check the reliability of the results and

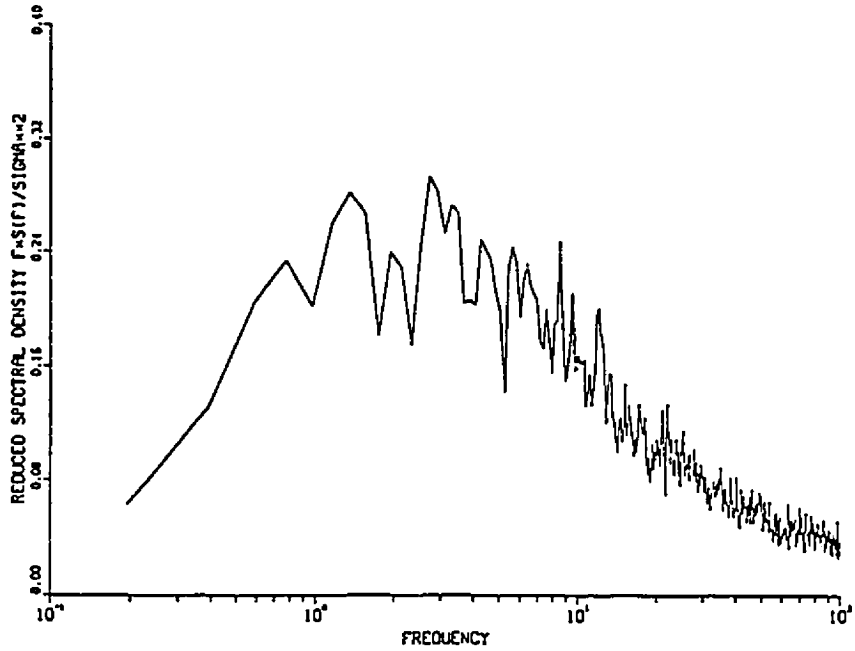

Fig. (7.7): Velocity spectrum for open country exposure

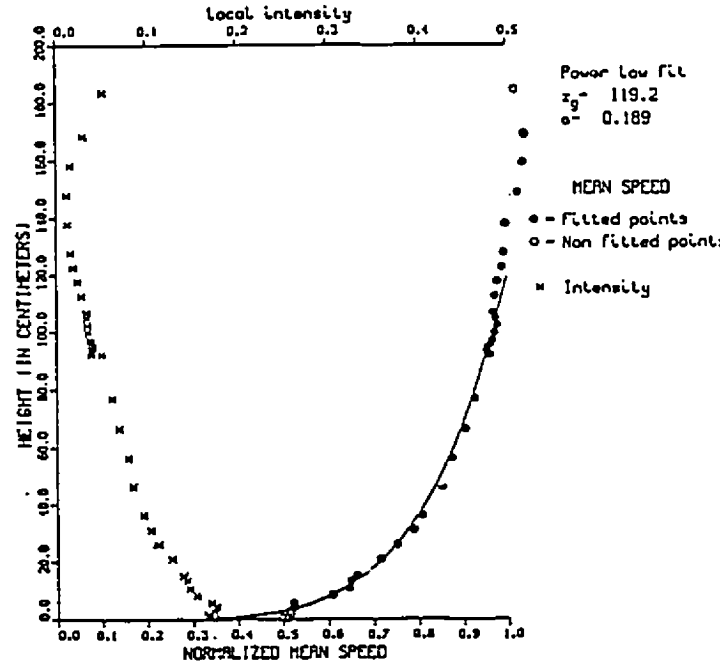

Fig. (7.8): Velocity profile for open country exposure

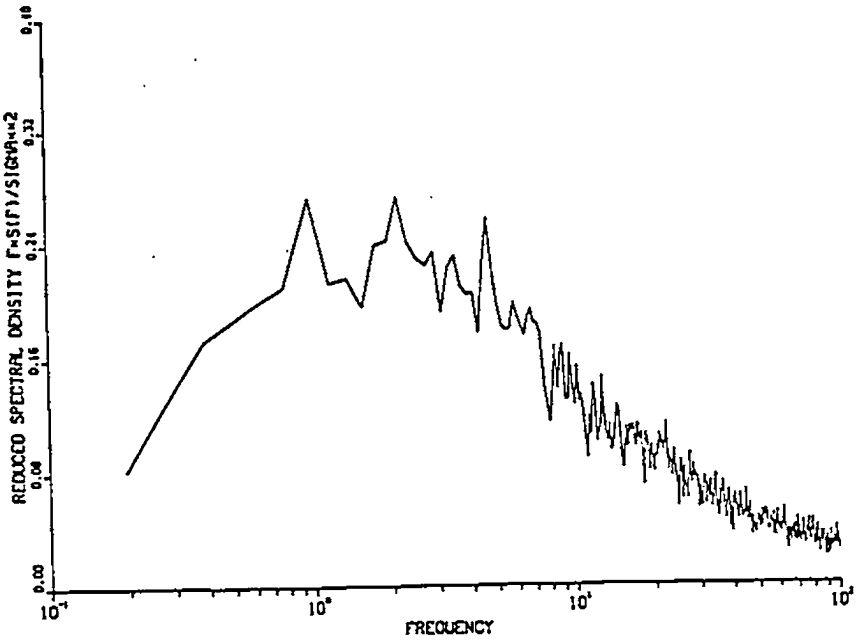

Fig. (7.9): Velocity spectrum for suburban exposure

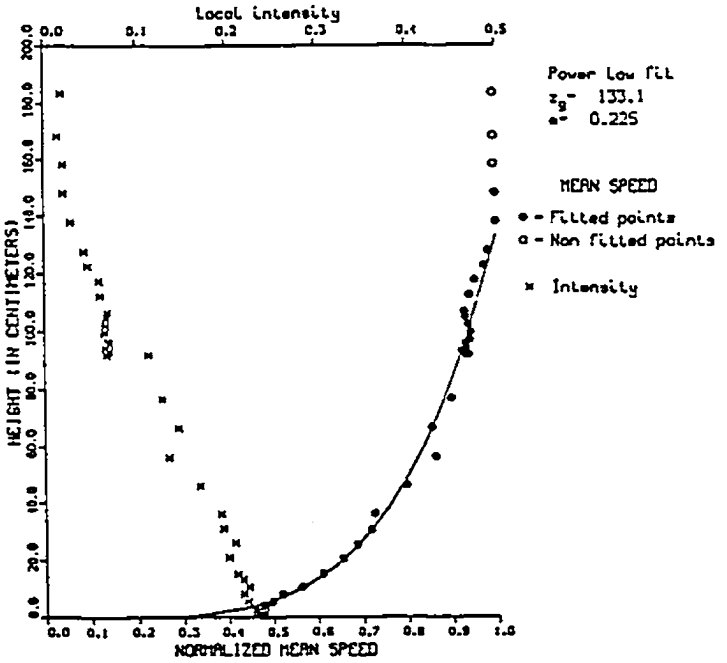

Fig. (7.10): Velocity profile for suburban exposure

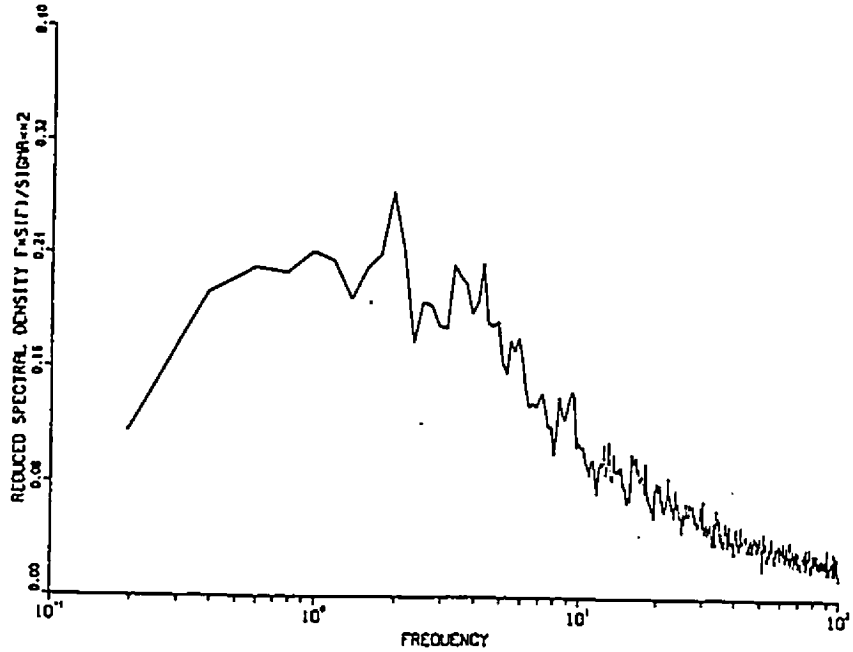

Fig. (7.11): Velocity spectrum for urban exposure

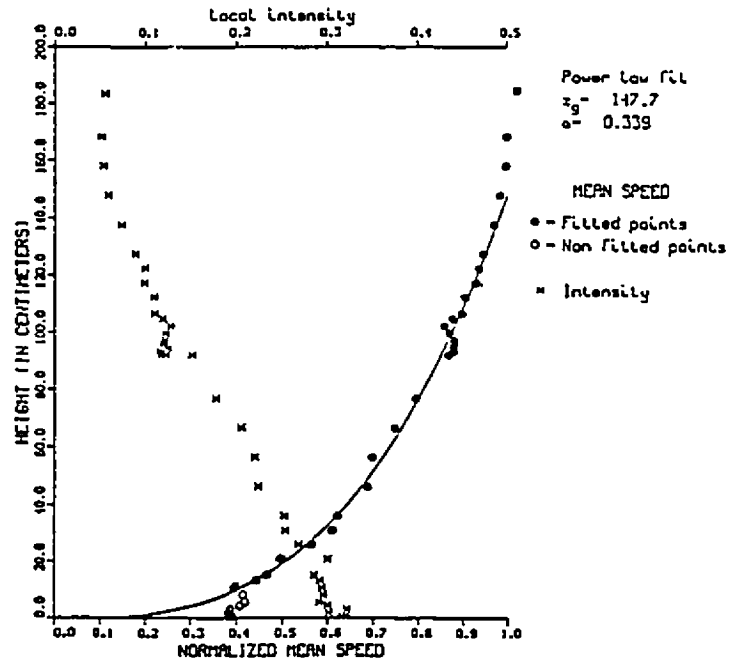

Fig. (7.12): Velocity profile for urban exposure

to cover a large number of points on the roof surface. The angles of rotation were 22.5°, 45°, 90°, 270°, and 315°.

The hemispherical aeroelastic model was instrumented to permit quantitative measurements of the mean and dynamic wind-induced membrane deflections and internal pressure fluctuations. The perpendicular displacements of the roof were measured at the five locations shown in Figure (7.2) using Kaman probes. In all cases, the measured deflections were perpendicular to the roof surface, and are given with respect to its initial geometry for a particular internal pressure. To study the internal pressure fluctuations within the model cavity due to the membrane movement under turbulent wind, a Setra pressure transducer was used. The outputs of both the displacement and pressure transducers were passed through a filter and an oscilloscope, then connected either to the on-line computer or to the HP analyzer. The arrangement of the testing procedure is shown in Figure (7.13).

The digital data acquisition system was used to obtain the maximum, minimum, mean, and RMS values of both the roof response and the internal pressure. Also, it was used to obtain the auto-spectra of both the membrane responses at the five locations, and the dynamic internal pressure. The deflections at all probe locations and the internal pressure fluctuations were simultaneously measured over an averaging period corresponding to approximately one hour in full scale for all test series. The HP analyzer was employed for the computation

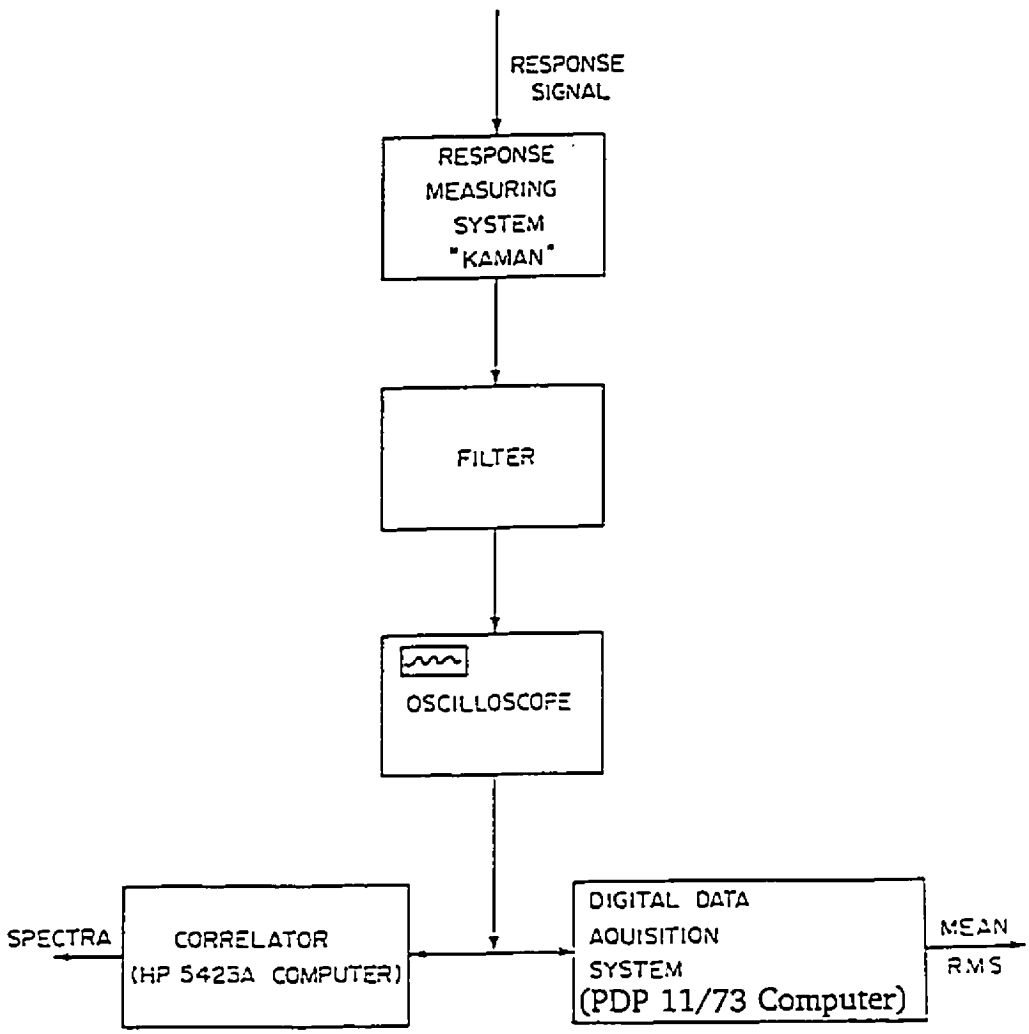

Fig. (7.13): Wind tunnel experimental set-up

of the auto-spectra, cross-spectra, auto-correlation and cross-correlation of the roof deflections at all probe locations. A photograph of the aeroelastic model in the wind tunnel is displayed in Plate (7.1).

7.8 AEROELASTIC MODEL RESPONSE

The aeroelastic model remained aerodynamically stable for all of the different internal pressures and wind speeds tested. Measured mean and RMS membrane deflections, and internal pressure fluctuations for the various test configurations are discussed below.

7.8.1 Effect of Wind Speed

Typical variations of the mean and RMS membrane deflections with wind speed for all internal pressures are presented in Figures (7.14a), (7.14b), and (7.15). It can be seen that the mean response is proportional to the square of the wind speed, and the RMS response increases almost linearly with the wind speed. This shows that the structural response is due only to gusting wind, and that there is no effect of vortex shedding or aerodynamic instability in the range of the internal pressures and wind speeds considered. The RMS deflections were typically small in comparison with the mean deflections.

The vortex shedding frequency (calculated on the basis of a Strouhal number equals 0.20) is about 10 Hz, which is well below the fundamental frequency of the model for the internal pressure range considered. Therefore, vortex shedding had no effect on the model response. It is important to emphasize

that vortex shedding may be a problem in air-supported structures if the internal pressure suddenly drops for any reason. The drop in the internal pressure causes the fundamental frequency of the structure to fall and approach the vortex shedding frequency, which may lead to destructive oscillations and flutter.

The power spectra of the roof response at various locations and for different conditions were measured using the on-line computer and the HP analyzer. Examples of the power spectra of response are shown in Figures (7.16), (7.17), and (7.18) for the open country exposure, gradient wind speed of 15 m/sec, and an internal pressure of 40 Pa. Spectra of response for other exposures and internal pressures are given in Appendix A. Examining the power spectra of the membrane response, the dynamic deflections were broad band random processes with no indication of pronounced resonant components at the natural frequencies. This may be because of the high damping.

An overlay of the response and external pressure spectra at probe 5, and the wind velocity is given in Figure (7.18) for open country exposure, gradient wind speed of 15 m/sec, and an internal pressure of 40 Pa. It can be seen that the energy is similarly distributed in all spectra and that the spectral values start to decrease gradually at high frequencies. The response of the structure is mainly at frequencies well below the fundamental frequency of the structure, which may be because the structure is heavily damped.

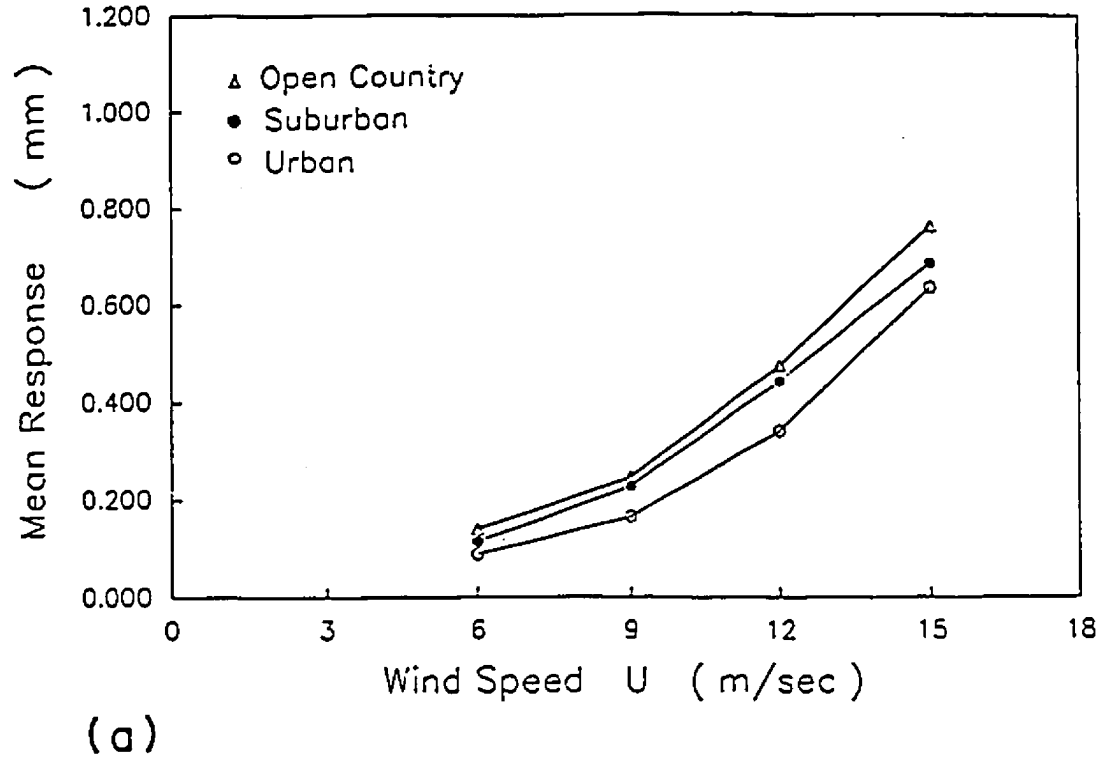

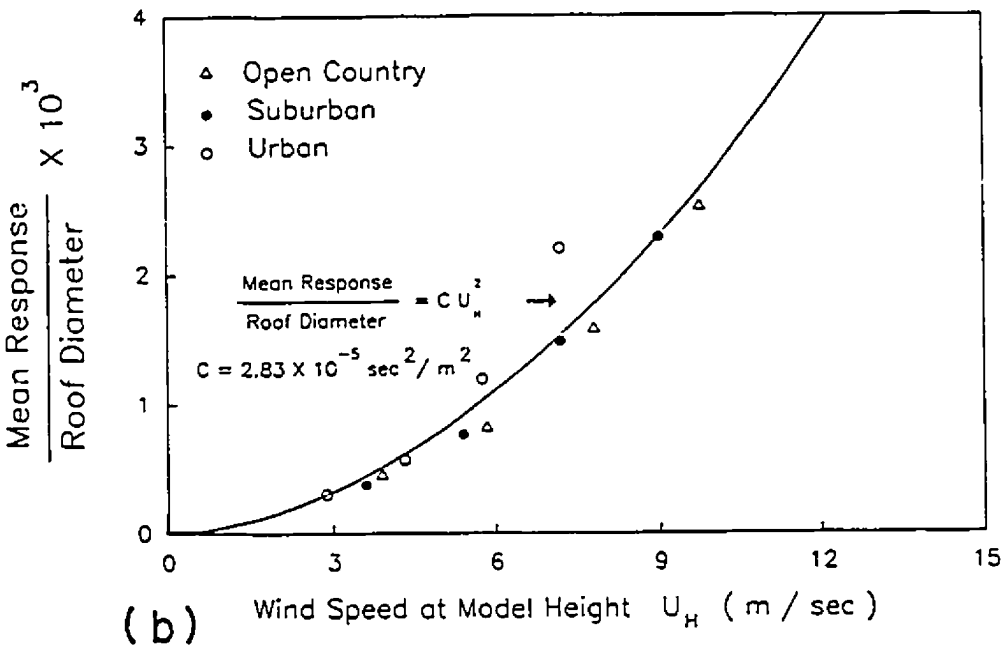

Fig. (7.14) : Mean response at roof center for different exposures (q_o = 40 Pa)

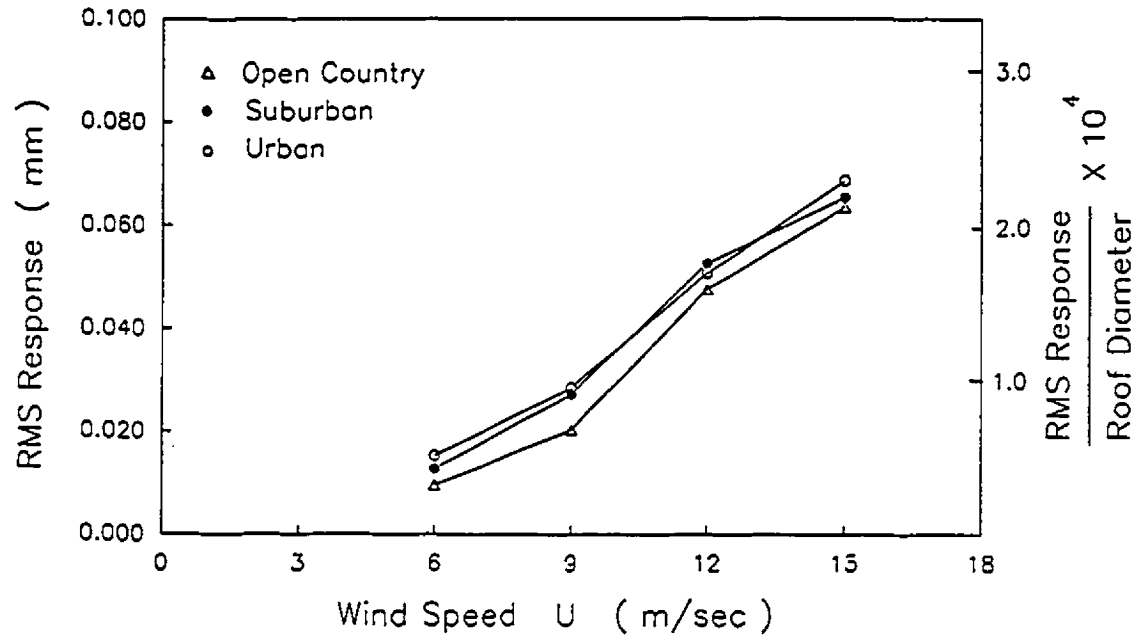

Fig. (7.15) : RMS response at roof center for different exposures (q_o = 40 Pa)

7.8.2 Effect of Exposure

It can be seen that the open country exposure gives higher mean and smaller RMS deflections as shown in Figures (7.14a), (7.14b), and (7.15) for an internal pressure of 40 Pa. Similar trends were found at the other locations. This could be because for the open country exposure, the mean wind speed at roof height is higher than those for other exposures, yielding higher values of mean response. In contrast, the urban exposure has more turbulence at roof height than the other exposures, yielding higher RMS deflections. Examples of the measure spectra of response for different exposures are given in Figures (7.16), (7.17), (7.18), and in Appendix A.

The normalized mean response of the roof center is plotted versus the wind speed at the top of the model, U_H, as shown in Figure (7.14b) for different exposures and an internal pressure of 40 Pa. It can be seen that the mean response for different exposures is proportional to the square of U_H. This trend is similar to that of the response of conventional structures to gusting wind.

It can also be seen from Figure (7.14b) that the normalized mean response, plotted versus the mean wind velocity at the top of the model, U_H, is independent of the terrain roughness. This is because the mean response basically depends on the mean wind speed at the top of the model, U_H, and for the same U_H the response is the same, regardless of the exposure condition.

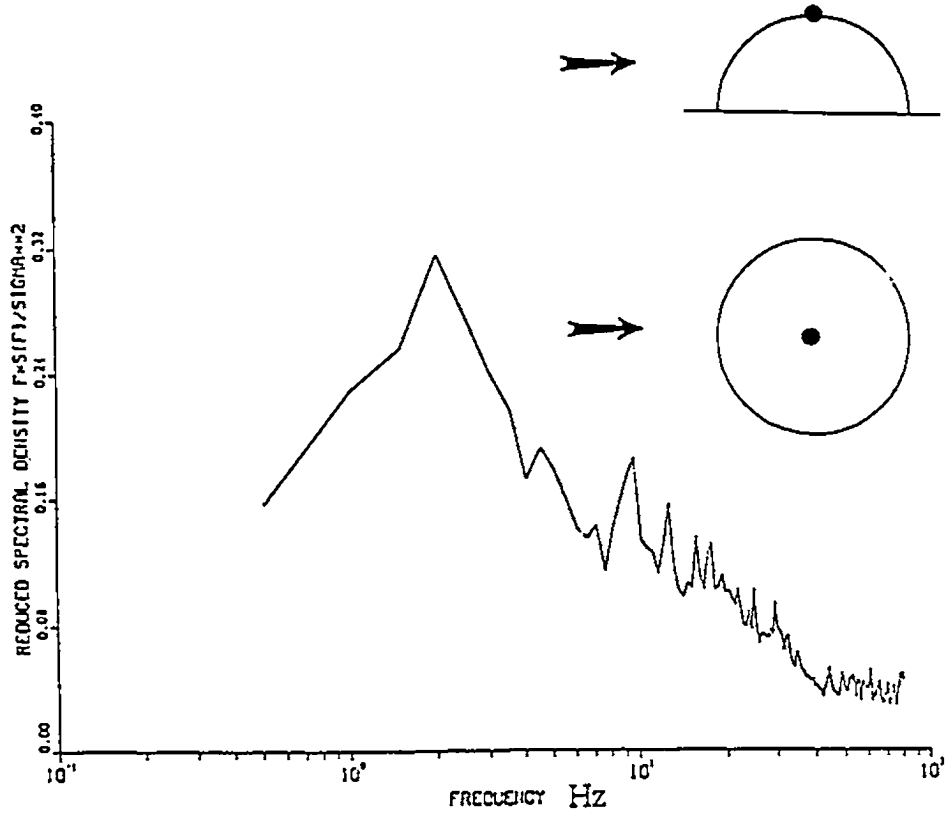

Fig. (7.16): Power spectrum of response at roof center
(open country exposure, U = 15 m/sec, and q_o = 40 Pa)

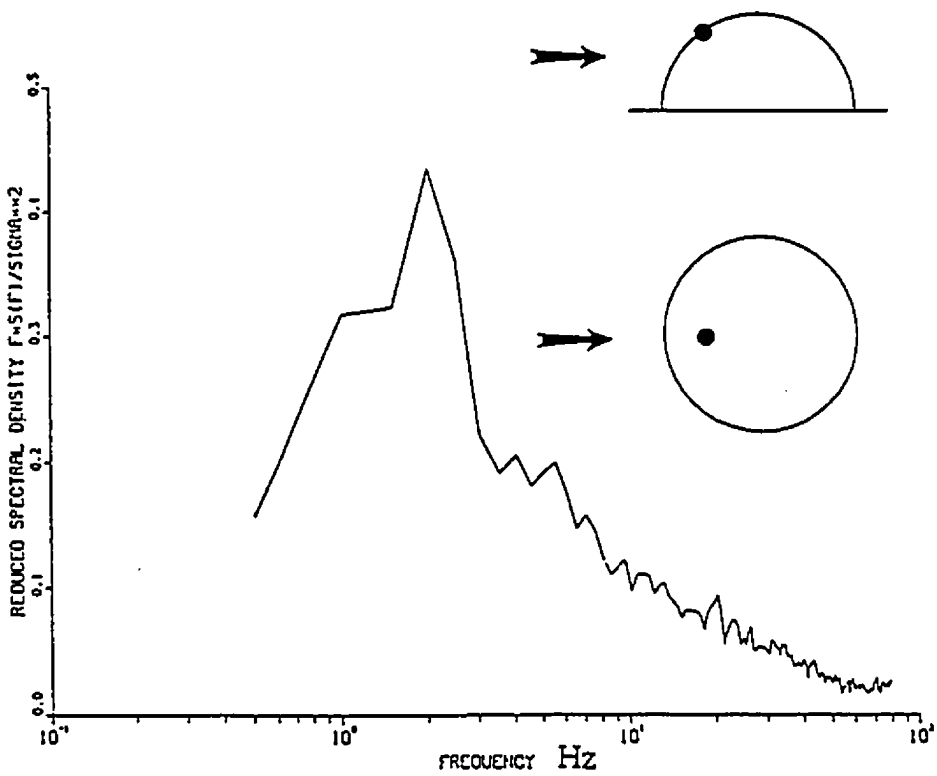

Fig. (7.17) : Power spectrum of response at probe 2 (open country exposure, U = 15 m/sec, and q_o = 40 Pa)

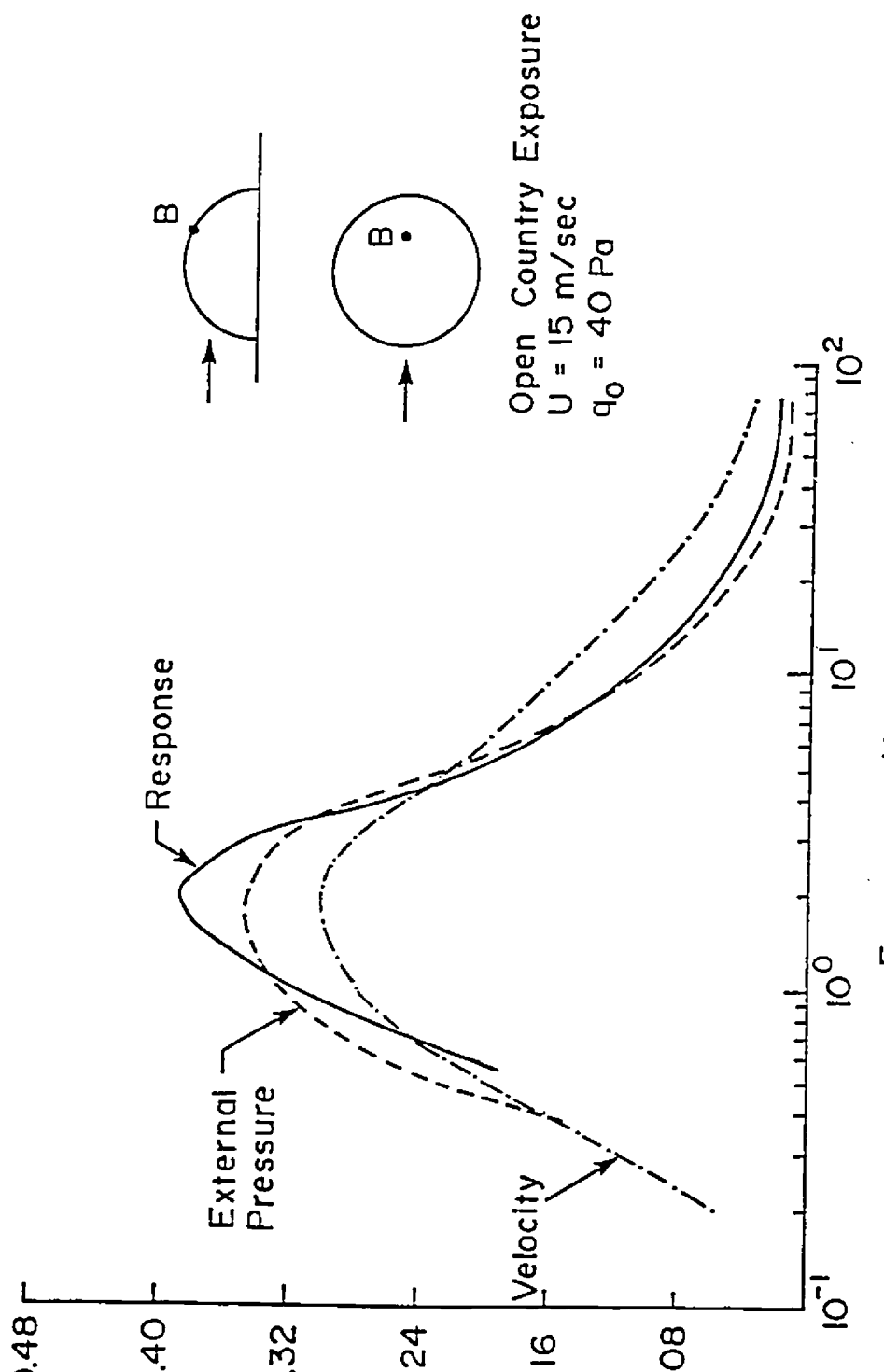

Fig. (7.18) : Comparison between wind velocity, external pressure, and response spectra

7.8.3 Internal Pressure Effect

To study the effect of the internal pressure on the measured wind-induced response, three values of internal pressures were used: 40, 80, and 120 Pa. The measured mean and RMS deflections at roof center for these three internal pressures are presented in Figures (7.19a), (7.19b), and (7.20). Examples of the response spectra for open country exposure; U = 15 m/sec and q_o = 40 Pa are shown in Figures (7.16), (7.17), and (7.18). Spectra of other exposures and internal pressures are given in Appendix A.

It can be seen from Figures (7.19a), (7.19b), and (7.20) that there is a tendency towards reduced mean and dynamic deflections at the center of the roof with increasing internal pressure for a specific wind speed. The mean response, in particular, was affected by the variation of the internal pressure over the range considered. This may be attributed to the reduction in the roof stiffness accompanying low values of internal pressure. The mean and RMS deflections at all other locations showed the same trend.

The normalized mean responses at the roof center (for different internal pressures and the condition of open country exposure) are plotted versus the nondimensional parameter $U_H/(f_{o1}d)$ as shown in Figure (7.19b), where f_{o1} is the fundamental frequency of the model and d is the model diameter. The fundamental frequency f_{o1} is used to normalize the results as it represents the total stiffness of the model for different internal pressures. It is important to emphasize

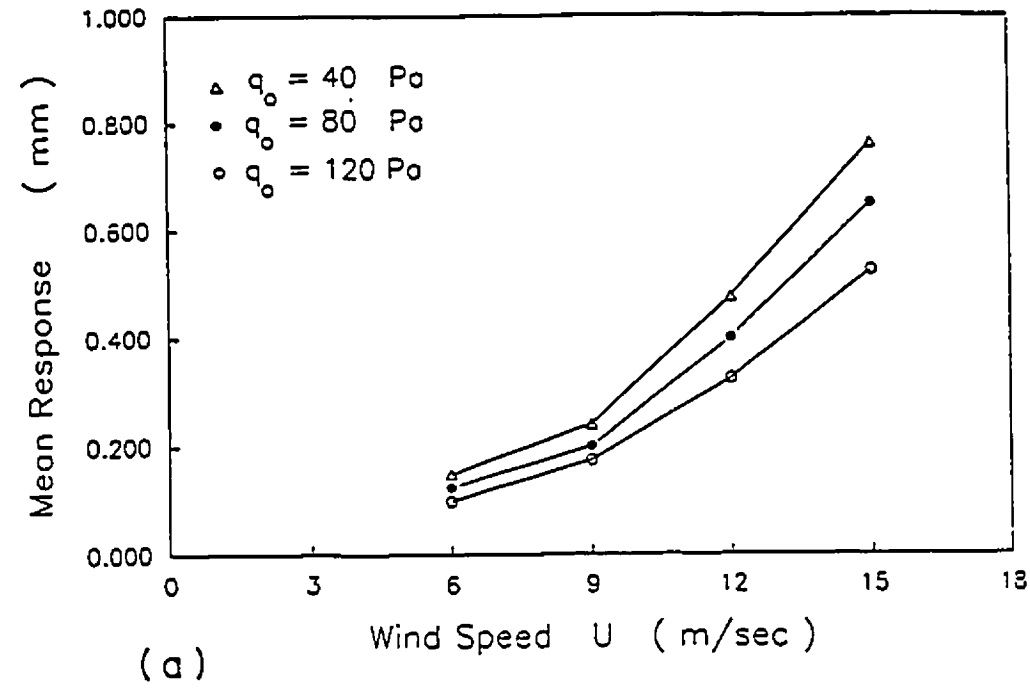

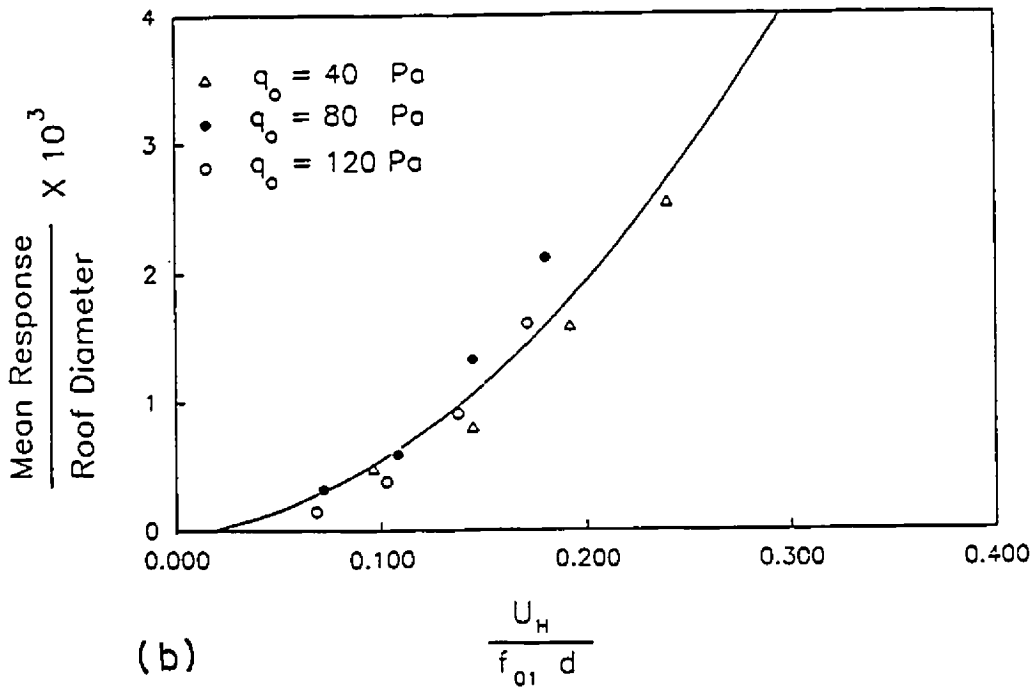

Fig. (7.19) : Mean response at roof center for different internal pressures (open country exposure)

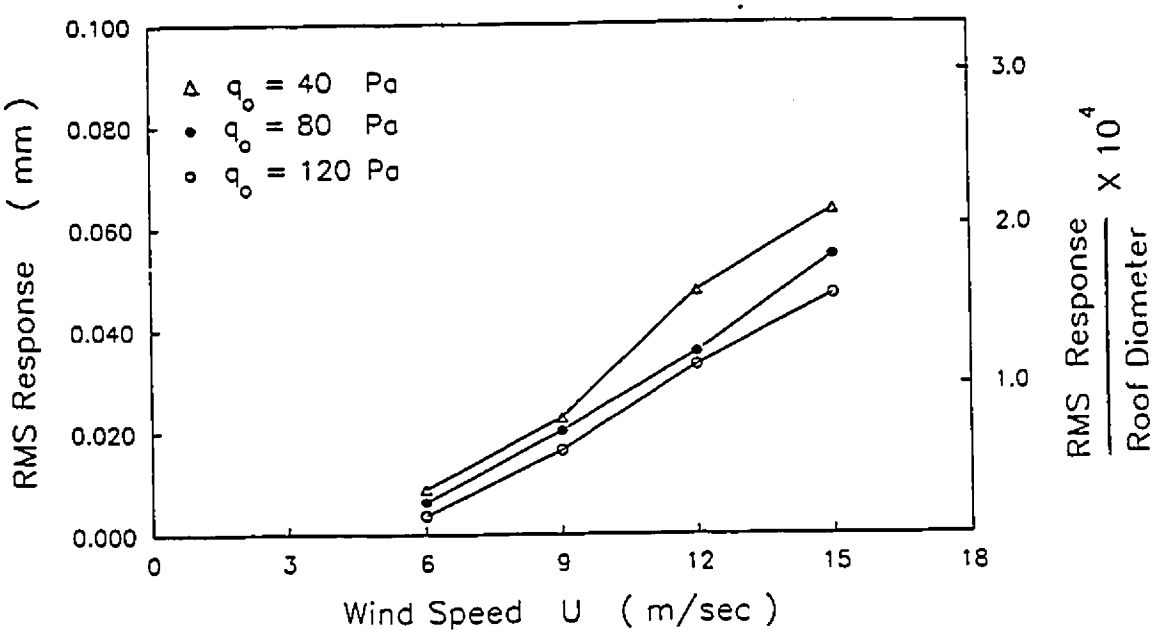

Fig. (7.20) : RMS response at roof center for different internal pressures (open country exposure)

that the total stiffness in air-supported structures stems from the elastic stiffness due to the tension of the membrane, the internal pressure q_o, and the compressibility of the enclosed air.

It can seen from Figure (7.19b) that the mean response results for different internal pressures fall on one curve. This means that the aerodynamic mean response of the model can be estimated for different internal pressures once the fundamental frequency of the model at that specific internal pressure is known, or in other words once a relation between the fundamental frequency of the model and the internal pressure is established. This relation can be established either theoretically using a finite element method or experimentally using an elastic model as discussed in Sections 7.5 and 7.6. It can also seen from Figure (7.19b) that the normalized mean response for different internal pressures is proportional to the square of U_H.

To observe the buckled shape, the internal pressure of the model was adjusted to about 13 Pa, and the wind speed was increased gradually until a part of the membrane on the windward side buckled. The buckled area increased as the wind speed was further increased. A photograph of the buckled shape of the membrane is displayed in Plate (7.2).

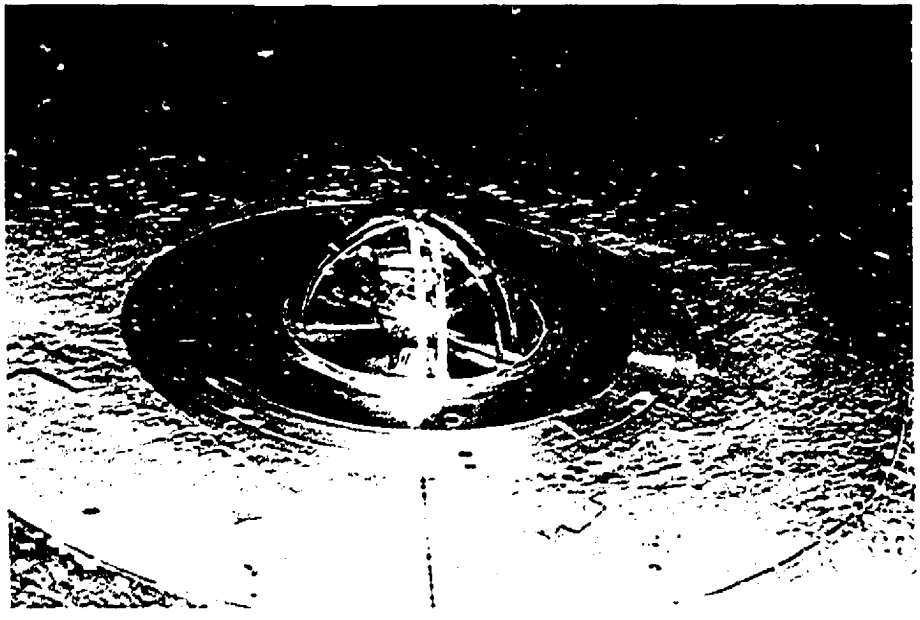

Plate (7.2): Local buckling of model on the windward side

7.8.4 Effect of Volume Scaling of Enclosure

In Chapter 4, it was mentioned that to achieve the dynamic stiffness scaling, the internal volume of the prototype needs to be exaggerated by a factor of $1/\lambda_V^2$ in excess of that indicated by direct geometric scaling. The tests described in this section were conducted to investigate the error that might arise from an incorrect volume scaling of the structure enclosure, and to examine the role of air compressibility. To study these effects, the volume of the chamber under the model was changed in three steps, as done in the free vibration tests. In these steps, the ratios of the chamber volume to the model volume were 8:1, 5.33:1 and 2.66:1.

The effect of the volume scaling on the measured wind-induced mean and RMS deflections of the model is shown in Tables (7.4) and (7.5), for the open country exposure and an internal pressure of 40 Pa. It can be seen that there is a tendency towards decreased static and dynamic deflections with decreasing chamber volume over the volume range tested, for a particular wind speed. This may be attributed to the increase in the roof stiffness accompanying smaller volume ratios. This increase in stiffness is due to a smaller volume of air being available to be compressed. This suggests that air compressibility plays a major role in increasing the overall stiffness of the roof for small enclosed air volumes. This effect, however, is less pronounced than that of increasing the internal pressure.

TABLE (7.4): MEAN RESPONSE AT MODEL CENTER FOR DIFFERENT ENCLOSED VOLUMES

(q_o = 40 Pa and open country exposure)

Tunnel Wind Speed (m/sec)	Model Mean deflection x (1 x 10^{-3}) mm		
	$\forall_{chamber}/\forall_{model}$		
	8.00	5.33	2.66
9	240	230	220
12	475	470	460
15	765	750	740

TABLE (7.5): RMS RESPONSE AT MODEL CENTER FOR DIFFERENT ENCLOSED VOLUMES

(q_o = 40 Pa and open country exposure)

Tunnel Wind Speed (m/sec)	Model RMS deflection x (1 x 10^{-3}) mm		
	$\forall_{chamber}/\forall_{model}$		
	8.00	5.33	2.66
9	25.00	22.50	20.00
12	47.50	45.00	40.00
15	65.00	62.50	57.50

7.9 INTERNAL PRESSURE FLUCTUATIONS

A Setra pressure transducer was mounted inside the model to monitor the internal pressure fluctuations induced by the membrane vibration. The internal pressure fluctuations were dependent on the distribution of the external pressures over the roof and the associated roof movement due to wind loading.

Examples of the power spectra of the internal pressure fluctuations for different internal pressures are presented in Figures (7.21) and (7.22). Appendix A includes spectra of internal pressure fluctuations for other conditions. Comparing the internal pressure spectra with those of the aeroelastic response at a specific point, it was found that the internal pressure spectra decrease rapidly at high frequencies than the response spectra do. This may be because the internal pressure fluctuations depend on the integrated external pressures over the roof surface and not on the external pressure or the roof response at a certain point.

The effects of the wind speeds, exposure conditions, and internal pressures on the RMS values of the internal pressure are also plotted in Figures (7.23) and (7.24). It can be seen from Figure (7.23) that the RMS values of the internal pressure increase as the wind speed increases, and that they monotonically increase with the changing of the exposure from open country to urban exposure, due to the accompanying turbulence intensity increase.

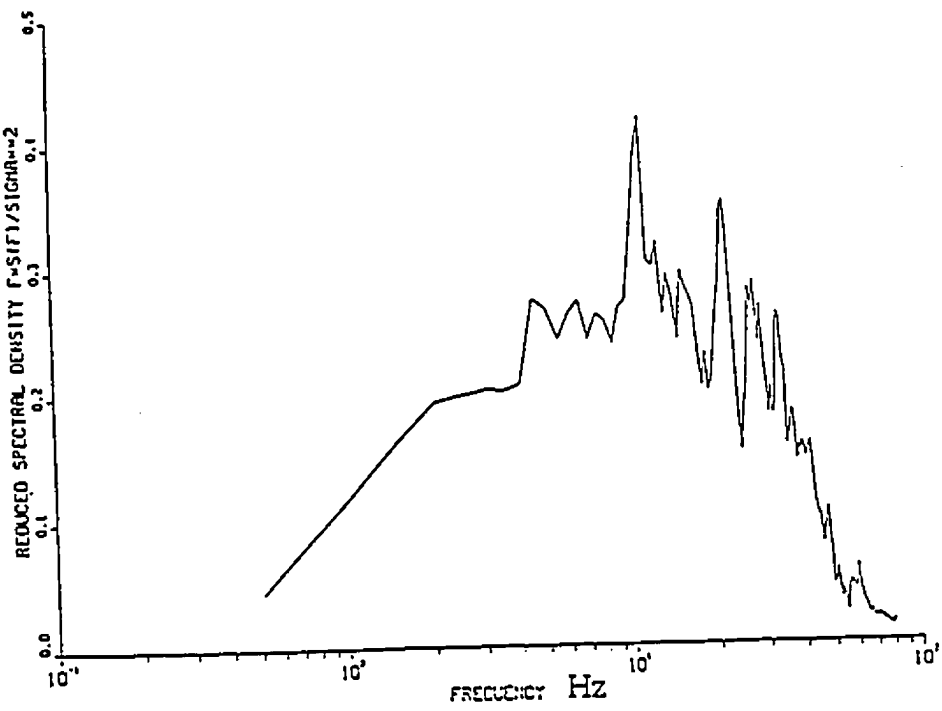

Fig. (7.21) : Power spectrum of internal pressure (open country exposure, U = 15 m/sec, and q_o = 40 Pa)

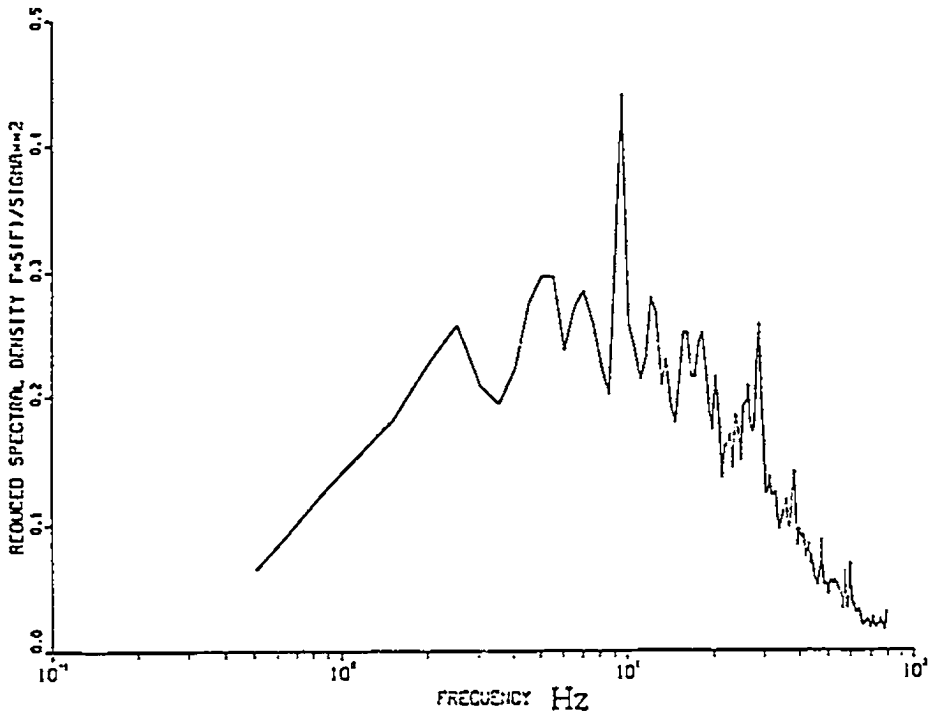

Fig. (7.22) : Power spectrum of internal pressure (open country exposure, U = 15 m/sec, and q_o = 80 Pa)

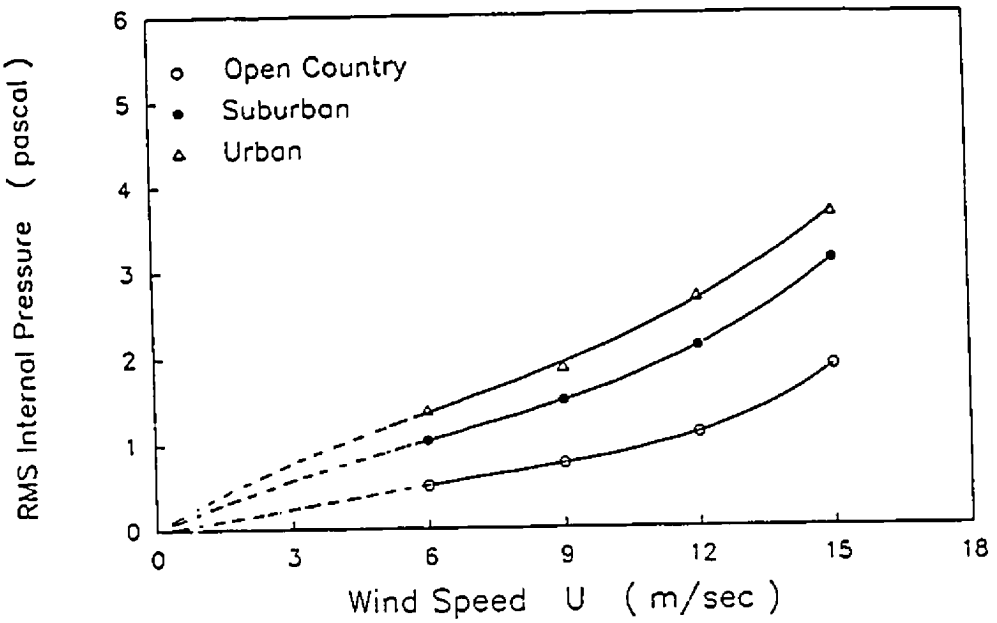

Fig. (7.23) : RMS internal pressure for different exposures (q_o = 40 Pa)

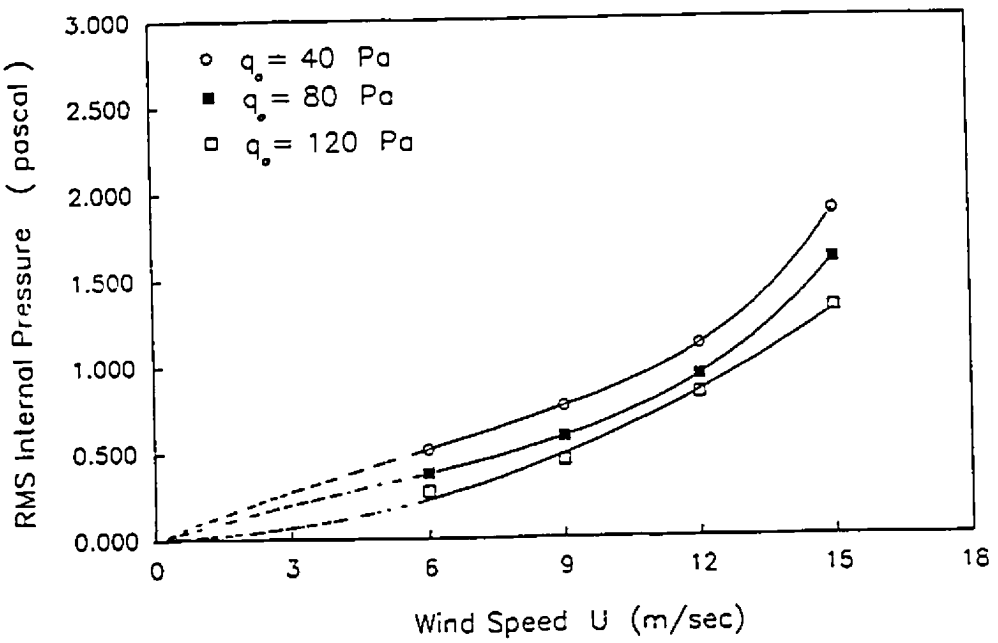

Fig. (7.24) : RMS internal pressure for different internal pressures (open country exposure)

The RMS values of internal pressure decrease with the increase of the mean value of the internal pressure as shown in Figure (7.24). This is similar to what was seen with the response, and is due to the increased stiffness and decreased motion of the roof under higher internal pressures.

The internal pressure fluctuations were also measured for different volume ratios. It was found that the RMS values of internal pressure slightly increase as the enclosure volume increases as shown in Table (7.6) for an internal pressure of 40 Pa and urban exposure. This is likely due to the effect of air compressibility, as discussed in Subsection 7.8.4.

In summary, the internal pressure fluctuations were generally small, being less than about 4 Pa for a gradient wind speed of about 15 m/sec. The peak departure of the model internal pressure from its mean value for this wind speed was in the order of 12 Pa for an internal pressure of 40 Pa.

It must be mentioned that the RMS internal pressure results in this section were corrected as they had zero intercepts when they were originally plotted. The zero intercepts are probably a combination of electronic noise and acoustic noise from the pressure regulator. The data were corrected by fitting a polynomial to the RMS internal pressure results from which the zero intercepts were determined. The corrected RMS internal pressure data are shown in Figures (7.23) and (7.24).

TABLE (7.6): RMS INTERNAL PRESSURE OF THE MODEL FOR DIFFERENT ENCLOSED VOLUMES

(q_o = 40 Pa and urban exposure)

Tunnel Wind Speed (m/sec)	RMS Internal Pressure (Pa)		
	$\forall_{chamber}/\forall_{model}$		
	8.00	5.33	2.66
9	1.90	1.70	1.20
12	2.60	2.30	2.00
15	3.70	3.42	2.90

CHAPTER 8

PREDICTION OF WIND-INDUCED RESPONSE OF HEMISPHERICAL AIR-SUPPORTED STRUCTURES

8.1 INTRODUCTION

In this study, a semi-analytical procedure for the prediction of wind-induced response of air-supported structures is formulated. This procedure is based on measurements of the external pressures using a rigid model, and also on the use of the influence surfaces of deflection, that can be determined analytically or experimentally using an elastic model.

A rigid model of the hemispherical air-supported roof (described in Chapter 7) was built and tested in The Boundary Layer Wind Tunnel Laboratory (BLWT II) at The University of Western Ontario, London, Ontario, Canada. The objective is to examine the applicability of the proposed semi-analytical approach for response prediction. The static and dynamic wind pressures were measured for different exposures. The influence surfaces of deflection were calculated using a finite element static analysis. The analytical results were compared to the experimental results that were previously obtained from the aeroelastic tests described in Chapter 7.

8.2 REVIEW OF PREVIOUS WORK ON DOME STRUCTURES

Models of domes and air-supported structures have previously been wind-tunnel tested to find the minimum internal pressure to prevent buckling. In wind tunnel tests on a model radome consisting of a three-quarter sphere on a cylindrical tower, the necessary internal pressure required to prevent buckling was equal to the full wind dynamic pressure q, while for a hemisphere mounted on the ground, the necessary internal pressure was only 0.7 q, (Beger, 1967). These tests were made in uniform flow which does not represent the boundary layer conditions in the natural wind.

A number of studies have dealt with hemispheres and domes immersed in turbulent boundary layers, but most of them were conducted at much lower Reynolds numbers than similarity would require for prototype structures. Taniguchi et al. (1982) studied a few hemispheres to establish a relationship between the distribution of the mean pressure coefficients, the aerodynamic forces, and the characteristics of the boundary layer.

Toy et al. (1983) investigated the flow around a hemisphere immersed in two turbulent boundary layers of different turbulence intensities and velocity profiles. The three-dimensional nature of the mechanism of separation and reattachment of the air flow was examined. Both the separation region and the reattachment points moved downstream with increasing turbulence intensity in the boundary layer.

Savory and Toy (1986) conducted a comprehensive study of the near wakes of hemispheres in three different boundary layers. The effects of changes in the flow or model geometry on the vorticity distributions and the development of the separated shear layers were assessed. The generation and development of vortex structures associated with the flow around the hemisphere were ascertained from water channel observations.

Newman (1984) studied the flow over three inflated domes with height to radius ratios of 0.5, 0.74, and 1.0, in a sparsely wooded area. The pressure distributions on the inflated domes were measured in a boundary layer wind tunnel, and a finite element analysis for thin shells was used to find the tension and shear forces in the membrane. Both rigid and flexible models were tested for all geometries at low Reynolds numbers.

Johnson and Surry (1985) studied the wind actions on five classes of small tent structures. The results for a dome with a height to radius ratio of 0.5 were slightly dependent on the Reynolds number, while the results for a hemispherical tent were strongly dependent on the Reynolds number.

Tamura et al. (1989) studied the unsteady flow patterns and pressures around a hemisphere situated on the ground at high Reynolds numbers. The study concentrated on the near wake of the hemisphere, and the unsteady flow patterns were investigated by computer simulation technique. Three-dimensional numerical

solutions of the flow were obtained by direct integration of the Navier-Stokes equations.

In summary, models for domes were wind-tunnel tested to establish a relationship between the distribution of the mean pressure coefficients and the characteristics of the boundary layer; and to study the nature of separation, reattachment of the air flow, and the near wakes of the domes for different Reynolds numbers.

In this study, a hemispherical rigid model was tested in a turbulent boundary layer flow to measure the external pressures. Pressure measurements were made for different exposure conditions (open country, suburban, and urban). These measurement were used for predicting the wind-induced response of a hemispherical air-supported model. The nature of the flow around the hemisphere is outside the scope of the study.

8.3 MEASUREMENTS OF SURFACE PRESSURES

Measurements of the wind-induced surface pressures were done using methods developed at The Boundary Layer Wind Tunnel Laboratory (BLWT II) at The University of Western Ontario, London, Ontario, Canada. A summary of the experimental technique used in pressure measurements is given in Appendix B. The Reynolds numbers achieved were low for reasons discussed in Chapter 7.

8.3.1 The Pressure Model

A 2.5 mm thick plexiglass hemispherical model was used, with the same dimensions as those of the aeroelastic model described in Chapter 7. The model was attached to a clamping ring before it was mounted to the wind tunnel turntable. The model surface was divided into thirty-two equal areas, (each with 6 pressure taps) and a total of 192 pressure taps were used in the pressure measurements. A plan of the model showing the 32 panels and the pressure tap distribution is given in Figure (8.1). A vertical cross-section of the pressure model showing the pressure tap locations is given in Figure (8.2). Also, a photograph of the pressure model is displayed in Plate (8.1).

8.3.2 Model Instrumentation

The hemispherical plexiglass model was drilled with 1 mm diameter holes for the pressure taps. The holes were connected with pressure tight brass stub tubes on the inside of the model that, in turn, provided the connection to plastic pressure tubing leads. The leads were connected to scanivalve pressure switching devices after being pneumatically averaged through pressure manifolds.

Pressure taps were distributed with 6 taps for each of the 32 panels as shown in Figures (8.1) and (8.2). Each hole was checked to ensure that the frequency content for a given pressure input was not distorted by the measuring techniques. The pressure taps of each panel were connected to a manifold to be pneumatically averaged, and the time history of the external wind pressure on

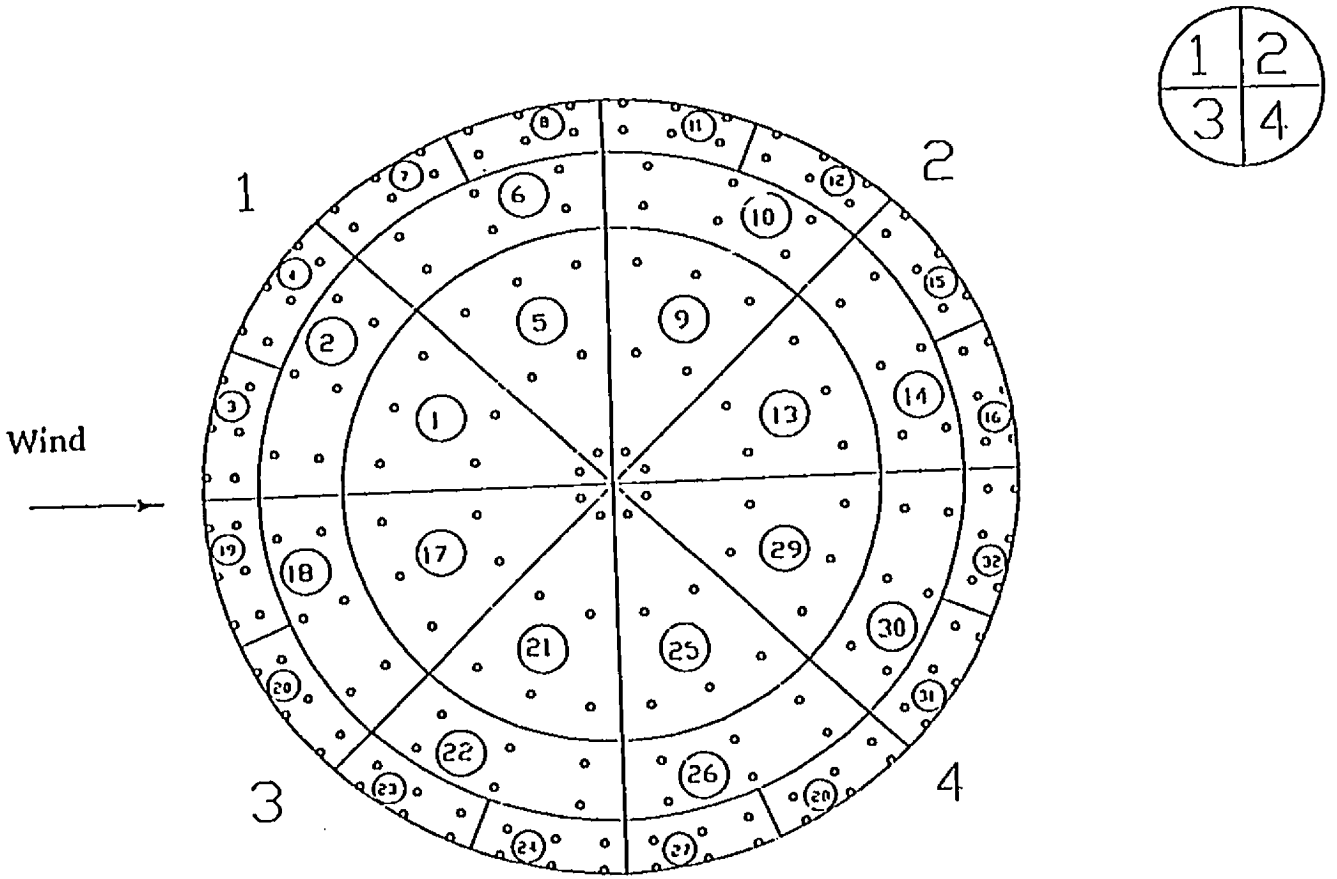

Fig. (8.1): Plan of pressure tap distribution and panel numbering

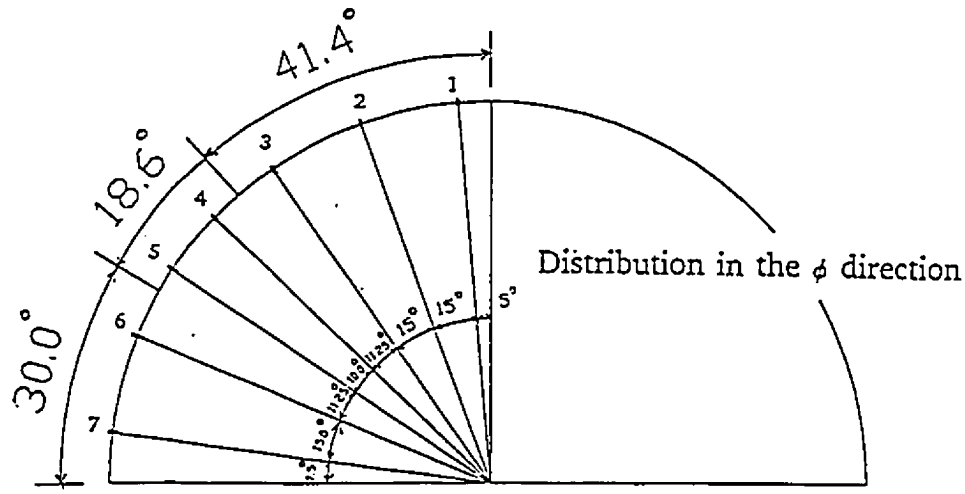

Group number	Distribution in θ direction	Total pressure taps
1	1@ 45°	8
2	1@ 22.5°	16
3	1@ 15°	24
4	1@ 15°	24
5	1@ 15°	24
6	1@ 7.5°	48
7	1@ 7.5°	48
		192

* Angles θ and ϕ are shown in Fig. (8.3)

Fig. (8.2): Vertical cross-section showing the pressure tap locations

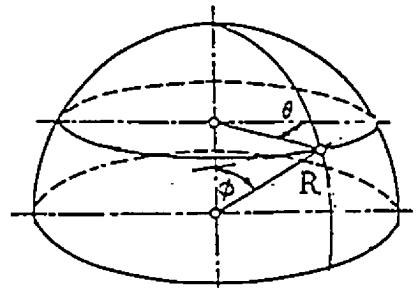

Fig. (8.3): Coordinates of a point on the hemisphere

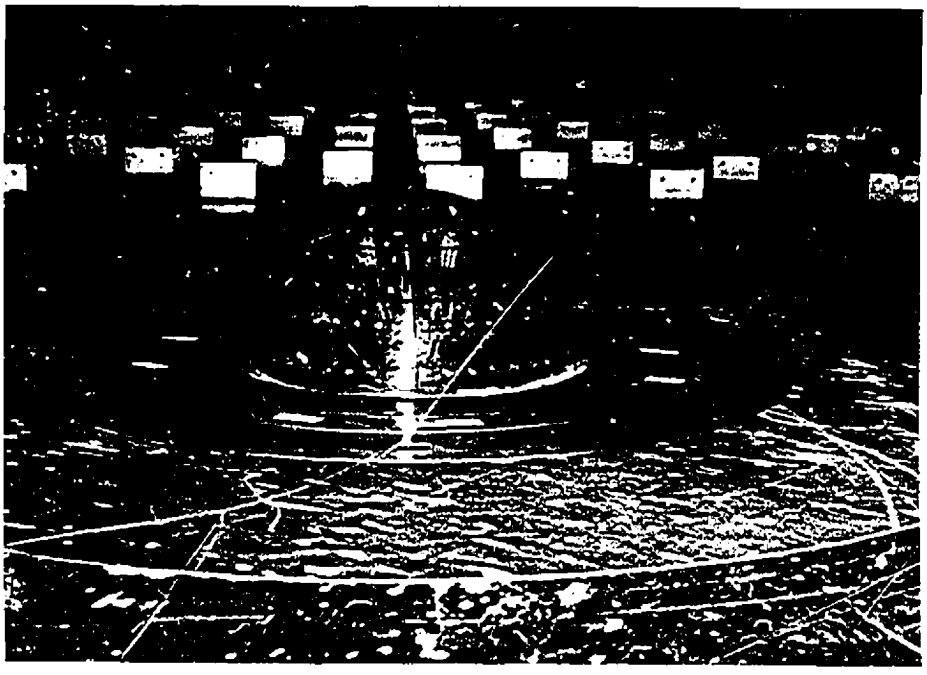

Plate (8.1): The pressure model

each panel was obtained using an on-line computer, (PDP 11/73 computer). The HP analyzer was also used in the pressure measurements. The pressure tests were carried out at a gradient wind speed of 15 m/sec ($R_e \approx 3 \times 10^5$). This Reynolds number is in the critical range, and is calculated with the length parameter equals 0.30 m which is the model diameter.

8.4 RESPONSE TO WIND LOADING

In Chapter 7, the response of the hemispherical, aeroelastic, air-supported model in turbulent wind showed no resonance effects, because of the associated high damping, and because the response occurred at frequencies well below the fundamental frequency of the model. Therefore, the influence surfaces of deflection were used together with the panel external pressure measurements to predict the wind-induced response of the hemispherical, air-supported model. The assumptions used in the analysis, i.e., that external pressures on the roof are independent of roof displacement, and that the internal pressure is independent of spatial location, are well-justified.

The response w at any point on the surface of a hemispherical roof (with radius R) at a time t due to random wind pressures can be represented in the form:

$$w = \overline{w} + w' \tag{8.1}$$

where $\overline{w}$ is the mean response and w' is the fluctuating component of the response w. The coordinates of any point, (θ,ϕ), on the surface of the hemisphere

is shown in Figure (8.3).

In this analysis, the total pressure at any point is $P(\theta,\phi,t)$, the mean pressure component is $\bar{P}(\theta,\phi)$, and the fluctuating component is $P'(\theta,\phi,t)$. The influence surface defining the response w at point B due to a unit load is $I_B(\theta,\phi)$ applied at a point with coordinates (θ,ϕ). For a quasi-static state, the response at point B can be given as

$$w_B = \int_A P(\theta,\phi,t)\, I_B(\theta,\phi)\, dA \tag{8.2}$$

where A is the surface area of the roof. The mean response can be written as

$$\bar{w}_B = \int_A \overline{P(\theta,\phi,t)}\; I_B(\theta,\phi)\, dA \tag{8.3}$$

The mean square response is

$$\overline{w'^2} = \iint_A \overline{P'(\theta_1,\phi_1,t)\, P'(\theta_2,\phi_2,t)}\, I_B(\theta_1,\phi_1)\, I_B(\theta_2,\phi_2)\, dA_1\, dA_2 \tag{8.4}$$

where $P'(\theta_1,\phi_1,t)$ and $P'(\theta_2,\phi_2,t)$ are the pressures at points 1, (θ_1,ϕ_1), and 2, (θ_2,ϕ_2), respectively.

In this study, the surface of the pressure model was discretized into 32 panels of equal area. All time histories and spectra of the external pressures were experimentally measured as mentioned earlier. Therefore, the problem of the response of the hemispherical air-supported structure is dealt with as a discrete system with 32 input forces which are correlated. The response at point B on the surface due to wind pressure can now be written as

$$w_B = \sum_{j=1}^{n} P_j(\theta_j,\phi_j,t)\, A_j\, I_B(\theta_j,\phi_j) \tag{8.5}$$

where A_j and P_j are the area and the pressure of panel j, respectively.

The mean response is

$$\bar{w}_B = \sum_{j=1}^{n} \bar{P}_j A_j I_B (\theta_j,\phi_j) \tag{8.6}$$

and the mean square response is

$$\overline{w_B'^2} = \sum_{i=1}^{n} \sum_{j=1}^{n} \overline{P_i' P_j'} A_i A_j I_B (\theta_i,\phi_i) I_B (\theta_j,\phi_j) \tag{8.7}$$

In the above equations i and j are panel numbers, and n is the total number of panels. The influence surfaces of deflection account for different internal pressures and accordingly different stiffnesses. The correlation function of any two fluctuating pressures P_i' and P_j' can be written as

$$R_{Pij}(\tau) = \overline{P_i'(\theta_1,\phi_1,t)\, P_j'(\theta_2,\phi_2,t+\tau)} \tag{8.8a}$$

$$= \lim_{T\to\infty} \frac{1}{2T} \int_{-T}^{T} P_i'(\theta_1,\phi_1,t)\, P_j'(\theta_2,\phi_2,t+\tau)\, d\tau \tag{8.8b}$$

The spectrum of the external pressure can be written as

$$S_{Pij}(f) = \int_{-\infty}^{\infty} R_{Pij}(\tau)\, e^{-2\pi f \tau i}\, d\tau \tag{8.9}$$

and the spectrum of response at a point B is

$$S_w(f) = \sum_{i=1}^{n} \sum_{j=1}^{n} S_{Pij}(f)\, A_i A_j I_B (\theta_i,\phi_i) I_B (\theta_j,\phi_j) \tag{8.10a}$$

or

$$S_w(f) = \sum_{i=1}^{n} \sum_{j=1}^{n} S_{Fij}(f)\, I_B (\theta_i,\phi_i) I_B (\theta_j,\phi_j) \tag{8.10b}$$

where

$S_{Pij}(f)$: spectrum of external pressure (auto-spectrum for i = j and cross-spectrum for $i \neq j$);

$S_{Fij}(f)$: spectrum of force;

$S_w(f)$: spectrum of response w at point B;

$I_B (\theta_i,\phi_i)$: deflection at point B due to unit load at panel i; and

$I_B (\theta_j,\phi_j)$: deflection at point B due to unit load at panel j.

The spectra S_{Fij} (f) and S_{Pij} (f) are related as

$$S_{Fij}(f) = \int_A \int S_{Pij}(f)\, dA_i\, dA_j \tag{8.11a}$$

$$= S_{Pij}(f)\, A_i\, A_j \tag{8.11b}$$

The variance of the response at point B can also be written as

$$\overline{w'^2} = \int_0^\infty S_w(f)\, df \tag{8.12}$$

where S_w (f) is given by Equation (8.10). Thus, the semi-analytical procedure can predict the mean, RMS, and spectrum of the wind-induced response at any point on the roof surface for different exposures and internal pressures. The wind pressures were measured in a wind tunnel using the rigid model for different exposures, and the influence surfaces of deflection were calculated theoretically for different internal pressures using a finite element static analysis.

8.5 INFLUENCE SURFACES OF DEFLECTION

The deflections of the roof due to a load at any point on the surface were theoretically calculated using the finite element program ABAQUS for different internal pressures considered. A static analysis was made to determine the roof deflections. In the finite element analysis, the roof surface was discretized into 4-node membrane elements and the deflections were evaluated for each value of the internal pressures corresponding to those of the aeroelastic model (40, 80, and 120 Pa). Vertical and horizontal cross-sections in a typical influence surface of deflection at point B is displayed in Figures (8.4a) and (8.4b). The deflections in these figures are normalized by the deflection at point B.

For comparison purposes, a few deflections were measured at the probe locations of the aeroelastic model described in Chapter 7. After calibrating the displacement transducers and setting up the required internal pressure, the hemispherical aeroelastic model was mounted on a shaker table to measure the roof deflections at the transducer locations. A load cell was calibrated and used to apply a load at several locations on the surface of the aeroelastic model. The load cell was mounted on a stand and was kept always perpendicular to the surface of the aeroelastic model as shown in Plate (8.2). The displacements of the five Kaman transducers were obtained using an on-line computer. Then, the model was rotated stepwise and the roof deflections at the transducer locations were accordingly monitored. The initial positions of the displacement transducers are shown in Figures (7.1) and (7.2). A comparison between the theoretical and experimental deflection results are given in Table (8.1). The agreement between the two approaches is good enough to confirm the theoretical deflection values obtained using the finite element method.

8.6 WIND TUNNEL PRESSURE TESTS

8.6.1 Flow Modelling

Three exposures were simulated in the wind tunnel; open country, suburban, and homogeneous urban exposures. The wind velocity at the top of the model was measured using a hot wire device. The measured flow properties which include the variation of the mean wind speed U(z), and the standard deviation of

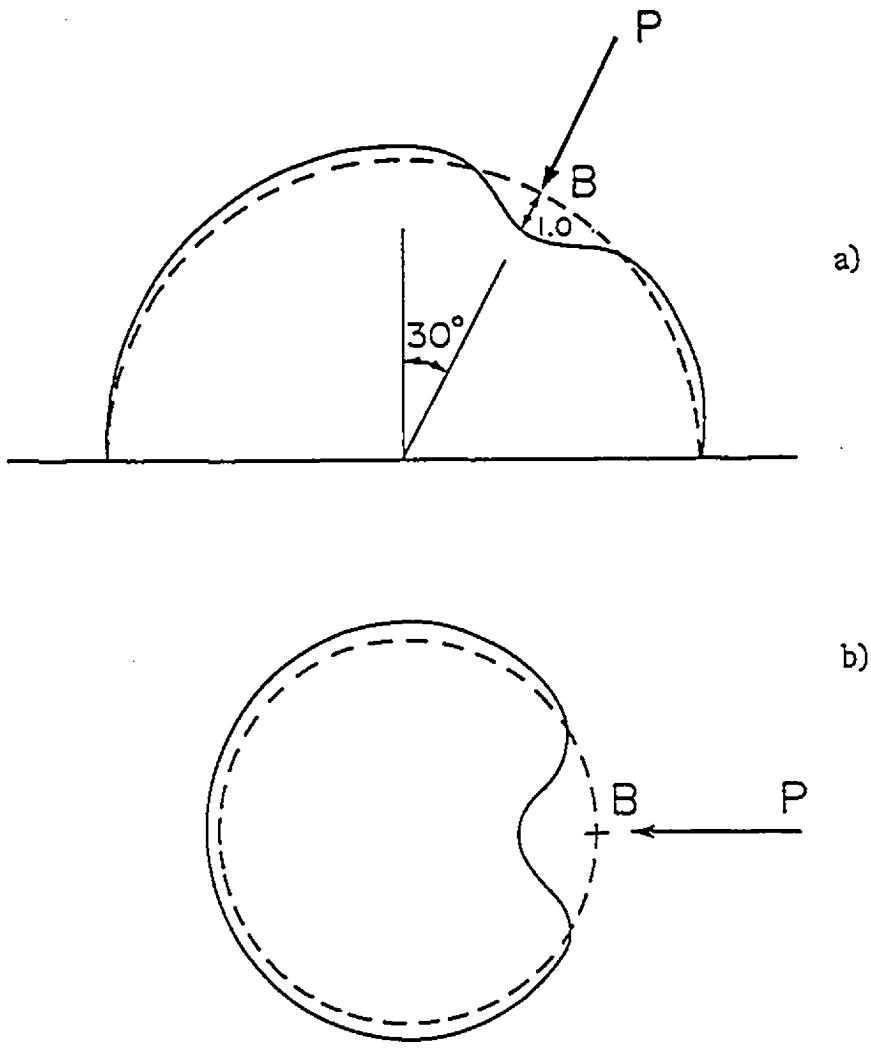

Fig. (8.4): Influence surface of deflection at point B

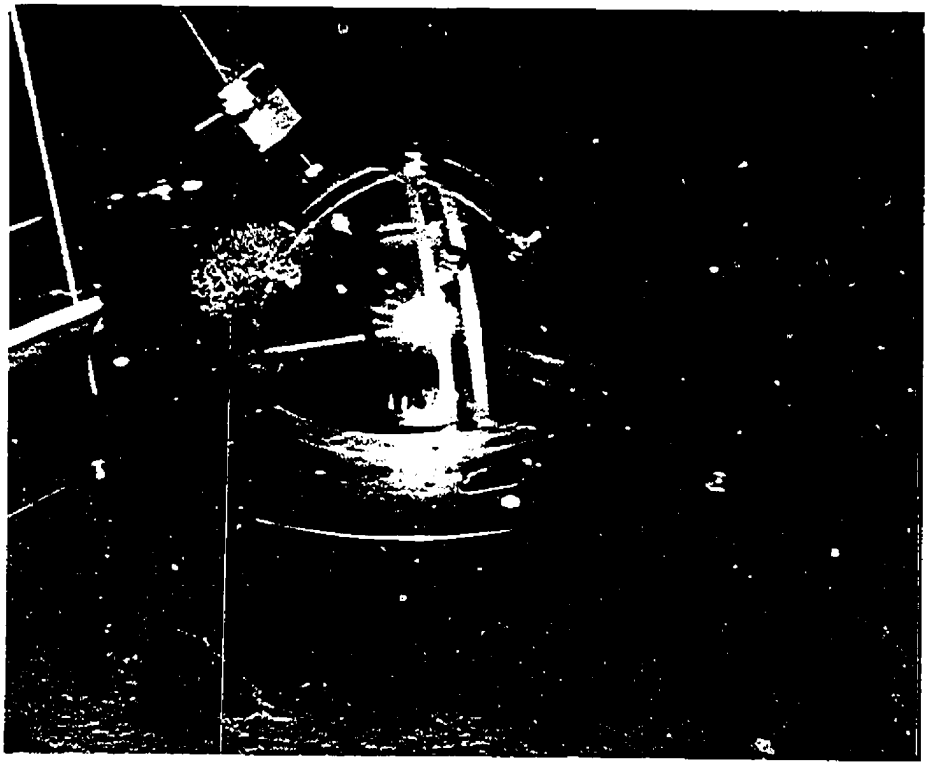

Plate (8.2): Measurements of influence surfaces of deflection

TABLE (8.1): COMPARISON BETWEEN THEORETICAL AND MEASURED STATIC DEFLECTIONS

(q_o = 40 Pa)

Probe Number	Measurements (1×10^{-3} mm)	Analytical
1	7.62	6.70
2	5.08	4.30
3	2.54	2.10
4	2.54	2.10
5	5.08	4.30

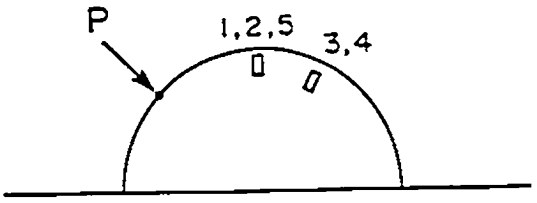

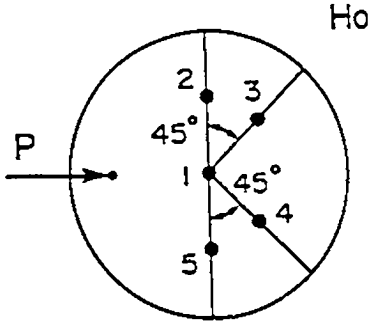

Sensor and Load Locations

the wind velocity fluctuation $\sigma_U(z)$ at the test section, were the same as those of the aeroelastic tests, Chapter 7.

8.6.2 Experimental Procedure

Pressure measurements were made for all three exposures. The model was also rotated; and the external pressures were measured to be used in the response prediction, and to check the reliability of the pressure measurements. The model was tested at rotation angles of 22.5°, 45°, and 90°.

The output signals of the pressure transducers were passed through a filter and monitored on an oscilloscope, and connected either to the on-line digital data acquisition system (PDP 11/73 Computer) or to the Hewlett-Packard Structural Dynamic Analyzer 5423A. The external wind pressures on the model were measured at a gradient wind speed of 15 m/sec. The on-line computer was used to obtain the time histories of the thirty-two panel pressures, each sixteen at a time. The pressure data of quarters 1 and 2, quarters 3 and 4, quarters 1 and 4, and quarters 3 and 2 were taken at an angle of attack o° as shown in Figure (8.1). To obtain the data of quarters 1 and 3, and quarters 2 and 4 the model was rotated 90°. From the pressure time histories the mean, RMS, and spectral information were calculated using the program CROSS on the wind tunnel mainframe computer. Also, the HP analyzer was used to measure the auto-spectra and cross-spectra of the external pressures directly for different panels.

The terrain roughness affected the panel external pressures. The mean external pressures for the open country exposure were higher than those for the other exposures. This is because the mean velocity at model height is higher for the open country exposure than it is for other exposures. The urban exposure resulted in higher RMS pressure values than other exposures due to the associated high turbulence intensity. The unsteady pressures and suctions are due to the natural gustiness of the wind and the unsteady character of the flow within the wake formed by the structure. Examples of the auto-spectra of external pressure for different exposures are shown in Figures (8.5) to (8.10).

8.7 COMPARISON OF ANALYTICAL AND EXPERIMENTAL RESPONSE RESULTS

The wind-induced response at any point on the surface of the hemispherical air-supported model can be predicted as explained in Section 8.4. The influence surfaces of deflection were calculated using the FEM analysis and used with the pressure measurements to predict the wind-induced response of the hemispherical, aeroelastic model. It may be mentioned that the prediction of response required considerable time and computational effort, as can be seen from Equations (8.6), (8.7), and (8.10). The calculation of the mean and RMS values of response as well as the response spectrum at a point (for a certain exposure and a specific internal pressure) required the use of the corresponding external pressures and deflection data.

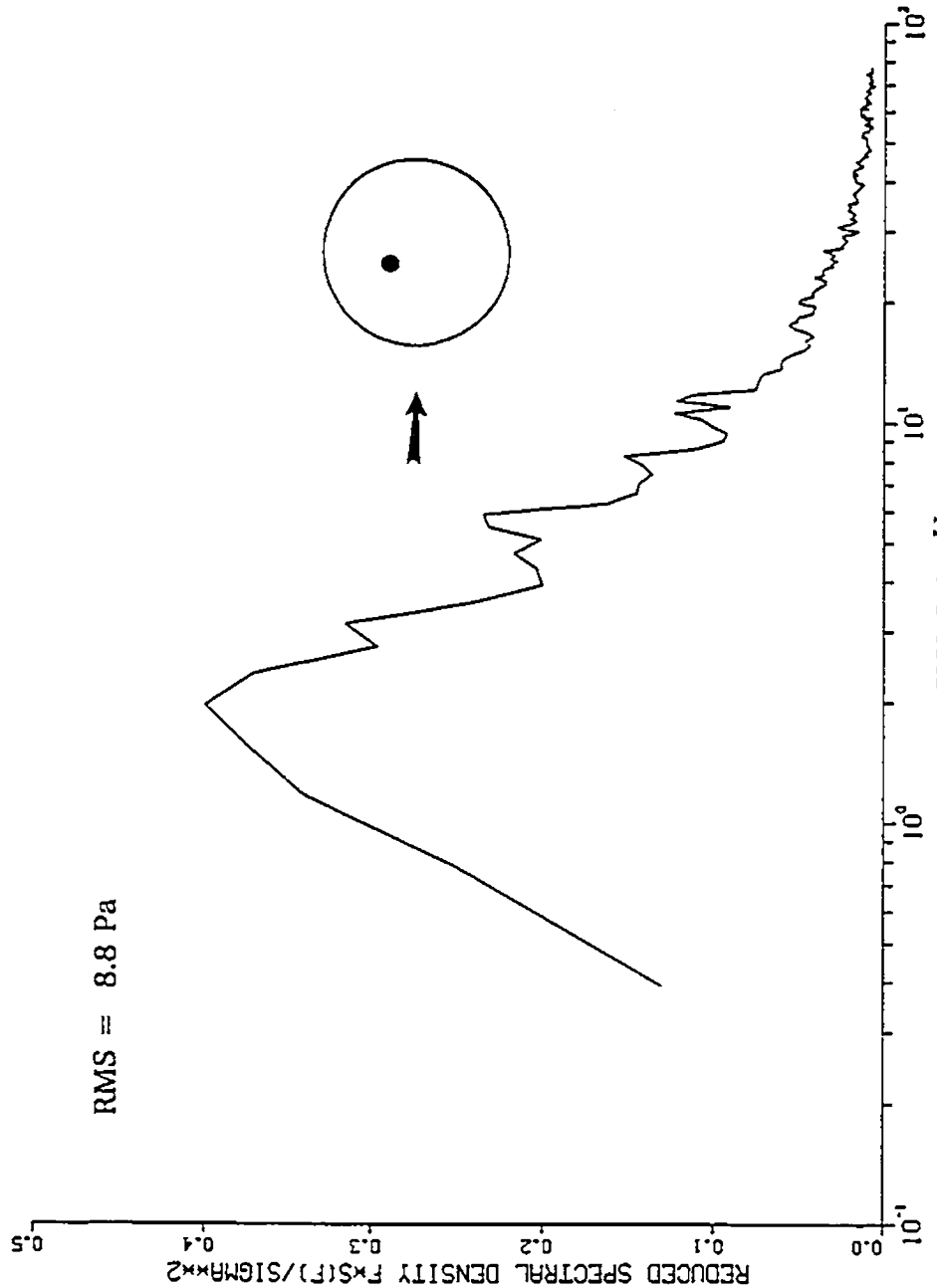

Fig. (8.5): Pressure spectrum of panel 5 for open country exposure

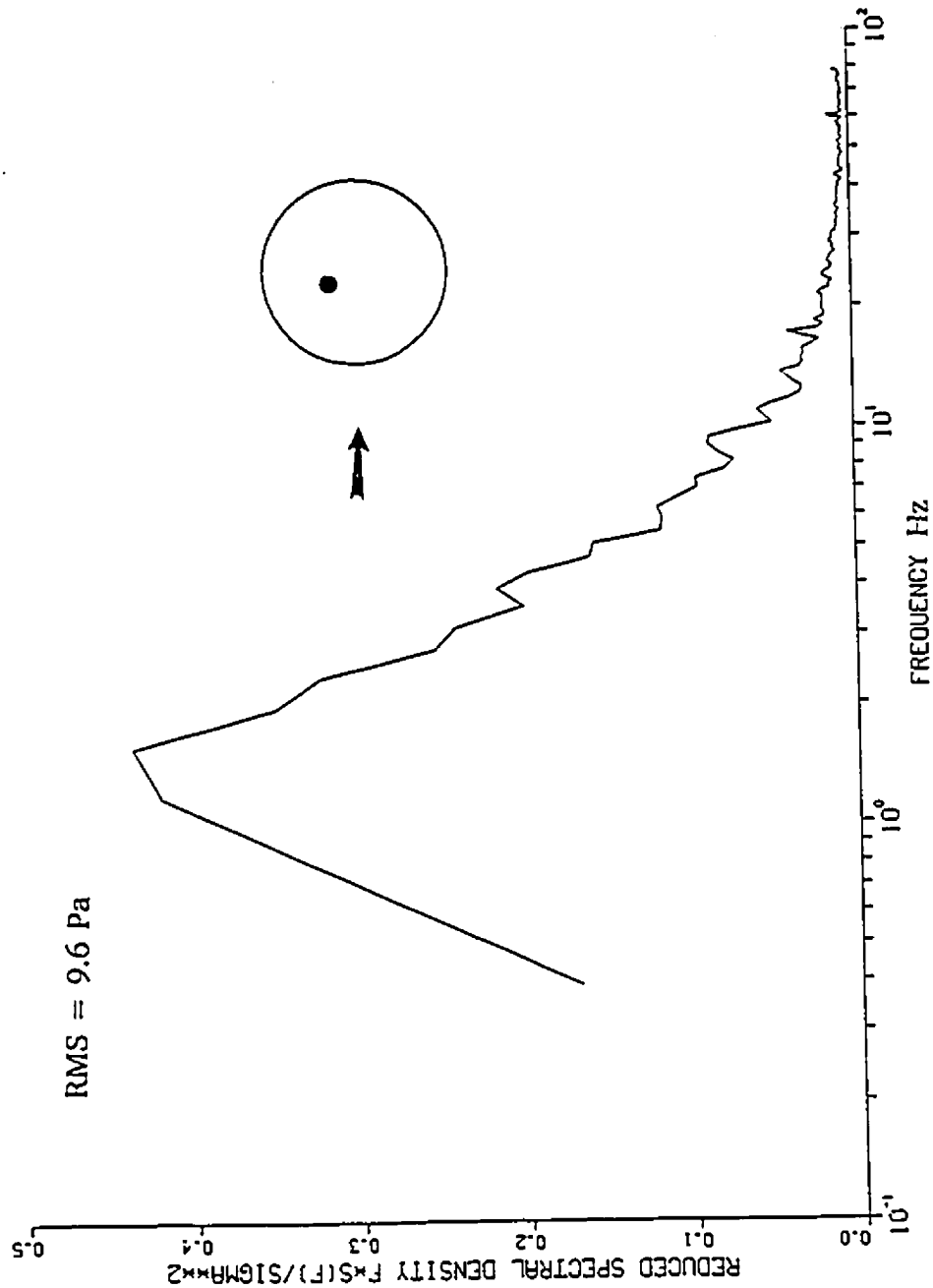

Fig. (8.6): Pressure spectrum of panel 5 for suburban exposure

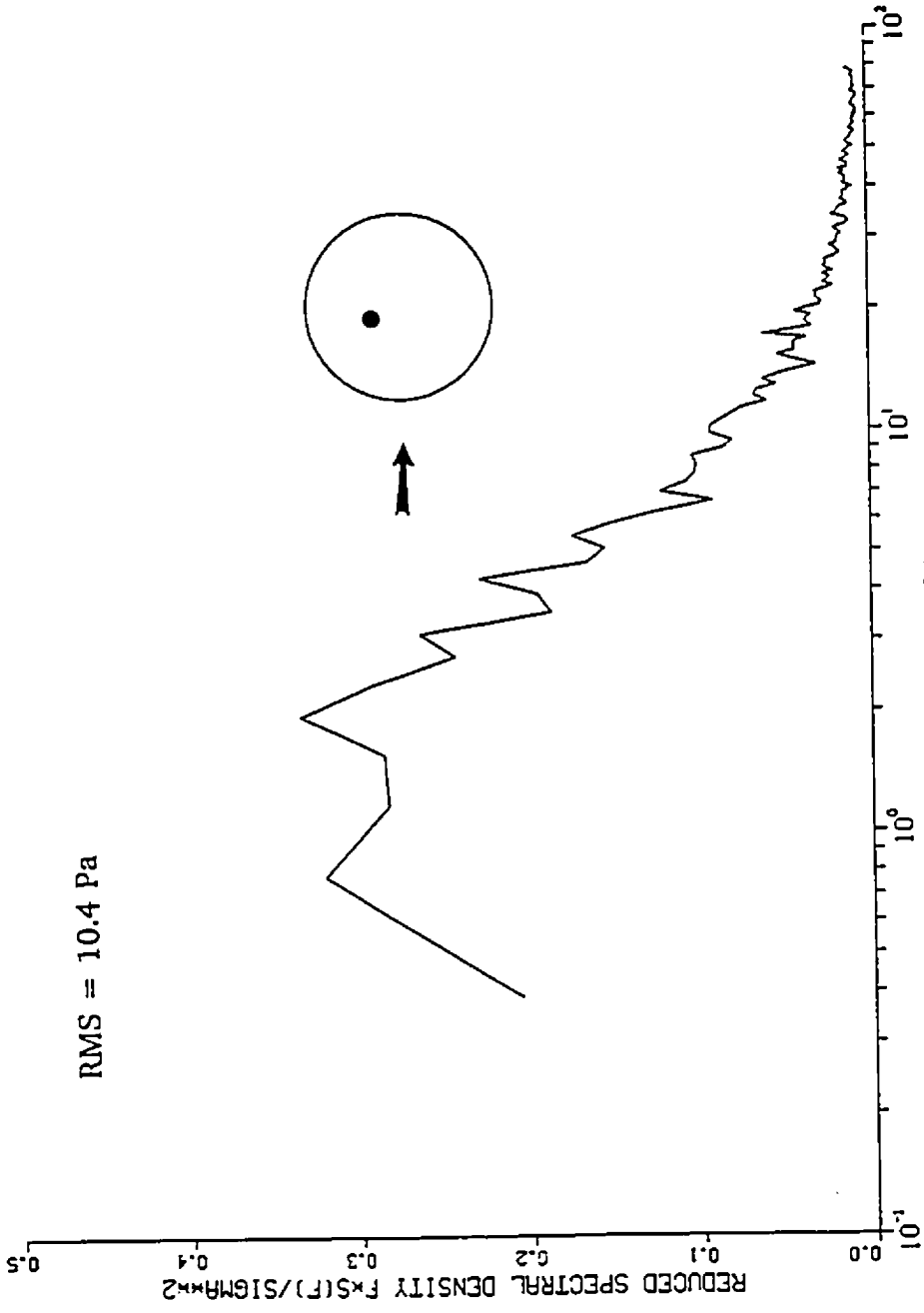

Fig. (8.7): Pressure spectrum of panel 5 for urban exposure

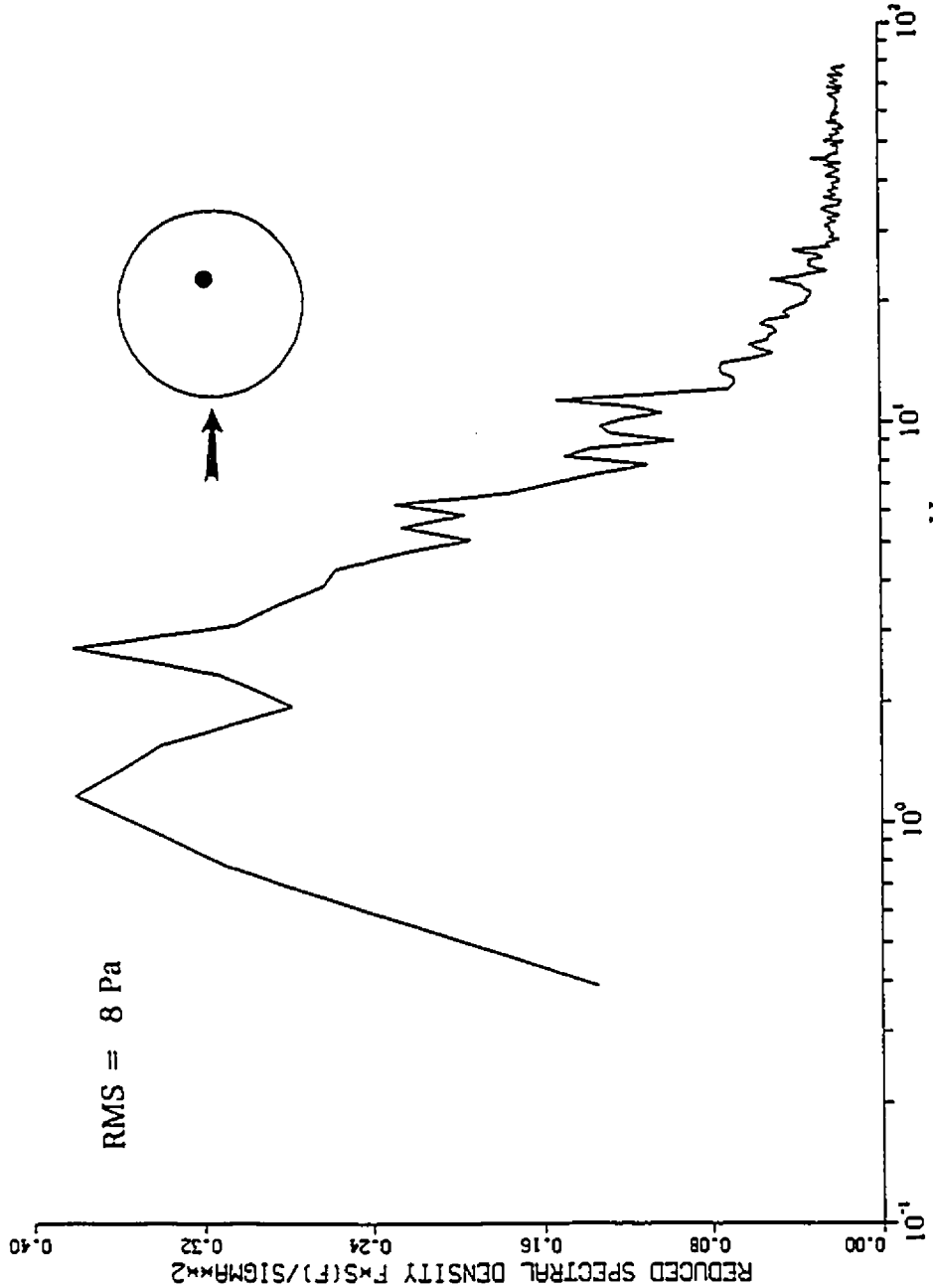

Fig. (8.8): Pressure spectrum of panel 13 for open country exposure

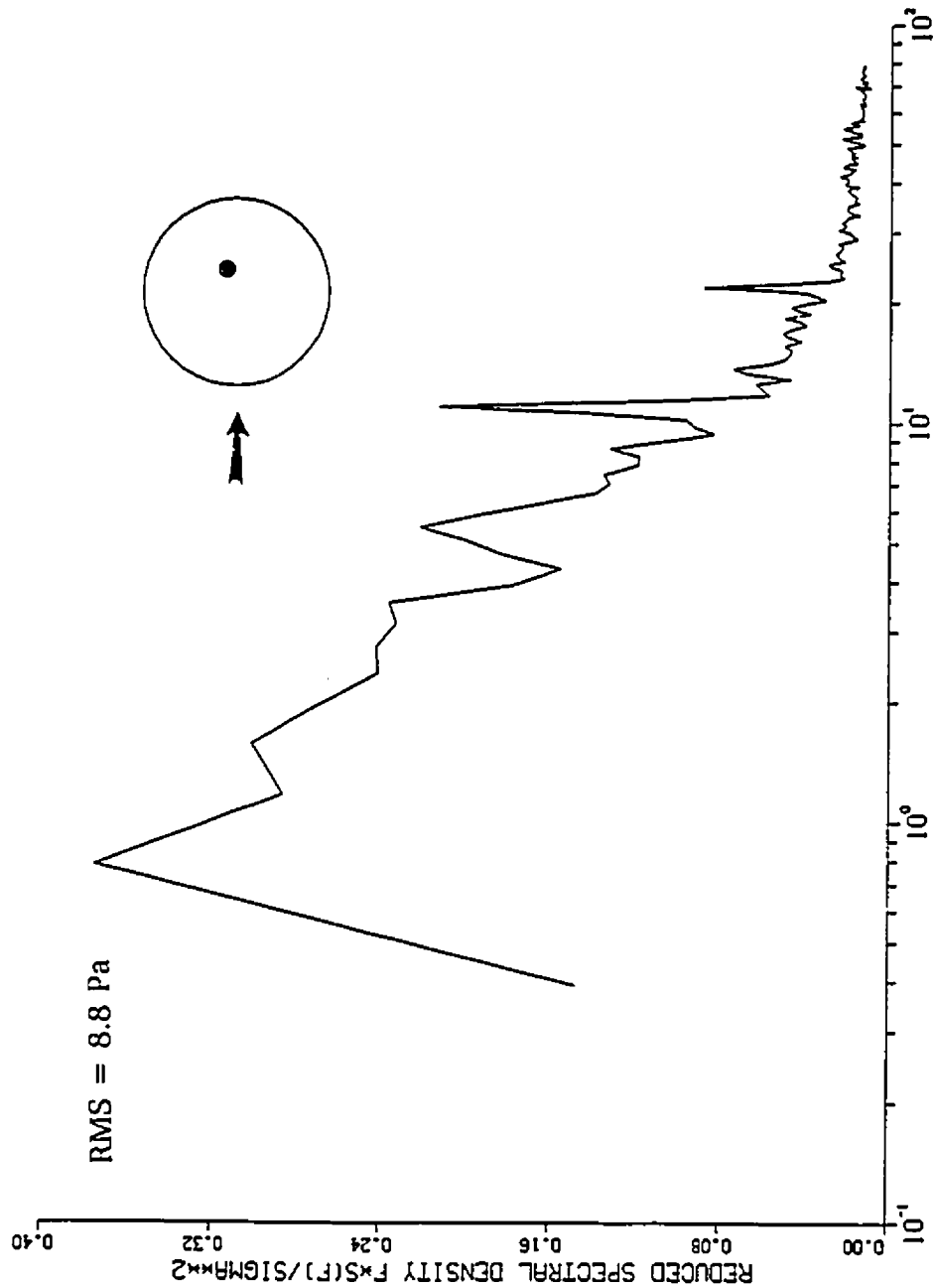

Fig. (8.9): Pressure spectrum of panel 13 for suburban exposure

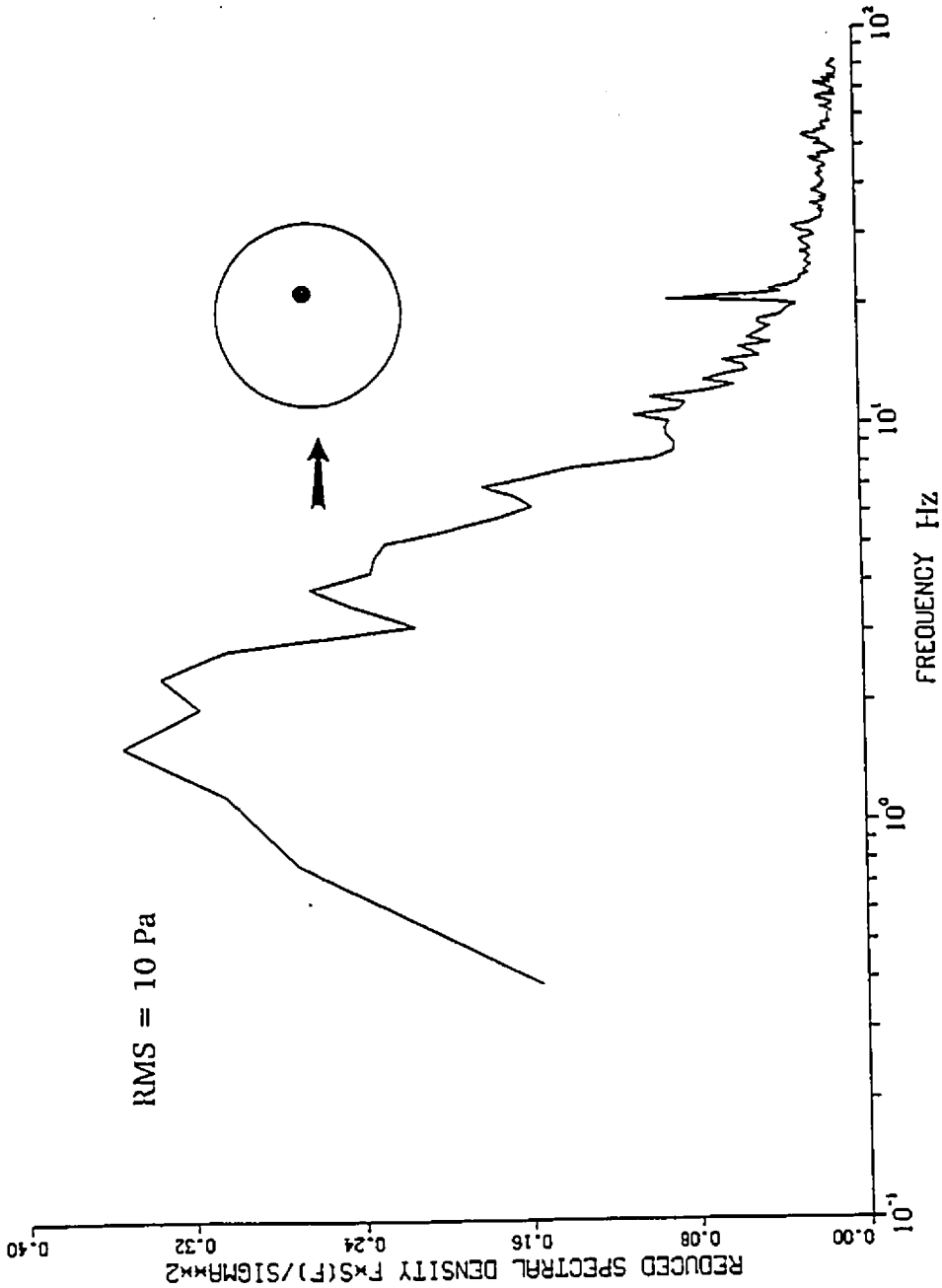

Fig. (8.10): Pressure spectrum of panel 13 for urban exposure

Examples of the predicted and measured (mean and RMS) deflections calculated using equations (8.6) and (8.7) are given in Tables (8.2) and (8.3) for different internal pressures and exposure conditions. It can be seen that the analytical results compare reasonably well with the experimental ones for the internal pressures and exposures considered.

The formulated semi-analytical procedure was also used to predict the spectra of response of the hemispherical air-supported model due to wind load using Equation (8.10). Examples of the analytical and experimental spectra of response are displayed in Figures (8.11) to (8.13) for different exposure conditions. The internal pressure of the aeroelastic model in this case was 40 Pa.

An overlay of the analytical and measured response spectra indicates that the analysis is adequate for predicting the wind-induced response of air-supported roofs. The analytical and measured response spectra show that the dynamic deflections are broad band random processes with no indication of resonance effects.

It can be seen from Tables (8.2) and (8.3) that the open country exposure gives slightly higher mean deflections than other exposures, as the mean wind speed at the model top is higher than those for other exposures. The urban exposure resulted in higher RMS deflections due to the associated high turbulence intensity. Both the measured and predicted response results showed that as the internal pressure of the model increases, the mean and RMS deflections decrease.

TABLE (8.2): MEAN RESPONSE AT POINT B FOR DIFFERENT EXPOSURES AND INTERNAL PRESSURES

Internal pressure (Pa)	Model Mean deflection x (1 x 10^{-3}) mm					
	Exposure					
	Open		Suburban		Urban	
	Anal.	Exp.	Anal.	Exp.	Anal.	Exp.
40	760	740	730	720	710	670
80	665	670	625	600	605	570
120	560	500	470	480	460	440

TABLE (8.3): RMS RESPONSE AT POINT B FOR DIFFERENT EXPOSURES AND INTERNAL PRESSURES

Internal pressure (Pa)	Model RMS deflection x (1 x 10^{-3}) mm					
	Exposure					
	Open		Suburban		Urban	
	Anal.	Exp.	Anal.	Exp.	Anal.	Exp.
40	74.10	65.00	85.70	80.00	96.50	110.00
80	69.20	62.50	78.70	72.50	86.40	90.00
120	62.70	55.00	72.40	65.00	78.70	82.50

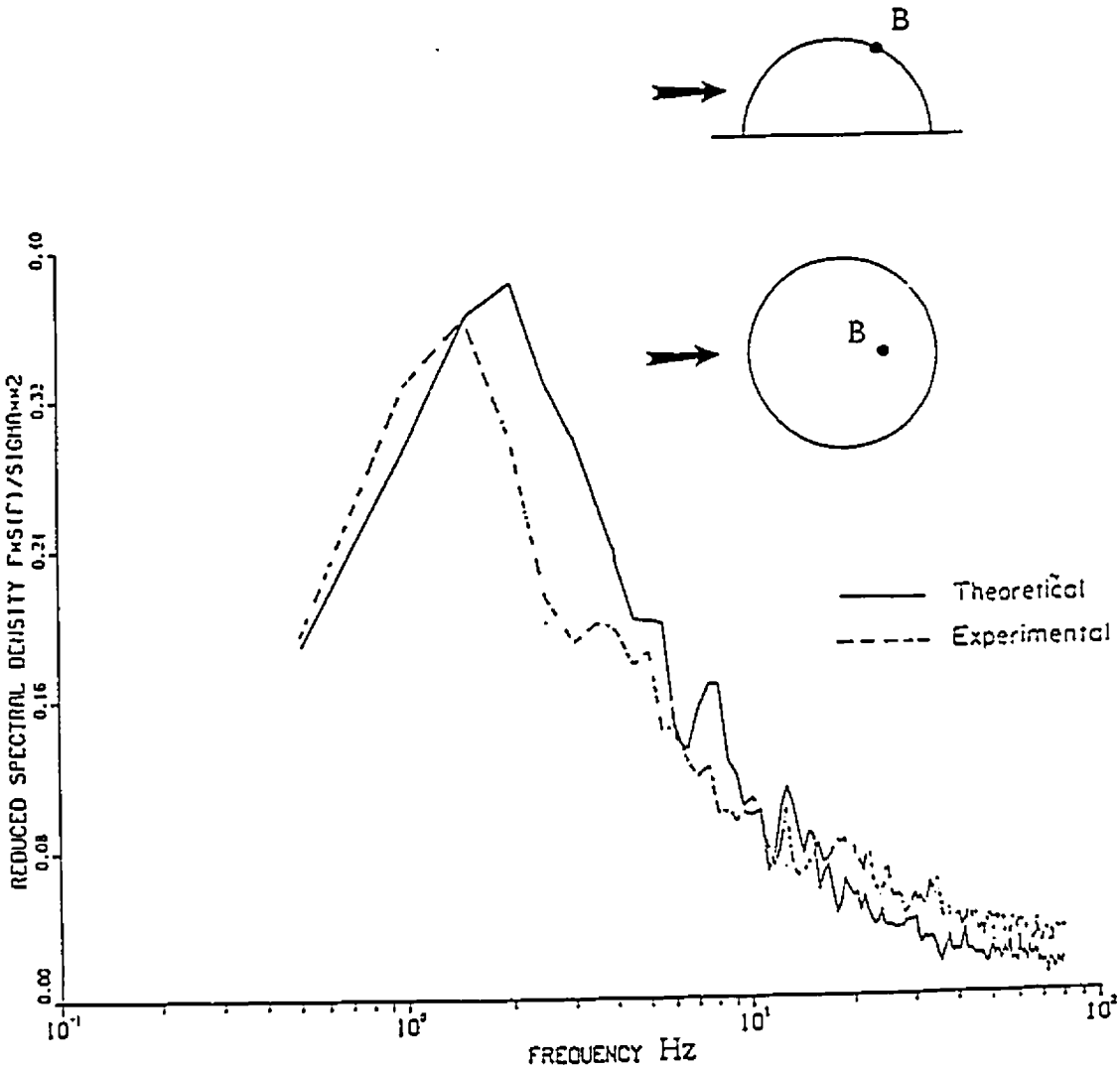

Fig. (8.11): Predicted and measured response spectra at point B (open country exposure, q_o = 40 Pa)

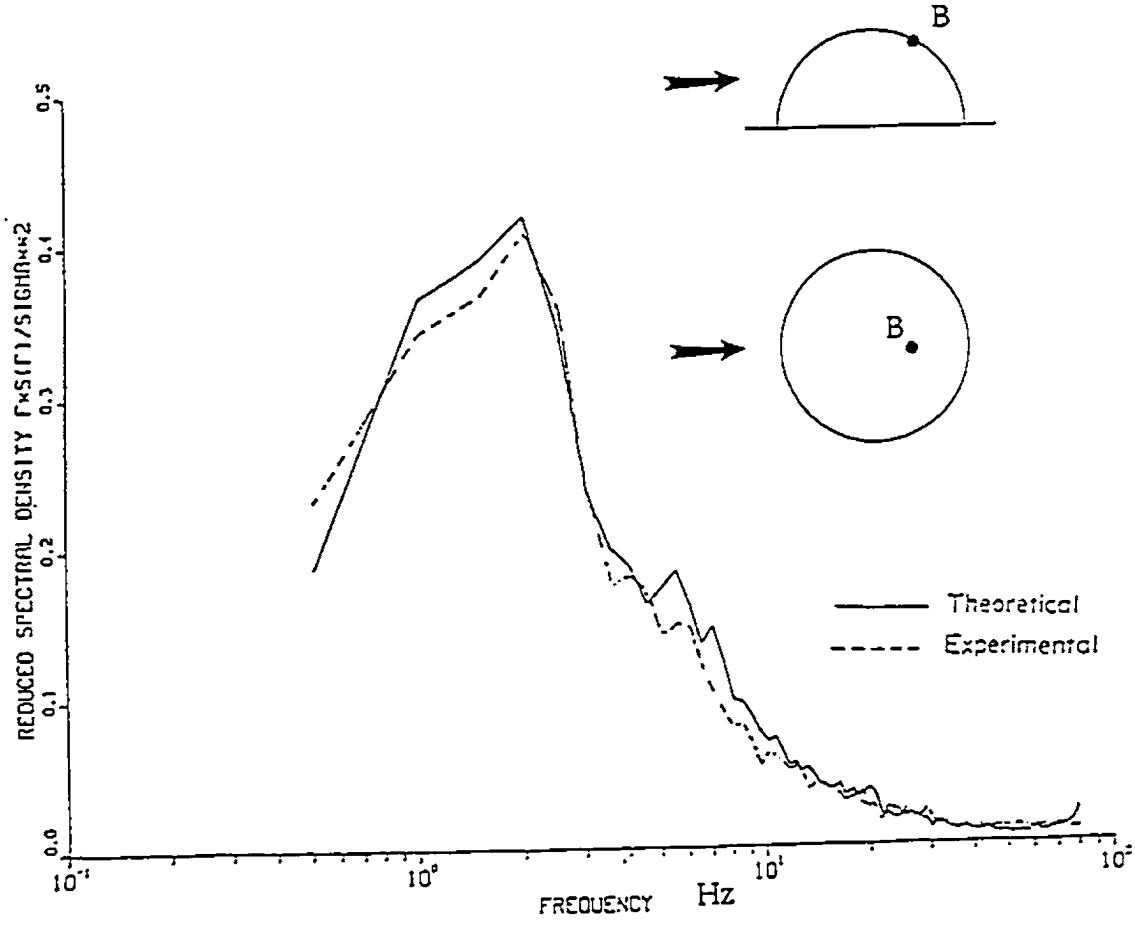

Fig. (8.12): Predicted and measured response spectra at point B (suburban exposure, q_o = 40 Pa)

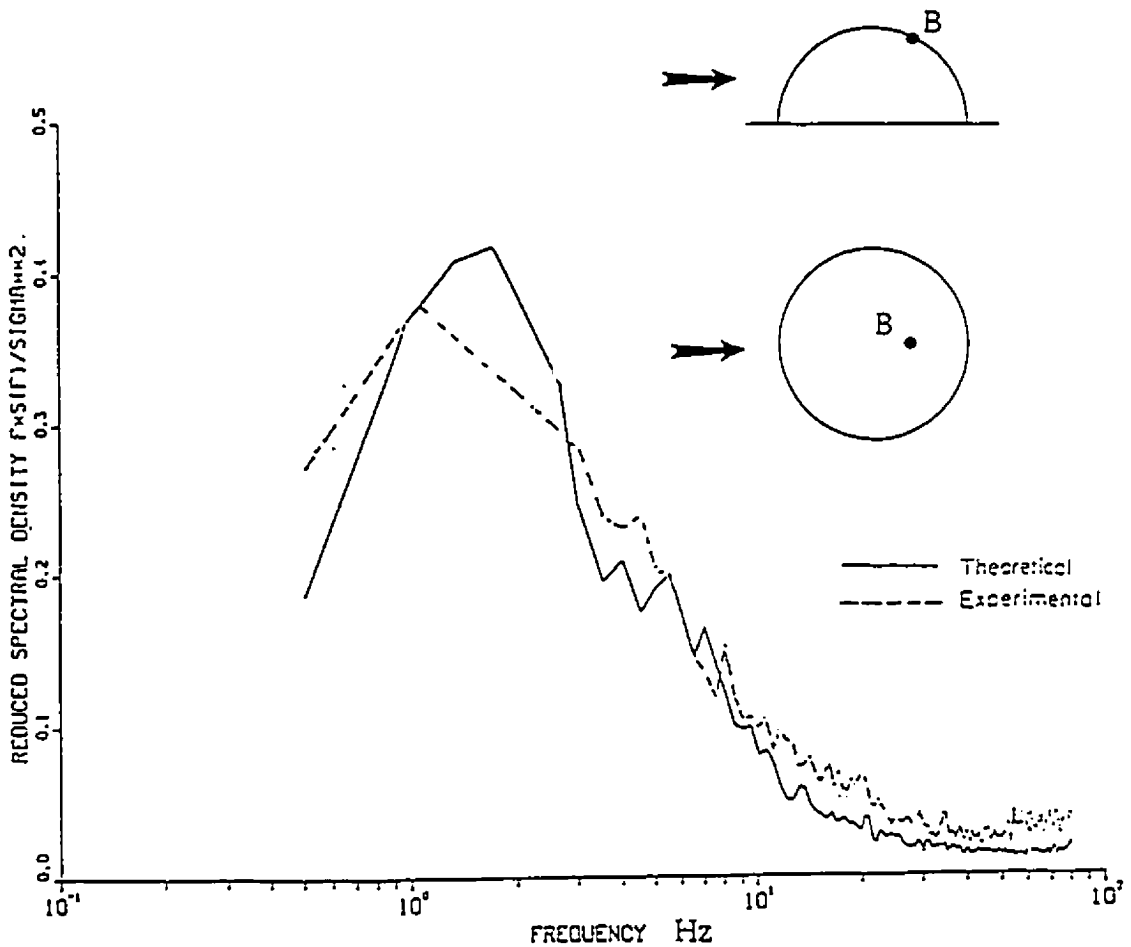

Fig. (8.13): Predicted and measured response spectra at point B (urban exposure, q_o = 40 Pa)

This is so because as the internal pressure increases, the roof stiffness increases.

It can be seen from Figures (8.11) to (8.13) and from Tables (8.2) and (8.3) that the agreement is quite good between the predicted and measured deflection values. Thus, the semi-analytical approach is a good estimate of the mean and RMS deflection values as well as the wind-induced response spectra. The maximum difference between the analytical and experimental results is about 14% which is acceptable in engineering practice. This difference might be because the external pressures on the aeroelastic model are somewhat different from those on the rigid model, being affected by the roof motion.

Finally, to improve the reliability of the suggested semi-analytical procedure, studies may be needed to find the distributions of the external pressure coefficients and the correlation functions for different terrain exposures and wide ranges of Reynolds numbers, particularly for very high Reynolds numbers.

The good agreement between the experiment and the theoretical results proves the applicability of the proposed semi-analytical approach. The great advantage of this approach is that the external pressures can be established on rigid models and then be used repeatedly to predict the response of different hemispherical roofs featuring various flexibilities, masses, internal pressures, and damping. This procedure reduces the need for aeroelastic testing, which is desirable because the aeroelastic models are costly and difficult to make.

CHAPTER 9

CONCLUSIONS AND RECOMMENDATIONS

In the first part of the study, free vibration of self-supported, large span roofs backed by cavities with openings was investigated. A simplified theoretical approach was formulated to evaluate the roof modal parameters, considering the structural and acoustical damping for the roof and the openings. The accuracy of the approximate formulae for the evaluation of roof modal properties was assessed by comparisons with a complex eigenvalue analysis and with an exact solution for a circular membrane. The theoretical approach was verified by conducting free vibration tests on two different structural models: a membrane roof and a plate roof. Closed form solutions were also derived for the damped response of a circular membrane backed by a cavity with openings.

The second part of the study was devoted to air-supported structures. Free vibration of cylindrical and spherical structures was theoretically investigated and the results were compared with those of a finite element solution. Wind tunnel tests were conducted on an aeroelastic model of a hemispherical air-supported structure to study the wind-induced response and the accompanying internal pressure fluctuations. The aeroelastic model was tested for different gradient wind speeds, exposures, enclosure volumes and internal pressures. A semi-analytical approach to predict the wind-induced response of air-supported structures was established. This approach is based on external pressure measurements conducted on a rigid model in the wind tunnel. The theoretical wind-induced response was

compared with the measured response established from the aeroelastic tests.

The conclusions of the study can be summarized as follows:

9.1 SELF-SUPPORTED ROOFS BACKED BY CAVITIES WITH OPENINGS

The main conclusions of the free vibration analysis of self-supported, lightweight roofs backed by cavities with openings are:

1. The free vibration of lightweight roofs in fundamental symmetrical modes is governed by the area of wall openings and by the pneumatic stiffness of the cavity, together with the shape, mass and elastic stiffness of the roof.
2. The pneumatic stiffness of the enclosure depends on the opening areas.
3. The lowest fundamental frequency of the roof-air system increases with the increase in the opening areas, as in a Helmholtz oscillator, and ultimately reaches the frequency of a roof vibrating in a vacuum.
4. The effects of wall openings on the second symmetrical mode are much less pronounced than on the first symmetrical mode and are very small for the antisymmetrical mode shapes.
5. The total damping of large span, lightweight roofs vibrating in still air stems from the structural and acoustical damping.
6. Theoretically predicted frequencies and damping ratios are in very good agreement with experimental values. This shows that the suggested generalized two-mass analytical model can provide reasonable estimates of the natural frequencies and modal damping of the roof-air system.

7. In still air, the volume of the enclosure under the roof significantly affects the frequency of the fundamental symmetrical modes of vibration in the absence of wall openings, but has little effect when wall openings are present. This effect is much less pronounced for the second symmetrical mode of vibration.

9.2 AIR-SUPPORTED STRUCTURES

9.2.1 Free Vibration Analysis of Cylindrical and Shallow Spherical Structures

The free vibration of cylindrical and spherical air-supported structures was theoretically examined for the condition of still air. Closed form solutions for the modal parameters of such structures were derived. The results were compared with the theoretical ones obtained using the finite element method.

The main conclusions are:

1. For both the cylindrical and spherical air-supported structures, the natural frequencies calculated analytically using the derived closed form solutions and using the finite element method are in good agreement.
2. As the internal pressure of the structure increases, the natural frequencies increase because of the accompanying increase in the stiffness of the structure. Conversely, decreasing the internal pressure may lead to a loss of the membrane stiffness, which subsequently leads to a substantial decrease in the natural frequencies.
3 Cylindrical air-supported structures with length to lateral projection ratios greater than 4 can be considered as infinitely long, as the effects of the ends

diminish. The damped frequencies and modal damping ratios of such structures can be evaluated using the derived closed form solutions.

4. Spherical air-supported structures with rise to lateral projection ratios less than 1/5 can be considered as shallow. The modal parameters of such structures can be estimated using the derived closed form solutions, which address the analogy between shallow spherical and flat circular membranes.

9.2.2 Free Vibration Analysis of Hemispherical Structures

The free vibration of hemispherical air-supported structures was examined both theoretically and experimentally. The main conclusions are:

1. The free vibration of air-supported structures is governed by the internal pressure, the mass, and the elastic stiffness of the roof.
2. The pneumatic stiffness is proportional to the internal pressure and inversely proportional to the enclosure volume.
3. The total damping of large span air-supported structures vibrating in still air is higher than that of conventional structures and stems from the structural damping and acoustical damping.
4. The enclosure volume under the roof significantly affects the frequency of the fundamental axisymmetrical mode of vibration for a particular internal pressure. This effect is much less pronounced for the second axisymmetrical mode of vibration.

9.2.3 Wind Tunnel Tests

Wind Tunnel tests were conducted on both aeroelastic and rigid models of a hemispherical air-supported structure. The parameters in these tests were the wind speed, the exposure, the internal pressure and the enclosure volume.

The main conclusions are:

1. The mean membrane deflections of the hemispherical air-supported structure in strong winds are very large compared to conventional structures and are mostly outward except the windward side, where the deflections are inward.
2. Dynamically, the membrane responds instantaneously and locally to wind induced pressure fluctuations.
3. The dynamic response is broad band in character, typical of a quasi-steady excitation or low frequency buffeting referred to as the background turbulence response, without resonance contributions. In this regard, the response of the hemispherical membrane is typical of a highly damped structure.
4. The dynamic response is generally small compared to the mean deflections.
5. The open country exposure gives higher mean and smaller RMS deflections than those for other exposures. In contrast, the urban exposure has more turbulence than other exposures, and produces higher RMS deflections.
6. Variations in the mean internal pressure have a significant effect on the roof response. A marked increase of the wind induced response occurs when the internal pressure is reduced.

7. Variations in the volume scaling affect the mean and RMS values of the roof response. Reductions of the roof responses occur when the model volume is significantly reduced.
8. The RMS internal pressure fluctuations are generally small. The RMS values of internal pressure grow with the wind speed and increase with changing the exposure from open country to urban, with the associated turbulence intensity increase. The RMS values of internal pressure are also inversely proportional to the internal mean pressure and proportional to the volume of the enclosure. This is similar to what was seen with the response.
9. The open country exposure gives higher mean and smaller RMS external pressures than other exposures. This is because the mean velocity at roof height is higher and the turbulence intensity is lower for the open country exposure than it is for rougher exposures.
10. The predicted mean and RMS deflections compare well with the experimental ones for the internal pressures and exposures considered. This indicates that the proposed semi-analytical approach can provide reasonable estimates of the wind-induced response of air-supported structures.

9.3 RECOMMENDATIONS FOR FUTURE RESEARCH

Several recommendations may be made for future research into free vibration and the dynamic response of more complex shapes of large span, lightweight roofs. Paraboloids and double curved shapes are among the complex shapes requiring further research. Dynamic analysis is also needed for air-

supported structures of more complex shapes such as cylindrical shapes with spherical or parabolic ends.

The terrain roughness has significant influence on wind loading. A detailed study may be needed to investigate the transition from local roughness introduced by one or two obstacles surrounding the structure, to general roughness introduced by a homogeneous urban environment. A full-scale study is needed to clarify the roof behaviour for high Reynolds numbers and to examine other features of wind-induced response of air-supported structures.

To improve the reliability of the semi-analytical approach formulated for predicting the wind-induced response of air-supported structures, further research into the distributions of external pressure coefficients and their correlation functions for different terrain exposures and high Reynolds numbers is needed. Finally, the analysis should be extended to allow for structural non-linearities.

APPENDIX A

SPECTRA OF RESPONSE AND INTERNAL PRESSURE FLUCTUATIONS

This appendix contains the power spectra of response as well as the internal pressure fluctuations due to turbulent wind for the aeroelastic hemispherical air-supported model described in Chapter 7, for different terrain exposures and internal pressures.

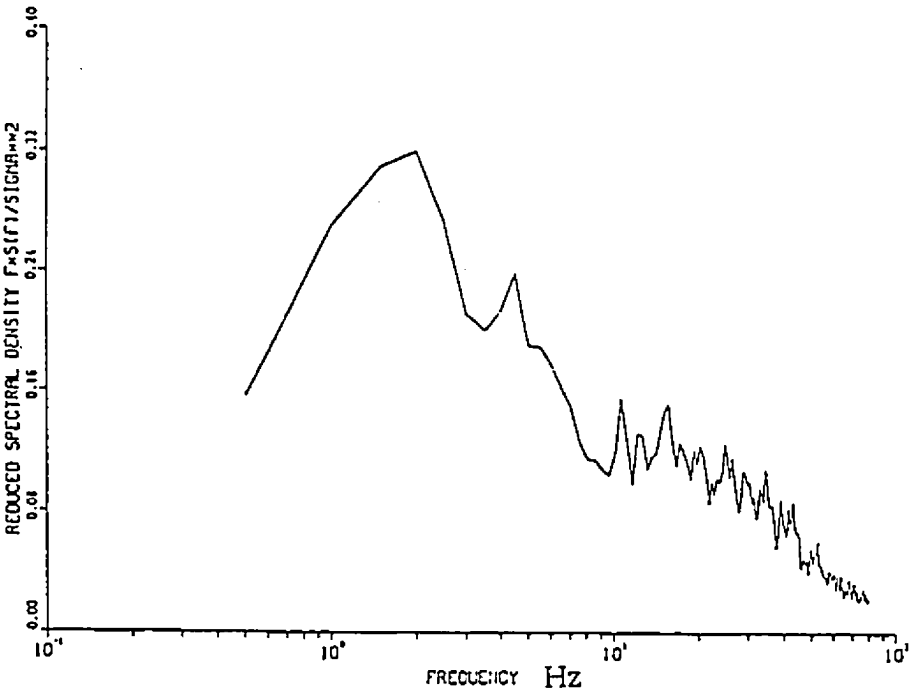

Fig. (A.1): Power spectrum of response at roof center (suburban exposure, U = 15 m/sec, and q_o = 40 Pa)

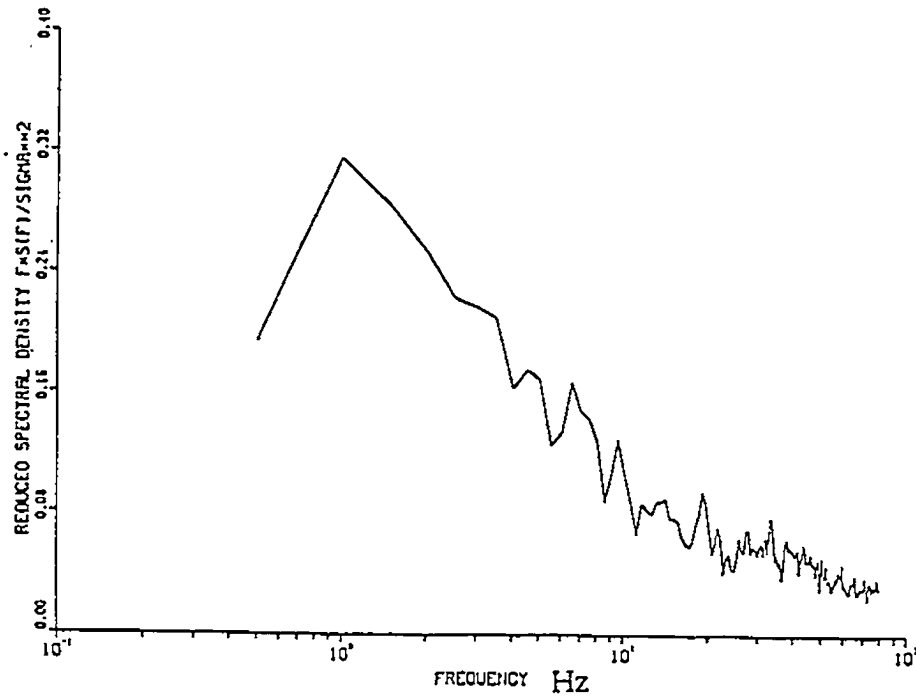

Fig. (A.2): Power spectrum of response at roof center (urban exposure, U = 15 m/sec, and q_o = 40 Pa)

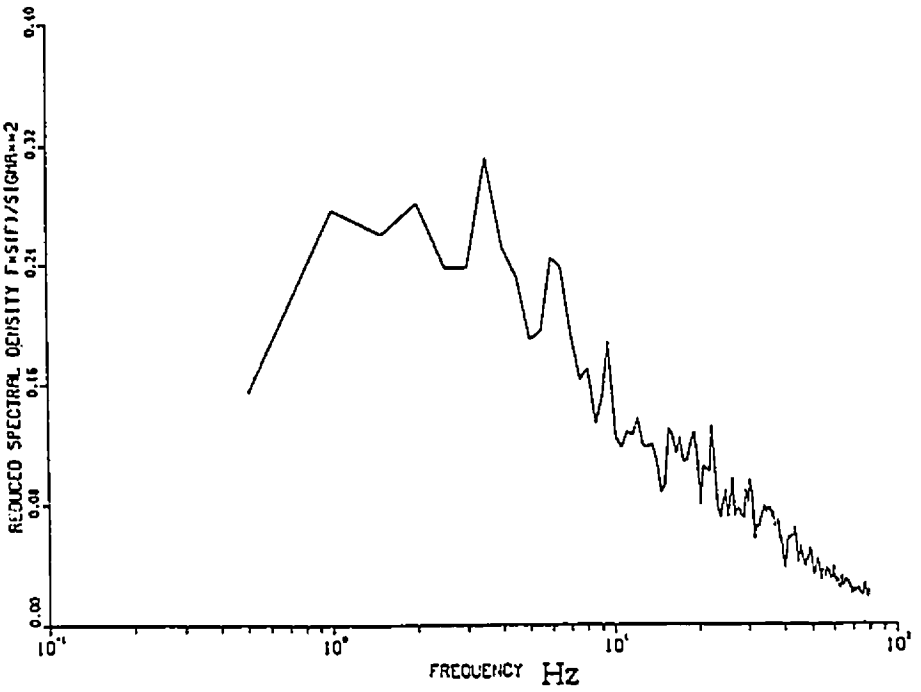

Fig. (A.3): Power spectrum of response at probe 2 (suburban exposure, U = 15 m/sec, and q_o = 40 Pa)

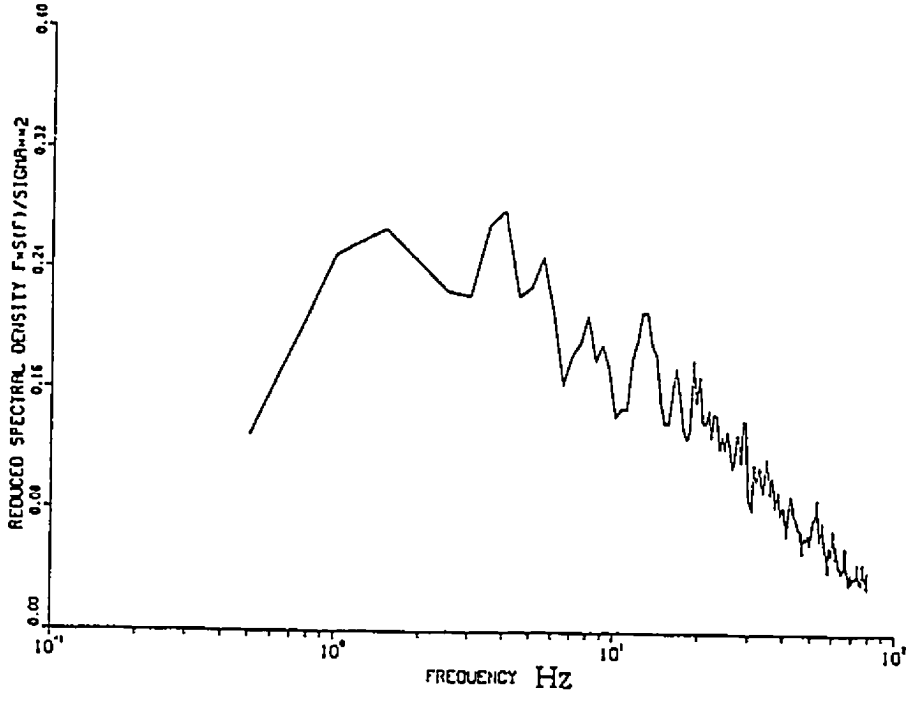

Fig. (A.4): Power spectrum of response at probe 2 (urban exposure, U = 15 m/sec, and q_o = 40 Pa)

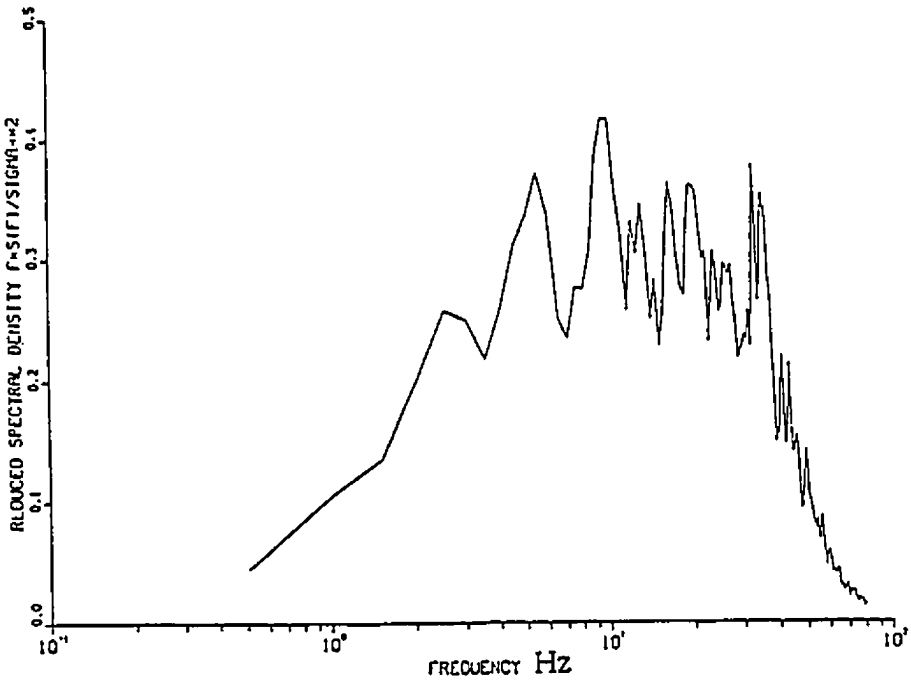

Fig. (A.5): Power spectrum of internal pressure (suburban exposure, U = 15 m/sec, and q_o = 40 Pa)

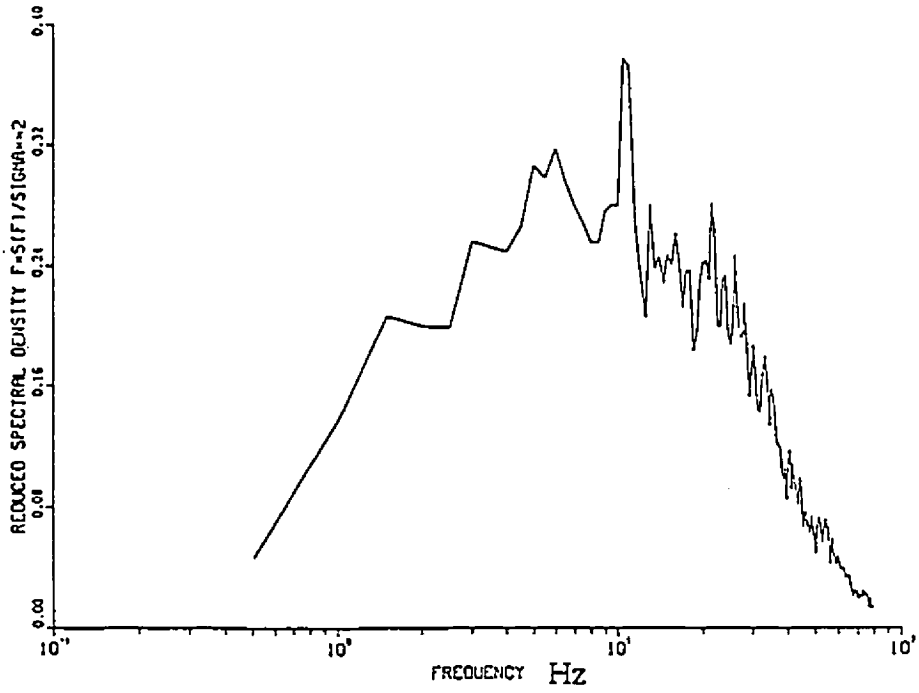

Fig. (A.6): Power spectrum of internal pressure (urban exposure, U = 15 m/sec, and q_o = 40 Pa)

APPENDIX B

MEASUREMENTS OF SURFACE PRESSURES *

Measurements of the wind-induced surface pressure at a point are accomplished by allowing the surface pressure to act on a transducer which provides an electrical analogue of the pressure. The electrical signal is processed using standardized instrumentation techniques and digitized to allow the on-line analysis by a small computer and peripherals.

In practice, the transmission of the surface pressure to the pressure transducer is complicated in two ways. First, there are usually a large number of measuring positions requiring the use of multiple pressure switches - in this case scanivalves - to provide a reasonable trade-off between a large number of transducers and a lengthy testing time. Second, the model is generally too small to allow the pressure switches and transducers to be very close to the measuring locations. The resulting use of long lengths of pneumatic tubing leads to the modification of the pressure at the transducer compared to that at the model surface. These problems are dealt with as follows: pressure taps on the model are connected pneumatically to one of several scanivalves, each is capable of handling 48 different taps. Each scanivalve contains a pressure transducer to which individual taps are connected on computer command. The pneumatic connection

---

* This appendix is adopted from a standard appendix to reports issued by the Boundary Layer Wind Tunnel Laboratory at the University of Western Ontario, London, Ontario, Canada.

between the model and the scanivalve is typically 1.50 mm ID plastic tubing containing a restricting insert of small bore at a specific point along its length. The function of the restrictor is to add damping to the resonant system made up of the pressure tube and the connecting volume adjacent to the pressure transducer. The resulting pressure system with 0.60 m long tubes, responds with negligible attenuation or distortion to the surface pressure fluctuations with frequencies up to about 100 Hz.

The on-line digital data acquisition system, consisting of a PDP 11/73 computer and peripherals, simultaneously samples the signal from each of the pressure transducers at a rate of about 500 times per second for sixteen inputs. Typically, sampling is continued for one minute in real time during which the computer records, for each input the time history, maximum and minimum values that occur, and computes the mean and the RMS pressure values. This sampling period was sufficiently long to provide statistically stable estimates of the mean and RMS pressures. The reference dynamic pressure, usually measured in the free stream above the boundary layer, is monitored similarly. After the sampling period, the measured maximum, minimum, mean and RMS pressure values for each channel are converted to pressure coefficients by dividing each by the reference dynamic pressure. These are stored on a disk for later analysis. Besides the sampling and the on-line calculations, the computer controls the experimental hardware such as the stepping of the scanivalves, the rotation of the wind tunnel turntable on which the pressure model is mounted and the wind speed.

Definition of the Pressure Coefficients

Pressures are usually measured with respect to the mean static pressure in the wind tunnel test section. Pressure coefficients are obtained by normalizing the measured pressures by the mean dynamic pressure measured at a convenient reference height, usually selected to be somewhat higher than the top of the boundary layer. The pressure coefficients are defined as follows:

Mean pressure coefficient

$$C_p = [\ \frac{1}{T}\int_0^T P(t)\ dt\ ]\ /\ q \qquad (B.1)$$

RMS pressure coefficient

$$C_p' = [\ \frac{1}{T}\int_0^T \{\ P(t) - \bar{P}\ \}^2\ dt\ ]^{\frac{1}{2}}\ /\ q \qquad (B.2)$$

Maximum pressure coefficient

$$\hat{C_p} = P_{max}\ /\ q \qquad (B.3)$$

and the minimum pressure coefficient is

$$C_p^{\vee} = P_{min}\ /\ q \qquad (B.4)$$

where P(t) is the instantaneous surface pressure measured with respect to the mean static reference pressure; t is the time; $\bar{P}$ is the temporal mean surface pressure defined with respect to the mean static reference pressure; and P_{max} and P_{min} are the maximum and minimum values of the surface pressure P(t) for the sampling period T, respectively. The reference mean dynamic pressure q is

$$q = \tfrac{1}{2}\ \rho_o\ \bar{U}^2 \qquad (B.5)$$

where ρ_o is the air density and $\bar{U}$ is the reference wind speed, normally measured in the free stream above the boundary layer in which case it corresponds to the hourly mean gradient wind speed at full scale.

REFERENCES

Architectural Fabric Structures Institute, AFSI (1977). "Air structures design and standards manual", ASI-77 AFSI, Glenview, Il., USA, Reproduced 1986, pp. 1-96.

Ahmadi, G. and Glockner, P. G. (1983). "Collapse by ponding of pneumatic elastic spherical caps under distributed loads", Canadian Journal of Civil Engineering, Vol. 10, PP. 740-747.

Beger, G. and Macher, E. (1967). "Results of wind tunnel tests on some pneumatic structures", Stuttgart, West Germany, pp. 142-146.

Bird, W. W. (1971). "Economic considerations in the use of air structures", Proceeding of the International Symposium on Pneumatic Structures, Delft, Netherlands, Vol. 1, Sep. 20-22.

Blevins, R. O. (1979). "Formulas for natural frequency and mode shape", Van Nostrand Reinhold Company, New York, U.S.A., pp. 224-232.

Bendat, J. L., and Piersol, A. G. (1971). "Random data: Analysis and measurements procedures", Wiley-Interscience, New York, U.S.A.

Bird, W. W. (1972). "Economic consideration in the use of air structures", Proceedings of the International Symposium on Pneumatic Structures, Delft, Netherlands, Vol. 1, Sept. 20-22.

Blessman, J. (1971). "Pressures on Domes with Several wind profiles", Proceeding of the Third International conference on Wind Effects on Buildings and Structures, Tokyo.

Bobrowski, J. and Partners Ltd. (1981). "Structural assessment of alternative roof designs for the Calgary Olympic Coliseum", Feb. 17.

Bobrowski, J. (1987)."The Saddledome: the Olympic ice stadium in Calgary", Canadian Journal of Civil Engineering, Vol. 14, April, pp. 239-256.

Boehler, B. J. (1989). "Cost, efficiency and analysis of air-supported structures", ES 400 Project Report in partial fulfilment of the requirement for the Degree of Bachelor of Engineering Science, University of Western Ontario, London, Ontario, Canada.

Buchhold, H. A. (1985). "An introduction to cable roof structures", Cambridge University Press, Cambridge, U.K.

Campbell, W. F. (1982). "The added mass of some rectangular and circular flat plates and diaphragms", Laboratory Technical Report LTR-LA-223, National Research Council Canada, July, Ottawa, Canada.

Canadian Standards Association (CSA), (1981). "Air-supported structures", National Standard of Canada, CAN3-S367-M81, Rexdale, Canada.

Davenport, A. G. (1961). "The application of statistical concepts to the wind loading of structures", Proceeding of the Institute of Civil Engineering, London, England, Vol. 19, 6480, pp. 449-472.

Davenport, A. G. (1963). "The relationship of wind structure to wind loading", Proceeding of the International Conference on Wind Effects on Buildings and Structures, N.P.L., Teddington, U.K., June.

Davenport, A. G. (1964). "The distribution of largest values of random function with application to gust loading", Proceeding of ICE, London, Vol. 28, pp. 187-196.

Davenport, A. G. (1967). "Gust loading factors", Journal of Structural Division, ASCE, Vol. 93, No. ST3, June, pp. 11-34.

Davenport, A. G. (1979). "The influence of turbulence on the aeroelastic responses of tall structures to wind" in IAHR/IUTAM Symposium Karlsruhe 1979 on "Practical experiences with flow-induced vibrations", Springer Verlag, ed Naudascher & Rockwell.

Davenport, A. G., Holm, E. and Surry, D. (1981). "A report of the wind tunnel measurements on the Olympic Coliseum, Calgary, Alberta", Boundary Layer Wind Tunnel Laboratory Report BLWT-SS11-1981, The University of Western Ontario, London, Ontario, Canada.

Davenport, A. G. and Surry, D. (1983). "The estimation of internal pressures due to wind with application to cladding pressures and infiltration", Presented at the ASCE Structural Engineering Conference, Houston, Texas, Oct., Published in Proc. Wind Pressure Workshop, Belgium, 1984.

Davenport, A. G. (1984). "The response of chimneys to wind", Proceedings, 5th International Chimney Congress, October 3 - 5, Essen, West Germany.

Davenport, A. G. "Industrial aerodynamics and meteorology", Graduate Course Notes, Faculty of Engineering Science, University of Western Ontario, London, Ontario, Canada.

Daw, D. J. (1987). " The static and dynamic response of semi-circular cylindrical structures to turbulent cross winds", Thesis presented in partial fulfilment of M. Sc. Degree, University of Western Ontario, London, Ontario, Canada.

Daw, D. J. and Davenport, A. G. (1985). "Fluctuating pressures and aerodynamic derivatives on a semi-circular roof", Presented at the Fifth U.S. International Conference on Wind Engineering, Lubbock, Texas, U.S.A.

Daw, D. J. and Davenport, A. G. (1939). "Aerodynamic damping and stiffness of a semi-circular roof in turbulent flow", Journal of Wind Engineering and Industrial Aerodynamics, Vol. 32, pp. 83-92.

Dent, R. N. (1971). "Principles of pneumatic architecture", The Architectural Press, London, England.

Donalson, M. W. and McNicholas, J. B. (1972). "First steps in the developments of a photoelastic model technique for the study of pneumatic structures", Proceedings of the International Symposium on Pneumatic Structures, Delft, Netherlands, Vol. 1, Sept. 20-22.

Draisey, S. (1987). "The influence of wall openings on the dynamic behaviour of large span roofs", Thesis presented in partial fulfilment of M. Sc. Degree, University of Western Ontario, London, Ontario, Canada.

Dym, C. L. (1973). "Some new results for the vibrations of circular cylinders", Journal of Sound and Vibrations, Vol. 29, pp. 189-205.

El-Ashkar, I. D. (1974). "Dynamic response of tension roofs to turbulent wind", Thesis presented in partial fulfilment of M. Sc. Degree, University of Western Ontario, London, Ontario, Canada.

El-Ashkar, I. D. and Novak, M. (1983). "Wind tunnel studies of cable roofs", Proceeding of the Sixth International Conference on Wind Engineering, The International Association of Wind Engineering, Gold Coast, Australia, pp. 407-419.

El-Ashkar, I. D. (1983). "Response of cable roofs to wind", Thesis presented in partial fulfilment of Ph. D Degree, University of Western Ontario, London, Ontario, Canada.

Engineering Science Data Unit (ESDU), (1974). "Characteristics of atmospheric turbulence near the ground (Part II - Single point data for strong winds), U.K.

Fahrtash, M. and Liu, H. (1989). "Internal pressure of low-rise building - field measurements", Proceeding of the Sixth U.S. National Conference on Wind Engineering, University of Houston, Houston, Texas, U.S.A, March 8-10, pp. B8-11 to B8-20.

Farell, C. and Arroyave, J. (1989). "On uniform flow around rough circular cylinders at critical Reynolds Numbers", Proceeding of the Sixth U.S. National Conference on Wind Engineering, University of Houston, Houston, Texas, U.S.A, March 8-10, pp. B4-32 to B4-42.

Firt, V. (1983). "Statics, form-finding and dynamics of air-supported cylindrical structures", Martinus Nijhoff Publisher, London, England.

Flugge, W. (1973). "Stresses in shells", Second Edition, Springer-Verlag, New York, U.S.A.

Fournier, B. M. and Greenberg, D. P. (1972). "A graphical analysis approach for pneumatic spherical membrane structures", Proceedings of the International Symposium on Pneumatic Structures, Delft, Netherlands, Vol. 1, Sept. 20-22.

Geiger, D. H. and Dick, J. S. (1976). "Design, fabrication and erection of Uni Dome Stadium", Journal of Prestressed Concrete Institute, PCI, pp. 95-107.

Glockner, P. G. and Malcolm, D. J. (1981). "Some problems in using cable-reinforced inflatables in greenhousing", Bulletin of the International Association of Shell and Spatial Structures, Vol. 22-1, No. 75, April, pp. 3-18.

Glockner, P. G. and Szyszkowski, W. (1986). "Some behaviourial features of cylindrical inflatables under line loads and ponding", Bulletin of the International Association for Shell and Spatial Structures, IASS, No. 90, Vol. XXVII-1, April, pp.57-63.

Haug, E. (1972). "Finite element analysis of pneumatic structures", Proceedings of the International Symposium on Pneumatic Structures, Delft, Netherlands, Vol. 1, Sept. 20-22.

Hibbitt, Karlsson, and Sorensen Inc. (1985). "ABAQUS User's Manual".

Holmes, J. D. (1979). "Mean and fluctuating internal pressures induced by wind", Proceeding of the Fifth International Conference on Wind Engineering, Colorado State University, Fort Collins, Colorado, U.S.A., Pergamon Press, Oxford, England and Elmsford, N.Y. 1980, pp. 435-450.

Hoxey, R. P. and Richardson, G. M. (1983). "Wind loads on film plastic greenhouses", Journal of Wind Engineering and Industrial Aerodynamics, Vol. 11, pp. 225-237.

Howell, J. F. (1973). "The wind response of a model suspension roof structure", M. Eng. Report, University of Western Ontario, London, Ontario, Canada.

Ikoma, T. and Sugizaki, K. (1985). "Full-scaled model tests and numerical analysis of air-supported structure", Proceedings of the International Association for Shell and Spatial Structures, Moscow, USSR, Sept. 23-28, pp. 126-140.

Irvin, H. M. (1981). "Cable structures", The MIT Press, Cambridge, Mass., U.S.A.

Irwin, H. P. A. H. and Wardlaw, R. L. (1979). "A wind tunnel investigation of the retractable fabric roof for the Montreal Olympic Stadium", Proceedings of the Fifth International Conference on Wind Engineering, Colorado State University, Fort Collins, Colorado, U.S.A., Pergamon Press, Oxford, England and Elmsford, N.Y. 1980, pp. 925-938.

Irwin, H. P. A. H., Wardlaw, R. L., Wood, K. N. and Bateman, K. W. (1979). "A wind tunnel investigation of the Montreal Olympic Stadium roof", Laboratory Technical Report LTR-L-228, National Research Council Canada, pp. 27-34, May, Ottawa, Canada.

Irwin, H. P. A. H., Cooper, K. R. and Girard, R. (1979). "Correction of distortion effects caused by tubing systems in measurements of fluctuating pressures", Journal of Wind Engineering and Industrial Aerodynamics, Vol. 5, pp. 93-107.

Jackson, P. S. (1983). "Flexible tent structures under dynamic wind loading", Boundary Layer Wind Tunnel, Research Report BLWT-1-1983, The University of Western Ontario, London, Ontario, Canada.

Johnson, G. L. and Surry, D. (1985). "Unsteady wind loads on tents", Boundary Layer Wind Tunnel Report, Research Report BLWT-SS5-1985, The University of Western Ontario, London, Ontario, Canada.

Kalnins, A. (1967). "Discussion of some experiments on a hemispherical shell", Journal of Applied Mechanics, Vol. 34, pp. 792-794.

Kapania, R. K. (1989). "Stability of cylindrical shells under combined snow and wind loads", Proceeding of the Sixth U.S. National Conference on Wind Engineering, University of Houston, Houston, Texas, U.S.A, March 8-10.

Kareem, A. (1989). "Measurements of pressure and force fields on building models in simulated atmospheric flows", Proceeding of the Sixth U.S. National Conference on Wind Engineering, University of Houston, Houston, Texas, U.S.A, March 8-10, pp. B4-11 to B4-21.

Kawmura, S. and Kiuchi, T. (1986). "An experimental study of a one-membrane type pneumatic structure - wind load and response", Journal of Wind Engineering and Industrial Aerodynamics, Vol. 23, pp. 127-140.

Kind, R. J. (1982). "Aeroelastic modelling of membrane structures", Proceedings of the International Workshop on Wind Tunnel Modelling Criteria and Techniques in Civil Engineering Applications, Gaithersburg, MD, Cambridge University Press, Cambridge, pp. 428-439.

Kind, R. J. (1984). "Pneumatic stiffness and damping in air supported structures", Journal of Wind Engineering and Industrial Aerodynamics, Vol. 17, No. 3, Sept., pp. 295-304.

Kinsler, L. E. and Frey, A. R. (1962). "Fundamentals of acoustics", Second Edition, John Wiley and Sons Inc., New York, U.S.A., pp. 81-196.

Kolousek, V., Pirner, M., Fischer, O. and Naprslek, J. (1983). "Wind effects on civil engineering structures", Academia, Prague, Czechoslovakia.

Kramer, C. and Gerhardt, H. J. (1989). "Wind effects on roofs and roofing systems", Proceeding of the Sixth U.S. National Conference on Wind Engineering, University of Houston, Houston, Texas, U.S.A, March 8-10.

Kraus, H. (1967). "Thin Elastic Shells", John Wiley, New York, U.S.A.

Krishna, P., (1978). "Cable-suspended roofs", McGraw-hill Book Company, New York, U.S.A.

Kunieda, H. (1984). "Flexural axisymmetrical free vibrations of a spherical dome: exact results and approximate solutions", Journal of Sound and Vibration, Vol. 92, pp. 1-10.

Lamb, H. (1932). "Hydrodynamics", Princeton University Press, Revised Edition, U.S.A.

Leonard, J. W. (1972). "Inflatable shells - A review", Proceedings of the IASS Calgary, pp. 519-530.

Lissa, A. W. (1969). "Vibration of plates", NASA Report NASA-SP-160, Ohio State University, Ohio, U.S.A.

Lissa, A. W. (1973). "Vibration of shells", NASA Report NASA-SP-288, Ohio State University, Ohio, U.S.A. .

Liu, H. and Rhee, K. H. (1986). "Helmholtz oscillation in building models", Journal of Wind Engineering and Industrial Aerodynamics, Vol. 24, pp. 95-115.

Lukasiewicz, S. and Glockner, P. G. (1983). "Lateral stability of lofty air-supported spherical membranes", International Journal of Nonlinear Mechanics, Vol. 18, No. 6, pp. 491-499.

Lukasiewicz, S. and Glockner, P. G. (1983). "Ponding instability of air-supported membranes under nonsymmetrical loading", Journal of Structural Mechanics, Vol. 10, No. 4, pp. 419-435.

Lukasiewicz, S., and Glockner, P. G. (1983). "Stability of lofty air-supported cylindrical membranes", Journal of Structural Mechanics, Vol. 12, No. 4, pp. 543-555.

Maaskant, R. and Rooda, J. (1985). "Stability of cylindrical air-supported structures", Journal of Engineering Mechanics, Vol. 111, No. 12, Dec., pp. 1487-1501.

Malcolm, D. J., and Glockner, P. G. (1978). "Collapse by ponding of air-supported membranes", Journal of the Structural Division, ASCE, Vol. 104, No. ST9, PP. 1525-1532.

Malcolm, D. J., and Glockner, P. G. (1979). "Optimum cable configuration for air-supported structures", Journal of the Structural Division, ASCE, Vol. 105, No. ST2, PP. 421-435.

Malcolm, D. J., and Glockner, P. G. (1981). "Collapse by ponding of air-supported spherical caps", Journal of the Structural Division, ASCE, Vol. 107, No. ST9, PP. 1731-1743.

Mataki, Y., Iwasa, Y., Fukao, Y. and Okada, A. (1985). "Experimental research on the structural characteristics of low-profile cable-reinforced air-supported structures" and "Wind pressure distribution and statistical behaviour under wind load", Proceedings of the International Association for Shell and Spatial Structures, Moscow, USSR, Sep. 23-28, pp 111-125.

Meirovitch, L. (1967). "Analytical methods in vibrations", The MacMillan Company, London, U.K.

Meirovitch, L. (1975). "Elements of vibration analysis", McGraw-Hill, Inc., New York, U.S.A.

Milne-Thompson, L. M. (1968). "Theoretical hydrodynamics", MacMillan Co. Ltd, 5th Edition, London, England.

Morse, P. M. (1948). "Vibration and sound", McGraw-hill Book Co., New York, U.S.A.

Naghdi, P. M. and Kalnins, A. (1962). "On vibrations of elastic spherical shells", Journal of Applied Mechanics, Vol. 29, pp. 65-72.

National Building Code, Associate Committee, "The supplement to National Building Code", National Research Council of Canada, NRCC 17724, Ottawa, Canada.

Newman, B. G., Ganguli, V. and Shrivastava, S. C. (1984). "Flow over spherical inflated buildings", Journal of Wind Engineering and Industrial Aerodynamics, Vol. 17, pp. 305-327.

Ng, H. T. and Mehta, K. C. (1989). "Pressure measuring system for wind induced pressures on building surfaces", Proceeding of the Sixth U.S. National Conference on Wind Engineering, University of Houston, Houston, Texas, U.S.A, March 8-10, pp. C2-22 to C2-31.

Ng, W. K. (1983). "The external and internal pressures induced under the turbulent wind action on arch-roof structures", M. E. Sc. Thesis, The University of Western Ontario, London, Ontario, Canada.

Niemann, H. J. (1972). "Wind tunnel experiments on aeroelastic models of air-supported structures: results and conclusions", Proceedings of the International Symposium on Pneumatic Structures, Delft, Netherlands, Vol. 1, Sept. 20-22.

Novak, M. and El-Hifnawy, L. (1983). "Effect of soil-structure interaction on damping of structures", Journal of Earthquake Engineering and Structural Dynamics, Vol. 11, pp. 595-621, Issue No. 5, Sept.- Oct.

Novak, M. "Advanced structural dynamics II", Graduate Course Notes, Faculty of Engineering Science, University of Western Ontario, London, Ontario, Canada.

Nowacki, W. (1963). "Dynamics of elastic systems", John Wiley and Sons Inc., New York, U.S.A.

Oniashvili, O. D. (1957). "Certain dynamic problems of the theory of shells", Press of the Academy of Sciences of the USSR, Moscow.

Rayliegh, J. W. S. (1945). " The theory of sound", First American Edition, Dover Publication, New York, U.S.A.

Reissner, E. (1955). "On transverse vibrations of thin, shallow elastic shells", Quart. Appl. Math., Vol. 13, pp. 169-176.

Reissner, E. (1955). "On axi-symmetrical vibration of shallow spherical shells", Quart. Appl. Math., Vol. 13, pp. 279-290.

Reitmeier, G. F. and Punnett, M B. (1972). "Design developments in large span cabled structures", Proceedings of the International Symposium on Pneumatic Structures, Delft, Netherlands, Vol. 1, Sept. 20-22.

Rice, S. O. (1954). "Mathematical analysis of random noise", Selected Papers on Noise and Stochastic Processes, Edited by Wax, N., Dover Publications, New York, U.S.A.

Richardson, G. M., Robertson, A. P., Hoxey, R. P. and Surry, D. (1989). "Full-scale and model investigations of pressures on an industrial agriculture building", Proceeding of the Sixth U.S. National Conference on Wind Engineering, University of Houston, Houston, Texas, U.S.A, March 8-10, pp. B7-17 to B7-26.

Robson, J. D. (1970). "An introduction to random vibrations", Edinburgh University Press, Edinburgh, U.K.

Roshko, A. (1961). "Experiments on the flow past a circular cylinder at very high Reynolds number", Journal of Fluid Mechanics, pp. 345-356.

Sachs, P. (1972). "Wind Forces in Engineering", Pergamon Press Ltd., Oxford, U.K.

Saiful-Islam, M., Ellingwood, B. and Corotis, R. B. (1989). "Transfer function models for determining dynamic wind loads on buildings", Proceeding of the Sixth U.S. National Conference on Wind Engineering, University of Houston, Houston, Texas, U.S.A, March 8-10, pp. B3-36 to B3-45.

Savory, E. and Toy, N. (1986). "Hemispheres and hemisphere-cylinders in turbulent boundary layers", Journal of Wind Engineering and Industrial Aerodynamics, Vol. 23, pp. 345-364.

Sharma, C. B. (1971). "Vibration characteristics of a clamped-free and clamped-ring-stiffened circular cylindrical shell", Journal of Sound and Vibrations, Vol. 14, pp. 459-474.

Sharma, C. B. (1973). "Frequencies of clamped-free circular cylindrical shells", Journal of Sound and Vibrations, Vol. 30, pp. 525-528.

Sill, B. L. and Fang C. (1989). "Effect of upstream roughness element distribution on wind loads on low rise structures", Proceeding of the Sixth U.S. National Conference on Wind Engineering, University of Houston, Houston, Texas, U.S.A, March 8-10, pp. A9-11 to A9-19.

Simiu, E. and Scanlan, R. H. (1978). " Wind effects on structures." A Wiley-Interscience Publication, John Wiley & Sons, New York, U.S.A.

Soarce, M. (1967). "Application of finite difference equations to shell analysis", Pergamon Press, Oxford, England.

Soedel, W. (1973). "A natural frequency analogy between spherically curved panels and flat plates", Journal of Sound and Vibration, Vol. 29, pp. 457-461.

Soedel, W. (1981). "Vibration of shells and plates", Marcel Dekker, Inc., New York, U.S.A.

Spinelli, P. (1978). "Wind effects on a cylindrical air-supported structure", Proceeding of the Third Colloquium on Industrial Aerodynamics, Building Aerodynamics, Aachen, West Germany, June 14-16, pp. 179-193.

Srivastava, N. ; Turkkan, N. and Dickey, R. (1984). "Wind tunnel study of a flexible membrane structure", Proceeding of the Third International Conference on Space Structures, Guildford, England, Sep. 11-14, pp. 785-790.

Srinivasan, R. S. and Krishnan, P. A. (1987). "Free vibration of conical shell panels", Journal of Sound and Vibration, Vol. 117,pp. 153-160.

Stathopoulous, T., Surry, D. and Davenport, A. G. (1979). "Internal pressure characteristics of low-rise buildings due to wind actions", Proceeding of the Fifth International Conference on Wind Engineering, Colorado State University, Fort Collins, Colorado, U.S.A., Pergamon Press, Oxford, England and Elmsford N.Y. 1980, Vol. 1, pp. 451-463.

Stathopoulous, T. (1979). "Turbulent wind actions on low-rise buildings", Thesis presented in partial fulfilment of Ph. D Degree, University of Western Ontario, London, Ontario, Canada.

Steckely, A., Vickery, B. J. and Isyumov, N. (1989). "On the measurements of motion induced forces on models in turbulent shear flow", Proceeding of the Sixth U.S. National Conference on Wind Engineering, University of Houston, Houston, Texas, U.S.A, March 8-10, pp. C2-10 to C2-21.

Stone, G. K., Surry, D. and Vickery, B. J. (1985). "A study of wind loading on the proposed Tampa Bay Coliseum, Florida", Boundary Layer Wind Tunnel Research report BLWT SS9-1985, The University of Western Ontario, London, Ontario, Canada.

Szyszkowski, W., and Glockner, P. G. (1984). "Finite deformation and stability behaviour of spherical inflatables subjected to axi-symmetric hydrostatic loading", International Journal of Solids and Structures, Vol. 20, No. 11/12, pp. 1021-1036.

Tahouri, B., Toy, N. and Savory, E. (1989). "Surface pressures and wake flows associated with highly curved agricultural buildings", Proceeding of the Sixth U.S. National Conference on Wind Engineering, University of Houston, Houston, Texas, U.S.A, March 8-10, pp. B2-31 to B2-39.

Tamura, T., Kuwahara, K. and Suzuki, M. (1989). "Numerical study of wind pressures on a domed roof and near wake flows", Proceeding of the Sixth U.S. National Conference on Wind Engineering, University of Houston, Houston, Texas, U.S.A, March 8-10, pp. A7-1 to A7-10.

Tanaka, H. 1977. "Wind properties at the Olympic Stadium, Montreal", Boundary Layer Wind Tunnel, Engineering Research Report BLWT-SS5-7, University of Western Ontario, London, Ontario, Canada.

Taniguchi, S., Sakamoto, H., Kiya, M. and Erie, M. (1982). "Time-averaged aerodynamic forces acting on hemisphere immersed in a turbulent boundary", Journal of Wind Engineering and Industrial Aerodynamics, Vol. 9, pp. 257-273.

Timoshenko, S., and Krieger, S. W. (1968). " Theory of plates and shells", McGraw-Hill Book Company, Inc., New York, U.S.A.

Timoshenko, S., and Goodier, J. N. (1970). " Theory of elasticity", McGraw-Hill Book Company, Inc., Second Edition, New York, U.S.A.

Toy, N., Moss, W. D. and Savory, E. (1983). "Wind tunnel studies on a dome in turbulent boundary layers", Journal of Wind Engineering and Industrial Aerodynamics, Vol. 11, pp. 201-212.

Tryggvason, B. V. and Isyumov, N. (1977). "A study of the wind induced response of the air-supported roof for the Dalhousie University Sports Complex", Research Report BLWT-SS7-1977, Boundary Layer Wind Tunnel Laboratory, University of Western Ontario, London, Ontario, Canada.

Tryggvason, B. V. and Surry, D., Davenport, A. G. (1978)."A study of the wind-induced response of the Haj terminal roof in Jeddah, Saudi Arabia - Phase II - An Aeroelastic Investigation", Research Report BLWT-SS7-1978, Boundary Layer Wind Tunnel Laboratory, University of Western Ontario, London, Ontario, Canada.

Tryggvason, B. V. (1979). "Aeroelastic modelling of pneumatic and tensioned fabric structures", Proceedings of The Fifth International Conference on Wind Engineering, Colorado State University, Fort Collins, Colorado, U.S.A., Pergamon Press, Oxford, England, and Elmsford, N.Y. 1980, pp. 1061-1072.

Uchiyama, K. and Uematsu, Y. (1987). "Experiments on the deflection and buckling behaviour of ring-stiffened cylindrical shells under wind pressure", Journal of Wind Engineering and Industrial Aerodynamics, Vol. 26, pp. 195-211.

Uematsu, Y. and Uchiyama, K. (1982). "Wind-induced dynamic behaviour of suspended roofs", Technology Reports, Tohoku University, Vol. 47, No.2, pp. 243-261.

Uematsu, Y. and Uchiyama, K. (1985). "Deflection and buckling behaviour of thin, circular cylindrical shells under wind loads", Journal of Wind Engineering and Industrial Aerodynamics, Vol. 18, pp. 245-261.

Uematsu, Y. and Uchiyama, K. (1986). "Aeroelastic behaviour of an H.P. shaped suspended roof", Proceeding of IASS Symposium of Shells, Membranes and Space Frames, Vol. 2, pp. 241-248.

Uematsu, Y. and Uchiyama, K. (1988). "Ovalling oscillations of thin circular cylindrical shells in a cross flow", Journal of Fluids and Structures, Vol. 2, pp. 285-307.

Uemura, M. (1971). "Membrane tension and deformation in cylindrical pneumatic structures subject to wind loads", Proceeding of the IASS Pacific Symposium, Part II, on Tension Structures and Space Frames, Tokyo and Kyoto, Japan, Oct. 17-23, pp. 199-210, (1972).

Vickery, B. J., Davenport, A. G. and Surry, D. (1984). "Internal pressure in low-rise buildings", Fourth Canadian Workshop on Wind Engineering.

Vickery, B. J. (1986). "Gust-factors for internal pressures in low rise buildings", Journal of Wind Engineering and Industrial Aerodynamics, Vol. 23, pp. 259-271.

Vickery, B. J. "Advanced structural Dynamics I", Graduate Course Notes, Faculty of Engineering Science, University of Western Ontario, London, Ontario, Canada.

Vickery, B. J. and Georgiou, P. N. (1989). "A simplified approach to the determination of the influence of internal pressures on the dynamics of large span roofs", Proceeding of the 8th Colloquium on Industrial Aerodynamics, Aachen, West Germany, Sep. 4-7.

Vinogradov, O. G., Malcolm, D. J., and Glockner, P. G. (1981). "Vibration of cable-reinforced inflatable structures", Journal of the Structural Division, ASCE, Vol. 107, No. ST10, Oct., PP. 1985-1999.

Vlasov, V. Z. and Leont'ev, U. N. (1960). "Beams, plates and shells on elastic foundations", Israel Program for Scientific Translations, Jerusalem.

Vol'mir, A. S. (1972). "The nonlinear dynamics of plates and shells", Nelineynaya Dinamika Plastinok i Obolocheck, Edited Translation, pp. 1-432.

Wellesley-Miller, S. R. (1972). "Control aspects of pneumatic structures", Proceedings of the International Symposium on Pneumatic Structures, Delft, Netherlands, Vol. 1, Sept. 20-22.

Whitbread, R. E. (1963). "Model simulation of wind effects on structures", Vol. 1, Symposium, Wind Effects on Buildings and Structures, National Physical Laboratory, U.K., June, HMSO.

Williams, C. J. (1985). "Form-finding and analysis of cable nets, tents and air-supported structures", Proceeding of the International Conference of Numerical Methods in Engineering: Theory and Applications, Swansea, Wales, England, Jan. 7-11, Publ. by A. A. Balkema, Rotterdam, Neth and Boston, Ma, USA pp 885-896.

Zetlin, L. (1968). "Suspension roofs", McGraw-hill Book Company, Inc., New York, U.S.A.